

**A hidden mystery: root adaptive responses to environmental
factors in *Nicotiana attenuata***

DISSERTATION

zur Erlangung des akademischen Grades
„doctor rerum naturalium“ (Dr. rer. nat.)

vorgelegt dem Rat der Fakultät für Biowissenschaften
der Friedrich-Schiller- Universität Jena

von

Ming Wang, M.S.
geboren am 19.05.1986 in China

Gutachter:

1.

2.

3.

Beginn der Promotion: 15.08.2013

Eingereicht am:

Tag der Verteidigung:

Table of Contents

1. General Introduction

1.1.	Root architecture formation and developmental regulation.....	1
1.1.1.	Auxin.....	2
1.1.2.	Cytokinins.....	5
1.1.3.	Gibberellins.....	6
1.1.4.	Reactive oxygen species (ROS)	7
1.2.	<i>Nicotiana attenuata</i> : a model system to study physiologically adapted re-sponses to comprehensive environmental factors.....	8
1.3.	Abiotic environmental factors: critical impacts on root plasticity.....	10
1.4.	Biotic environmental factors: friends and foes.....	13
1.4.1.	A native growth-promoting bacterial isolate, <i>Bacillus</i> sp. B55, can rescue defects in ethylene deficient plants.....	13
1.4.2.	Native bacterial consortiums enhance pathogenic resistance against sudden wilt disease.....	15
1.4.3.	Arbuscular mycorrhizal fungi, a mutualistic partner with <i>N. attenuata</i> in the field.....	16
1.5.	Scope of this thesis.....	20

2. Manuscript Overview & Author Contributions.....23

3. Manuscripts

3.1.	Manuscript I: Catechol, a major component of smoke, influences primary root growth and root hair elongation through reactive oxygen species-mediated redox signaling.....	26
3.2.	Manuscript II: <i>Nicotiana attenuata</i> 's capacity to interact with arbuscular mycorrhiza alters its competitive ability and elicits major changes in the leaf transcriptome.....	51

3.3.	Manuscript III: Blumenols as effective shoot markers for root symbiosis with arbuscular mycorrhizal fungi.....	83
4.	Discussion	
4.1.	From the abiotic perspective: a new compound, catechol, which exists in natural environments, is involved in root growth.....	134
4.2.	Auxin is not the main regulator that mediates catechol-induced root morphological changes.....	135
4.3.	Spatial ROS homeostasis interruption caused by catechol treatment accounts for root defects.....	136
4.4.	From the biotic perspective: growth responses of plant communities in mesocosms colonized with arbuscular mycorrhizal fungi	140
4.5.	AMF-mediated preferential Pi uptake in EV plants leads to better growth.....	141
4.6.	Interactive model aspect summarized from foliar DEGs: the third regulator behind differential plants growth.....	143
4.7.	Additive model aspect 1: predication of AMF-indicative markers genes in leaves.....	145
4.8.	Additive model aspect 2: searching AMF-indicative chemicals in leaves.....	147
4.9.	Functional implication of blumenol accumulation and transport.....	150
4.10.	Using AMF-indicative blumenols as a powerful tool for research and plant breeding.....	151
5.	Summary	152
6.	Zusammenfassung	154
7.	References	156
8.	Acknowledgment	167
9.	Curriculum Vitae	168
10.	Eigenständigkeitserklärung	170

1. General Introduction

Terrestrial root systems are dynamic regulators of plant shoot physiology, morphology, biochemistry, flowering and synthesis of metabolites, both directly and indirectly. The root system of a plant maintains a continuous conductivity link to the stem and leaves and is a good model organ to study interactions with environmental factors that play essential roles in plant development and growth, biomass production, survival, and reproduction. Roots are subjected to many changing environmental aspects, which are commonly categorized into two broad areas: abiotic factors (e.g. temperature, soil moisture, ecohydrology, soil fertility, etc.) and biotic factors (e.g. pathogens, rhizobia, mycorrhizae, herbivores, etc.). Roots evolved diversified mechanisms to cope with multifaceted environmental factors and the interactions among them. In the last few decades, the development of advanced techniques, particularly in molecular biology, has facilitated a better understanding of the mechanisms by which plants perceive environmental signals, transmit these signals to cellular machinery to activate adaptive responses, and ultimately coordinate responses in molecular, biochemical and physiological aspects.

1.1. Root architecture formation and developmental regulation

The growth of a plant root results from a continuous and sustainable cell division process localized in the root apical meristem (RAM). After a few rounds of cell proliferation, root meristematic cells will progress exit the cell cycle, transition to elongation phases, and then differentiate. These successive stages ultimately confer a longitudinal formation to the root (Figure 1). Close to the root tip is the stem cell niche (SCN) with a quiescent center (QC), where a small group of peripheral stem cells forming a circuit are located, referred to as the “initials” (or “founders”). A specific root cell file derives from a specifically determined initial. Differentiation of stem cells ahead of the QC in the root tip gives rise to columella cells containing statoliths that are crucial to gravity sensing. Laterally, stem cells alongside the QC divide and symmetrically differentiate into the lateral root cap. Other stem cells determined by their own initials ultimately develop into cell files of stele, pericycle, endodermis, cortex and epidermis cells radially from the center to the exterior. The number of cells in each cell file differs by plant species, but root radial organization into concentric circles is conserved in all

land plants. In *Arabidopsis thaliana*, a model plant with extensively studied root structure, only one layer of endodermal and cortical cells are present, and a lateral slice of the root reveals that each root stele contains two protoxylem at opposing sides and two protophloem half way between the protoxylems, also on opposing sides. This radially organized primary root pattern is genetically inherited from embryogenesis and the cell specification and patterning are post-embryonically maintained, usually by the SCN and the precise engagement of phytohormones, peptides and reactive oxygen species (ROS) regulation (Willemsen & Scheres, 2004; De Smet *et al.*, 2008; Matsuzaki *et al.*, 2010). Here we recapitulate the importance of ROS signals and phytohormones including auxin, cytokinin and gibberellins in root development and growth.

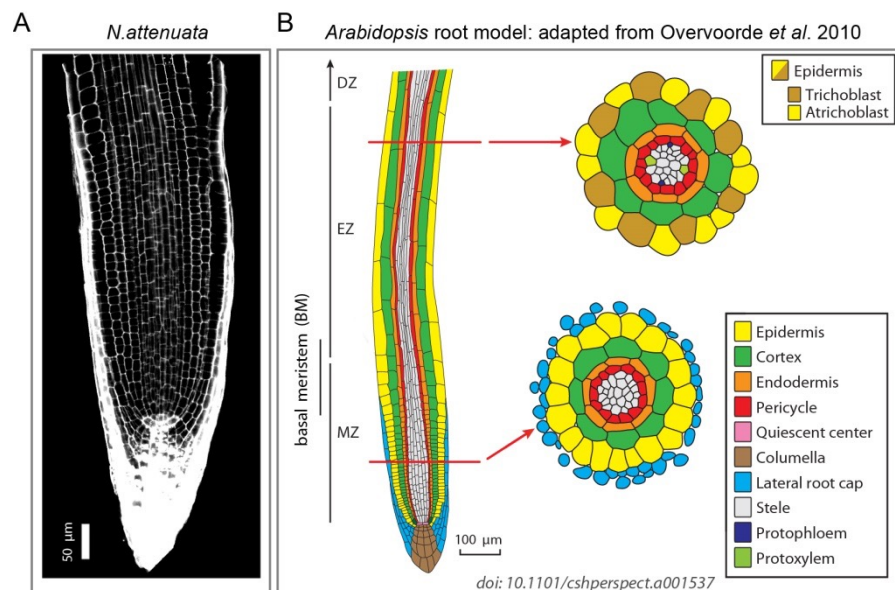


Fig 1. The root structure of *Nicotiana attenuata* is similar to that of the model plant *Arabidopsis thaliana*.

A. Fine root structure of *N. attenuata* in a seedling, 7 days post-germination. B. Cellular organization on a proximal-distal axis of an *A. thaliana* root. MZ: meristem zone; EZ: elongation zone; DZ: differentiation zone. Scheme is adapted from Overvoorde *et al.* (Overvoorde *et al.*, 2010).

1.1.1. Auxin

Auxin has long been known to orchestrate nearly all aspects of plant growth and development, across all organs and throughout a plant's lifespan. Auxin regulates root architecture formation through downstream agents of auxin signaling which interact with root transportation, production and conjugate inactivation.

Indole-3-acetic acid (IAA) is the most bioactive form of auxin in plants and is mainly biosynthesized in young leaves and cotyledons through proposed tryptophan (Trp)-independent and -dependent pathways (Mashiguchi *et al.*, 2011; Won *et al.*, 2011). Though auxin has been identified as a growth regulator over centuries, a clear auxin biosynthesis pathway has still not been fully unraveled. For the hypothesized Trp-dependent pathways, potential branches to define the biosynthesis network include: 1) the IPA (indole-3-pyruvic acid) pathway, 2) the TAM (tryptamine) pathway, 3) the IAM (indole-3-acetamide) pathway and one specialized in Brassicaceae species, 4) the IAOx (indole-3-acetaldoxime) pathway. In the potential Trp-independent pathway, IAA is proposed to be initiated directly from indole as a substrate instead of from Trp via mostly unknown steps. However, the inactivation process of IAA is simpler: like most phytohormones, oxidative conjugation is the most common catabolic process to inactivate IAA.

The process of acropetal auxin allocation generally originates from production sites such as young leaves and results in accumulation of auxin in the roots. A model for the transportation of auxin during this process has been widely accepted to be the combination of two types of machineries defined by allocation distance. Long-distance (also known as long-range) transportation is dependent on the mature phloem, and mobilizes auxin mainly from the synthesizing locations of young shoot tissues to roots, similar to the allocation of carbohydrates from “source” to “sink” tissue. The second transport machinery complements this long-distance vasculature translocation by unloading and loading auxin cargo from the phloem and distributing it to the nearby tissues (Swarup *et al.*, 2001; Marchant *et al.*, 2002). This is known as short-distance (or short-range) transportation and is a cell-to-cell transport system crossing through plasma membranes via specialized transporters dynamically docked on the membranes. In *A. thaliana*, three main classes of transporters were identified: influx carriers such as AUX1

(AUXIN RESISTANCE 1) and LAX (LIKE AUX), efflux carriers including PINs (PIN FORMED), and ABCB/MDR/PGP carriers (ATP-binding cassette group B/ multi-drug resistance/P-glycoprotein -like). These carriers mediate both influx and efflux, which coordinate to form a short-range transport system, referred to as polar auxin transport (PAT) [reviewed in (Friml, 2003; Reinhardt *et al.*, 2003)]. This sophisticated transport system organizes a directional auxin flux loop that has been metaphorically called “inverted fountains”, and eventually form an auxin gradient mainly depending on the type of cells in the immediate area (i.e. creating the highest concentration of auxin in the QC). Interactive tuning between biosynthesis and mobilization ultimately ensures the status of auxin homeostasis.

In plant cells, free IAA brings one of the several nuclear receptors TRANSPORT INHIBITOR RESPONSE 1/AUXIN SIGNALING F-BOX (TIR1/AFB) and members of transcriptional repressors AUX/IAA together as molecular glue. As subunits of ubiquitin ligase complex SCF^{TIR1}, TIR1/AFB belonging to an F-box component interact with Skp1 via its F-box motif. Instead of inducing conformational changes in TIR1 or AFB, such interaction leads to the complete assembly of a complex with two other components (Cullin and RBX1), which transfers activated ubiquitin to targeted proteins, namely AUX/IAA. With the ubiquitination by the proteasome, AUX/IAA is degraded, and previously repressed AUXIN RESPONSE FACTOR (ARF) transcription factors are sequentially released, ultimately activating down-stream responsive genes [reviewed in (Leyser, 2017)].

In the root, local auxin biosynthesis coupled with PAT is clearly engaged in balancing cell proliferation and differentiation along the apical-basal axis. An output from the interplay between biosynthesis and mobilization of auxin is represented by the gradient of auxin around the QC, where the highest levels of IAA in the QC result in minimal mitotic activity, and slightly reduced auxin content in the SCN still produces only a compromised level of mitotic activity. In contrast, in the meristematic zone (MZ), lower auxin levels relative to that in the SCN are positively associated with rapid cell proliferation, and these levels progressively decrease toward the basal axis of the root until they reach their lowest level at the onset of the transition zone

(TZ). This decreasing gradient is inversely correlated with cell proliferation (Grieneisen *et al.*, 2007).

Through new developments in biochemistry and analytical chemistry techniques and technologies, the discovery of auxin synthetic analogues (e.g. NAA, 2,4-D), synthesis inhibitors (Yucasin, Kyn), transport inhibitors (NPA), and PINs trafficking inhibitors (BFA) has been made possible [reviewed in (Kerr & Bennett, 2007)]. Advanced optical visualization techniques, coupled with specific staining dyes or trackable proteins with fluorescence, and also isotopic labeling equipped with ultra-high resolution quantification methodologies, have remarkably improved the understanding of auxin biosynthesis and its transport from different aspects. In addition, forward and reverse genetic manipulation strategies coupled with improved computational methods largely help current research to better mechanically reveal the importance of auxin in plant growth and development.

1.1.2. Cytokinins

Cytokinins (CKs) are crucial regulators involved in plant's environmental responses, growth and development, such as in the differentiation of the root and shoot [reviewed (Sakakibara, 2006)].

CKs were discovered in 1955 as a class of adenine derivatives mainly enriched in juvenile tissues like shoot apical meristems (SAM), immature seeds, and young leaves [reviewed in (Amasino, 2005)]. In *A. thaliana*, they are biochemically classified into 4 groups depending on their chemical properties, specifically, their side chains: aromatic, isopentenyladenine (iP)-type, cis-zeatin-type (cZ)-type and transzeatin-type (tZ)-type. Only the iP and tZ CKs are derived from iP hydroxylation and are thought to be bioactive. CK biosynthesis initiates with a rate-limiting step delivering an isopentenyl moiety from dimethylallyldiphosphate (DMAPP) to an adenine nucleotide (iP nucleotide) by IPT (ATP/ADP-ISOPENTYL-TRANSFERASE) (Miyawaki *et al.*, 2004; Takei *et al.*, 2004). Inactive forms of biosynthesized iP nucleotides include iPRTP, iPRDP, and iPRMP, and these can be converted to tZ nucleotides by cytochrome P450 monooxygenase (CYP735A). However, they are still inactive. Inactive tZ/iP nucleotide forms, including iPRMP and tZRMP, can be either directly converted to the bioactive freebase by LONELY GUY (LOG) proteins with a one-step reaction or by an activation process through a two-step reactions

(Kyoizuka, 2007). Metabolic CK's inactivation process mostly relies on the catabolic activity of the CYTOKININ OXIDASE/DEHYDROGENASE (CKX) protein family (Werner *et al.*, 2001; Werner *et al.*, 2003). Though it's hard to distinguish the functional specificities between iP-type and tZ-type CKs, both types can be translocated to other tissues by subsets of nucleoside transporters and purine permeases (Gillissen *et al.*, 2000; Bürkle *et al.*, 2003; Hirose *et al.*, 2005). CK signals transmit via a two-components signaling pathway that involves three independent histidine kinase receptors (AHK2/3/4) docking on the plasma membrane that triggered the cascade of phosphorylation to successively phosphorylates *ARABIDOPSIS* RESPONSE REGULATORS (ARR) and subsequently activates AP2 transcription factors to progressively complete signaling transduction and eventually activate target genes (Hwang *et al.*, 2012).

CKs attenuate the size of the RAM mainly by accelerating differentiation rate of meristematic cells. Exogenous supplementation of cytokinins to plant roots negatively regulates the root meristem size (Dello Ioio *et al.*, 2007), and in contrast, CK-biosynthetic deficient mutants or over-expressing CKX plants, which inactivate bioactive forms of CK, exhibit longer roots with clear increases in the number of meristematic cells (Werner *et al.*, 2003). The external supplementation of CKs does not appear to modify stem cell niche (SCN) activity or cell division rate of meristematic cells in the root tip, whereas CKs definitely affect the cell differentiation rate when specifically added to the vascular tissue at the MZ/EZ transition zone in the presence of auxin, causing an acceleration in cell differentiation in the distal meristem to enter transition zone/elongation zone (TZ/EZ) (Dello Ioio *et al.*, 2007). Root responses to CKs are not linear: a small decrease in CK content or in the sensitivity of CK signaling can lead to an increase in root size, while a reduction beyond this threshold - such as complete depletion of CK presence in root or thorough block signaling transduction (e.g., *ahk2/3/4*) - may lead to an obvious inhibition in root growth.

1.1.3. Gibberellins

Gibberellins (GAs) regulate multiple aspects of plant growth and development such as root elongation and size modification of the RAM. GAs are biosynthesized and act mainly in rapidly growing tissues such as the tips of shoots and roots, developing flowers and seeds (Silverstone *et*

al., 1997). GA biosynthesis initiates from geranylgeranyl diphosphate (GGDP) and successive synthesis and oxygenation steps ultimately form a large number of products, of which only a small portion of GAs are biologically active (e.g., in *A. thaliana*, GA1, GA3, GA4 are active; of those, GA7 and GA4 are the most active forms). Bioactive GAs bind to the *GIBBERELLIN INSENSITIVE DWARF1* (GID1) receptor with high affinity, whereas inactive GAs have nearly no affinity for this receptor. This binding leads to the degradation of DELLA proteins, commonly accepted as repressors of down-stream transcription factors that mediate GA responses and the regulation of their associated target genes (Sun & Gubler, 2004). GAs regulate root growth and development mainly by controlling cell proliferation and elongation in an DELLA-dependent manner. A decrease in endogenous GA content in plants through biochemical or genetic approaches causes the formation of shorter roots with reduced RAM size. The *gai* mutant in *A. thaliana*, which has a gain-of-function mutation and produces a stabilized DELLA which is not degraded when GA binds, displays inhibited root growth. It has been shown that bioactive GAs increase the size of MZ via the promotion of cell proliferation without interfering with SCN specification or activity (Ubeda-Tomás *et al.*, 2009).

1.1.4. Reactive oxygen species (ROS)

Reactive oxygen species (ROS) are important signaling molecules and not only play a role in response to biotic and abiotic stress but are also critical for root growth and development (Gapper & Dolan, 2006). In plants, superoxide (O_2^-) is produced by NADPH oxidases (RBOH), and converted into H_2O_2 by superoxide dismutases (SODs) and other enzymes including apoplastic oxalate oxidase, diamine oxidase and class III peroxidases. H_2O_2 can be enzymatically catabolized to H_2O by catalase (CAT), glutathione peroxidase (GPX), and ascorbate peroxidase (APX), or non-enzymatically consumed by Fenton reactions when Fe^{2+} is available, a reaction highly dependent on pH and other indicators of subcellular reactivity [reviewed in (Apel & Hirt, 2004)]. As demonstrated by mutants in *A. thaliana*, the main ROS species appear to have their own zones of accumulation, and their homeostasis is genetically regulated by a bHLH transcription factor UPBEAT (UPB1); *upb1* mutation in *A. thaliana* caused a longer primary roots resulting from the increase of meristem cell numbers and the increase of cell length in TZ/

EZ. Chip-Seq helped to find direct target genes of UPB1, and these included a large set of peroxidases which led to a focus on ROS. As a result, it was found that in *upb1* mutants, superoxides accumulate in the meristematic zone during root growth, while H₂O₂ presence decreases in the elongation/differentiation zone (Tsukagoshi *et al.*, 2010). Additional evidence corroborated that amounts of superoxides in the MZ are highly associated with the number of meristem cells, while H₂O₂ appears to be negatively correlated to these cell numbers. From the investigation with *upb1*, it was demonstrated that a UPB1-regulated ROS balance modified root morphology in an auxin-independent way. Another genetic research study in *A. thaliana* reported MED25/PFT1 as a mediator that controls root hair differentiation and primary root elongation by regulating redox-related gene expression, which critically alter the balance of H₂O₂ and O₂⁻ (Sundaravelpandian *et al.*, 2013; Raya-González *et al.*, 2014)

1.2. *Nicotiana attenuata*: a model system to study physiologically adapted responses to comprehensive environmental factors

Fires are one of the major drivers of vegetative diversity and have occurred on Earth since the beginning of land plant existence. It is to be expected that plants have acquired a myriad of responses to benefit from fires, and in extreme cases, some plant species depend on fires to complete their whole life cycle when, for instance, they have fire-activated germination. Fires provide plants with unique environmental factors by removing canopies and leaf litter, therefore changing the light availability in both quality and quantity, and further, fertilize the soil with extra nutrients and moisture, which may modify the structures and members of peripheral microbe communities. Fire is an exothermic chemical process of combustion to rapidly oxidize substances, releasing heat, light, and various reaction products, which consequently confer a unique condition to selectively shape many characteristically fire-promoted biomes around the world (Baldwin & Morse, 1994; Baldwin *et al.*, 1994; Lynds & Baldwin, 1998).

Nicotiana attenuata, an annual wild tobacco species native to the Great Basin Desert of the United States, exists mostly as ephemeral near-monoculture populations which occur most abundantly in post-fire habitats but also exist in smaller persistent groups found in washes (Bahulikar *et al.*, 2004). Dormant *N. attenuata* seeds from long-lived seed banks usually

germinate in sagebrush and pinyon-juniper areas when fires both remove allelochemicals in litter which may inhibit their germination, and provide smoke-derived germination cues that are permeate into the soil (Baldwin & Morse, 1994; Baldwin *et al.*, 1994). The elements of these germination cues are easily transported by floods or wind to areas nearby to the burned area, though they are still predominantly contained within the burned area. In 2004, the main bioactive compound to promote seed germination in smoke was isolated and identified: karrikin, a molecule new to science (Flematti *et al.*, 2004). Fire may be one of nature's most powerful forces to mold the vegetation landscape, but other abiotic and biotic factors also determine the final outcome (Fig 2). In this study, we probe into environmental factors occurring in our Utah Field Station, located in the Great Basin Desert in *N. attenuata*'s natural habitat, to evaluate their impact on the performance of these plants, and we test these factors in both glasshouse and field assays.

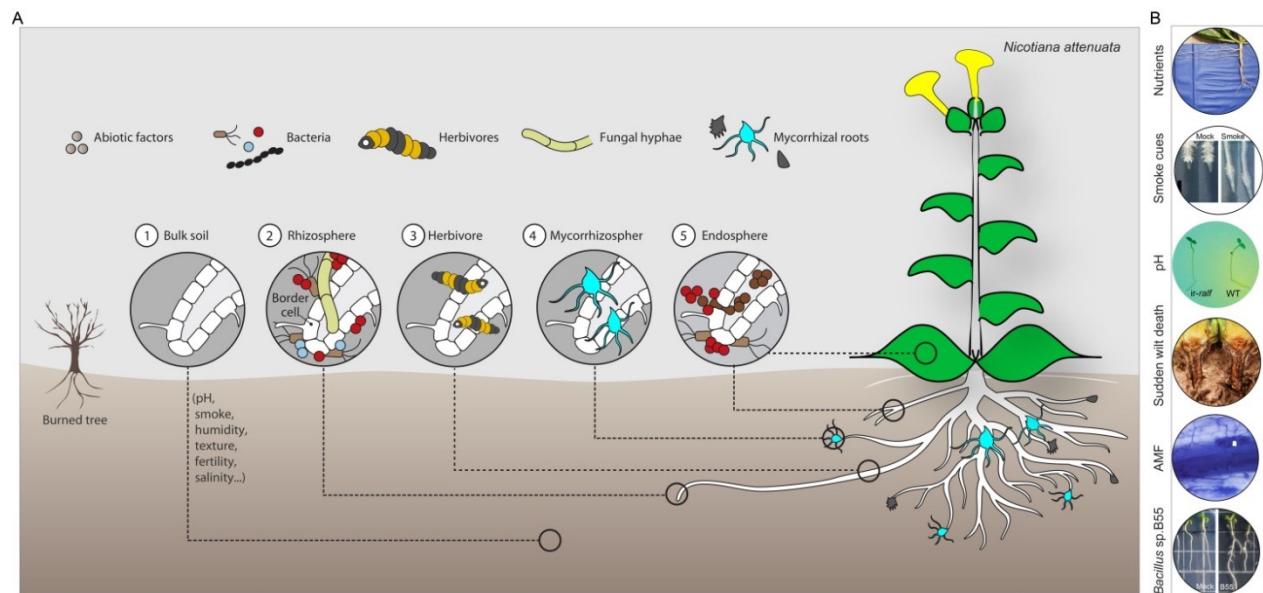


Fig 2. The interaction complex in the soil of Utah desert and known factors for *Nicotiana attenuata*

A. The potential interactions occurring in the soil with *N. attenuata* roots depend on abiotic factors such as pH, smoke cues, and soil fertility. In addition, they depend on biotic factors including microbes and insects in the soil. This figure is adapted from (Martin *et al.*, 2017). B. Representative and observed interactions between *N. attenuata*'s plant roots and different environmental factors in the last 2 decades in its natural habitat at our field station (Great Basin Desert, UT, USA) include, from top to bottom, nutritional variance (Ferrieri *et al.*, 2017), presence of smoke cues from burns (Wang *et al.*, 2017), differences in soil pH (Wu *et al.*, 2007), presence of a wilt-causing pathogen (Santhanam *et al.*, 2015), mycorrhizal interactions (Groten *et al.*, 2015a) and *Bacillus* sp. Infections (Meldau *et al.*, 2012; Meldau *et al.*, 2013).

1.3. Abiotic environmental factors: critical impacts on root plasticity

Nutritional products such as those which result from a fire's combustion of old leaf and plant material have been intensely investigated since they are important to the whole lifespan of plants. Fires increase nitrogen soil content in the form of NO_3^- , as well as phosphorus (P), manganese (Mn), calcium (Ca) and magnesium (Mg), although such fire-elevated nutrients can be easily washed out with, for example, a flood, which in turn confers an ephemeral and highly heterogeneous nutrient distribution in burned areas (Baldwin & Morse, 1994; Baldwin *et al.*, 1994). Root architecture in such environments plastically adapts to these conditions. As reported, excavated *N. attenuata* roots of naturally growing populations in Utah consist of a single primary root and few, well developed lateral roots extending outward into the shallow layers of the soil. In contrast, root systems of glasshouse-grown plants under stable and homogenous growth conditions contain multiple, twisted primary and lateral roots. Bulk soil surrounding foraging lateral roots of *N. attenuata* plants were harvested for nutrient gradient estimation. Indeed, it was found that lateral root placement was associated with a higher concentration of soil micronutrient levels relative to root-free transects, and root foraging behavior was observed in Petri dish bioassays toward micronutrient patches in a concentration-dependent manner. By genetically manipulating *N. attenuata* plants, root chemotropic responses causing them to head to

nutritionally concentrated zones can be compromised. The *N. attenuata* lines which eliminated this specific root directional growth towards nutrients were deficient in jasmonates and ethylene. In sum, under natural growth conditions, nutrients in the soil, which result both directly and indirectly from fires in the area, are distributed unevenly, and phenotypic plasticity in root growth and development enables plants to adapt to such variation and effectively forage for nutrients that are critical to their survival in nature (Baldwin & Morse, 1994; Baldwin *et al.*, 1994; Ferrieri *et al.*, 2017)

Another independent survey was performed in the Mediterranean Basin, where fire is also one of the major sculptors of vegetation diversity, to understand the underlying ecological roles of smoke cues in seedling emergence and establishment. Field plots received applications of liquid smoke, which is commonly used as replacement for fire smoke, and data were recorded mainly on seedling emergence and establishment, including community composition at the family and species level and plant types (annual or perennial). The results were that liquid smoke addition had a significantly positive effect on seedlings recruitment, hence increasing seedling emergence and seedling establishment at community level (Tormo *et al.*, 2014).

Given the positive effect of smoke cues on seed germination and seedling emergence and establishment, the persistence of smoke cues in soil for years is understandable. The question of how smoke cues mechanistically engage in the process of morphological plasticity has been addressed. However, particularly in a burned area, belowground roots emerge and also come into contact with these smoke cues in the rhizosphere. The hypothesis that these roots, while still hidden in the soil, are also immediately and inevitably influenced in growth and development by the omniscient presence of these smoke cues (derived from wildfire) has been proposed and investigated **in manuscript I**.

pH is another notable factor that regulates root growth and development, and it is commonly known that higher pHs diminish plant growth. In our Utah field station, soil pH ranges from 6.5 to over 7.5 (Kratsch & Heflebower, 2013). It has long been reported that pH values in and around roots are not necessarily constant, and changes in pH are frequently observed. However, pH changes over physical ranges under extreme conditions will cause

irreversible damage, for instance, the effect of oxygen deprivation on flooding-intolerant plants is particularly severe when paired with an acidification of the cytoplasm that will further lead to cell death in this condition (Roberts *et al.*, 1984a; Roberts *et al.*, 1984b). Genetic evidence reveals how *N. attenuata* roots adapt to high pH growth conditions common to their natural habitat. *NaRALF* (rapid alkalization factor) is a peptide consisting of 49 amino acids that was named after its activity consisting of fast alkalization of cultivated tobacco cell cultures (Pearce *et al.*, 2001). Plants silenced in *NaRALF* transcripts display wild-type (WT)- like aerial parts, but deficient roots with enhanced root growth showing longer primary roots and flawed trichoblasts that led to a failure in the process of root hair formation. The abnormal root hair phenotype in *irRALF* was ascribed to the disturbance of apoplastic pH oscillations exhibiting a logy rhythm with lower frequency and higher amplitude, and resulted in an abnormally high pH status at the tips of trichoblasts. pH indicators illustrated that WT root progressively acidify the root surrounding area during growth, showing a yellowish color on the petri-dish, but *irRALF* did not make these similar pH changes as there were no petri-media color changes. The inhibition of root hair growth was partially suppressed by a low-pH-buffered growth medium, and such defects in root hair were phenocopied with a high-pH-buffered medium in WT plants. This suggests that the disruption of physical pH adjustment in *irRALF* mainly contributed to the hairless phenotype. On the other hand, as reported, reactive oxygen species (ROS) are critical regulators for root hair formation and growth, and the lack of ROS accumulation at the root hair initiation zone of *irRALF* appeared partially involved in root hair defects as well. Field assays were performed by planting *irRALF* and WT into the basic soils of *N. attenuata*'s native habitat, and *irRALF* plants displayed diminished fitness traits including smaller leaves, shorter stalks, and far less flowers and seed capsules than that of the WT control plants. This was mainly due to *irRALF* plants not being capable of acidifying the rhizosphere to accommodate root growth in basic soil. *NaRALF* is an indispensable regulator to control the transition from root hair initiation to tip growth by tuning the balance of root hair extracellular pH and the status of ROS, and provides plants with an adaptive strategy to better survive and reproduce when growing in basic soil (Wu *et al.*, 2007).

1.4. Biotic environmental factors: friends and foes

When seed germination occurs in a seed bank, the primary root will physically emerge and protrude into soil, and the peripheral root tissues will form a local complex microcosm that provides a broadly selective different habitats for the recruitment of a myriad of microorganisms such as bacteria including actinomycetes, as well as nematodes, microalgae, and fungi. With advances in sequencing and microbial culturing, the relationships of plants with microbial associates have been unraveled rapidly in the last decades. Plants provide associated microbes with food and shelter, while for plants, the best-characterized benefits from associating with a microbiome are generally classified into two groups: 1) growth promotion: plant growth-promoting microbes, which promote growth by several direct or indirect means such as enhancement of nutrient acquisition or through increased drought tolerance; and 2) defense enhancement: microbes which trigger induced systemic resistance (ISR) by activating defensive signaling pathways including jasmonic acid (JA) and ethylene (ET) pathways, conferring hosts with a greater ability to endure disease (Newman, 1978; Leach *et al.*, 2017).

1.4.1. A native growth-promoting bacterial isolate, *Bacillus* sp. B55, can rescue defects in ethylene deficient plants.

For the wild coyote tobacco *Nicotiana attenuata*, the strategic reshaping of its root system results from adaption to different associations with complex communities of microbes. In turn, microbial consortium composition is influenced by the plant, for example via flavonoids and strigolactones in root exudates which may be used to recruit and stimulate mycorrhizae (Bais *et al.*, 2006). From field assays, in four types of native soils that differed mainly in organic and mineral nutrients (carbon and nitrogen) bacterial endophytes were isolated and identified by sequencing from the cleaned roots of wild plants. The results indicated that the root-associated community composition was largely diverse in different type of soil of Utah and such composition in the same type of soil also differentiated with the specificity of root recruitment depending on root type, secretions, or metabolism. For example, plant ethylene emission has been corroborated to be one of the regulators that coordinate the bacterial endophyte composition after comparison of microbial taxonomy by using isogenic transformed plants either deficient in

ethylene (ET) production (*ir-aco1*) or perception (*35S-etr1*). Moreover, plants grown in organic (vs mineral) soils consisted of a more dynamic community composition, and plants flawed in the ethylene pathway exhibited less diversity in their root microbial composition than in that of wild-type plants (Long *et al.*, 2010).

Among cultivable bacteria isolated from native *N. attenuata* roots, the impact of each on morphological traits were assessed, and one strain of *Bacillus* sp. B55 was isolated owing to its obvious promotion effect on plant growth and its potential ability to improve the survival of ethylene (ET) deficient plants in the field. An ET-perception impaired line, *35S-etr1*, is severely defective in root growth and root hair development, displaying longer but hairless roots, and subsequently it has strongly reduced survivorship in field conditions compared to control plants (Meldau *et al.*, 2012). However, inoculation with the isolated *Bacillus* sp. B55 strain caused the mortality of *35S-etr1* to remarkably decrease in two successive field season tests, and other fitness traits of these plants such as plant height and number of flowers were much better than that of the same genotype without the B55 strain. This effect was further studied to better understand how the *Bacillus* sp. B55 strain inoculation promotes *N. attenuata* seedling growth, including an increase in leaf surface area and number of lateral roots, though to a certain extent there was still a decrease in primary root growth. Firstly, auxin content and ethylene emission measurements were performed to exclude the potential roles of these two main root architects in this regulation; they were found to be the same with or without B55 inoculation. Through quantification of the content of phosphate in B55 inoculated and non-inoculated plants, barely any detectable differences were found and this reduced the possibility of nutritional aspects contributing (Meldau *et al.*, 2012; Meldau *et al.*, 2013), at least in the case of Pi deficiency. The following assay tested whether volatile organic compound (VOC) blends were the players involved in the morphological changes. A bipartite petri-dish culturing system was established to separate B55 and seedlings physically, while still allowing “dialogue” through the air. Indeed, the plant growth promoting effect was still clearly observed, and VOCs were focused on as the regulator engaged in this morphological manipulation. An elegant experiment was then designed to distinguish which compound in the VOC blend was active. B55 culturing resulted in a high abundance of the S-containing compound dimethyl disulfide (DMDS) by GC-MS detection after

a solid phase microextraction. Interestingly, the total amount of DMDS in the bipartite system negatively and significantly correlated with the number of inoculated seedlings (more plants inoculated, less DMDS, and vice versa), which provided evidence that plants may be able to absorb this compound. It is known that 35S-*etr1* constitutively produces a far larger amount of ethylene at base level, ascribed to a negative feedback loop from not perceiving ethylene, and this comes at the cost of excessive consumption of substrates involved in ethylene biosynthesis including sulfur metabolites such as Methionine (Met). Though 35S-*etr1* plants absorbed more sulfur (S) as observed through an isotope 35S labeling assay, continuous catabolism of S still kept plants in a the S-starvation status and exhibited a higher transcript levels of genes related to S metabolism. External sulfate or DMDS addition partially rescued morphological defects in 35S-*etr1* plants, indicating the abnormal S metabolism in this genetically modified line. This indicated sulfur supplementation as a mechanism for the effect of DMDS emitted by native isolate *Bacillus* sp. B55 in suppressing the defects in ethylene-deficient plants. Field assays then helped to better understand the ecological roles of native associates of *Bacillus* sp.B55 for *N. attenuata* plants grown in natural conditions, particularly in environments with a shortage of S (Meldau *et al.*, 2013).

1.4.2. Native bacterial consortiums enhance pathogenic resistance against sudden wilt disease

Regarding the enhancement of disease resistance in plants, the machinery engaged in this resistance has been extensively characterized in wheat associated with a disease of its root caused by *Gaeumannomyces graminis* var *Tritici* infections, referred to as “take-all” disease. This investigation started with wheat cropping, successive cropping in the same field for many years with a few disease outbreaks, when suddenly such outbreaks waned. Apparently, with environmental stress selection, wheat evolved an adaptive strategy against disease invasion through renewal of its own defensive system to antagonize *Pseudomonas* spp (Weller *et al.*, 2002). Our group has used *N. attenuata* as a model species to perform field assays in its natural habitat in order to study interactions with natural environmental factors for over 20 years. Since 1991, the field has had symptoms of a sudden wilt disease which was sporadically observed. Plants were observed to weather and die quickly if infected in the elongation stage, and

additionally the natural white roots of the plants became black. It is standard to diagnose such sudden wilt disease showing wilting and black roots symptoms together. Mortality characterized from this disease increased progressively since 1991 until it reached levels over 50% in 2012, and nearly wiped out all efforts in the 2012 field season (Santhanam *et al.*, 2015).

The occurrence of the sudden wilt disease is referred to as a common agricultural disease caused by many years of continuous cropping and the reemployment of the same plotting area for years, bringing on a quantitative accumulation of plant pathogens. To further understand the potential causal agents resulting in sudden wilt disease, roots of plants infected by this disease were analyzed for bacteria or fungus. From more than 100 cultivable isolates consisting of around 70 bacterial and 36 fungal isolates, the high abundance of *Fusarium spp.* and *Alternaria spp.* were eventually demonstrated to cause symptoms of this sudden wilt disease. To evade the damages resulting from sudden wilt disease, crop rotation is a general farming strategy, but it is not an easily applicable solution for our field station because of our research focus. Therefore a biocontrol strategy is an alternative, means of controlling antagonistic pathogen partners. Six native bacterial isolates from the healthy roots of *N. attenuata* plants in the same field location were tested as an inoculation mixture. Interestingly, in a 2013 field season test, plants planted with bacterial mixtures together exhibited a consistent decline of mortality with a statistically significant decrease compared with the non-inoculated plants without additional costs from other morphological traits such as plant biomass and reproductive output. Because of the disease resistance effect from the inoculation of bacterial mixture, the subgroups were tested in the 2014 field season and they confirmed that the core consortium of bacteria is collectively needed to provide protection, rather than just a single dominant strain. These results indicate the complex interactions among pathogens, protective bacterial communities, and plants, and also provide an investigational platform to disentangle how *Nicotiana attenuata* plants cope with biotic stresses (Santhanam *et al.*, 2015).

1.4.3. Arbuscular mycorrhizal fungi, a mutualistic partner with *N. attenuata* in the field

One of the most widespread symbionts, ectomycorrhizae, can establish association with about 2% plants around the world of which most of these plants are trees. However, more than 80% of all terrestrial plant species, including crop plants, can establish symbiotic associations with arbuscular mycorrhizal fungi (AMF) (Brundrett & Tedersoo, 2018). In the AMF symbiotic process, plant root exudates such as flavonoids and strigolactones stimulate fungal spore germination and hyphal branching, and extraradical hyphae then penetrate the rhizodermis by initially anchoring hyphopodia on the root surface, then they transcellularly infect the roots of the plant. Eventually, a main trunk with highly branched intracellular structures named arbuscules is formed in the inner cortex to establish a mutualistic partnership with the host plants (Parniske, 2008). Arbuscules are formed as transient structures due to the branched structures shortly entering the stage of degradation, and are generally considered as the main location of nutrient exchange (Harrison, 2005). They are regarded as the “heart” structure of AMF. The fungus facilitates the more efficient uptake of nutrients, in particular phosphorous (Pi) and nitrogen for the plant, and in turn, the plant supplies the fungus with a carbon source (Helber *et al.*, 2011; Bravo, Armando *et al.*, 2017; Jiang *et al.*, 2017; Keymer *et al.*, 2017; Luginbuehl *et al.*, 2017; Rich *et al.*, 2017).

The interaction between host plants and AMF initiates with a binary negotiation prior to physical contact. Plant-derived secretions activates the life cycle of AMF by promoting spore germination. AMF release factors, referred to as mycorrhizal factors, which have been widely accepted and confirmed to lipochitooligosaccharides (Myc-LCOs)(Maillet *et al.*, 2011), and short-chain chitin oligomers (CO) (Genre *et al.*, 2013) which are elicitors of a signaling cascade in the plant. During the complicated signal transmission process, a large set of regulatory core genes have been predicted and corroborated. Among them, some are implicated in both rhizobial symbioses and mycorrhizal symbioses, and encode for proteins which participate in the so called Common Symbiosis Signaling Pathway (CSSP) (Oldroyd, 2013). To trigger this pathway, released Myc-factors are recognized by putative plasma membrane-localized receptors, though these are still not fully deciphered, and it is speculated that specific LysM domain-containing receptor-like kinases (LysM-RLKs) play a critical role in this process. Interestingly, in rhizobial/mycorrhizal model plant species such as *Medicago truncatula*, *Lotus japonicum* and *Oryza*

sativa, MtLYK3/LjNFR1/OsCERK1 were required for a full AMF colonization and potentially encode proteins necessary for Myc-factor (Myc-LCOs or COs) perception. The sequential calcium spiking in root cells (mainly epidermal), is mediated by a plasma membrane LRR (leucine-rich-repeat) receptor kinase (MtDMI2/LjSYMRK) (Endre et al., 2002; Stracke et al., 2002) and a potassium channel located at the nuclear envelope (MtDMI1, LjCASTOR and LjPOLLUX) (Ané et al., 2004; Imaizumi- Anraku et al., 2005; Peiter et al., 2007; Riely et al., 2007). These calcium oscillations are successfully transduced into nuclei and perceived by a calcium-calmodulin-dependent kinase (LjCCaMK/MtDMI3) which can directly interact with the transcription factor MtIPD3/LjCYCLOPS to relay downstream signaling and finally activate target genes related to the symbiosis with AMF (Oldroyd, 2013).

The interactions occurring between AMF and host plants are overall beneficial for plant growth (Rooney *et al.*, 2009; Adolfsson *et al.*, 2015) and improve the resistance of plants to various abiotic and biotic stresses (Pineda *et al.*, 2010; Vannette *et al.*, 2013; Chitarra *et al.*, 2016; Sharma *et al.*, 2017). Besides the aforementioned adverse biotic stress in the natural habitat of *N. attenuata*, within its dynamic microbe compositions, mutualistic associates with arbuscular mycorrhizal fungi (AMF) are also observed. The isolates from roots excavated from the field site contain AMF species of *Rhizophagus irregularis* and *Funelliformis mosseae*, identified by sequencing. The heart structure of the symbiosis, the arbuscule, was clearly observed in field samples of *N. attenuata* roots, showing that *N.attenuata* is one of the host species with AMF symbionts in natural growth conditions. These findings allow us to investigate such mutualistic interactions between *N. attenuata* and AMF.

To test the ecological consequences from impaired symbiotic relationship establishment in the field, the *NaCCaMK* gene (Calcium- and calmodulin-dependent protein kinase) was silenced by RNAi to cause an incomplete establishment of a mutualistic relationship with AMF. Through tests in the glasshouse and field, three independent lines were screened and showed no infection with *R. irregularis* or native fungal inoculum. Comparisons between these three lines with empty vector (EV) plants revealed similar growth and fitness traits in the glasshouse and in field growth conditions between irCCaMK and EV. Also, the basal levels of jasmonates (JA),

salicylic acid (SA) and abscisic acid (ABA) was nearly the same in the transgenic lines as in controls, and the inducibility of these phytohormones after herbivore attack did not differ, indicating that activation of these canonical defense pathways is not dependent on the CCaMK protein. Despite these similarities, there were still some differences in other traits, such as bacterial community recruitment differences by alpha-diversity parameters of bacterial OTUs, though overall fungal community recruitment did not differ significantly between EV and irCCaMK plants under field conditions (Groten *et al.*, 2015a).

In addition to ecological and genetic advances, progress in metabolic research regarding AMF interactions took a big step forward with, for example, the discovery of Myc-LCO and CO elicitors that trigger AMF-inoculation related signal transduction. There still remain major questions however, as it is well known that AMF interactions influence whole-plant performance (i.e., plant growth is commonly impacted by AMF colonization (Rooney *et al.*, 2009)) and thus systemic metabolic responses are to be expected, and yet, no common AMF-specific responses have been found in systemic tissues. Although AMF colonization morphologically takes places only in the roots, the search continues for potential responses in other tissues, and related questions continue to be interesting (Schweiger *et al.*, 2014a; Schweiger *et al.*, 2014b; Aliferis *et al.*, 2015; Gerlach *et al.*, 2015; Schweiger & Muller, 2015; Desalegn *et al.*, 2016).

Studies in this direction have been approached for years. Several studies revealed changes in leaf primary metabolites, consisting of carbohydrates, proteins, and amino acids, after AMF inoculation. Moreover, hypotheses that AMF-mediated symbiosis increases the content of secondary metabolites was demonstrated with the findings of higher concentrations of gallic acid, anthraquinone derivatives, phenolic acids, iridoid glycosides and various alkaloids in AMF-inoculated leaves. These studies mainly implement targeted approaches to quantify particular chemical compounds, but the lack of consistent evidence of these changes in even detecting such limited numbers of compounds among different plant species largely motivates researchers to search for a common metabolic response in systemic tissues, and related ecological functions are expected.

Another motivation behind this work is to identify AMF-indicative chemical markers in shoots which are indicators of root colonization. Technically, quantification of root colonization has been achieved in several ways. Complete or partial destructive root harvesting is always the first step; the sequential steps of staining and microscopic examination follow to document the structures of hyphae, arbuscules and vesicles within the stained roots. From Phillips and Hayman's proposed staining method in 1970 through the heating of roots in KOH and staining of fungal cell walls with trypan blue, to McGonigle's standardized quantification method in 1990, along with the development of fluorescence dyes for staining and advanced optical microscopy for observing, efficiency and accuracy of quantification has largely improved. However, characterization of AMF-associations is still laborious and time-consuming. The chase for a shoot AMF-indicative marker is on (Phillips & Hayman, 1970).

However, challenges remain to target AMF-specific compounds within systemic tissues. AMF generally has a plant growth-promoting effect, and discrepancies in plant developmental stages thus often occur under AMF presence versus absence. Besides, differences in abundance of metabolites among below- and above-ground tissues and inconsistency of inducibility of AMF-mediated compounds across plant species (or across plants subject to different species of AMF inoculum) exacerbates the difficulties of disentangling ubiquitous metabolic changes. Notably, such putative compounds generally produce structural modifications among plant species, which makes finding a pattern much harder. To more precisely target these metabolic changes, a few recent studies started to implement comprehensive metabolic approaches to investigate the effects of AMF on a wide range of metabolites (the metabolome) in both targeted and untargeted ways.

These tools provided much broader insights in quantitative AMF-mediated changes. Many more metabolite classes were successfully discovered, and systemic responses of leaf compounds were found in various plant species. Schweiger and co-workers performed a comparative study on AMF effects on the polar leaf metabolomes of five plant species inoculated with one AMF species (*Rhizophagus irregularis*), and plenty of AMF-mediated changes were detected in the leaves of the five plant species such as succinate and ribonate (Schweiger *et al.*,

2014a; Schweiger *et al.*, 2014b). However, only very few metabolites in leaves were commonly modulated with similar trends by AMF inoculation in most species, though all plant species shared at least 850 metabolic features. Interestingly, there was a significant decline in concentrations of several organic acids of the citrate cycle in most species, which may be the universal pattern as AMF-indicative makers reflecting AMF colonization in roots. However, a lack of statistical correlation between the amount of such metabolites in leaves and root colonization in these studies is not enough to clearly claim the robustness as AMF-indicative markers.

1.5. Scope of this thesis

The overall scope of this thesis is to combine multiple toolboxes including those for transcriptomics, metabolomics, and plant transformation, in order to perform environmental factor-plant interaction studies. *Nicotiana attenuata*, an annual wild tobacco species native to the Great Basin Desert of United States, was developed as a model plant to investigate plant growth and development, species evolution, and various types of plant interactions with abiotic or biotic factors. Fire is a natural, ancient force which has sculpted the Earth's landscape of vegetation for millions of years. Some fire-acquired traits have been evolutionarily seared into a plant's genome, leading to the development of a set of fire responses such as the promotion of its seeds to germinate by smoke cues. Another ancient player that has served to evolutionary sculpt *N. attenuata* is arbuscular mycorrhizae, which largely ecologically benefits plants by increasing their phosphate acquisition and stress tolerance. Roots are the primary locus in nearly all below-ground interactions of plants, but the roots do maintain a continuous conductivity link to aerial tissues and so these interactions without a doubt effect plant performance as a whole. In order to better understand root-environmental factor interactions, we explore concise and specific questions addressing *N.attenuata*'s root performance under smoke or mycorrhizae saturated growth conditions, and provide answers for these questions in the manuscripts of this thesis.

Manuscript I: What are root responses to smoke cues? What are the active compounds in smoke cues that reshape root morphology? Are these smoke-cued root responses triggered by the

same components in smoke that enhance seed germination? What is the potential mechanism behind smoke causing root morphological changes?

Manuscript II: Within a mesocosm saturated with AMF, similar to a natural, communal, competition growth environment, what is the growth response between an AMF symbiotic-plant and an AMF non-symbiotic plant? What does the role AMF play? Is there a common molecular response in the leaf that may help to indicate AMF root colonization and what is it?

Manuscript III: Is there a common chemical response in the root that indicates AMF root colonization and what is it? Are these root indicative markers positively associated with root colonization? Can these root indicative markers be found in leaves? Are the amounts of root markers in leaves positively reflective of root colonization? Could these foliar markers distinguish a plant impaired in its symbiosis with AMF? To what extent can we distinguish plants impaired in AMF symbiosis sampled from field trials using these markers? Can these AMF-indicative markers be broadly applied for forward genetic screening? Are these foliar AMF-indicative markers transported from roots or are they locally biosynthesized? Are these AMF-indicative markers universal across species?

2. Manuscript Overview & Author Contributions

Manuscript I:

Catechol, a major component of smoke, influences primary root growth and root hair elongation through ROS-mediated redox signaling

Ming Wang, Matthias Schoettner, Shuqing Xu, Christian Paetz, Julia Wilde, Ian T. Baldwin, Karin Groten

Published in *New Phytologist* (2016)

doi:10.1111/nph.14317

In **manuscript I**, the morphological root appearance of *N.attenuata* seedlings was altered by external addition of liquid smoke, resulting in longer and hairless roots. Bioassay-driven fractionation enabled the identification of an active compound, catechol, from liquid smoke. Root transcriptome changes by a kinetic treatment of the active fraction isolated from liquid smoke shed light on potential regulatory mechanisms through the ROS signaling pathway, rather than through the conventional auxin pathway. Chemical complementation assays corroborated that imbalance of polar ROS distribution in the roots leads to an increase of cell length resulting from cell wall loosening, and hence eventually confers longer roots.

MW, ITB and KG planned and designed the research and wrote the manuscript; MW performed the research and data analysis, MS guided the fractionation of catechol and its analysis by HPLC; MS and SX annotated the RNAseq data and helped with RNAseq data analysis; JW contributed to data collection.

Manuscript II:

***Nicotiana attenuata*'s capacity to interact with arbuscular mycorrhiza alters its competitive ability and elicits major changes in the leaf transcriptome**

Ming Wang, Julia Wilde, Ian T. Baldwin and Karin Groten

Published in *Journal of Integrative Plant Biology* (2017)

doi: 10.1111/jipb.12609

In manuscript II, under glasshouse conditions, when EV and irCCaMK are co-cultured in the same pot with a limited phosphate nutrition supply, the growth of irCCaMK plants is highly inhibited in the presence of AMF inoculum, in comparison to in the absence of this inoculum. To further understand the potential transcriptome changes in leaves between EV and irCCaMK plants, a microarray for transcriptome profiling was performed. Expected AMF-indicative shoot molecular markers were not found, but *NaPT5* (phosphate transporter) in the root was unexpectedly targeted. *NaPT5* is one of the AMF-indicative marker genes in root, and is differentially detected in leaves between EV and irCCaMK: it is up-regulated in irCCaMK plants while simultaneously down-regulated in EV plants within the same treatment with AMF inoculum. Within phosphate- plants without AMF inoculation, *NaPT5* lost its high inducibility in roots, but increased transcript abundance in leaves was still observed, suggesting the potential functional differentiation of *NaPT5* within specific tissues.

MW, JW, KG and ITB designed the study. MW, JW and KG setup the experiments, recorded plant growth and harvested the material. MW, JW and KG drafted the manuscript. ITB and KG revised the manuscript.

Manuscript III:
**Blumenols as effective shoot markers for root symbiosis with arbuscular
mycorrhizal fungi**

Ming Wang, Martin Schäfer, Dapeng Li, Rayko Halitschke, Chuanfu Dong, Erica McGale, Christian Paetz, Yuanyuan Song, Suhua Li, Junfu Dong, Sven Heiling, Karin Groten, Philipp Franken, Michael Bitterlich, Maria Harrison, Uta Paszkowski and Ian T. Baldwin

Submitted to *eLife* (2018)

In manuscript III, the hypothesis was addressed that a subset of the AMF-induced root metabolites could accumulate in shoots as a result of transport or systemic signaling. A comparative metabolomics study was performed and potential AMF-indicative markers were documented in roots. Among them, blumenols were particularly focused on due to their high inducibility with AMF inoculation, and their abundance. By means of a targeted approach, a subgroup of blumenols including hydroxy- and carboxyblumenol-C-glucosides was detected in shoots as well, which were shown to also reflect root colonization by AMF, via validation by statistical correlation. A subsequent QTL analysis corroborated the potential application of this chemical marker by allowing leaf sampling on a RIL population resulting in clear loci from this marker, and the blumenol derivatives found from different plant species broadened the scope of this marker as being part of a general AMF-responsive compound class.

Conceptualization, MW, MS, DL, RH, KG and ITB; Methodology, MW, MS, DL and RH; Software, DL, RH and EM; Validation, MW, MS, DL, RH and SH; Formal Analysis, MW, MS, DL, RH, EM and CP; Investigation, MW, MS, DL, RH, CD, EM, CP, YS, SL, JD, SH and MB; Resources, CP, PF, MB, MH, UP and ITB; Data Curation, MW, MS, DL, RH, EM and CP; Writing – Original Draft, MW, MS, RH and ITB; Writing – Review & Editing, MW, MS, DL, RH, CD, EM, CP, YS, SL, JD, SH, KG, PF, MB, MH, UP and ITB; Visualization, MW, MS, DL, RH, EM and ITB; Supervision, RH, CP, KG, PF, MH, UP and ITB; Project Administration, RH and ITB; Funding Acquisition, ITB

3. Manuscripts

Manuscript I

Manuscript I:

**Catechol, a major component of smoke, influences primary root growth and root hair
elongation through ROS-mediated redox signaling**

Ming Wang, Matthias Schoettner, Shuqing Xu, Christian Paetz, Julia Wilde, Ian T. Baldwin, Karin Groten

Published in *New Phytologist* (2016)

doi:10.1111/nph.14317

Catechol, a major component of smoke, influences primary root growth and root hair elongation through reactive oxygen species-mediated redox signaling

Ming Wang¹, Matthias Schoettner¹, Shuqing Xu¹, Christian Paetz², Julia Wilde¹, Ian T. Baldwin¹ and Karin Groten¹

¹Department of Molecular Ecology, Max Planck Institute for Chemical Ecology, Hans-Knoell-Str. 8, 07745 Jena, Germany; ²NMR Group, Max Planck Institute for Chemical Ecology,

Hans-Knoell-Str. 8, 07745 Jena, Germany

Summary

Author for correspondence:

Karin Groten

Tel: +49 3641 571000

Email: kgroten@ice.mpg.de

Received: 3 May 2016

Accepted: 29 September 2016

New Phytologist (2017) 213: 1755–1770

doi: 10.1111/nph.14317

Key words: antioxidant, auxin, catechol, *Nicotiana attenuata*, post-fire annual, reactive oxygen species (ROS), smoke.

- *Nicotiana attenuata* germinates from long-lived seedbanks in native soils after fires. Although smoke signals have been known to break seed dormancy, whether they also affect seedling establishment and root development remains unclear.
- In order to test this, seedlings were treated with smoke solutions. Seedlings responded in a dose-dependent manner with significantly increased primary root lengths, due mainly to longitudinal cell elongation, increased numbers of lateral roots and impaired root hair development. Bioassay-driven fractionations and NMR were used to identify catechol as the main active compound for the smoke-induced root phenotype.
- The transcriptome analysis revealed that mainly genes related to auxin biosynthesis and redox homeostasis were altered after catechol treatment. However, histochemical analyses of reactive oxygen species (ROS) and the inability of auxin applications to rescue the phenotype clearly indicated that highly localized changes in the root's redox-status, rather than in levels of auxin, are the primary effector. Moreover, H₂O₂ application rescued the phenotype in a dose-dependent manner.
- Chemical cues in smoke not only initiate seed germination, but also influence seedling root growth; understanding how these cues work provides new insights into the molecular mechanisms by which plants adapt to post-fire environments.

Introduction

Fire is a predictably irregular natural event in many regions of the world; fire frees up space, nutrients and light, allowing seedlings to become established (Rundel, 1981; Baldwin *et al.*, 1994; Nelson *et al.*, 2009). Regrowth, reproduction and germination are synchronized in the immediate post-fire environment. Some plant species are classified as fire ephemerals, which germinate synchronously only after fires that start in long-lived seedbanks in the soil (Keeley & Pizzorno, 1986; Baldwin & Morse, 1994; Preston & Baldwin, 1999). One of the key compounds of smoke that promotes seed germination and is required for synchronizing mass germination after fire has been identified as 3-methyl-2H-furo[2,3-c]-pyran-2-one, also known as karrikin1 (KAR1) (Flematti *et al.*, 2004a,b); by contrast, catechol, a major constituent in smoke, does not induce germination (Baldwin *et al.*, 1994). Catechol is known to interact with both organic compounds (e.g. amino acids) and inorganic compounds (e.g. metal ions) (Yang *et al.*, 2014), and has a complex redox chemistry in the presence of metal ions (Schweigert *et al.*, 2001).

Treatments with smoke water and smoke extracts not only induce germination, but also enhance root growth in rice (Kulkarni *et al.*, 2006), tomato (Taylor & Van Staden, 1998), jatropha (Abdelgadir *et al.*, 2012), rapeseed (Abdollahi, 2012), papaya (Chumpookam *et al.*, 2012) and maize (Soós *et al.*, 2009). However, for most of this work, it is not clear which compound(s) in smoke is(are) responsible for the improved growth and how the signals that result in growth promotion are transduced into cellular processes.

Primary root growth requires two main physiological processes: the proliferation of daughter cells in the apical meristem and the enlargement of differentiated cells that are no longer in the meristem. When cells stop expanding, they are considered morphologically to belong to the mature zone, which is characterized by root hair development and vascular tissue formation (Petricka *et al.*, 2012). All of these developmental processes are regulated by different plant hormones, among which auxins are the best studied (Sabatini *et al.*, 1999; Galinha *et al.*, 2007; Dinnyes & Benfey, 2008). That the control of auxin biosynthesis and signaling is important for root growth and development has been shown by external applications of auxins, which result in increased cell

division but decreased root growth in *Arabidopsis* (Rahman *et al.*, 2007; Zhou *et al.*, 2011), whereas the addition of auxin biosynthesis inhibitors, L-kynurenine (Kyn) (He *et al.*, 2011) and yucasin (Nishimura *et al.*, 2014) leads to increased primary root growth. Auxin gradients are also regulated by transport systems (Tromas & Perrot-Rechenmann, 2010; Zhou *et al.*, 2011; Adamowski & Friml, 2015; Draelants *et al.*, 2015; Rodríguez-Sanz *et al.*, 2015). Furthermore, among other factors, auxin-regulated gene expression is controlled by the *SHY2* (short hypocotyl) gene encoding IAA3, a member of the Aux/IAA family (Tian *et al.*, 2002).

In addition to auxin, reactive oxygen species (ROS) are important signaling molecules that play a role not only in plants' responses to biotic and abiotic stress, but also in plant growth and development (Gapper & Dolan, 2006; Petrov & Van Breusegem, 2012; Foyer & Noctor, 2013). *In planta*, O_2^- is produced by NADPH oxidases (RBOH) and can be further converted into H_2O_2 by superoxide dismutases (SODs) and other enzymes, including apoplastic oxalate oxidase, diamine oxidase and class III peroxidases. H_2O_2 can be catabolized enzymatically to H_2O by catalase (CAT), glutathione peroxidase (GPX) and ascorbate peroxidase (APX) or it can be consumed nonenzymatically by Fenton reactions when Fe^{2+} is available; such a reaction depends greatly on pH and other indicators of subcellular reactivity. As demonstrated by mutants, the main ROS appear to have different zones of accumulation within roots, and their generation and balance is controlled by the bHLH transcription factor UPBEAT; superoxide accumulates in the meristematic zone, whereas H_2O_2 accumulates in the elongation/differentiation zone (Tsukagoshi *et al.*, 2010). Furthermore, the presence and localization of ROS in the growing root hair, in particular the root tip, is decisive for the growth of the hair, and *Arabidopsis* RBOHC mutants impaired in H_2O_2 production are defective in root hair elongation (Foreman *et al.*, 2003).

The cell wall plays an important role in cell expansion, and the primary cell walls are composed primarily of microfibrils, hemicelluloses, pectins and structural proteins such as hydroxyproline-rich O-glycoprotein extensins (EXT) (Velasquez *et al.*, 2011; Nguema-Ona *et al.*, 2014; Xiong *et al.*, 2015). ROS can contribute to the tightening and the loosening of cell walls. Cell-wall tightening is assumed to be due to the cross-linking of cell-wall components. This process is concentration-dependent: moderate levels of H_2O_2 and proper cross-linking are essential for root growth, whereas excessive levels of H_2O_2 dramatically inhibit cell expansion and may be directly toxic, oxidizing DNA, proteins and metabolites (Tenhaken, 2014; Kärkönen & Kuchitsu, 2015). Cell-wall loosening and underlying root elongation were suggested to be at least partly due to the production of the hydroxyl radical; this radical can be produced from H_2O_2 in the presence of metal ions through the Fenton reaction (Liszky *et al.*, 2004) and leads to the cleavage of cell-wall polysaccharides (Fry *et al.*, 2001; Carol & Dolan, 2006; Kim *et al.*, 2014).

At the molecular level, members of the receptor-like kinase CrRLK1 family have been shown to control cell wall properties and cell expansion (Anders *et al.*, 2014), and in *Arabidopsis*, MED25/PFT1 has been reported as a mediator that controls root hair differentiation and primary root elongation by regulating the

expression of several genes encoding redox-active proteins; the expression of these genes critically alters the balance of H_2O_2 and O_2^- (Sundaravelpandian *et al.*, 2013; Raya-González *et al.*, 2014).

Nicotiana attenuata, or wild tobacco, is a summer annual native to the Great Basin desert of California, Nevada, Idaho and Utah, USA; it primarily occurs ephemerally for up to three growing seasons after wildfires and persistently in certain areas that do not accumulate leaf litter (Goodspeed, 1955; Preston & Baldwin, 1999). As a fire-chasing species, *N. attenuata* seed germination after fires has been studied extensively (Baldwin & Morse, 1994; Baldwin *et al.*, 1994), and a wealth of ecological and molecular knowledge is available for this species. However, surprisingly, little is known about the additional effects of smoke on the establishment of seedlings and their root growth in the post-fire habitat.

Here we tested the hypothesis that smoke has additional effects on the growth of *N. attenuata* seedlings with a root morphology-guided approach. We identified catechol as the main active compound in smoke which shapes root architecture in a dose-dependent manner. Histological, transcriptome and analytical results provide evidence that ROS, and not auxin, are the primary regulators of the catechol-induced root phenotype; the phenotype results from alterations in ROS homeostasis in the root cortex of the elongation zone, in root hairs and within the roots.

Materials and Methods

Plant material and growth

In all experiments, wild-type *Nicotiana attenuata* Torr. Ex Watts seeds of the 31st generation inbred line were used. Seed germination and plant growth were performed as described (Kruegel *et al.*, 2002). In brief, seeds were sterilized and germinated on agar with Gamborg B5 (Duchefa, The Netherlands, <http://www.duchefa.com>) after soaking for 1 h in a 1 : 50 (v/v) diluted liquid smoke (House of Herbs, Passaic, NY, USA) supplemented with 1 mM of gibberellic acid (GA_3). Seedlings were grown vertically in Percival chambers (Perry, IA, USA) at 28°C, under long-day conditions (16 h : 8 h, light : dark). Seedlings were either directly germinated on the supplemented media (long-term treatment) or transferred 5 d post-germination (dpg) to the supplemented media (short-term treatment). For the long-term treatment (13 dpg, data for Fig. 1), liquid smoke was added to the GB5 medium before autoclaving. For all other short-term treatments, the chemicals were added to cooled GB5 media (*c.* 45–50°C), using the concentrations indicated in the text and figures, and seedlings were phenotyped hours or days after treatment.

Chemicals and stock solutions

Stock solution were prepared and filtered with 22-nm sterilized filters: Indole-3-acetic acid (IAA, CAS-no. 87-51-4, Duchefa, <https://www.duchefa-biochemie.com/>), dissolved in ethanol), 1-naphthaleneacetic acid (NAA, CAS-no. 86-87-3, dissolved in 1 M NaOH), N-1-naphthylphthalamic acid (NPA, CAS-no. 132-66-1, Santa Cruz Biotechnology, dissolved in DMSO), L-kynurenine (Kyn, CAS-no. 2922-83-0,

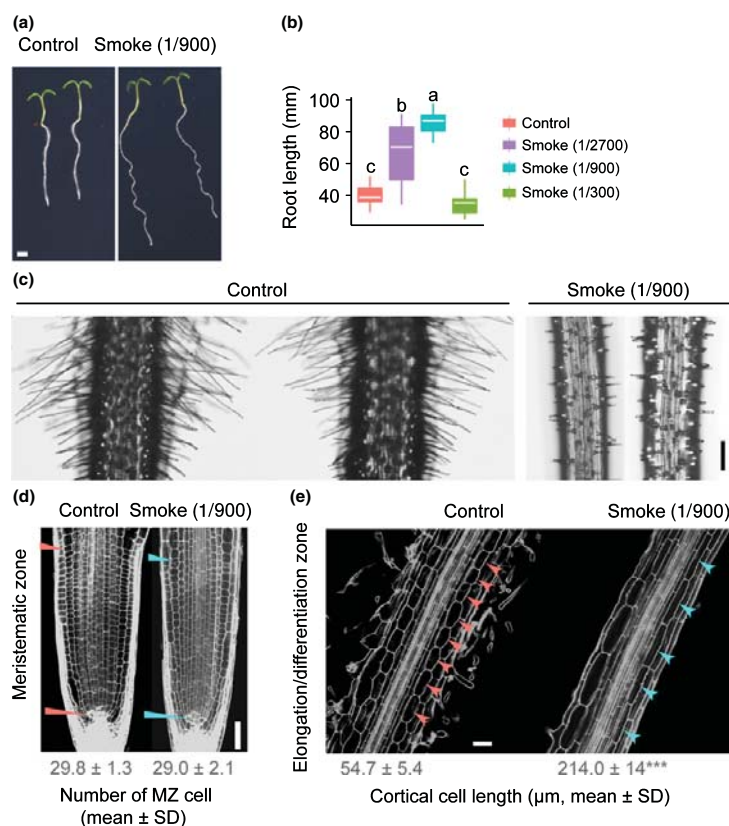


Fig. 1 Treatment of *Nicotiana attenuata* seedlings with liquid smoke increases primary root growth and decreases root hair elongation. Root phenotype is induced by smoke treatment. *Nicotiana attenuata* seedlings were germinated on GB5 medium containing liquid smoke (v/v = 1/900) and compared to mock-treated roots. Measurements were taken 13 d post-germination (dpg). (a) A scan of seedlings revealed the increase in primary root length after smoke treatment. Bar, 0.2 mm. (b) The effect of smoke treatment is concentration-dependent ($n = 6$, for each biological replicate 25–30 seedlings per Petri dish were measured); different letters indicate significant differences ($P \leq 0.05$, one-way ANOVA followed by Tukey's HSD), box plots show the medium (white horizontal line), the upper and lower quartile (upper and lower end of the box) and the minimum and maximum (whiskers). (c) Root hair phenotype was observed by Zeiss ApoTome imaging under bright-field. Bar, 10 μm . (d, e) Confocal microscope imaging after propidium iodide (PI) staining to visualize the cell walls. (d) The number of meristem cells did not change after smoke treatment. The distances of meristem zone (MZ; left half only) for measuring are marked by arrow-heads. (e) After smoke treatment, cells in the elongation zone were significantly longer than cells in the elongation zone of controls. Only cells in the cortex layer were measured (see also Supporting Information Fig. S2). A representative picture of the elongation/differentiation zones (EZ/DZ) is shown. The arrowheads point to the elongated cells. Data are means \pm SD (20–25 seedlings were measured), significant differences are indicated by asterisks (Student's t -test: ***, $P \leq 0.001$) (see also Fig. S1).

Sigma-Aldrich, dissolved in DMSO), 5-(4-chlorophenyl)-4H-1,2,4-triazole-3-thiol (yucasin, CAS-no. 26028-65-9, Sigma-Aldrich, dissolved in DMSO), diphenyleioidonium chloride (DPI, CAS-no. 4673-26-1, Sigma-Aldrich, dissolved in DMSO), BES-H₂O₂-AC (WAKO, www.wako-chem.co.jp/english/labchem/, dissolved in DMSO), 1,2-dihydroxybenzene (catechol, CAS-no. 120-80-9, Sigma-Aldrich, dissolved in 80% methanol), 1,3-dihydroxybenzene (resorcinol, CAS-no. 108-46-3, Sigma-Aldrich, dissolved in 80% methanol), 1,4-dihydroxybenzene (hydroquinone, CAS-no. 123-31-9, Sigma-Aldrich, dissolved in 80% methanol), 2-methoxyphenol (guaiacol, CAS-no. 90-05-1, Sigma-Aldrich, dissolved in 80%

methanol) and nitro blue tetrazolium (NBT, CAS-no. 298-83-9, Sigma-Aldrich, in 20 mM phosphate buffer pH 6.1).

Phenotyping experiments

In order to determine the length of primary roots, pictures of seedlings were scanned using a desktop scanner at 600 dpi. These scanned pictures were further measured using IMAGEJ (NIH). For root hair phenotyping, macro-images were taken under a stereomicroscope (MZ16, Leica, Wetzlar, Germany) and micro-images were taken by ApoTome (Zeiss, Oberkochen, Germany) microscope.

Extraction, fractionation and purification of liquid smoke and burnt soil

Solid phase extraction (Multi 96 HR-XC (96 × 25 mg) column (Macherey Nagel, Düren, Germany) was used as first step of liquid smoke fractionation to isolate the active compound. In brief, 0.8 ml undiluted liquid smoke (House of Herbs, Passaic, NY, USA) was loaded onto an activated column and flow-through was collected as S0, then successively eluted with 1 ml each of 1 M HCOOH, 80% methanol in HCOOH, 100% methanol, 0.35 M NH₄OH, 0.35 M NH₄OH in 60% methanol and 2 M NH₄OH in acetone. At each step the eluted flow-through was collected and desiccated as S0–S6 fractions, dissolved eventually in methanol and the obtained fractions used for further bio-assay and high power liquid chromatography (HPLC) fractionation. A detailed description of HPLC fractionation, mass acquisition by UPLC/electrospray ionization-time of flight (ESI-TOF) and catechol quantification is provided in the Supporting Information Methods S1.

Soil was collected from a burn in 2016 from the native habitat of *N. attenuata* in Arizona, USA. Milled soil was dissolved in methanol (80%) and analyzed after solid phase extraction. The same method was employed for catechol quantification as already described. Catechol content was measured by UPLC/ESI-qTOF with the standard curve method.

Structure elucidation by NMR

Collected fractions were dried completely in a vacuum concentrator (3.7 mbar, Concentrator 5301, Eppendorf). The merged active HPLC-fractions 'd3' and 'd4' were used for structure elucidation by nuclear magnetic resonance spectroscopy (NMR). ¹H NMR, ¹³C NMR and ¹H-¹³C HSQC spectra were recorded on an Avance500 NMR spectrometer (Bruker-Biospin, Karlsruhe, Germany) at 300 K using a 5 mm TCI CryoProbe™. Chemical shift values (δ) are given relative to the residual solvent peaks at δ_H 3.31 and δ_C 49.05, respectively. Coupling constants are given in hertz (Hz).

RNA isolation

For our large-scale gene expression analysis, roots were treated with the S2 fraction or the same amount of methanol as a control. Root tips were harvested 2 and 6 h after treatment. At least 200 seedlings were harvested as one replicate and kept in RNeasy Lysis Buffer (Qiagen, <https://www.qiagen.com/de/>) until being extracted. In total, three replicates per time-point and treatment were harvested. RNA was extracted using Qiagen RNeasy Mini Kit columns (Qiagen) according to manufacturer's protocols, in combination with on-column DNase-I treatment (Qiagen). Aliquots (1 µl) of purified RNA were pipetted for quantification and quality assessment of total RNA using the Agilent 2100 Bio-analyser system in combination with RNA 6000 n kit (Agilent, Santa Clara, CA, USA). Only RNA that displayed intact 18S and 25S peaks was sent for RNA-seq profiling (Max Planck Genome Centre Cologne, Germany). All libraries were sequenced on the Illumina HiSeq 3000 (Illumina, <https://www.illumina.com/>).

RNA-seq data analysis

For data analysis, we followed the descriptions of Ling *et al.* (2015). Briefly, the raw reads were trimmed with ADAPTERREMOVAL (Lindgreen, 2012), which were subsequently aligned to the *N. attenuata* genome assembly (release 1.0) using TOPHAT2 (Kim *et al.*, 2013). The genes were assembled by CUFFLINKS in combination with *N. attenuata* genome annotation as the reference. Re-mapping all trimmed reads to the assembled transcripts via RSEM was used to estimate the expression level of the assembled transcripts. Read count were calculated using HT-SEQ (Anders *et al.*, 2014) using *N. attenuata* genome annotation. The trimmed mean of M-values (TMM) normalized fragment per kb of transcript per million mapped reads (FPKM) was calculated using TRINITY (Haas *et al.*, 2013). The differentially expressed genes (DEG) were identified using EDGE package (Grman & Robinson, 2013). Genes with the absolute fold-change of > 2 and with a false discovery rate (FDR)-adjusted *P*-value of < 0.05 were considered as differentially expressed genes (DEGs). The gene ontology (GO) annotations of *N. attenuata* genes were derived from its genome annotation (S. Xu, T. Brockmüller, A. Navarro-Quezada, H. Kuhl, K. Gase, Z. Ling, W. Zhou, C. Kreitzer, M. Stanke, H. Tang, E. Lyons, P. Pandey, S. P. Pandey, B. Timmermann, E. Gaquerel & I. T. Baldwin, unpublished). The functional enrichment analysis was computed by CLUGO. The levels of significance of enriched GO terms were determined by Bonferroni corrected *P*-values (*P* ≤ 0.05).

Indole-3-acetic acid (IAA) extraction and measurement

Root and leaf tissues were separated, and roots dissected after long-term treatment with smoke (5 dpg) and short-term treatment with catechol (48 h) and immediately frozen in liquid nitrogen. After being ground to a fine power, IAA was extracted and concentration was determined as described in detail by Schaefer *et al.* (2016). In brief, total IAA was extracted with extraction buffer (methanol : 1 M formic acid = 4 : 1 (v/v)), and IAA was measured relative to labeled D-IAA by a Bruker Elite EvoQ Triple quad-MS equipped with a HESI (heated electrospray ionization) ion source (Bruker Daltonik, Bremen, Germany).

Superoxide anion (O₂⁻) and hydrogen peroxide (H₂O₂) staining and quantification

Seedlings grown on GB5 media were transferred to media supplemented with smoke, catechol, and inhibitors of ROS and H₂O₂ for the indicated time-points. For superoxide anion staining with NBT, seedlings were stained for 15 min in a solution of 2 mM NBT in 20 mM phosphate buffer (pH 6.1). Transferring stained seedlings into distilled water stopped the reaction. Pictures were taken by Leica stereomicroscope (MZ16, Leica, Wetzlar, Germany). Settings were exactly identical for all of the pictures in the same experiment. To visualize H₂O₂, seedlings were incubated in 50 µM BES-H₂O₂-AC for 30 min in the dark; and for the simultaneous visualization of H₂O₂ and plant cell walls in a single specimen, seedlings were double-stained by

incubation in 100 μM of propidium iodide (PI) and 50 μM of BES- H_2O_2 -AC for 30 min in the dark. After three quick rinses, pictures were immediately taken by LSM 510 (Zeiss, Jena, Germany). The excitation wavelength for PI-stained samples was 536 nm, and emission was collected at 617 nm; for BES- H_2O_2 -AC stained samples excitation was 485 ± 20 nm, and emission collected at 515 ± 20 nm. For imaging after NBT and BES- H_2O_2 -AC staining, all of the instrumental parameters were retained in an independent experiment.

IMAGEJ software (NIH, <https://imagej.nih.gov/ij/>) was used to assess the average intensity of NBT-stained signals and the relative amount of H_2O_2 fluorescence intensity by BES- H_2O_2 -AC. Briefly, original captured images were loaded and inverted to 8-bit mode, and then the images were processed under the menu of 'Process' to subtract background, followed by calibration under the menu of 'Analyze', the default value of the threshold of 'Adjust' was kept for measuring the next step. All of the 'IntDen' values were exported to Microsoft EXCEL for statistical analysis.

The H_2O_2 content of the roots after staining with BES- H_2O_2 -AC staining was analyzed by Amplex Red hydrogen peroxide/peroxidase assay kit (Thermo Fisher Scientific, <https://www.thermofisher.com>, USA) according to the manufacturer's instruction. Briefly, six root sections of 1–1.5 cm length (from tip to shoot) as one replicate were incubated in the reaction mixture for 30 min in the dark at room temperature. The fluorescence intensity was quantified with a fluorescence microplate reader (Infinite[®] 200 PRO; Tecan, Maennedorf, Switzerland) with an excitation at 540 nm and emission at 610 nm. Different concentrations of H_2O_2 solution were used to prepare the standard curve. The reaction mixture without the substrate or root material served as a control.

Statistical analysis

For all of the pairwise comparisons relative to control groups, Student's *t*-test was performed ($P \leq 0.05$). In the experiments of NAA/IAA complementation with or without smoke addition, linear regression modeling was performed and ANOVA was applied for significance test. For all other experiments, one-way ANOVA was conducted, followed by either Tukey's HSD for symmetric groups or Fisher's protected LSD for unequal groups.

Nucleotide sequence accession numbers

The RNA sequencing data have been deposited in the National Center for Biotechnology Information (NCBI) under project number PRJNA320036.

Results

Smoke cues impair root hair elongation and increase primary root length by regulating cell expansion in the elongation/differentiation zone

In order to determine the potential roles of smoke cues for establishing seedlings, we germinated *Nicotiana attenuata* on media

containing different amounts of liquid smoke and observed root morphology. After being treated with liquid smoke, *N. attenuata* primary roots were significantly longer and had more lateral roots, whereas root hair elongation was impaired (Fig. 1). Hypocotyl length did not change. The effect of smoke on root growth and lateral formation was dose-dependent: growth was promoted at low concentrations and inhibited at high concentrations (Figs 1a, S1a,b).

In order to examine whether an increase in cell division in the meristem zone (MZ) or increase in cell expansion in the elongation/differentiation zone (EZ/DZ) accounted for the increase in root length, the number of cortex cells was counted from the quiescent center (QC) to the first elongated cell as a measure of meristem size (Fig. S2a). The number of cells in the MZ did not increase significantly (Fig. 1d); however, the cortical cell length in the EZ/DZ increased significantly (Fig. 1e). Short-term treatments (16 h) with smoke showed the same result as long-term treatments. These results indicate that an increase in longitudinal cell expansion in the EZ/DZ was mainly responsible for the accelerated root growth by smoke cues (Fig. S2).

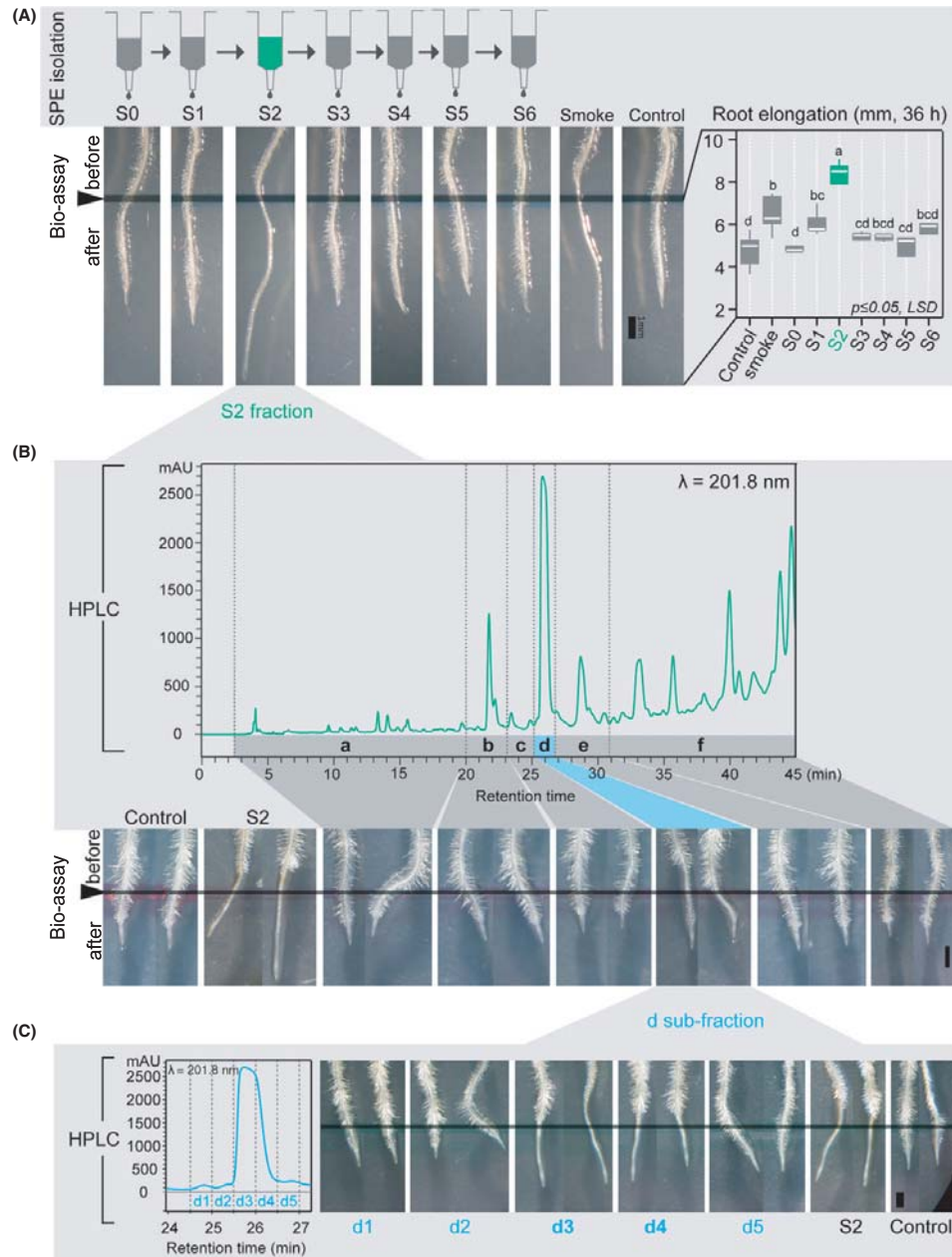
Catechol, but not karrikins, is the main active compound in smoke that affects root growth

Karrikins were identified in smoke and their effect on seed germination and seedling growth has been well described. However, although treatment with KAR1 dramatically increased the seed germination ratio and decreased hypocotyl elongation, as reported earlier (Flematti *et al.*, 2004a; Nelson *et al.*, 2009), no significant changes in root growth were observed after treatment (Fig. S1c–f).

In order to identify the potential compounds in liquid smoke responsible for the observed increase in primary root elongation and the decrease in root hair growth, bioassay-driven SPE was applied as the first fractionation step. Among the seven collected fractions (S0–S6), only fraction S2 induced the smoke-elicited root phenotype: root length increased and root hair expansion was impaired (Figs 2a, S3). In contrast to the strong acidic smoke solution (1/900, pH 4.2), fraction S2 did not alter the pH of the culture medium, allowing us to rule out the hypothesis that pH changes in the medium are responsible for the root phenotype.

Further fractionation of the active S2 fraction was performed by HPLC. Bioassays were conducted with pooled elutions as indicated in Fig. 2(b). Only treatment with one of the fractions ('d') was able to mimic the root phenotype elicited by S2 (Fig. 2b). Five subfractions (d1–d5) of fraction 'd' were collected, and the application of fraction d3 and d4 resulted in impaired root hair elongation (Fig. 2c).

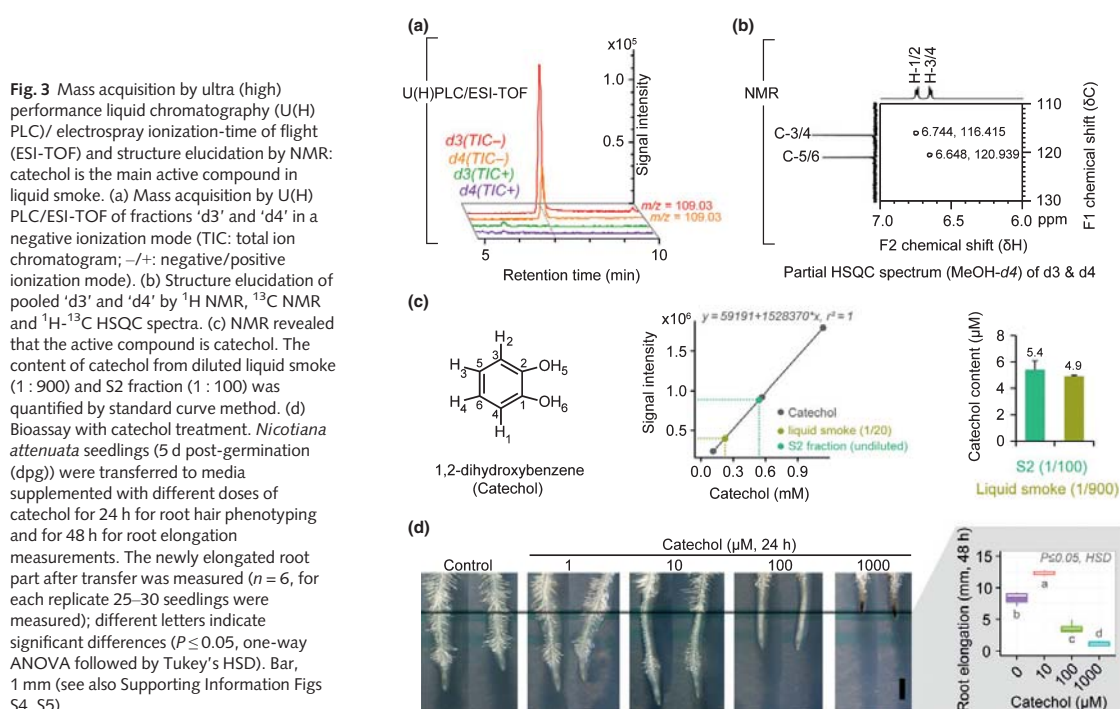
Based on the acquired masses and retention time, fractions d3 and d4 were identical (Fig. 3a) and pooled for one-dimensional (^1H and ^{13}C NMR) and two-dimensional (HSQC) NMR. The ^1H NMR spectrum showed two multiplet signals (*ddd*, 3.7/3.7/9.5 Hz) in the aromatic range, at δ_{H} 6.74 and δ_{H} 6.65, respectively, which is typical for a symmetrically 1,2-disubstituted aromatic ring. ^{13}C NMR showed, in accordance with the expectation symmetry, three signals at δ_{C} 116.4, 120.9 and 146.4. Correlations in the ^1H - ^{13}C HSQC allowed for the final identification of 1,2-dihydroxybenzene (catechol) (Fig. 3b). The



amounts of catechol in liquid smoke (1/900) and active S2 (1/100) were measured by U(H)PLC/ESI-TOF using different catechol concentrations for a standard curve. Both solutions contained approximately half ($5.4 \mu\text{M}$ and $4.9 \mu\text{M}$, respectively,

Fig. 3c) of the concentration of pure catechol ($10 \mu\text{M}$) required to elicit a similar extent of root elongation (Fig. 3d). In order to verify whether catechol is the active compound leading to the same root phenotype as that induced by smoke, the bioassay was

Fig. 2 Bioassay-driven solid phase extraction (SPE) and high performance liquid chromatography (HPLC) fractionation: The elution S2 and HPLC fractions d3/d4 are the bioactive fractions in liquid smoke. (A) Scheme of the SPE fractionation procedure and root-phenotype-guided activity assay. Elution S2 is the active fraction of the SPE fractionation. Liquid smoke was loaded onto reverse/cation exchange phase column; the initial flow-through was called S0, and subsequent flow-throughs were referred to as S1–S6. For the bioassay, seedlings were transferred from mock GB5 media to media supplemented with the different elutions (S0–S6). 36 h after transfer, the newly elongated part of the root was measured ($n = 3$, for each biological replicate, 8–12 *Nicotiana attenuata* seedlings per Petri dish were measured); different letters indicate significant differences ($P \leq 0.05$, one-way ANOVA followed by Fisher's LSD). For additional replicates of root hair phenotype, see Supporting Information Fig. S3. The light-colored 'roots' in the pictures are reflections of the roots on the medium due to the photographing technique. (B) HPLC fractionation of SPE-elution S2 on a reversed phase C18 column. Fractions were collected every 30 s; and based on the chromatogram fractions 2.5–20 min, 20–23 min, 23–25 min, 25–27 min, 27–31 min and 31–45 min, fractions were pooled and labeled 'a' through 'f' respectively. Only fraction 'd' inhibited root hair elongation. (C) The further fractionation of fraction 'd', the 5 sub-fractions (d1–d5, starting at 24.5 min) were collected and used for bioassays; both 'd3' and 'd4' decreased root hair elongation. (B, C) Seedlings (5 d post-germination (dpg)) were transferred to media supplemented with the different fraction for 24 h for root hair phenotyping (for each group, 8–10 seedlings per Petri dish were observed). Bars, 1 mm.



performed using different concentrations of commercially available pure catechol. Both catechol and smoke/S2 showed the same dose-dependent root morphology (Fig. 3d). Interestingly, root elongation was reliably increased up to a concentration of 60 μM , whereas root hair formation was partially impaired by the addition of 10 μM catechol and fully abolished at catechol concentrations higher than 20 μM (Fig. S4).

Several substances whose chemical structures are similar to the structure of catechol but show different levels of redox reactivity, such as resorcinol, hydroquinone and guaiacol, also have been identified in liquid smoke (Baldwin *et al.*, 1994). A comparison of the three isomers of dihydroxybenzene (1,2-dihydroxybenzene-catechol; 1,3-dihydroxybenzene-resorcinol; and 1,4-dihydroxybenzene-hydroquinone) revealed that only

catechol impaired root hair elongation and induced root elongation at a concentration of 10 μM , whereas for the para-isomer hydroquinone, a higher concentration was required to observe the effect on root hair growth, and for the meta-isomer resorcinol as well as for guaiacol, a higher concentration was required to induce both, root hair growth and primary root elongation (Fig. S5). Taken together, roots were most sensitive to catechol. We assume that catechol is the main active compound in smoke responsible for inducing the root morphology.

In order to prove that catechol is present not only in liquid smoke, but also under natural conditions, we collected freshly burnt soil from *N. attenuata*'s habitat in Arizona, USA, and c. 10.1 μg of catechol in 12.5 g of soil was measured by U(H) PLC/ESI-qTOF (Fig. 4).

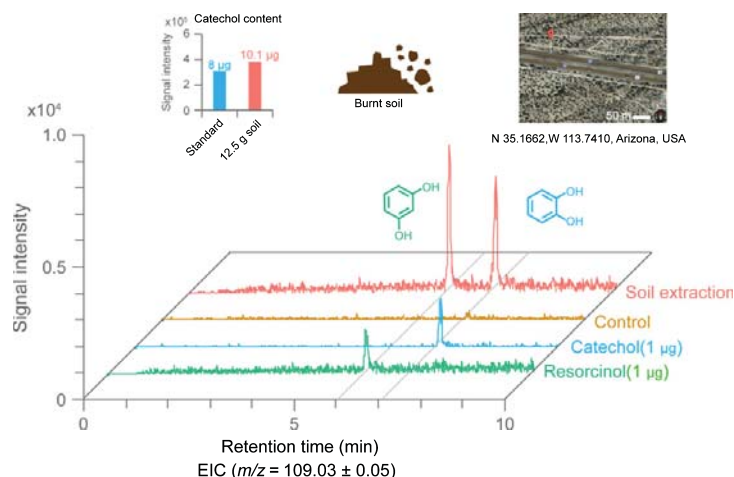


Fig. 4 Catechol occurs in high concentrations ($\mu\text{g g}^{-1}$) in burnt soil collected from the native habitat of *Nicotiana attenuata*. Catechol and resorcinol were detected by ultra performance liquid chromatography (UPLC)/ electrospray ionization-quadrupole time of flight (ESI-qTOF) in extracts from burnt soil. Extracted ion chromatograms (EIC, $m/z = 109.03 \pm 0.05$) of soil extraction (pink) and standards including catechol (cyan) and resorcinol (green). Burnt soil was collected in 2016 from the native habitat of *N. attenuata* in Arizona, USA (inset: Google Map image of collection site).

Smoke-treatment leads to massive changes in gene expression

In order to dissect the potential mechanisms leading to the smoke-induced changes in root morphology, transcriptome profiling was performed by RNA-seq. We used roots treated with the S2 fraction for these analyses, because in contrast to the nonfractionated liquid smoke solution, S2 did not affect the pH of the medium; however, it is more stable than pure catechol, presumably due to the presence of additional compounds in the smoke solution which protect catechol from oxidation. Seedlings were treated with S2-free or S2-containing medium for 2 and 6 h (Fig. 5a). After sequencing, a total of 1391 differentially expressed genes (DEG) were identified ($|\log_2\text{FC}| > 1$, $\text{FDR} \leq 0.05$; Fig. 5a,b; Table S1).

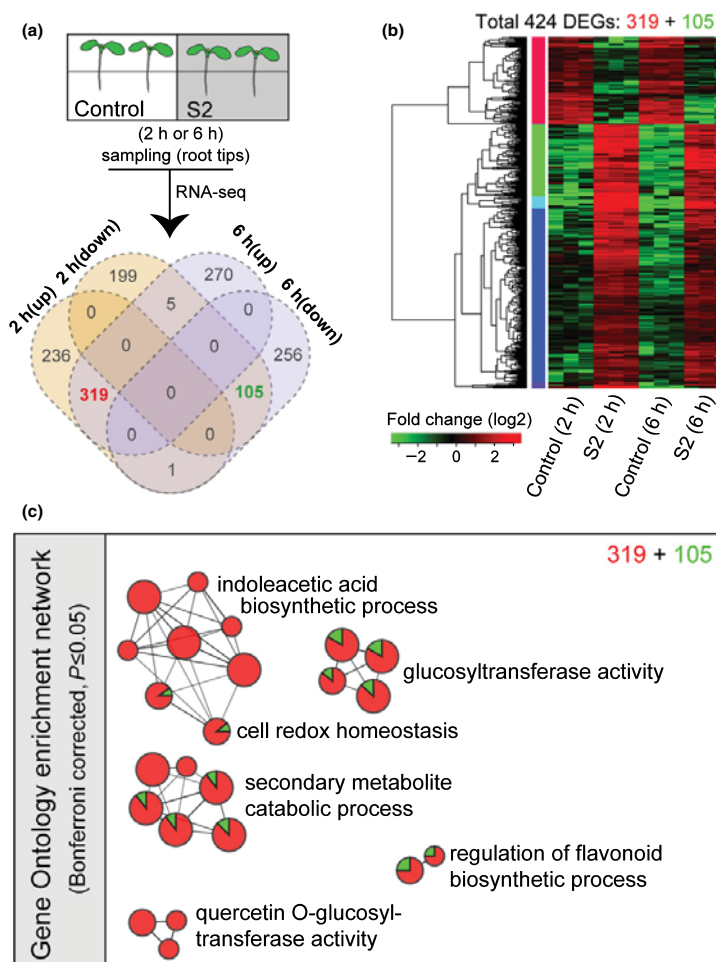
In order to reveal the main regulatory pathway(s), DEGs at both time points were considered first (424 DEGs; Fig. 5b). Among these, several extensin-like proteins were most strongly downregulated after treatment with smoke (Fig. S6c), whereas a number of glucosyltransferases – *ap2* *erf* domain-containing transcription factors and glutathione-S-transferases – were most strongly upregulated (Table S1). A GO analysis of these DEGs showed that enriched networks were mapped mainly to flavonoid biosynthesis, secondary metabolite catabolism, glucosyltransferase, cell redox homeostasis and auxin biosynthesis (Fig. 5c). The two enriched processes – auxin biosynthesis (Zhao, 2010) and cell redox homeostasis (Tsukagoshi, 2016) – are known to play major roles in root development and growth. Networks of enriched GOs for genes differentially expressed only after 2 or 6 h were mainly related to programmed cell death, water transport and general functions such as nucleosome assembly, ribosome and carbohydrate catabolism (Fig. S6a,b).

The smoke-induced root phenotype is not primarily regulated by auxin

We first tested the hypothesis that smoke-induced primary root growth was due to changes in auxin production. Two auxin biosynthesis inhibitors, Kyn and yucasin, were applied and the root phenotypes observed. Kyn is an alternative substrate for L-tryptophan-pyruvate aminotransferase 1 (TAA1) and decreases root-derived auxin production through competition (He *et al.*, 2011). Yucasin is a potent auxin biosynthesis inhibitor that blocks the conversion of indole-3-pyruvic acid (IPyA) to IAA by targeting the YUC enzymes (Nishimura *et al.*, 2014) (Fig. 6a). *Nicotiana attenuata* seedlings grown on medium supplemented with either a range of Kyn concentrations or yucasin, showed increased root length and impaired root hair growth (Fig. 6b,c). By contrast, seedlings grown on NPA-supplemented medium, which is a polar auxin transport inhibitor (Jensen *et al.*, 1998), had an inhibitory effect on root growth (Fig. 6c). At first glance, these results suggested that reduced auxin biosynthesis might be responsible for the smoke-induced phenotype but not for polar auxin transport. However, the quantification of auxin levels in roots after long-term treatment with smoke and short-term treatment with catechol resulted in higher levels of IAA (Fig. 7a) and not the lower levels suggested by the application of the auxin biosynthesis inhibitors. Additionally, we monitored the auxin response in real time by using an auxin reporter line from *Arabidopsis* (DII-VENUS) which negatively correlates auxin responses with fluorescence intensity. As expected, the application of the auxin biosynthesis inhibitor Kyn resulted in more fluorescence and the application of external auxin resulted in less fluorescence. The addition of smoke and S2 fractions led to an intermediate reduction in fluorescence intensity indicating an increase in auxin levels, as was expected (Fig. S7a,b).

In order to further dissect a possible role for auxin in the smoke-induced root phenotype, we performed a histochemical analysis. The addition of the synthetic auxin NAA (1 nM) led to a significant

Fig. 5 Hierarchical clustering and the functional enrichment of differentially expressed genes (DEGs) in *Nicotiana attenuata* roots after treatment with the active SPE-elution S2 for 2 and 6 h: genes related to cell redox-homeostasis and auxin biosynthesis are enriched among the upregulated genes at both time-points after treatment. Seedlings (5 d post-germination (dpg)) were transferred to media with or without the S2 fraction, and root tips were harvested for RNA-seq. Three replicates were sequenced for each group (~300 seedlings were harvested from 10 Petri dishes and pooled as one replicate). (a) Sample preparation and data analysis ($|\log_2FC| > 1$, $FDR \leq 0.05$); Venn-diagrams show the number of up- and downregulated genes in root tips after treatment with S2 fraction for 2 and 6 h compared to control groups. Numbers in red (upregulation) and green (downregulation) indicate DEGs (319 + 109) showing the same expression pattern at both time points. (b) Hierarchical cluster analysis of these 424 DEGs. (c) Gene ontology (GO) enrichment analysis of the 424 DEGs was computed with CLUGO according to the GO categories 'Biological Process' and 'Molecular Function' (two-sided hypergeometric test, Bonferroni corrected, $P \leq 0.05$) (see also Supporting Information Fig. S6).



increase in the number of MZ cells, whereas the addition of smoke did not significantly alter the number of MZ cells (Fig. 7b). Furthermore, a chemical complementation assay demonstrated that the smoke-induced phenotype could neither be mimicked nor rescued by IAA/NAA treatments (Fig. 7c). Moreover, *SHY2/IAA3*, a key transcription factor involved in controlling the balance of cell division and cell differentiation and considered as a molecular marker of auxin activity, did not respond to S2 fraction incubation based on RNA-seq datasets (Fig. S7c). Taken together, these results indicate that auxin is not the primary signal responsible for the smoke-induced changes in primary root growth and root hair elongation.

Redox processes regulate root growth and root hair elongation in response to smoke

H_2O_2 and O_2^- , two important ROS in roots, are differentially distributed and fulfill different developmental functions. Based

on the GO enrichment analysis from the RNA-seq data, we hypothesized that the observed increased cell expansion in the EZ/DZ was due to redox changes. We quantified the content of H_2O_2 and O_2^- in roots before and after catechol exposure, and also exposed roots to salicylhydroxamic acid (SHAM), an inhibitor of peroxidase activity (Brouwer *et al.*, 1986), and DPI, which primarily inhibits NADPH oxidase activity (Li & Trush, 1998). The two inhibitors confirmed the validity of the methodology; their application strongly reduced O_2^- levels. Treating seedlings with different concentrations of catechol also reduced O_2^- production compared to controls (Fig. 8a,b). By contrast, H_2O_2 content did not change in response to catechol treatment (10 μM), but slightly and significantly increased with higher amounts of catechol (Fig. 8c).

In order to understand how catechol treatment affects the levels and distribution of H_2O_2 in the roots, we investigated the spatial distribution of H_2O_2 in response to catechol treatment

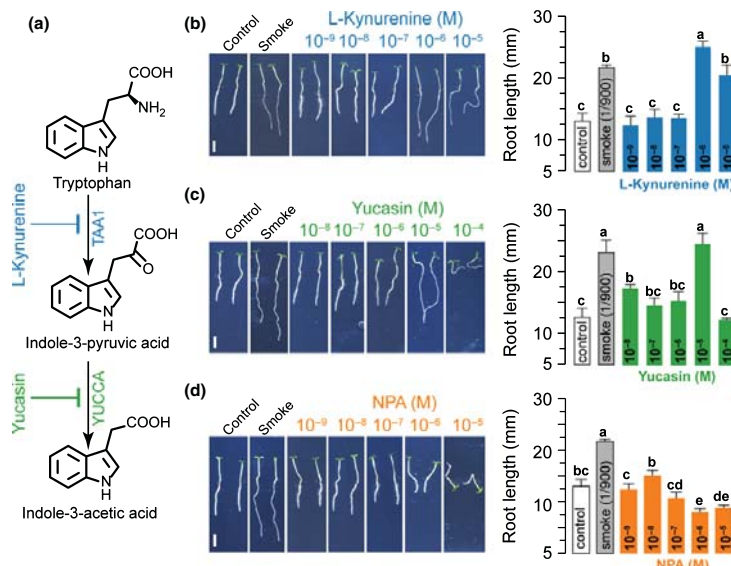


Fig. 6 The root phenotype induced by smoke is mimicked by the application of auxin biosynthesis inhibitors, but not by an auxin transport inhibitor. To investigate if auxin levels are responsible for the smoke-induced root phenotype, auxin biosynthesis and transport inhibitors were applied in an attempt to mimic smoke-induced root phenotype. (a) Auxin biosynthesis is inhibited by L-kynurenine (Kyn) and yucasin. (b, c) Both Kyn and yucasin application mimicked the smoke-induced root phenotype in a concentration-dependent manner. (d) Roots were treated with 1-N-naphthylphthalamic acid (NPA), an inhibitor of polar auxin transport. After treatment, root elongation was significantly decreased. (b–d) *Nicotiana attenuata* seedlings were grown on GB5 medium supplemented with different concentrations of Kyn, yucasin and NPA for 9 d (7 d post-germination (dpg)). Data are means \pm SD ($n = 6$, for each replicate 25–30 seedlings per Petri dish were measured); different letters indicate significant differences ($P \leq 0.05$, one-way ANOVA followed by Tukey's HSD). Bars, 5 mm.

using the highly specific H_2O_2 fluorescent indicator BES- H_2O_2 -AC (Maeda, 2008). In controls, H_2O_2 fluorescence was particularly enriched in the expanding root hairs and in the EZ/DZ of primary roots. The strongest signal was found in the cortical cells close to the cell wall, whereas the remaining root parts did not show detectable fluorescence (Fig. 8d). This distribution of ROS is consistent with that found in previous studies (Dunand *et al.*, 2007). However, after catechol treatment, the H_2O_2 fluorescence signal was enriched mainly in the inner tissue surrounding the central cylinder in the EZ/DZ, whereas it disappeared from the outer layers (Fig. 8d). Counterstaining with PI corroborated the observation that after catechol treatment, H_2O_2 was detected in the stele but not around the cortical cell walls, as was observed in the controls (Fig. 6e). We therefore inferred that treating roots with catechol leads to the redistribution of H_2O_2 . We speculated that the locally reduced H_2O_2 levels around the cortical cells might be one important factor controlling cell expansion and root hair elongation.

In order to test this hypothesis, we supplemented the catechol-treated roots with H_2O_2 . The application of H_2O_2 could partly rescue the catechol-induced phenotype, and a weak H_2O_2 fluorescent signal was detected around the cell walls of the outer layer of cortical cells (Fig. 8e). Furthermore, the additional H_2O_2 supplementation reversed the inhibitory effect of catechol on root hair elongation, and primary root growth rates were similar to those of controls (Fig. 9). However, the

phenotype was fully restored only when $100 \mu\text{M}$ H_2O_2 and $10 \mu\text{M}$ catechol were applied, whereas higher catechol concentrations and $100 \mu\text{M}$ H_2O_2 were not able to rescue the root hair development and resulted in significantly reduced root growth (Fig. 9). Based on these results, we conclude that catechol profoundly influences the root morphology by locally decreasing H_2O_2 levels in the cell wall of the cortical layer in the EZ/DZ and thereby increasing H_2O_2 levels in and around the stele.

Discussion

The effects of smoke on seed germination and on the isolation and characterization of active compounds from smoke for enhancing germination have been well documented (Nelson *et al.*, 2012). However, the role of smoke signals on root growth and development is poorly understood. As primary root growth for nutrient uptake is a crucial factor for seedling establishment, it plays a central role in *Nicotiana attenuata*'s ability to colonize the post-fire environment. Here, we identified catechol – which has been shown previously to be highly abundant in smoke (Baldwin *et al.*, 1994; Montazeri *et al.*, 2013) – as the active effector in smoke that morphologically promotes root growth and lateral root formation, while repressing root hair elongation of *N. attenuata* seedlings. We could rule out the germination stimulant karrikin from causing this effect (Figs 1, S1), which indicates

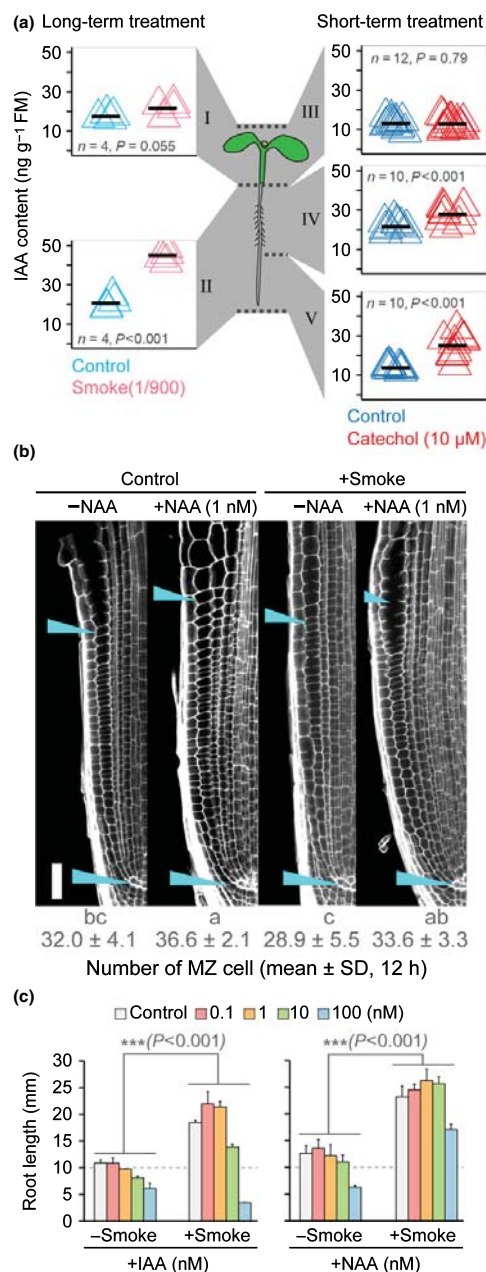


Fig. 7 The smoke-induced root phenotype is not primarily regulated by auxin. (a) Auxin levels were slightly but significantly increased by long-term (left panel) and short-term (right panel) treatment. For long-term treatment, *Nicotiana attenuata* seedlings were grown on media supplemented with liquid smoke for 7 d (5 d post-germination (dpg)); shoot (I) and root (II) were harvested separately. For short-term treatments, seedlings (5 dpg) were treated with catechol (10 μ M) for 48 h, and three parts were collected separately (shoot part (III), newly elongated root part after transfer (V) and the remaining part (IV)). Auxin (IAA) was measured by high-resolution LC/MS relative to labeled D-IAA. Cross-bars in the strip plot indicate the means, Student's *t*-test. 420–450 seedlings from 15 Petri dishes were collected as one replicate. (b) The size of the meristem was not significantly altered by smoke induction compared to its size in control groups. Short-term (12 h) application of NAA (1 nM) increased the number of meristem zone (MZ) cells, but results from treatment with external smoke plus supplementation with NAA did not significantly differ from results from the application of NAA only. The distances of MZ (left half only) for measuring are marked by arrow-heads. Data are means \pm SD (15–20 seedlings were analyzed, only the left half of root was counted), different letters indicate significances ($P \leq 0.05$, one-way ANOVA followed by Fisher's LSD). (c) Chemical complementation assay. Indole-acetic acid (IAA) and the synthetic auxin, 1-naphthaleneacetic acid (NAA) did not rescue the faster primary root elongation induced by smoke ($v/v = 1/900$) application. Seedlings were grown on GB5 media with external supplementations as indicated (7 dpg). Data are means \pm SD ($n = 6$, for each replicate 25–30 seedlings per Petri dish were measured; linear regression model was applied followed by ANOVA test: $***$, $P \leq 0.001$) (see also Supporting Information Fig. S7).

redox-homeostasis were affected by smoke cues. Previous studies characterizing the morphology of the roots of *Arabidopsis* auxin biosynthesis mutants (Pitts *et al.*, 1998) and of roots exposed to an imbalance of H_2O_2 and O_2^- (Takeda *et al.*, 2008) describe similar phenotypes. Based on the similarities of the observed root phenotype after treatment with smoke and the auxin-biosynthesis inhibitors Kyn and yucasin (Nishimura *et al.*, 2014), we initially assumed that the inhibition of auxin biosynthesis and, hence, decreased auxin levels, might be an important factor in tobacco's response to smoke. However, our results strongly suggest that auxin biosynthesis does not play a primary role in the smoke- and catechol-induced root phenotype because (1) supplementing the smoke-treated roots with auxins could not rescue the phenotype, (2) the total amounts of auxin showed the opposite pattern – they increased in smoke/catechol-treated roots, and (3) the expression of the molecular marker *NaSHY2* regulated by auxin did not significantly change after treatment. Additionally, in agreement with previous publications (Peng *et al.*, 2013; Perrot-Rechenmann, 2013), the treatment of roots with the synthetic auxin NAA increased the number of cells in the meristem zone, whereas the application of smoke did not. Further evidence against a central role of auxin in the smoke-induced phenotype was provided by the *Arabidopsis* DII-VENUS line, which confirmed a slight increase in auxin levels after smoke treatment; however, this increase in auxin levels was not accompanied by an increased number of MZ cells (Figs 6, 7, S7). It may be that the increase of IAA is a byproduct or secondary signal from the plants' primary physiological responses to smoke treatment. However, an effect of the increased auxin levels on meristem

that *N. attenuata* perceives different substances in smoke responsible for germinating and establishing seedlings.

The transcriptome profiling and gene ontology (GO) network analysis indicated that auxin biosynthesis and

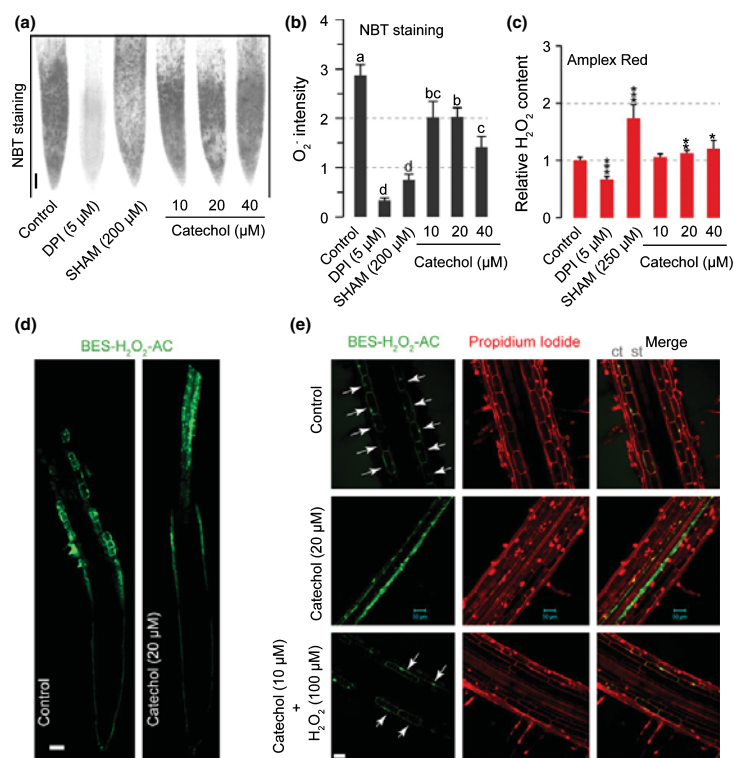


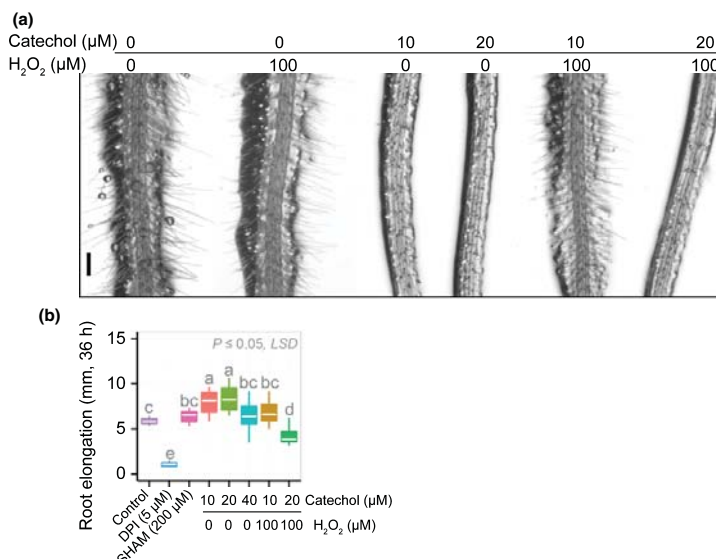
Fig. 8 Localization and total amounts of hydrogen peroxide (H_2O_2) in *Nicotiana attenuata* roots are altered by catechol treatment. (a) Histochemical localization of superoxide anions (O_2^-) by nitroblue tetrazolium (NBT) staining. Seedlings (5 d post-germination (dpg)) were transferred to media containing different concentrations of catechol, diphenyleneiodonium (DPI, NADPH oxidase inhibitor), and salicylhydroxamic acid (SHAM, peroxidase inhibitor), and pictures were taken 12 h after transfer. Bar, 100 μ m. (b) O_2^- amounts in roots significantly decreased after catechol incubation by quantification of NBT-stained signals in (a) (data are means \pm SD, 15–20 seedlings were measured). Different letters indicate significant differences ($P \leq 0.05$, one-way ANOVA followed by Fisher's LSD). (c) Total amounts of H_2O_2 slightly but significantly increased as the concentration of catechol increased in the treatment by Amplex red staining 24 h after induction (means \pm SD, $n = 4$, for each replicate, 6 newly elongated root parts after transfer were pooled as one replicate). Significant differences relative to the control group are indicated by asterisks (Student's t -test: **, $P \leq 0.01$; ***, $P \leq 0.001$). (d) Imaging after BES- H_2O_2 -AC staining with LSM 510 microscope (ZEISS) to visualize H_2O_2 spatial distribution in root tip. Bar, 100 μ m. (e) Counterstaining BES- H_2O_2 -AC with propidium iodide (PI) showed that without treatment, H_2O_2 was enriched around the cortical cells, whereas after catechol treatment, H_2O_2 was mainly enriched in the area around the stele. Seedlings were transferred to media supplemented with catechol and H_2O_2 for 24 h before staining. Arrows indicate H_2O_2 localization around cortical cells (6–10 roots were analyzed). st, stele; ct, cortex. Bars, 50 μ m.

zone (MZ) cell proliferation might have been countered by decreased O_2^- levels.

In addition to changes in biosynthesis, signaling and the temporal and spatial distribution of auxin are also crucial to fully evaluate the effects of auxin on growth (Ljung, 2013); in particular, the cell-to-cell transport of auxin can generate auxin gradients that elicit growth responses (Sauer *et al.*, 2013). However, in the present study, the inhibition of auxin transport was unable to mimic the smoke-induced phenotype, which supports the inference that auxin is not the primary effector. Nevertheless, based on the data provided here, highly local cell-to-cell changes in auxin concentrations cannot be ruled out completely.

The observed induction of reactive oxygen species (ROS)-related genes corresponds with the analysis of the transcriptome

of maize embryos treated with liquid smoke solution for 24 h; this analysis also demonstrated a GO enrichment for redox processes (Soós *et al.*, 2009). ROS are well-known from the signal transduction pathways that regulate plant growth, development and defense responses (Considine *et al.*, 2015), and their production is tightly controlled and locally restricted (Schmidt & Schippers, 2015). As was shown in histochemical studies in several other plant species (Schopfer, 1994; Dunand *et al.*, 2007; Tsukagoshi *et al.*, 2010), in *N. attenuata* O_2^- was present mainly in inner tissues of the young elongation zone, and, to a lesser extent, in the meristem zone and in the stele along the roots (Fig. 8a). By contrast, H_2O_2 was highly abundant around cell walls of the cortical layer in the elongation/differentiation zone (EZ/DZ) confined to the apoplast and in the expanding root



2011). Considering the gene expression changes in ROS-related genes and the strong downregulation of EXTs upon elicitation with smoke cues, we propose that catechol/smoke treatment weakens the cross-linking in the cell wall we propose that catechol/smoke treatment weakens the cross-linking in the cell wall and that this weakening is due to the lack of structural extensins. However, to confirm this hypothesis, the signal leading to reduced EXT expression still has to be elucidated.

Recent results indicate that five members of an RLK subfamily in Arabidopsis are cell wall sensors; homologs of two (*RLK-theseus 1* and *-feronia*) (Cheung & Wu, 2011; Lindner *et al.*, 2012) are also regulated after smoke treatment (Table S1). RLK-feronia has been thought to activate the production of ROS, and these regulate growth (Cheung & Wu, 2011). It is tempting to speculate that ROS perceive local changes in the redox-state in the apoplast in the presence of smoke-inducing signaling cascades, and that these changes ultimately result in growth effects.

catechol at high concentrations has been well described as a highly toxic organic industrial waste product (Petriccione *et al.*, 2013), yet its role in root growth for fire ephemerals has not been studied previously. In the present study we show that catechol is not only present in liquid smoke solution, but also occurs at high concentrations ($\mu\text{g g}^{-1}$) in freshly burned soil from the wild tobacco plant's native habitat (Fig. 4). Plant roots forage in the soil for minerals and water (Trewavas, 2014). We assume that the root phenotype observed *in vitro* is of ecological importance. The catechol-induced root elongation and increase in the number of lateral roots may enable the roots to grow more quickly into areas of the highest nutrient concentrations. However, additional research is needed to better understand the local distribution and persistence of catechol in burned soil and its correlation with the presence of nutrients, and to fully understand its ecological role as an environmental signal.

In conclusion, we provide evidence that, depending on the dose, smoke can induce root growth and suppress root hair elongation in *N. attenuata* seedlings. Smoke-induced root development changes were mainly mediated by catechol. Transcriptomic sequencing suggests that although the expression of genes from both auxin biosynthesis and ROS pathways was significantly altered by smoke treatment, only ROS were found to be involved directly in smoke-induced root development changes and these acted by altering the distribution of H_2O_2 in the elongation zone. Further experiments will be required to elucidate how the catechol-induced changes in the redox state are sensed in the root, if catechol is also transported into the cells, and whether the presence of catechol in the soil will promote plant growth and fitness in the field.

Acknowledgements

We thank Nam Nguyen, Zach Liechty and Irem Tuyusz for help with seedling growth and harvest; Klaus Gase for assistance with RNA-seq data submission, Jürgen Rybak for LSM instructions and Emily Wheeler for editorial assistance. This study was funded by the Max Planck Society, by Advanced Grant 293926 from the European Research Council to ITB, and by the

Collaborative Research Centre 'Chemical Mediators in Complex Biosystems – ChemBioSys' (SFB 1127). S.X. acknowledges funding by the SNF (PEBZP3-142886) and a Marie Curie Intra-European-Fellowship (328935).

Author contributions

M.W., I.T.B. and K.G. planned and designed the research and wrote the manuscript; M.W. performed the research and analyzed the data; M.S. guided the fractionation of catechol and its analysis by HPLC and MS; S.X. annotated the RNA-seq data and helped with RNA-seq data analysis; C.P. undertook the NMR analysis; and J.W. contributed to data collection.

References

- Abdelgadir H, Kulkarni M, Arruda M, Van Staden J. 2012. Enhancing seedling growth of *Jatropha curcas*—a potential oil seed crop for biodiesel. *South African Journal of Botany* 78: 88–95.
- Abdollahi M. 2012. Effect of plant-derived smoke on germination, seedling vigour and growth of rapeseed (*Brassica napus*) under laboratory and greenhouse conditions. *Seed Science and Technology* 40: 437–442.
- Adamowski M, Friml J. 2015. PIN-dependent auxin transport: action, regulation, and evolution. *Plant Cell* 27: 20–32.
- Anders S, Pyl PT, Huber W. 2014. HTSeq – a Python framework to work with high-throughput sequencing data. *Bioinformatics* 31: 166–169.
- Baldwin IT, Morse L. 1994. Up in smoke 2. Germination of *Nicotiana attenuata* in response to smoke-derived cues and nutrients in burned and unburned soils. *Journal of Chemical Ecology* 20: 2373–2391.
- Baldwin IT, Staszakozinski L, Davidson R. 1994. Up in smoke 1. Smoke-derived germination cues for postfire annual, *Nicotiana attenuata* Torr ex Watson. *Journal of Chemical Ecology* 20: 2345–2371.
- Bendary E, Francis R, Ali H, Sarwat M, El Hady S. 2013. Antioxidant and structure–activity relationships (SARs) of some phenolic and anilines compounds. *Annals of Agricultural Sciences* 58: 173–181.
- Brouwer KS, van Valen T, Day DA, Lambers H. 1986. Hydroxamate-stimulated O_2 uptake in roots of *Pisum sativum* and *Zea mays*, mediated by a peroxidase its consequences for respiration measurements. *Plant Physiology* 82: 236–240.
- Carol RJ, Dolan L. 2006. The role of reactive oxygen species in cell growth: lessons from root hairs. *Journal of Experimental Botany* 57: 1829–1834.
- Cheung AY, Wu H-M. 2011. THESEUS 1, FERONIA and relatives: a family of cell wall-sensing receptor kinases? *Current Opinion in Plant Biology* 14: 632–641.
- Chumpookam J, Lin H-L, Shiesh C-C. 2012. Effect of smoke-water on seed germination and seedling growth of papaya (*Carica papaya* cv. Tainung No. 2). *Horticultural Science* 47: 741–744.
- Considine MJ, Maria Sandalio L, Foyer CH. 2015. Unravelling how plants benefit from ROS and NO reactions, while resisting oxidative stress PREFACE. *Annals of Botany* 116: 469–473.
- Dinneny JR, Benfey PN. 2008. Plant stem cell niches: standing the test of time. *Cell* 132: 553–557.
- Draelants D, Avitabile D, Vanroose W. 2015. Localized auxin peaks in concentration-based transport models of the shoot apical meristem. *Journal of The Royal Society Interface* 12: 20141407.
- Dunand C, Crèvecoeur M, Penel C. 2007. Distribution of superoxide and hydrogen peroxide in Arabidopsis root and their influence on root development: possible interaction with peroxidases. *New Phytologist* 174: 332–341.
- Flematti GR, Ghisalberti EL, Dixon KW, Trengove RD. 2004a. A compound from smoke that promotes seed germination. *Science* 305: 977.
- Flematti GR, Ghisalberti EL, Dixon KW, Trengove RD. 2004b. Molecular weight of a germination-enhancing compound in smoke. *Plant and Soil* 263: 1–4.

- Foreman J, Demidchik V, Bothwell JH, Mylona P, Miedema H, Torres MA, Linstead P, Costa S, Brownlee C, Jones JD. 2003. Reactive oxygen species produced by NADPH oxidase regulate plant cell growth. *Nature* 422: 442–446.
- Foyer CH, Noctor G. 2013. Redox signaling in plants. *Antioxidants and Redox Signaling* 18: 2087–2090.
- Fry SC, Dumville JC, Miller JG. 2001. Fingerprinting of polysaccharides attacked by hydroxyl radicals *in vitro* and in the cell walls of ripening pear fruit. *Biochemical Journal* 357: 729–737.
- Galinha C, Hofhuis H, Luijten M, Willemsen V, Blilou I, Scheres RHB. 2007. PLETHORA proteins as dose-dependent master regulators of Arabidopsis root development. *Nature* 449: 1053–1057.
- Gapper C, Dolan L. 2006. Control of plant development by reactive oxygen species. *Plant Physiology* 141: 341–345.
- Goodspeed TH. 1955. *The genus Nicotiana*. Waltham, MA, USA: Chronica Botanica Company.
- Grman E, Robinson TMP. 2013. Resource availability and imbalance affect plant–mycorrhizal interactions: a field test of three hypotheses. *Ecology* 94: 62–71.
- Haas BJ, Papanicolaou A, Yassour M, Grabherr M, Blood PD, Bowden J, Couger MB, Eccles D, Li B, Lieber M *et al.* 2013. De novo transcript sequence reconstruction from RNA-Seq: reference generation and analysis with Trinity. *Nature Protocols* 8: 1494–1512.
- He W, Brumos J, Li H, Ji Y, Ke M, Gong X, Zeng Q, Li W, Zhang X, An F. 2011. A small-molecule screen identifies L-kynurenine as a competitive inhibitor of TAA1/TAR activity in ethylene-directed auxin biosynthesis and root growth in Arabidopsis. *The Plant Cell* 23: 3944–3960.
- Jensen PJ, Hangarter RP, Estelle M. 1998. Auxin transport is required for hypocotyl elongation in light-grown but not dark-grown Arabidopsis. *Plant Physiology* 116: 455–462.
- Kärkönen A, Kuchitsu K. 2015. Reactive oxygen species in cell wall metabolism and development in plants. *Phytochemistry* 112: 22–32.
- Keeley SC, Pizzorno M. 1986. Charred wood stimulated germination of two fire-following herbs of the California chaparral and the role of hemicellulose. *American Journal of Botany* 73: 1289–1297.
- Kim JH, Lee Y, Kim EJ, Gu S, Sohn EJ, Seo YS, An HJ, Chang YS. 2014. Exposure of iron nanoparticles to *Arabidopsis thaliana* enhances root elongation by triggering cell wall loosening. *Environmental Science & Technology* 48: 3477–3485.
- Kim D, Pertege G, Trapnell C, Pimentel H, Kelley R, Salzberg SL. 2013. TopHat2: accurate alignment of transcriptomes in the presence of insertions, deletions and gene fusions. *Genome Biology* 14: 1–13.
- Kruegel T, Lim M, Gase K, Halitschke R, Baldwin IT. 2002. *Agrobacterium*-mediated transformation of *Nicotiana attenuata*, a model ecological expression system. *Chemoecology* 12: 177–183.
- Kulkarni M, Sparg S, Light M, Van Staden J. 2006. Stimulation of rice (*Oryza sativa* L.) seedling vigour by smoke-water and butenolide. *Journal of Agronomy and Crop Science* 192: 395–398.
- Li Y, Trush MA. 1998. Diphenyleneiodonium, an NAD (P) H oxidase inhibitor, also potentially inhibits mitochondrial reactive oxygen species production. *Biochemical and Biophysical Research Communications* 253: 295–299.
- Lindgreen S. 2012. AdapterRemoval: easy cleaning of next-generation sequencing reads. *BMC Research Notes* 5: 1–7.
- Lindner H, Mueller LM, Boisson-Dernier A, Grossniklaus U. 2012. CrRLK1L receptor-like kinases: not just another brick in the wall. *Current Opinion in Plant Biology* 15: 659–669.
- Ling Z, Zhou W, Baldwin IT, Xu S. 2015. Insect herbivory elicits genome-wide alternative splicing responses in *Nicotiana attenuata*. *Plant Journal* 84: 228–243.
- Liszkay A, van der Zalm E, Schopfer P. 2004. Production of reactive oxygen intermediates (O_2^- , H_2O_2 , and OH) by maize roots and their role in wall loosening and elongation growth. *Plant Physiology* 136: 3114–3123.
- Ljung K. 2013. Auxin metabolism and homeostasis during plant development. *Development* 140: 943–950.
- Maeda H. 2008. Which are you watching, an individual reactive oxygen species or total oxidative stress? *Annals of the New York Academy of Sciences* 1130: 149–156.
- Montazeri N, Oliveira AC, Himelbloom BH, Leigh MB, Crapo CA. 2013. Chemical characterization of commercial liquid smoke products. *Food Science and Nutrition* 1: 102–115.
- Nelson DC, Flematti GR, Ghisalberti EL, Dixon KW, Smith SM. 2012. Regulation of seed germination and seedling growth by chemical signals from burning vegetation. *Plant Biology* 63: 107–130.
- Nelson DC, Riseborough JA, Flematti GR, Stevens J, Ghisalberti EL, Dixon KW, Smith SM. 2009. Karrikins discovered in smoke trigger Arabidopsis seed germination by a mechanism requiring gibberellic acid synthesis and light. *Plant Physiology* 149: 863–873.
- Nguema-Ona E, Vire-Gibouin M, Gotte M, Plancot B, Lerouge P, Bardor M, Driouch A. 2014. Cell wall O-glycoproteins and N-glycoproteins: aspects of biosynthesis and function. *Frontiers in Plant Science* 5: 12.
- Nishimura T, Ki Hayashi, Suzuki H, Gyohda A, Takaoka C, Sakaguchi Y, Matsumoto S, Kasahara H, Sakai T, Ji Kato. 2014. Yucasin is a potent inhibitor of YUCCA, a key enzyme in auxin biosynthesis. *Plant Journal* 77: 352–366.
- Passardi F, Longet D, Penel C, Dunand C. 2004a. The class III peroxidase multigenic in land plants family in rice and its evolution. *Phytochemistry* 65: 1879–1893.
- Passardi F, Penel C, Dunand C. 2004b. Performing the paradoxical: how plant peroxidases modify the cell wall. *Trends in Plant Science* 9: 534–540.
- Peng Q, Wang H, Tong J, Kabir MH, Huang Z, Xiao L. 2013. Effects of indole-3-acetic acid and auxin transport inhibitor on auxin distribution and development of peanut at pegging stage. *Scientia Horticulturae* 162: 76–81.
- Perrot-Rechenmann C. 2013. *Auxin signaling in primary roots*. Boca Raton, FL, USA: CRC Press.
- Petriccione M, Forte V, Valente D, Ciniglia C. 2013. DNA integrity of onion root cells under catechol influence. *Environmental Science and Pollution Research* 20: 4859–4871.
- Petriccia JJ, Winter CM, Benfey PN. 2012. Control of Arabidopsis root development. *Annual Review of Plant Biology* 63: 563.
- Petrov VD, Van Breusegem F. 2012. Hydrogen peroxide – a central hub for information flow in plant cells. *AoB Plants* 2012: pls014.
- Pitts RJ, Cernac A, Estelle M. 1998. Auxin and ethylene promote root hair elongation in Arabidopsis. *Plant Journal* 16: 553–560.
- Preston CA, Baldwin IT. 1999. Positive and negative signals regulate germination in the post-fire annual, *Nicotiana attenuata*. *Ecology* 80: 481–494.
- Price NJ, Pinheiro C, Soares CM, Ashford DA, Ricardo CP, Jackson PA. 2003. A biochemical and molecular characterization of LEP1, an extensin peroxidase from lupin. *Journal of Biological Chemistry* 278: 41389–41399.
- Rahman A, Bannigan A, Sulaman W, Pechter P, Blancaflor EB, Baskin TI. 2007. Auxin, actin and growth of the *Arabidopsis thaliana* primary root. *Plant Journal* 50: 514–528.
- Raya-González J, Ortiz-Castro R, Ruiz-Herrera LF, Kazan K, López-Bucio J. 2014. PHYTOCHROME AND FLOWERING TIME1/MEDIATOR25 regulates lateral root formation via auxin signaling in Arabidopsis. *Plant Physiology* 165: 880–894.
- Ringli C. 2010. The hydroxyproline-rich glycoprotein domain of the Arabidopsis LRX1 requires Tyr for function but not for insolubilization in the cell wall. *Plant Journal* 63: 662–669.
- Rodríguez-Sanz H, Solís M-T, López M-F, Gómez-Cadenas A, Risueño MC, Testillano PS. 2015. Auxin biosynthesis, accumulation, action and transport are involved in stress-induced microspore embryogenesis initiation and progression in *Brassica napus*. *Plant and Cell Physiology* 56: 1401–1417.
- Rundel P. 1981. Fire as an ecological factor. In: Lange OL, Nobel BS, Osmond CB, Ziegler H, eds. *Physiological plant ecology*, vol. 12. A of the series Encyclopedia of Plant Physiology. Berlin: Springer, 501–538.
- Sabatini S, Beis D, Wolkenfelt H, Murfett J, Guilfoyle T, Malamy J, Benfey P, Leyser O, Bechtold N, Weisbeek P *et al.* 1999. An auxin-dependent distal organizer of pattern and polarity in the Arabidopsis root. *Cell* 99: 463–472.
- Sauer M, Robert S, Kleine-Vehn J. 2013. Auxin: simply complicated. *Journal of Experimental Botany* 64: 2565–2577.
- Schaefer M, Bruttig C, Baldwin IT, Kallenbach M. 2016. High-throughput quantification of more than 100 primary- and secondary-metabolites, and

- phytohormones by a single solid-phase extraction based sample preparation with analysis by UHPLC-HESI-MS/MS. *Plant Methods* 12: 30.
- Schmidt R, Schippers JH. 2015. ROS-mediated redox signaling during cell differentiation in plants. *Biochimica et Biophysica Acta* 1850: 1497–1508.
- Schopfer P. 1994. Histochemical demonstration and localization of H₂O₂ in organs of higher plants by tissue printing on nitrocellulose paper. *Plant Physiology* 104: 1269–1275.
- Schopfer P. 2001. Hydroxyl radical-induced cell-wall loosening in vitro and *in vivo*: implications for the control of elongation growth. *Plant Journal* 28: 679–688.
- Schweigert N, Zehnder AJB, Eggen RIL. 2001. Chemical properties of catechols and their molecular modes of toxic action in cells, from microorganisms to mammals. *Environmental Microbiology* 3: 81–91.
- Soós V, Sebestyén E, Juhász A, Pintér J, Light ME, Van Staden J, Balázs E. 2009. Stress-related genes define essential steps in the response of maize seedlings to smoke-water. *Functional and Integrative Genomics* 9: 231–242.
- Sundaravelpandian K, Chandrika NNP, Schmidt W. 2013. PFT1, a transcriptional mediator complex subunit, controls root hair differentiation through reactive oxygen species (ROS) distribution in Arabidopsis. *New Phytologist* 197: 151–161.
- Takeda S, Gapper C, Kaya H, Bell E, Kuchitsu K, Dolan L. 2008. Local positive feedback regulation determines cell shape in root hair cells. *Science* 319: 1241–1244.
- Taylor J, Van Staden J. 1998. Plant-derived smoke solutions stimulate the growth of *Lycopersicon esculentum* roots in vitro. *Plant Growth Regulation* 26: 77–83.
- Tenhaken R. 2014. Cell wall remodeling under abiotic stress. *Frontiers in Plant Science* 5: 771.
- Tian Q, Uhlir NJ, Reed JW. 2002. Arabidopsis SHY2/IAA3 inhibits auxin-regulated gene expression. *Plant Cell* 14: 301–319.
- Trewavas A. 2014. *Plant behaviour and intelligence*. Oxford, UK: Oxford University Press.
- Tromas A, Perrot-Rechenmann C. 2010. Recent progress in auxin biology. *Comptes Rendus Biologies* 333: 297–306.
- Tsukagoshi H. 2016. Control of root growth and development by reactive oxygen species. *Current Opinion in Plant Biology* 29: 57–63.
- Tsukagoshi H, Busch W, Benfey PN. 2010. Transcriptional regulation of ROS controls transition from proliferation to differentiation in the root. *Cell* 143: 606–616.
- Velasquez SM, Ricardi MM, Dorosz JG, Fernandez PV, Nadra AD, Pol-Fachin L, Egelund J, Gille S, Harholt J, Ciancia M *et al.* 2011. O-Glycosylated cell wall proteins are essential in root hair growth. *Science* 332: 1401–1403.
- Wolf S, Hematy K, Hofte H. 2012. Growth control and cell wall signaling in plants. *Annual Review of Plant Biology* 63: 381–407.
- Xiong J, Yang YJ, Fu GF, Tao LX. 2015. Novel roles of hydrogen peroxide (H₂O₂) in regulating pectin synthesis and demethylesterification in the cell wall of rice (*Oryza sativa*) root tips. *New Phytologist* 206: 118–126.
- Yang J, Cohen Stuart MA, Kamperman M. 2014. Jack of all trades: versatile catechol crosslinking mechanisms. *Chemical Society Reviews* 43: 8271–8298.
- Zhao Y. 2010. Auxin biosynthesis and its role in plant development. *Annual Review of Plant Biology* 61: 49.
- Zhou ZY, Zhang CG, Wu L, Zhang CG, Chai J, Wang M, Jha A, Jia PF, Cui SJ, Yang M *et al.* 2011. Functional characterization of the *CKRC1/TAA1* gene and dissection of hormonal actions in the Arabidopsis root. *Plant Journal* 66: 516–527.

Supporting Information

Additional Supporting Information may be found online in the Supporting Information tab for this article:

Fig. S1 Treatment with karrikin1 (KAR1) increases *Nicotiana attenuata* seed germination and decreases hypocotyl elongation, but does not induce changes in primary root length.

Fig. S2 Scheme of the meristem zone of *Nicotiana attenuata* roots and longitudinal elongation of cells in the elongation zone induced by smoke.

Fig. S3 Root hair phenotype induced by SPE elutions.

Fig. S4 Root phenotyping in response to different amounts of catechol.

Fig. S5 Comparison of the catechol-induced root phenotype induced by structurally similar di-hydroxy/-methoxy phenolics.

Fig. S6 Hierarchical clustering and functional enrichment analysis of differentially expressed genes (DEGs) in *Nicotiana attenuata* roots after treatment with SPE-fraction S2.

Fig. S7 Real-time auxin response monitoring (DII-VENUS, *Arabidopsis*) indicates increased auxin level after smoke and active fraction S2 incubation within 90 min.

Methods S1 Fractionation of liquid smoke and quantification of catechol.

Table S1 List of differentially expressed genes (DEG) identified by RNAseq.

Please note: Wiley Blackwell are not responsible for the content or functionality of any Supporting Information supplied by the authors. Any queries (other than missing material) should be directed to the *New Phytologist* Central Office.

New Phytologist Supporting Information

Article title: **Catechol, a major component of smoke, influences primary root growth and root hair elongation through ROS-mediated redox signaling**

Authors: Ming Wang, Matthias Schoettner, Shuqing Xu, Christian Paetz, Julia Wilde, Ian T. Baldwin, Karin Groten

Article acceptance date: 29 September 2016

The following Supporting Information is available for this article:

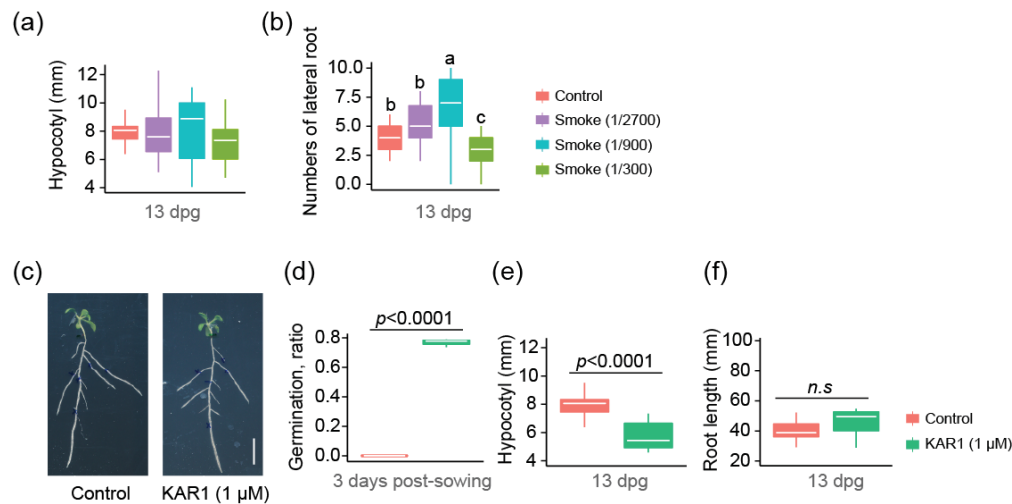


Fig. S1 Treatment with karrikin1 (KAR1) increases *N. attenuata* seed germination and decreases hypocotyl elongation, but does not induce changes in primary root length.

(a)-(b) The number of lateral roots was significantly increased by smoke treatment, while hypocotyl length did not change. Seedlings for measurements were the same as those described in Fig. 1. Different letters indicate significant differences, $p \leq 0.05$, one-way ANOVA followed by Tukey's HSD. Cross-bars in the box plots represent the median ($n=6$, for each biological replicate 25-30 seedlings per Petri dish were measured). (c) Morphology of seedlings treated by KAR1 (1 μ M), scale bar, 0.5 mm. (d) Positive effect of KAR1 treatment on seed germination ($n=3$, for each biological replicate 30 seeds per pot were analyzed 3 days after sowing). (e) Negative effect of KAR1 treatment on hypocotyl elongation. (f) No significant differences were observed in primary root elongation after KAR1 treatment compared to controls. (d)-(f) Student's *t*-test. *N. attenuata* seedlings were germinated on GB5 media containing KAR1 (1 μ M) or different doses of liquid smoke. Scans were taken 13 dpg for measurements.

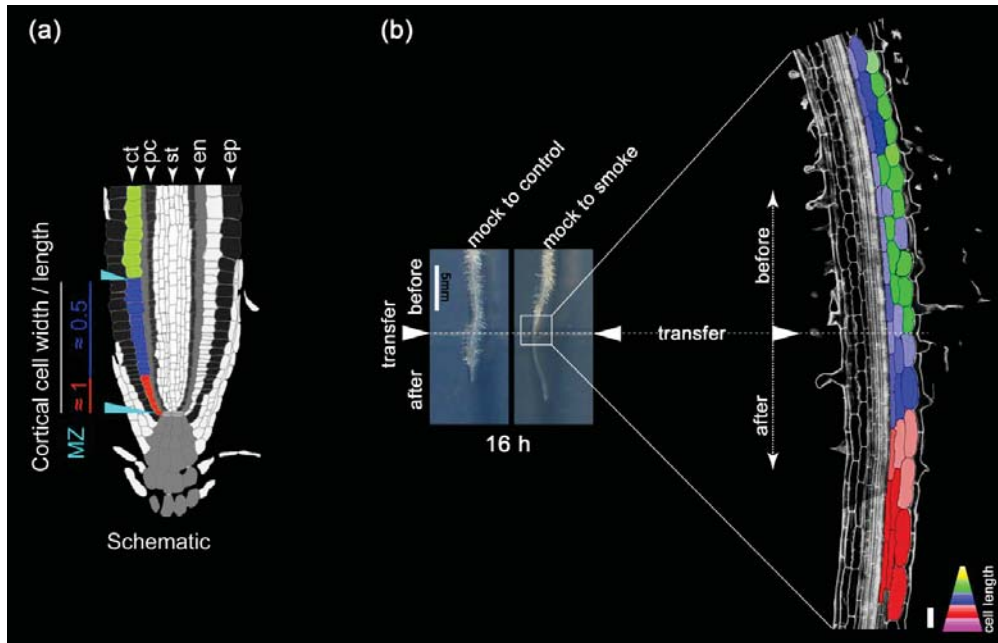


Fig. S2 Scheme of the meristem zone of *N. attenuata* roots and longitudinal elongation of cells in the elongation zone induced by smoke.

(a) Schematic presentation of width to length (w/l) ratio progression of cortex cell development in an *N. attenuata* root meristem zone (MZ), with the developing stem cell daughters in red (w/l ≈ 1.0) and intensive division zone in blue (w/l ≈ 0.5). Cells in both red and blue as MZ cells were counted (ep: epidermis, ct: cortex, en: endodermis, pc: pericycle, st: stele). (b) Root morphology after short-term application of smoke. Seedlings (5 dpv) were transferred from mock GB5 media to media containing liquid smoke (V:V = 1:900) for 16 h. Scale bar, 5 mm. Imaging by confocal LSM 510 (ZEISS) of roots before and after smoke-treatment stained with propidium iodide to visualize the cell walls. The color codes indicate the lengths of cells. 12-15 seedlings were tested, the experiment was repeated twice. Scale bar, 50 μ m.

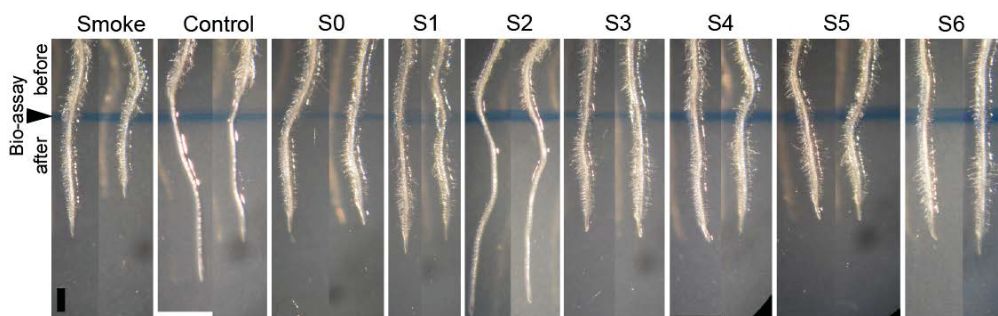


Fig. S3 Root hair phenotype induced by SPE elutions. Same set-up as described in Fig. 2(a), but additional replicates are shown. Scale bar, 1 mm.

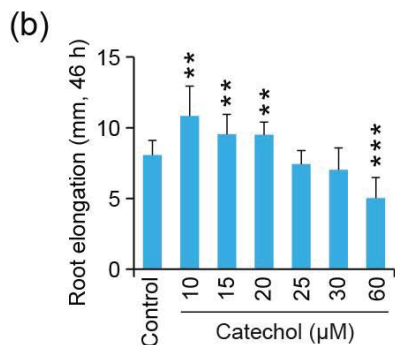
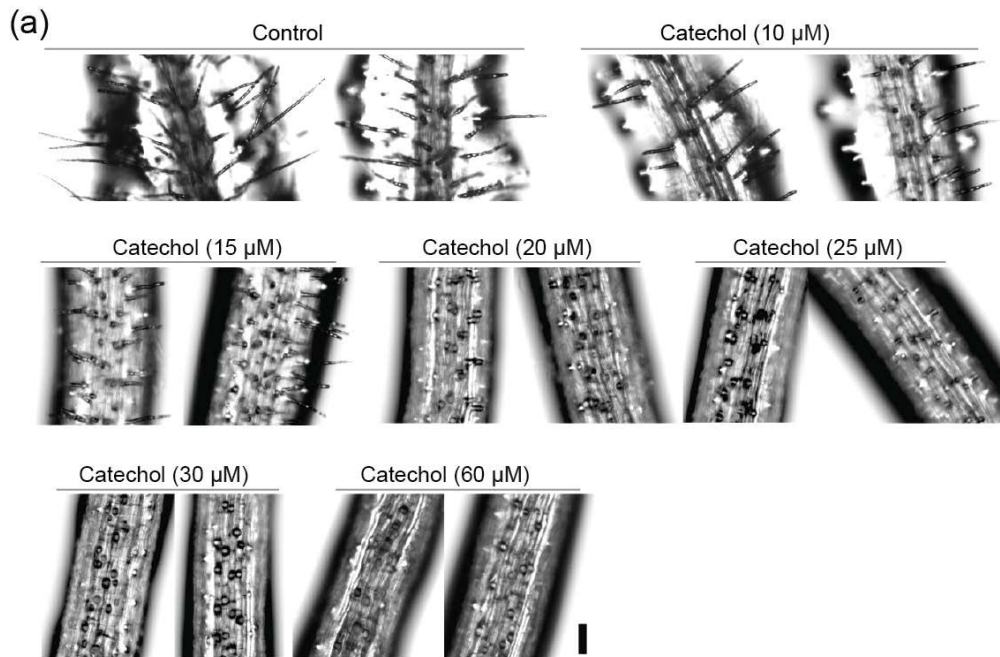


Fig. S4 Root phenotyping in response to different amounts of catechol. (a) Root hair phenotype 46 h after catechol incubation. At concentrations higher than 15 μ M, root hair elongation was strongly impaired. Scale bar, 100 μ m. (b) Primary root elongation induced by catechol treatment is concentration dependent. Seedlings (5 dpv) were transferred to catechol supplemented media for 46 h. Images were taken by ApoTome microscopy (ZEISS) for root hair phenotyping (8-10 seedlings were observed) and for root elongation measurements by desktop scanner (data are means \pm SD ($n=3$, for each biological replicate, 6-8 seedlings per Petri

dish were measured). Significant differences relative to the control group are indicated by asterisks (Student's *t*-test, ** $p \leq 0.01$, *** $p \leq 0.001$).

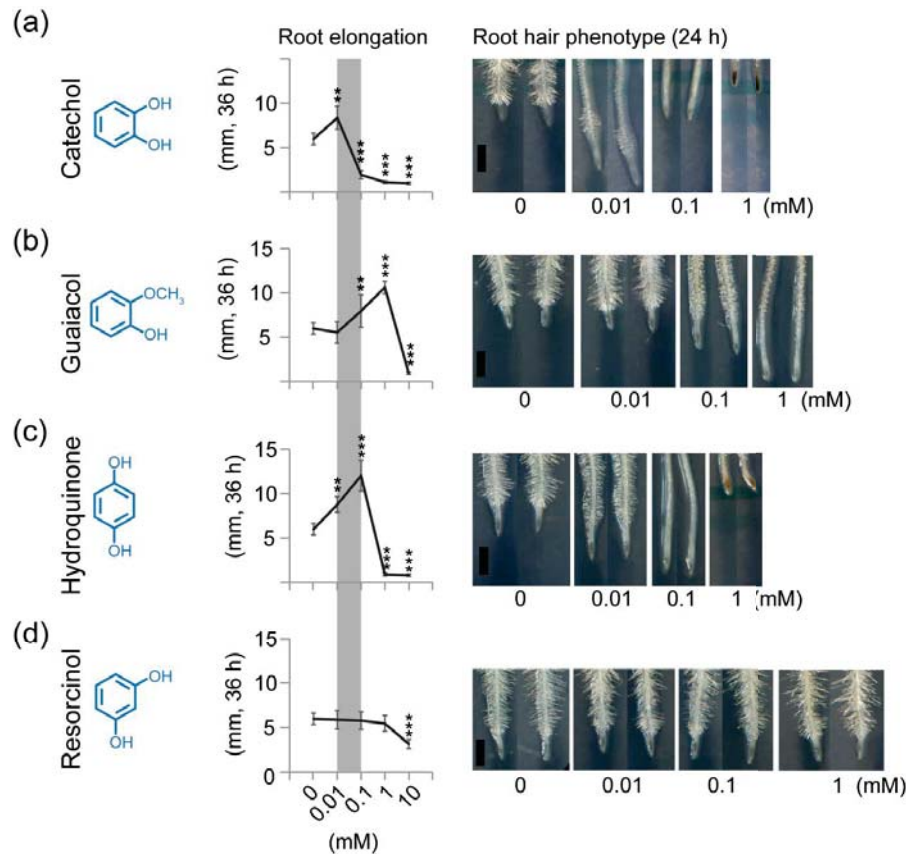


Fig. S5 Comparison of the catechol-induced root phenotype induced by structurally similar dihydroxy/-methoxy phenolics.

(a)-(d) Structurally related compounds of catechol, including resorcinol, guaiacol and hydroquinone, were tested for root elongation measurements (36 h) and root hair phenotyping (24 h). Catechol is the most active compound used to decrease root hair elongation (0.01 mM) and abolish root elongation (0.1 mM) among tested substances. Seedlings (5 dpv) were transferred from mock media to media supplemented with different concentrations of catechol (a), guaiacol (b), hydroquinone (c) and resorcinol (d). For root elongation measurements, data are means \pm SD ($n=6$, for each replicate 6-10 seedlings per Petri dish were measured). Significant differences relative to the control group are indicated by asterisks (Student's *t*-test, ** $p \leq 0.01$, *** $p \leq 0.001$). Scale bars, 1 mm.

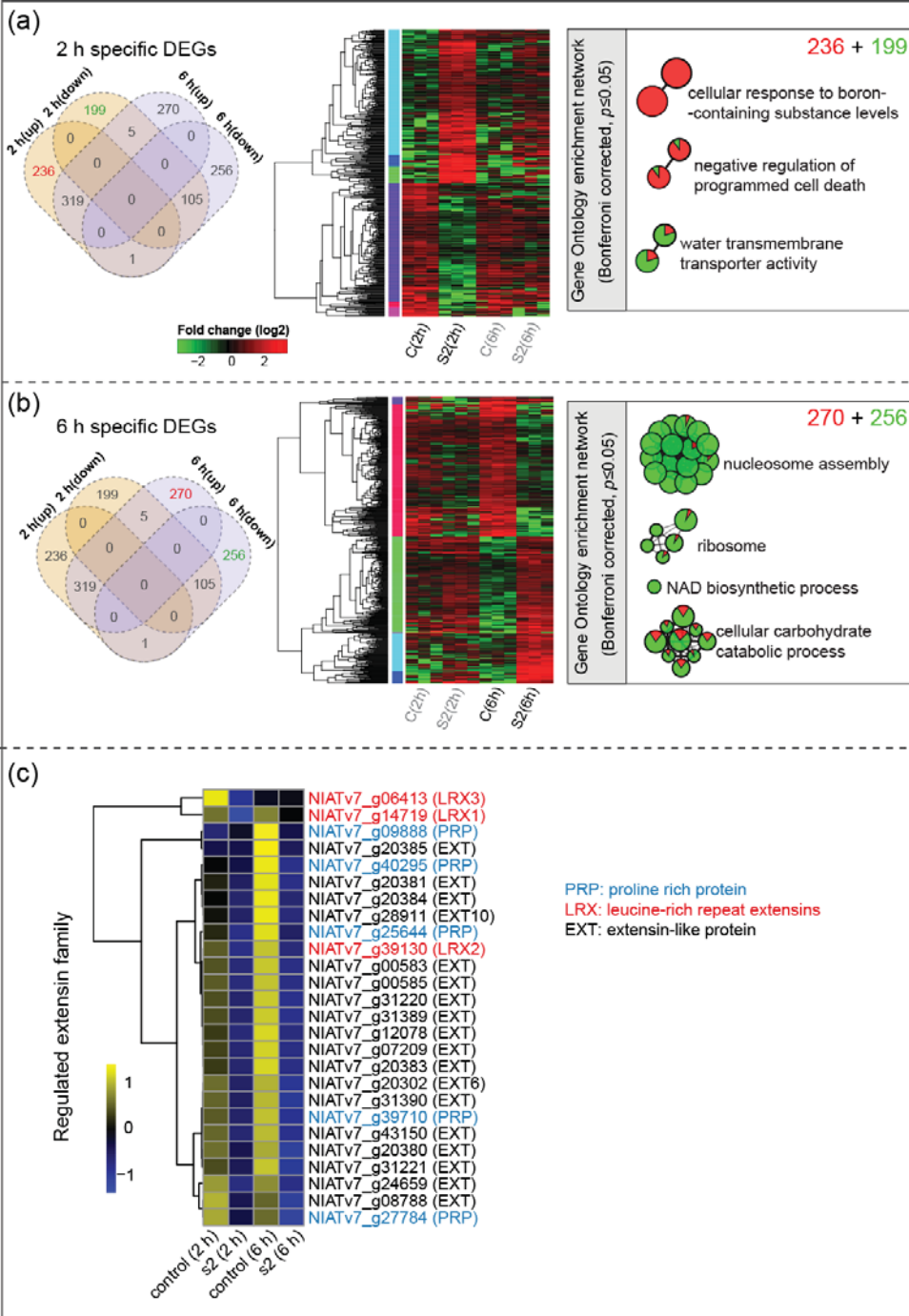


Fig.

S6 Hierarchical clustering and functional enrichment analysis of differentially expressed genes (DEGs) in *N. attenuata* roots after treatment with SPE-fraction S2.

The same analysis was performed as described in Fig. 4 ($|\log_2FC| > 1$, $FDR \leq 0.05$), but only the DEGs specifically regulated at either 2 h (a) or 6 h (b) are shown. Gene ontology (GO) enrichment analysis of the 1391 DEGs was computed with CluoGO according to the GO categories “Biological Process” and “Molecular Function” (two-sided hypergeometric test, Bonferroni corrected, $p \leq 0.05$). DEGs of 2 h with functions in programmed cell death were specifically enriched. Only 6 h after treatment, DEGs were mainly down-regulated and related to general cell functions.

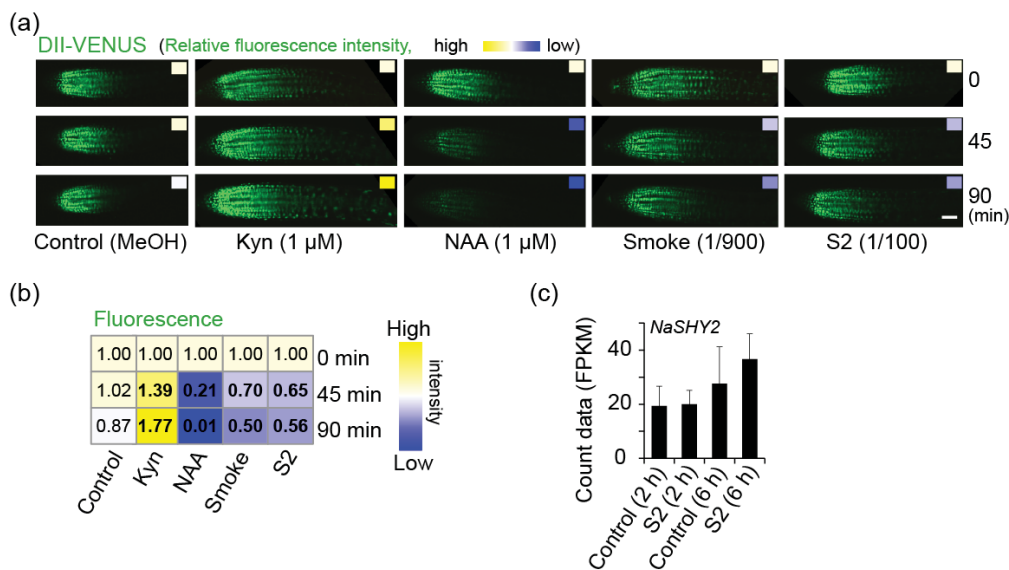


Fig. S7 Real-time auxin response monitoring (DII-VENUS, *Arabidopsis*) indicates increased auxin level after smoke and active fraction S2 incubation within 90 min.

DII-VENUS reporter line (*Arabidopsis*) was tested to monitor auxin response in a real time course after different treatments. (a) After the application of auxin biosynthesis inhibitor (L-kynurenine) and synthetic auxin (NAA), fluorescence strongly increased and decreased, respectively. Both liquid smoke and active SPE elution S2 slightly increased auxin level shown by decreased fluorescence intensity. Seedlings were scanned every 45 min for 90 min to follow the DII-VENUS signal, immediately after the beginning of treatment. Imaging was conducted by LSM-510 laser-scanning confocal microscope (Zeiss). Scale bar, 50 µm. To quantify fluorescence in the root tips, the average fluorescence intensity over the identical scanned portion of the root was extracted by ImageJ software. (b) All of the exported values of fluorescence intensity were visualized by heatmap using R. The values in the boxes and filled color codes indicate relative fluorescence intensities. The values in black bold indicate significant differences relative to the first time-point (0 min) (Student's *t*-test, $p \leq 0.05$). For each treatment, 4-6 seedlings were analyzed and the experiment was repeated twice. (c) *NaSHY2* expression profile

in *N. attenuata* seedlings. Data are normalized FPKM (Fragments per Kilobase Million) extracted from RNA-seq (means \pm SD, $n=3$).

Table S1 Provided as separate excel file

Methods S1 Extraction, fractionation of liquid smoke and quantification of catechol

Solid phase extraction (SPE, Multi 96 HR-XC (96 x 25 mg) column, Macherey-Nagel, <http://www.mn-net.com/>) was used as the first step of liquid smoke fractionation to isolate the active compound. In brief, 0.8 mL undiluted liquid smoke was loaded onto an activated column and flow-through was collected as S0, then successively eluted with 1 mL each of 1 M HCOOH, 80% methanol in HCOOH, 100% methanol, 0.35 M NH₄OH, 0.35 M NH₄OH in 60% methanol and 2 M NH₄OH in acetone. At each step the eluted flow-through was collected and desiccated as S0-S6 fractions and dissolved in methanol, and the obtained fractions were used for further bioassays and HPLC fractionation. The concentrated active S2 fraction was subjected to further fractionation using a reverse-phase HPLC (Luna C-18 (2), 250 \times 10 mm; Phenomenex) at a 3-mL min⁻¹ flow rate. The following binary gradient was used: Solvent A: millipore water (from Millipore model Milli-Q Advantage A10) and solvent B: HPLC grade methanol (Fluka, www.sigmaaldrich.com/germany.html). The details of Chromatographic solvent gradients were, from 0 to 5 min isocratic 15% of B, from 5 to 40 min linear gradient to 30% of B and from 40 to 45 min linear gradient to 100% of B. “d3” and “d4” were collected from fraction “d” (26 min and 26.5 min, respectively). These purified fractions were further profiled using a Dionex UltiMate 3000 RS (U)-HPLC system (Thermo Scientific, Waltham, MA, USA) equipped with a Thermo Scientific Acclaim RP-18 column 2.2 μ m, 120Å, 2.1x150 mm. The following binary gradient was applied for HPLC fractionation: 0 to 0.5 min isocratic 1% A (millipore water, 0.1% [v/v] acetonitrile [HPLC LC-MS grade, VWR, <https://de.vwr.com/>, Germany], and 0.05% formic acid), 5% B (acetonitrile and 0.05% formic acid); 0.5 to 3.5 min linear gradient to 15% B; 3.5 to 30.5 min linear gradient to 30% B; 30.5 to 36min linear gradient to 99% B with a flow rate of 400 μ L/min. Eluted compounds were detected by a Micro-ToF (Time of Flight) mass spectrometer (Bruker Daltonik, Bremen, Germany) equipped with an electrospray ionization source in a negative ionization mode. Instrument settings were as follows: capillary voltage, 4500 V; capillary exit, 130 V; dry gas temperature, 200°C; dry gas flow, 10 L/min. Ions were detected from m/z 50 to

1400 at a repetition rate of 2 Hz. Mass calibration was performed using sodium formate clusters (10 mM solution of NaOH in 50/50% v/v isopropanol/water containing 0.2% formic acid).

To quantify catechol levels in liquid smoke, S2 fraction and burnt soil, compounds were detected by UHPLC-ESI/qTOF mass spectrometer (Bruker Daltonik, Bremen, Germany) and analyzed using the method described above. Different concentrations of catechol were measured for a standard curve, and the content of catechol calculated was based on a comparison with the peak areas of the standard curve.

Manuscript II:

***Nicotiana attenuata*'s capacity to interact with arbuscular mycorrhiza alters its competitive ability and elicits major changes in the leaf transcriptome**

Ming Wang, Julia Wilde, Ian T. Baldwin and Karin Groten

Published in *Journal of Integrative Plant Biology* (2017)

doi: 10.1111/jipb.12609

Nicotiana attenuata's capacity to interact with arbuscular mycorrhiza alters its competitive ability and elicits major changes in the leaf transcriptome^{FA}

Ming Wang, Julia Wilde, Ian T. Baldwin and Karin Groten*

Department of Molecular Ecology, Max Planck Institute for Chemical Ecology, Hans-Knöll-Str. 8, Jena 07745, Germany

*Correspondence: Karin Groten (kgroten@ice.mpg.de)

doi: 10.1111/jipb.12609

High-Impact Article

Abstract To study the local and systemic effects of arbuscular mycorrhizal fungal (AMF) colonization, *Nicotiana attenuata* plants impaired in their interactions with AMF due to silencing of a calcium- and calmodulin dependent protein kinase (inverted repeat (ir)CCaMK) were grown competitively in pairs with empty vector (EV) plants, with and without two different types of inoculum. When inoculated, EV plants strongly outperformed irCCaMK plants. Foliar transcript profiling revealed that AMF colonization significantly changed gene expression of P-starvation and -transporter genes in irCCaMK plants. The Pht1 family phosphate transporter NaPT5 was not only specifically induced in roots after AMF colonization, but also in leaves of AMF-colonized irCCaMK plants, and in plants grown under low Pi conditions in the

absence of AMF. The P-starvation signature of inoculated irCCaMK plants corresponded with increases in selected amino acids and phenolic compounds in leaves. We also found a strong AMF-induced increase in amino acids and phenolic metabolites in roots. Plants impaired in their interactions with AMF clearly have a fitness disadvantage when competing for limited soil nutrients with a fully functional isogenic line. The additional role of the AMF-induced Pht1 family transporter NaPT5 in leaves under P-starvation conditions will require further experiments to fully resolve.

Edited by: William J. Lucas, University of California, Davis, USA
Received Oct. 17, 2017; **Accepted** Oct. 27, 2017; **Online on** Oct. 31, 2017

FA: Free Access

INTRODUCTION

The formation of arbuscular mycorrhizae, a symbiotic association of plants with soil fungi of the phylum Glomeromycota, can be found throughout terrestrial ecosystems (Smith and Read 2008) and has been dated to 400 million years ago when plants started to colonize land (Redecker et al. 2000). Arbuscular mycorrhizal fungi (AMF) are known to alter root morphology and increase the absorption surface in the soil, improving water and nutrient acquisition of plants, especially when these factors limit growth. AMF colonization elicits differential gene expression in roots and these have been extensively described for many species where many are conserved responses to AMF colonization (Guimil et al. 2005; Liu et al. 2007; Fiorilli et al. 2009;

Guether et al. 2009; Hogekamp and Kuester 2013; Groten et al. 2015b). A few large-scale gene expression studies have also investigated the systemic effects of AMF colonization that occurs in shoots (Guimil et al. 2005; Kogel et al. 2010; Cervantes-Gamez et al. 2016). However, there appears to be little conservation of the differentially expressed genes (DEGs) in leaves of AMF colonized and non-colonized plants among the different studies that have examined this question (Liu et al. 2007; Fiorilli et al. 2009). Further studies focused on root and foliar changes in metabolite levels after AMF colonization, and found changes in particular amino acids, carbohydrates and organic acids (Kogel et al. 2010; Fester et al. 2011; Schweiger et al. 2014).

Plants have a high demand in phosphorus for metabolism and overall development, yet the mobility

Free Access

and availability of inorganic phosphate (P_i) in the soil is low (Marschner 1996). The P-starvation response is well-characterized in plants and includes an increase in the root-to-shoot biomass ratio, root hair elongation, anthocyanin accumulation, increased foliar levels of free amino acids and other soluble nitrogenous compounds, lipid remodeling, and expression of many Pi starvation-induced (PSI) genes such as *MGDG3*, *PHO1*, *H1*, and *SPX3* (Chiou and Lin 2011; Schlueter et al. 2013; Gu et al. 2016).

The formation of arbuscular mycorrhizae can greatly enhance the P nutrition of plants, and in exchange for P, plants provide 4 to 20% of their photosynthates to the fungal partner (Jakobsen and Rosendahl 1990; Douds et al. 2000; Bonfante and Genre 2010; Smith et al. 2011). The AMF-related Pi uptake (indirect Pi uptake pathway) happens via the fungal hyphae and arbuscules, and has been shown to contribute up to 90%–100% to the plants' P requirements (Smith et al. 2004; Bucher 2007). In the direct pathway, P_i is directly taken up across the root-soil interface (Bucher 2007). The two pathways are tightly regulated, and depend on, among other factors, the availability of Pi and nitrogen in the soil (Nagy et al. 2009; Balzergue et al. 2011; Nouri et al. 2014). Under high soil Pi conditions, root AMF colonization is reduced; and in the presence of AMF, the direct Pi pathway is reduced or deactivated (Smith et al. 2011). Both pathways rely on the expression of phosphate transporter (PT) genes belonging to the phosphate transporter 1 (Pht1) family; these are either expressed in epidermal cells and root hairs or in cortical cells along the periarbuscular membrane, which surrounds the main sites of nutrient exchange between the plant and its fungal partner, the arbuscule (Daram et al. 1998; Rausch et al. 2001). The Pht1 family consists of 9–13 genes depending on the species examined. Most of the mycorrhizal-specific PTs belong to the family of active H^+/P_i symporters (Karandashov and Bucher 2005; Nagy et al. 2005; Bucher 2007) and have been identified for di-, as well as for monocots (Kai et al. 2002; Paszkowski et al. 2002; Karandashov et al. 2004; Nagy et al. 2005; Chen et al. 2007; Tamura et al. 2012). *PT4* and *PT5* in Solanaceous species, as well as their paralogs in other species, are in roots only expressed in cells containing arbuscules, while *PT3* is constitutively expressed in roots, but induced during symbiosis with AMF (Bucher 2007; Tan et al. 2012; Chen et al. 2014). Interestingly, recently it was demonstrated that Pht1 family member *PT4* in

Medicago and *Lotus* is not only specifically induced by AMF, but also in root tips under Pi starvation, under conditions that are independent of AMF colonization (Volpe et al. 2016). Thus, mycorrhizae-specific PT genes may play additional functions than previously thought.

In nature, plants interact with many different fungal and bacterial partners, who in turn interact with many different plants, to form belowground networks linking together plants of the same or different plant species (Lehmann et al. 2012; Merrild et al. 2013). The identity of the plant and fungal partners has been shown to alter competitive interactions among plants, changing growth and fitness outcomes (van der Heijden and Horton 2009; Walder et al. 2012; Wu et al. 2015; Yang et al. 2015). Similarly, plants of the same species grown in pairs, revealed that in the presence of some fungal species, genotypes with a lower capacity to interact with a fungus produced less biomass and received less Pi in comparison to their better interacting competitor (Facelli et al. 2010; Willmann et al. 2013; Facelli et al. 2014). However, the roles of the direct and indirect Pi uptake pathways in terms of PT gene expression remain unclear, and an in-depth analysis of the foliar changes in gene expression and metabolites (amino acids, phenolic compounds) of plants competing for the same limited amount of nutrients remains to be done.

The majority of the relevant molecular-ecological studies have been conducted either with crop plants such as rice, maize and tomato (Willmann et al. 2013; Gerlach et al. 2015; Jeong et al. 2015) or with legumes which not only associate with AMF but also with nitrogen-fixing bacteria (Harrison et al. 2002; Parniske 2008; Gutjahr and Parniske 2013). These additional relationships of legumes may confound the effects of AMF, as it is well known that nitrogen nutrition affects P nutrition and vice versa, and the third partner (plant, AMF, rhizobia) may also change the distribution of carbohydrate rewards (Wang et al. 2011). Investigations of wild plant species and their native fungal partner are few, but are essential if we are to evaluate our current understanding of plant AMF interactions in natural systems.

Here, we used *Nicotiana attenuata*, an annual plant native to the Great Basin Desert in North America. This fire-chasing annual plant shows synchronized mass germination from long-lived dormant seed-banks and monocultural growth with high intra-specific competition after fires in its native habitat (Baldwin and Morse

1994; Baldwin et al. 1994). An RNAi line, silenced in the expression of its calcium- and calmodulin-dependent protein kinase (inverted repeat (ir)CCaMK), a key enzyme facilitating the interaction with AMF, does not show arbuscule formation when grown in the field in native habitats and the glasshouse, and when grown in single pots, develops in a manner indistinguishable from wild type plants (Groten et al. 2015a), a prerequisite for comparative studies (Rillig et al. 2008). Many additional genes (e.g. SYMRK, CASTOR, POLLUX, NUP85, NUP133, CYCLOPS, NENA and Vapyrin) have been shown to be required for root colonization by AMF, and also for the root-nodule symbiosis with rhizobia in *Lotus japonicus* or in *Medicago truncatula* (Kistner et al. 2005; Tan et al. 2013). Mutants in these are impaired at different stages of development, and we selected CCaMK for RNAi because when the expression of this gene is silenced, hyphal growth is arrested in the epidermis and arbuscules fail to develop (Levy et al. 2004; Banba et al. 2008; Gutjahr et al. 2008).

The aim of this work was: (i) to investigate systemic changes in gene expression due to AMF colonization using an AMF inoculum native to the plant's native habitat; (ii) to determine the effects of AMF associations on plant competition; and (iii) to evaluate the regulation of direct and indirect phosphate transporter genes in *N. attenuata*. To address these objectives, we performed comparative whole-transcriptome profiling with 60k oligomicroarrays using two transgenic *N. attenuata* lines, empty vector (EV) plants capable of, and irCCaMK plants, impaired in AMF colonization grown under controlled, but competitive and P-limited conditions with a field-collected mycorrhizal mixture (native inoculum), and compared the results using the same experimental set-up but with a commercial *Rhizophagus irregularis* inoculum.

RESULTS

Roots grown in field mycorrhizal inoculum are colonized by *Funelliformis mossae* and *Rhizophagus irregularis*

In order to mimic natural intraspecific competition and AMF colonization, EV and irCCaMK plants were grown in competition with two different inocula, a native inoculum based on soil collected in the plant's natural habitat in Utah, USA (field mycorrhizal mixture,

FMM) and a commercial *Rhizophagus irregularis* inoculum, both under growth-limiting phosphate conditions (Figure 1). AMF communities of the FMM were characterized by amplifying a part of the 18S rDNA using a nested PCR approach. The most abundant species colonizing *N. attenuata* roots were identified as *F. mosseae* and *R. irregularis* (Figure 1) with strains related to *Rhizophagus* dominating the community. This composition of fungal species is similar to that reported from field grown-plants from the same soil in the plant's native habitat (Groten et al. 2015a), and hence mimics natural conditions well.

AMF inoculation increases growth disparities between EV and irCCaMK plants when grown in competition

When EV and irCCaMK plants competed for the same limited amount of nutrients in their shared pot without AMF inoculation, growth of the non-inoculated irCCaMK plants was similar (*R. irr.* -) or slightly attenuated compared to EV (FMM-). However, when AMF inoculated, irCCaMK plants were severely attenuated in their growth and this attenuation was independent of inoculum type, particularly for stalk elongation (Figure 2). The differences in stalk height between EV and irCCaMK plants were almost doubled when plants were associating with either of the two inocula types.

We used the known mycorrhizae-specific phosphate transporters, *NaPT4* and *NaPT5*, as markers of arbuscule colonization (Chen et al. 2007; Tan et al. 2012; Groten et al. 2015b). Their transcript abundance was strongly increased in response to inoculation in roots of both genotypes, though, the expression of this transporter was significantly higher (2–3 fold) in inoculated EV roots than in irCCaMK roots (Figure 2). The analysis of root colonization after staining revealed that irCCaMK plants also showed all of the typical AMF colonization structures (internal hyphae, arbuscules, vesicles), but relative abundance of arbuscules and vesicles was lower in irCCaMK than in EV plants for both inocula types (Table S1). As these results contradicted our previous characterization of the irCCaMK line, which did not find any evidence of internal colonization when plants were grown in single pots or in the field (Groten et al. 2015a), we re-analyzed the colonization patterns in different experimental set-ups so as to distinguish different hypotheses that could account for this apparent discrepancy. We used singly-grown plants in

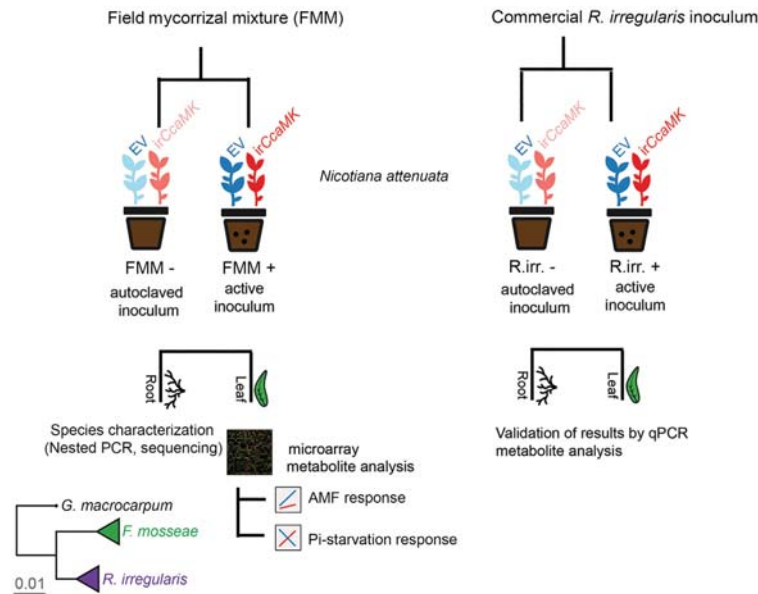


Figure 1. Experimental set-up, work-flow and characterization of the field mycorrhizal mixture (FMM)

Empty vector (EV) *Nicotiana attenuata* plants were co-cultured with transgenic lines silenced in the expression of calcium and calmodulin dependent protein kinase (irCcCaMK) in 2 L pots, with living and autoclaved arbuscular mycorrhizal inoculum originally collected from the plant's native habitat in Utah, USA, and with commercial *Rhizophagus irregularis* inoculum. Leaves were harvested at two time-points after inoculation (2 and 6 weeks post-inoculation (wpi)) for transcriptome profiling for FMM inoculation, metabolite analysis and validation of selected genes found by transcriptome profiling in leaves inoculated with the commercial inoculum. Roots were used for the characterization of the fungal strains of the field mycorrhizal mixture colonizing the roots based on the small subunit (SSU) rDNA genes after nested PCR with arbuscular mycorrhiza specific primers and cloning. Three replicate samples per transgenic line were used, and 24 clones per sample sequenced. The relative number of clones with highest homology to sequences in the NCBI database is shown (total number of positive sequenced clones: 141). Unweighted Pair Group Method with Arithmetic mean (UPGMA) phylogenetic tree. *Glomus macrocarpum* was used as the out-group. Branches with bootstraps lower than 60% were collapsed to polytomies. The scale bar indicates the SSUs per site.

1 L pots and competitively grown plants in 2 L pots with root barriers penetrable by hyphae. For both set-ups we did not find any internal AMF colonization structures, and, consistent with our previous results (Groten et al. 2015a), *NaPT4* was only upregulated in inoculated EV plants, but not in irCcCaMK (Figure S1A, S1B). To further elucidate why we obtained a different result in the present study, we decided to repeat the competitive set-up without a barrier, but instead of EV we used a transgenic *N. attenuata* line ectopically expressing a green fluorescent fusion protein (GFP-SPOR). Using this set-up we reproduced the results described above for competitively grown EV and irCcCaMK plants – roots of

GFP-SPOR plants showed much higher colonization rates and *NaPT4* transcript accumulation than for irCcCaMK, but some AMF-colonized roots and *NaPT4* transcripts were also detected in roots of irCcCaMK plants. Interestingly, the transcript abundance of *GFP* showed a similar pattern as *NaPT4* (Figure S1C). As *GFP* transcripts should only be present in GFP-SPOR plants, and indeed they were not present in singly grown irCcCaMK plants, we infer that the colonization pattern found for irCcCaMK is probably due to an incomplete separation of the root systems during harvest. This has no effect on the aboveground part, which is the focus of the present study. Furthermore, the incomplete

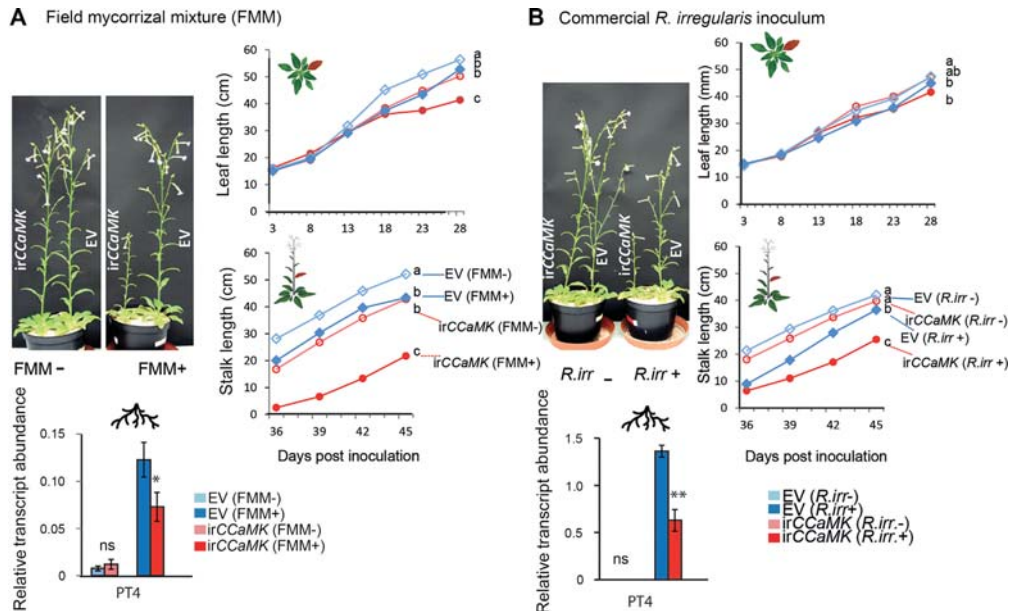


Figure 2. After inoculation with the field mycorrhizal mixture (FMM) (A) or with *R. irregularis* inoculum (*R. irr.*) (B) *N. attenuata* empty vector (EV) plants grown in competition with transgenic plants silenced in the expression of a key gene of arbuscular mycorrhizal signaling (irCCaMK) had significantly taller stalks than irCCaMK plants and showed higher levels of mycorrhiza-specific phosphate transporter transcript accumulation

For the experimental set-up see Figure 1. Representative pictures of the plants. Pictures were taken 45 d post-inoculation (dpi). Leaf and stalk length growth of the two transgenic lines, EV (blue diamonds) and irCCaMK (red circles) with (+, filled) and without (–, non-filled) mycorrhizal inoculum. Measurements were taken at indicated time points after inoculation; significant differences are shown by different letters (linear model of leaf and stalk length growth using the interaction of mycorrhizal treatment and transgenic line followed by Tukey's HSD, $P \leq 0.05$, $n = 10$). Leaves depicted in red indicate harvested leaves 2 and 6 wpi for further analysis. Relative expression of the arbuscular mycorrhiza-specific phosphate transporter *NaPT4* as marker of arbuscule activity in roots of EV and irCCaMK plants compared to elongation factor. Asterisks indicate significant differences among the two genotypes (paired Student's *t*-test, * $P \leq 0.05$, ** $P \leq 0.01$, ns, not significant, $n = 6$).

separation of the root systems turned out to be a good indicator of AMF-inducible metabolites in roots by using the characteristic additive expression pattern as a marker.

Total P content of inoculated irCCaMK leaves and roots is significantly lower than for competing EV plants

As inoculated EV and irCCaMK lines showed a strong difference in growth, we also quantified leaf and root biomass, P concentration and total P contents of the plants growing in FMM inoculated pots (Figure 3). Roots showed a very clear pattern: while root biomass

was similar for both treatment and lines, P concentration tended to be higher and total P content was significantly higher in inoculated EV roots. The shoots of inoculated irCCaMK plants had a significantly lower biomass than those of inoculated EV plants, while leaf P concentration was only significantly different when comparing the inoculated plants with non-inoculated EV plants; within a pot the two plant lines did not significantly differ in P leaf concentration. However, when considering total biomass as a measure of P gain over time and P leaf concentration, total P of inoculated irCCaMK plants was significantly lower than that of their competing EV plants. In short, inoculated irCCaMK

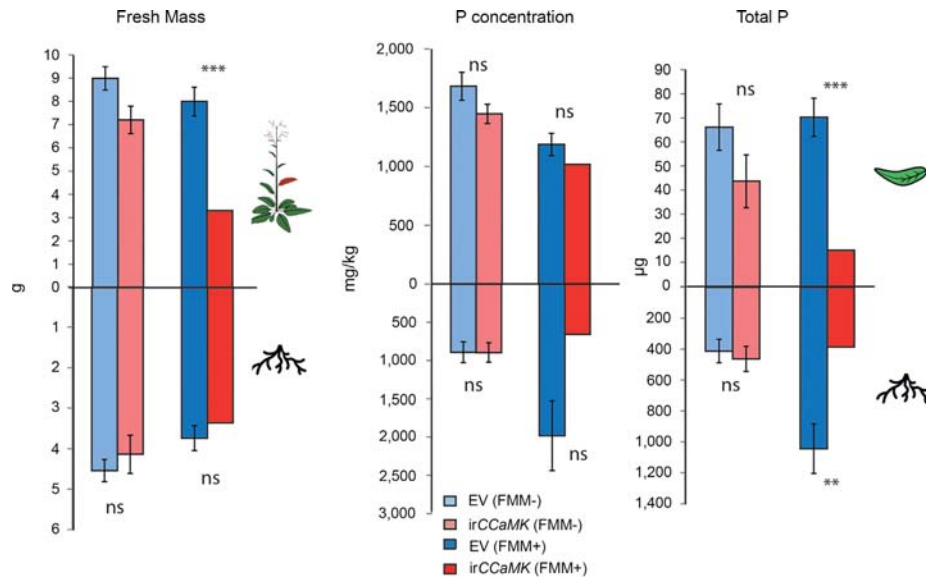


Figure 3. Total P content is significantly lower in FMM- inoculated irCCaMK compared to non-inoculated plants and to FMM-inoculated EV plants

Fresh mass of plants (roots and shoots) 6 weeks post-inoculation with field mycorrhizal mixture (FMM) and P concentration in stem leaves (1st–3rd leaf) were analyzed and the total P content in leaves and roots determined. Asterisks indicate significant differences among the two genotypes (paired Student's t test, ** $P \leq 0.01$, *** $P \leq 0.005$; ns, not significant; $n = 10$ for fresh mass, and $n = 3$ for P measurements).

plants grown in competition with EV plants acquired less P than did the competing EV plants.

Foliar fingerprinting revealed differentially expressed genes showing additive and interactive expression patterns for AMF colonization and genotype

To further investigate the systemic effects of AMF colonization for competing plants, we performed a foliar transcriptome analysis by microarray at two time-points after inoculation, 2 and 6 weeks. Quantile normalization and qRT-PCR validation revealed the robustness of this dataset (Figure S2B, S2D). Multi-dimensional scaling analysis grouped all the samples harvested at 2 weeks post-inoculation (wpi) together independently of genotype and colonization (Figure S2A). At 6 wpi, EV and irCCaMK samples (without AMF inoculation) also grouped, while they were clearly distinct after FMM inoculation (Figure S2A). There was almost no difference in the transcript abundances of EV and irCCaMK without AMF inoculation (0 DEG, 2 wpi; 12 DEGs, 6 wpi)

(Figure S2C) and these minor differences reflect the expression pattern of *CCaMK* in plants - *CCaMK* expression is absent in leaf tissues, while transcripts accumulate in roots and flowers (Figure S2E).

The microarray data analysis revealed that the number of DEGs in leaves was 15 times greater in irCCaMK than in EV leaves at both time points after FMM inoculation compared with the non-inoculated group (Figure 3B). This dramatic difference might result from the strong growth differences between EV and irCCaMK plants after FMM inoculation. Therefore, we first only considered DEGs overlapping at the two time-points (47 core DEGs: 14 from 2 wpi, 33 from 6 wpi) (Figure 4A). Hierarchical clustering analysis indicated two main effects among them, an additive effect and an interactive effect, in particular for DEGs at 6 wpi.

To evaluate whether this additive effect expression pattern induced by FMM was independently reproducible by *R. irregularis* alone, we used the same set-up with a commercially available *R. irregularis* inoculum (Figure

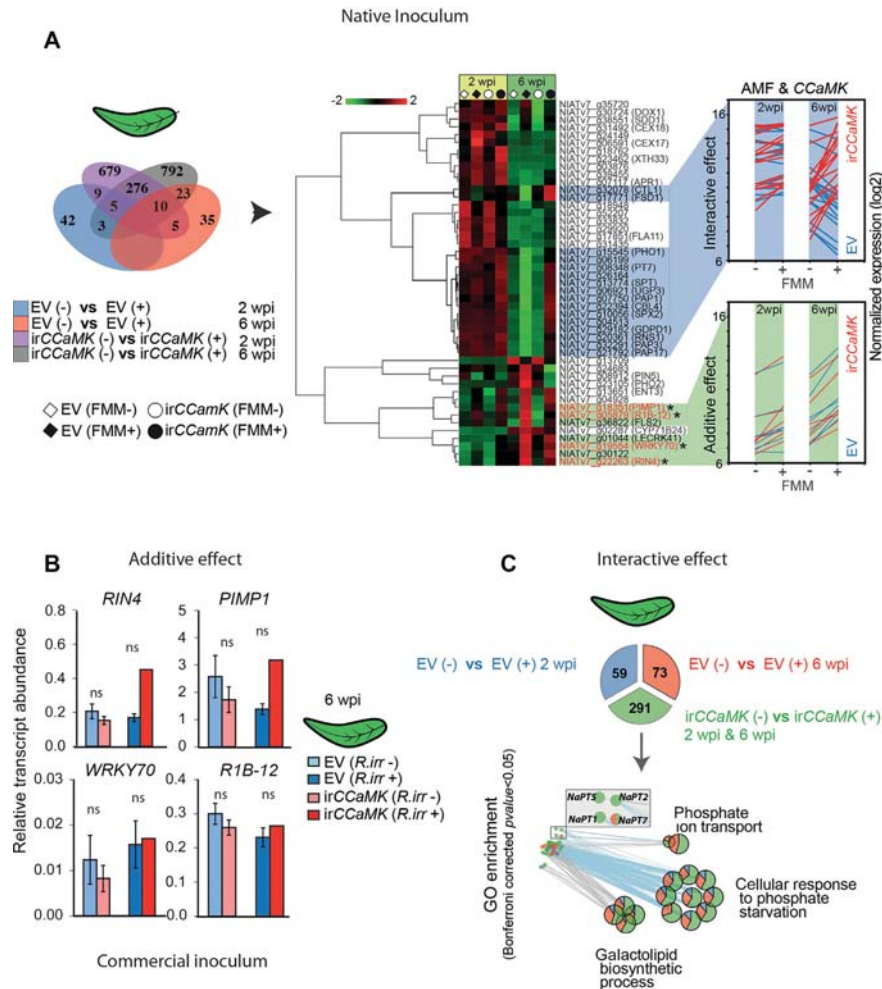


Figure 4. Transcriptome analysis in leaves of FMM-inoculated and non-inoculated EV and *irCCaMK* plants indicate strong interactive changes in expression of P-starvation genes and the additive effect of transcription factors and receptor kinases at 6 weeks post-inoculation (wpi)

(A) The Venn-diagram depicts the number of differentially expressed genes (DEG) when comparing FMM-inoculated and non-inoculated EV plants (in blue and pink) and *irCCaMK* plants (in violet and grey) at the early (2 wpi) and late harvests (6 wpi) of FMM inoculation. The pair-wise comparison was performed using R (fold change ≥ 1.5 or ≤ -1.5 , FDR ≤ 0.05). Hierarchical cluster analysis of 47 overlapping DEGs (in bold black). Strong interactive and additive effects between genotypes (EV/*irCCaMK*) and treatments (FMM -/+) were found at 6 wpi. The DEGs shown with a blue background show the opposite expression pattern in EV and *irCCaMK* after AMF inoculation, while DEGs with a green background show an additive effect, representing a significant increased expression level after inoculation, which is higher in EV than in *irCCaMK* leaves. Data shown are means \pm SE ($n = 3$) after quantile normalization and \log_2 -transformation. (B) Foliar genes showing an additive effect could not be confirmed to be specifically induced by arbuscular mycorrhizae using the same experimental set-up and the *R. irregularis* inoculum (see Figure 1). qPCR analysis of selected genes expressed in leaves; significance was tested by a paired Students t-test, $n = 6$; ns, not significant). (C) Pie-chart of DEGs selected from (A). GO enrichment analysis of 423 DEGs was computed with

4B). Four representative genes, *PIMP1*, *R1B-2*, *FLS2*, *WRKY70* and *RIN4*, were selected from the FMM induced foliar additive model (see Figure 4A) to more critically evaluate the observed expression pattern. However, the pattern found for the FMM-inoculated leaves could not be reproduced: *irCCaMK* leaves of plants inoculated with the *R. irregularis* AMF inoculum showed the same expression as non-inoculated plants and inoculated EV plants (Figure 4B). The lack of reproducibility after inoculation with commercial *R. irregularis* inoculum compared to FMM treatment suggests that foliar differential gene expression found for FMM inoculum following the additive model depends on other factors such as the type of partner or growth conditions (sand vs. expanded clay); and hence these DEGs found cannot be considered as general foliar markers of AMF colonization.

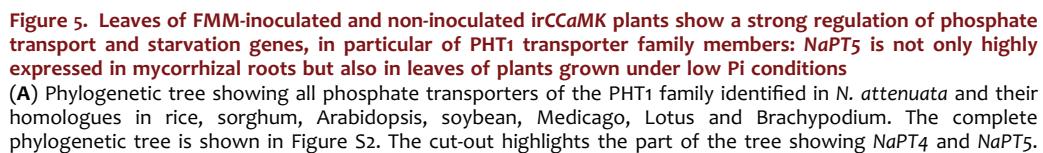
In the interactive model, patterns of transcript accumulation in EV and *irCCaMK* show opposite patterns. Many typical phosphate starvation-inducible genes exhibited such a pattern at 6 wpi, for example, phosphate transporter *PHO1*, purple acid phosphatases (PAP), SPX domain containing *SPX2* and *PHOSPHATE2* (*PHO2*), but these were not significantly changed at 2 wpi (Figure 4A). To further dissect the gene expression pattern showing an interactive model induced by FMM treatment, a detailed gene ontology (GO) enrichment analysis was conducted. The overlapping 276 core DEGs at 2 and 6 wpi in *irCCaMK* leaves were selected in combination with 59 DEGs (2 wpi) and 73 DEGs (6 wpi) of EV as GO enrichment analysis groups (Figure 4C). GO enrichment analysis showed that the GO terms of phosphate ion transport, galactolipid biosynthetic process and phosphate starvation responses were enriched. These results corresponded with the total P content of the leaves and are consistent with the hypothesis that *irCCaMK* plants sharing a 2 L-pot with EV plants were P starved after FMM inoculation.

NaPT5 is induced by P-starvation in leaves independently of AMF colonization

To further investigate the P-starvation signature of *irCCaMK* plants, we quantified the gene expression pattern of selected phosphate transporters. The *PHT1* family of plant membrane proteins is mainly responsible for the uptake of Pi from the soil. Based on a Blast search using published *PHT1* sequences from tomato, rice, Medicago and Arabidopsis, 11 orthologues were identified in *N. attenuata*. The maximum-likelihood phylogenetic tree based on protein sequences grouped *NaPT4* and *NaPT5* in the same clade with the well-characterized AMF-inducible phosphate transporters *MtPT4/5*, *LePT4/5* and *OsPT11* (Figures 5A, S3A). *NaPT3.1* was in the same clade as the AMF-specific phosphate transporter *LePT3* (Figure S3A). Tissue-specific expression clustering classified *NaPT4*, *NaPT3.1* and *NaPT5* in the same clade (Figure S3B).

To further elucidate the role of the selected phosphate transporters, we quantified their transcript levels by qRT-PCR and clustered the values after log₂ transformation. *NaPT4*, *NaPT3.1* and *NaPT5* were upregulated in FMM inoculated roots in EV and *irCCaMK* plants, while *NaPT1*, *NaPT7* and *NaPT5* were only upregulated in leaves of FMM inoculated *irCCaMK* plants (Figure 5B). Hence, *NaPT5* was not only upregulated in FMM inoculated roots of both genotypes (EV and *irCCaMK*), but also in P-starved leaf tissues of *irCCaMK* plants. The distinct role of *NaPT5* was corroborated by hierarchical clustering which revealed that *NaPT5* has its own distinct expression pattern compared to the clades of *NaPT4/3.1* and *NaPT1/7* (Figure 5B). These results were validated in a separate experiment using the same experimental set-up but with the commercial *Rhizophagus* inoculum (see Figure 1). The expression level of *PHO2*, an ubiquitin-conjugating E2 enzyme and important central negative regulator of the Pi response pathway (Chiou and Lin 2011), was significantly induced by *R. irregularis*

CluoGO + CluePedia according to the GO categories “Biological Process” and “Molecular Function” (Two-sided hypergeometric test, Bonferroni corrected test, $P \leq 0.05$). GO terms were associated to DEGs according to the best BlastX hits obtained from *Arabidopsis* TAIR10 proteome. The color proportion of GO terms (strokes in black) is positively correlated with the frequency of DEGs from the corresponding lists. Colors of associated nodes (without stroke) including regulated *PHT1* family members (inset) indicate overrepresented DEGs from the corresponding lists.



inoculation in EV leaves, and showed the same pattern as in FMM-inoculated plants. Similarly, the expression of *NaPT4* and *NaPT5* was the same for the commercial inoculum and the FMM (Figure 5C). To evaluate whether the high transcript abundance of *NaPT5* in leaves is a P starvation response irrespective of AMF colonization, plants were grown under two different P levels (low P: 0.02 and regular P: 0.50 mmol/L) without AMF inoculation. After irrigation with low P fertilizer (0.02 mmol/L), the molecular marker regulating Pi homeostasis *PHO2* was significantly downregulated in both leaf and root tissues (Figure 5D), and consistent with our expectations, *NaPT4* was neither expressed in root or leaf tissues, while *NaPT5* was not induced in root tissues, but significantly upregulated in leaves of P-starved plants (Figure 5D). In summary, from these data we conclude that *NaPT5* is not only induced by AMF colonization in roots, but is also induced by P starvation in leaves independently of AMF colonization.

Concentrations of particular amino acids are enriched in leaves of inoculated *irCCaMK* plants, while roots show a strong accumulation of amino acids and phenolics in AMF-treated EV roots.

To further evaluate the results obtained by gene expression analysis, we also analyzed amino acid levels, as it is thoroughly documented that amino acids and nitrogenous compounds increase during P limited growth (Willmann et al. 2013; Ganie et al. 2015), and AMF colonization is known to alter the foliar levels of asparagine, glutamine, glutamic acid and aspartic acid (Kogel et al. 2010; Fester et al. 2011). We used both types of inocula for a robust analysis and the results were largely consistent for both inocula. We did not find

a significant change in specific amino acids in leaves of AMF-inoculated EV plants. However, glutamic acid, aspartic acid, glutamine, serine and tryptophane were significantly increased in leaves of inoculated *irCCaMK* plants independently of inoculum type (Figure 6, Tables S2, S3). Hence, levels followed the interactive pattern found for genes known to be related to P-starvation (Figure 5C). Furthermore, the foliar levels of the phenolic compounds rutin, caffeoylputrescine, scopoletin and scopolin tended to be lower in inoculated EV plants, and increased in leaves of AMF-inoculated *irCCaMK* plants (Figure 6). The overall pattern was similar for the two different inocula (Tables S2, S3), but the absolute levels differed, with higher levels in plants inoculated with the commercial inoculum. In contrast to leaves, the levels of the majority of free amino acids in roots showed a similar additive pattern to that of *NaPT4* expression – amino acid levels increased with AMF inoculation, but levels were mostly higher for EV than for *irCCaMK* (Figure 6A; Tables S2, S3). The phenolic compounds sinapic acid, ferulic acid, cinnamic acid and scopolin also reflected this pattern, while other compounds showed similar AMF-induced levels in both genotypes or higher levels in *irCCaMK* plants (Figure 6, Tables S4, S5).

DISCUSSION

Plants have developed many strategies to adapt to local environments, in particular to cope with extreme environments such as nutrient and water deficiency. One strategy is to establish mutualistic symbiotic relationships with AMF. The interaction with the fungal partner leads to local large-scale reprogramming in the roots. Here, we focused on systemic effects in isogenic

(B) Hierarchical cluster analysis of PHT1 family members (*NaPT1*, *NaPT2*, *NaPT4*, *NaPT5*, *NaPT7*) of FMM inoculated and non-inoculated plants validated by qRT-PCR. Log₂-transformed transcript accumulation values are only shown for significant differences after pairwise comparisons among inoculated and non-inoculated samples of the same genotype. (C) *NaPT5* transcript accumulation was evaluated in response to *R. irregularis* inoculation (see Figure 1). Relative gene expression values of gene expression in EV (blue bar) and *irCCaMK* (red bar) with (*R. irr*+) and without (*R. irr*-) mycorrhizal inoculum 6 wpi is shown. Data represent the mean ± SE (n = 6); asterisks indicate significant differences among the two genotypes (paired Student's t-test and Wilcoxon Rank Sum test for *NaPT5* expression in leaves, * $P \leq 0.05$, ** $P \leq 0.01$, *** $P \leq 0.005$; ns, not significant). (D) EV plants were grown in a single pot under two different Pi levels, regular P (0.5 mmol/L) and low Pi (0.02 mmol/L), respectively, to evaluate *NaPT5* transcript accumulation in response to Pi-starvation. Asterisks indicate significant differences between the two P-treatments (Student's t-test, ** $P \leq 0.01$, *** $P \leq 0.005$). Relative transcript abundance of *NaPHO2*, *NaPT5* and *NaPT4* was compared to the housekeeping gene (eukaryotic translation initiation factor 5A-3 (*EIF5A3*); *NIATv7_g37283*) in leaves and roots.

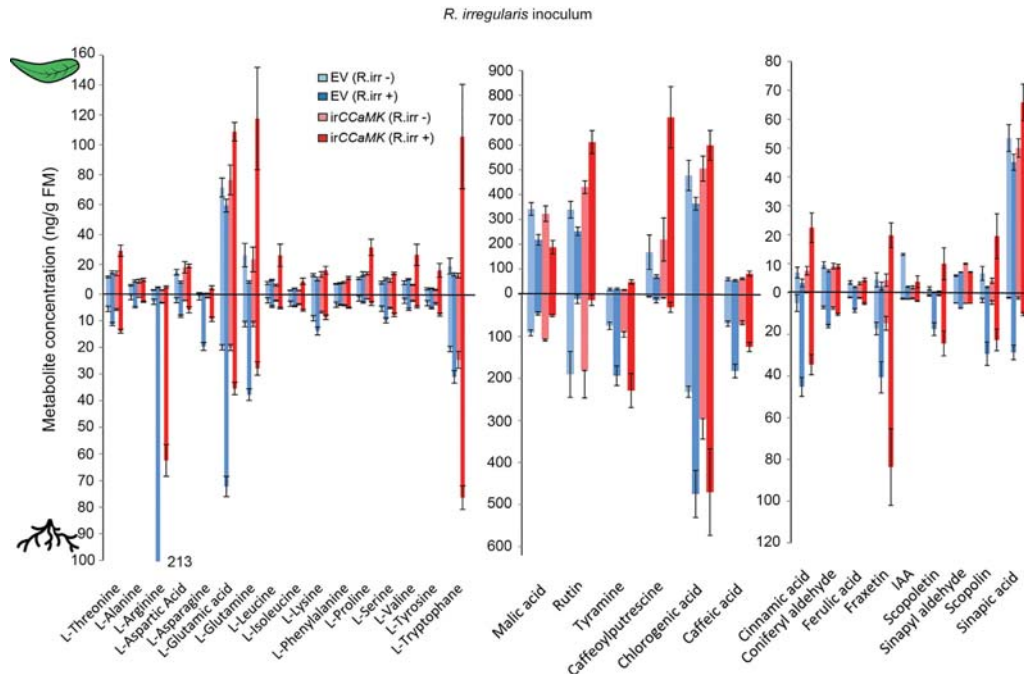


Figure 6. The foliar concentrations of many amino acids significantly increase in *R. irregularis* inoculated irCCaMK plants and decrease in the leaves of inoculated EV plants compared to non-inoculated plants of the same genotype, while in roots the majority of amino acid levels follow the additive pattern

Metabolites of leaves and roots of plants 6 wpi were extracted by solid-phase extraction based sample preparation and analyzed by UHPLC–HESI–MS/MS. Data shown are means \pm SE ($n=7$). Statistical results are provided in Table S3. In order to show several metabolites in one graph, data were transformed - for malic acid values were divided by 100, and for rutin, chlorogenic acid, caffeoylputrescine and scopolin by 10, while fraxetin and cinnamic acid values are shown at 100- and 10-fold levels than the measured values, respectively.

N. attenuata plants with different capabilities to interact with AMF. Plants were grown in competition in a native inoculum to mimic natural conditions, and for data validation compared to the results with a commercial *Rhizophagus irregularis* inoculum using the same experimental set-up. *N. attenuata* host plants (EV) and isogenic surrogate non-host plants silenced in a key enzyme to establish an AMF symbiosis (irCCaMK) were used to gain new insights into the regulation of AMF colonization and the complex expression patterns of PHT1 phosphate transporter family members.

Previously it has been shown that the two isogenic wild annual tobacco plants used in the present study do not differ in growth and fitness parameters when grown in single pots or in rows in the field (Groten et al. 2015a); the growth of both lines was impaired to the

same extent after inoculation with AMF compared to autoclaved inoculum (Groten et al. 2015a). Here, we observed the same growth difference for EV plants when comparing active and autoclaved inoculum. However, in contrast to the results obtained from plants grown singly in pots, when plants were grown in competition in the same pot – a condition which is similar to the natural situation in which plants due to their mass germination after fire also compete with their neighbors for light and nutrients (Lynds and Baldwin 1998) – the two lines showed a strong growth difference in the presence of AMF, with lines impaired in the interaction with the fungal partner being strongly reduced in growth compared to the fully functional competitor. This result was independent of the inoculum type. From these findings, we infer that AMF colonization

is not beneficial for *irCCaMK* plants when these AMF-impaired plants are grown in competition with a fully AMF-functional competitor. In accordance with the reduced stalk lengths, shoot biomass was also significantly reduced, and this was reflected in the significantly lower total P values, while AMF-colonized roots of EV plants had much higher P concentrations and total amounts of P. From these results we infer that these AMF-impaired plants took up less P than their EV competitors, and this inference was further corroborated by the microarray analysis of leaf tissues.

An in-depth analysis of foliar DEGs following the interactive pattern, in other words, genes that show the opposite expression pattern in EV and *irCCaMK*, revealed that a majority of GO functions directly (P starvation and P transport) or indirectly (galactolipid biosynthesis) were related to P nutrition (Figure 4C). The effect only became obvious 6 wpi, while after 2 weeks, only few changes in gene expression were observed between plants with and without inoculum (Figure 4A), and all samples clustered together (Figure S2A). The low colonization rates at this early stage in the interaction when the AMF network may not have been fully established in addition to the likely nutrient sufficiency of these smaller plants are likely responsible. From these observations, we infer that the competition for nutrients was less prominent at the early time-point, as expected. The transcriptome analysis corroborated the inference that AMF-mediated P acquisition and nutrition resulted in the P starvation of *irCCaMK* plants. P-uptake of plants via AMF occurs via inducible P-transporters located in the periarbuscular membrane, and these deserve further discussion.

NaPT4 and *NaPT5* show 93 and 94% similarity at the amino acid level with their orthologues *LePT4* and *LePT5*, in tomato, respectively (Karandashov et al. 2004; Nagy et al. 2005). Interestingly, *PT5*, which is known as a typical marker for AMF colonization (Tan et al. 2012), was not only expressed in AMF-inoculated roots but also in the leaves of inoculated *irCCaMK* plants. The expression was only observed for *NaPT5* and not for *NaPT4*, and correlated with significantly higher expression levels of the direct transporters *NaPT1* and *NaPT7*. In particular *PT1* is known to be induced by P-starvation in tomato (Liu et al. 1998). These findings strongly suggested that *NaPT5* is induced by Pi starvation, and the observations that 1) the same expression pattern

was observed with a different inoculum and 2) that high levels of *NaPT5* expression under low Pi conditions without AMF were observed (Figure 5) were consistent with this hypothesis. Interestingly, a recent study with tomato revealed that *LePT5* was significantly downregulated in leaves in response to *R. irregularis* inoculation. These plants were well-fertilized and did not suffer from P-starvation (Cervantes-Gamez et al. 2016), again providing evidence consistent with the hypothesis that *PT5* transcript levels negatively correlate with the P status of leaves. Additional direct evidence comes from an early study on the expression of P-transporter genes in three Solanaceous species which showed an induction of AMF-inducible *PT4* in leaves and roots of strongly P-starved eggplants, but not in pepper and *N. tabacum* (Chen et al. 2007), and a very weak expression of *PT5* was also observed in P-deprived tomato leaves (Chen et al. 2014), and of the AMF-inducible *PT3* in maize leaves (Nagy et al. 2006). Expression of genes known to be AMF-induced in other tissues were also reported for the AMF inducible *Pht1* gene *SbPT11* from sorghum, in reproductive tissue (stamen and pistil), and for *SbPT11*, *SbPT9*, *LuPT5* and *LuPT8* in leaves of sorghum and flax (Walder et al. 2016) all consistent with our findings that *PT5* is not only a mycorrhizal marker in roots, but also an indicator of P-starvation in leaves in *N. attenuata*. Furthermore, the AMF-inducible *PTs* *LjPT4* (*L. japonicus*) and *MtPT4* (*M. truncatula*) were found to be expressed in non-inoculated roots (Volpe et al. 2016). The transcript abundance of *LjPT4* and *MtPT4* highly increased with low P growth in non-mycorrhizal roots, and GUS histochemical staining indicated an enrichment in the root apex (Volpe et al. 2016). In the P starvation experiment presented here, we could not detect any changes in *NaPT4* transcript levels in roots. This discrepancy is likely due to the fact that we analyzed entire roots of which the root apices represent only a minor contributor.

The functional roles of the expression of these AMF-induced *PTs* in non-mycorrhizal tissues remain unknown. It has been speculated that *MtPT4* and *LjPT4* may function in the root apex act – in addition to their roles in Pi transport across the periarbuscular membrane – as phosphate sensors that regulate early root branching (Volpe et al. 2016). The foliar expression of AMF-inducible *PTs* may play a role in Pi mobilization

(Walder et al. 2016). However, further studies are needed to clearly distinguish if these AMF-inducible PTs are relevant for transport, remobilization, or signaling.

At the metabolite level we found an increase in foliar amounts of free amino acids, glutamine, glutamic acid, aspartic acid, serine and tryptophane in irCCaMK (Figure 6), a result which is consistent with the hypothesis that irCCaMK plants suffer from P starvation when competing with AMF-inoculated EV plants. Increased levels of these amino acids are known to occur in P-starved plants (Schlueter et al. 2013), while asparagine, aspartic acid, glutamine and glutamic acid have also been shown to be reduced in leaves of mycorrhizal *Lotus japonicus* probably due to improved P nutrition (Fester et al. 2011). Consistent with these findings, we also found a significant decrease in the amounts of proline, tryptophane, glutamine, glutamic acid and tyrosine after inoculation with the two different inocula when comparing inoculated and non-inoculated EV plants.

We also observed a decline in foliar concentrations of malic acid, rutin and chlorogenic acid in EV plants, while the same compounds also in addition to fraxetin, caffeoylputrescine, scopolin and scopoletin increased in AMF-inoculated irCCaMK plants, though not all differences were significant for both inocula. This result at first is surprising as rutin and chlorogenic acid are typically induced by herbivory (Lou and Baldwin 2004), involved in priming against herbivores (Bandoly et al. 2016) and bacterial pathogens (Yan et al. 2016) and scopolin and scopoletin are known as antifungal compounds (Sun et al. 2014). Moreover, AMF-inoculated plants are usually considered to be better defended against leaf-chewing herbivores than non-colonized plants (Jung et al. 2012). However, early publications on P-starvation reported a large increase in chlorogenic acid and phenolic compounds in leaves of P-starved plants and a leakage of scopolin and scopoletin from leaves of these plants (Koeppel et al. 1976; Juszczuk et al. 2004), results consistent with our observations that inoculated irCCaMK plants are P-starved when grown in competition with fully functional EV plants. An increase in foliar phenolic compounds is one way for plants to cope with environmental stress, and one hypothesis is that phenolics are produced to make use of carbon skeletons (carbon-nutrient balance theory) (Caretto et al. 2015). In

contrast to our findings, which rather showed a decline in some phenolic compounds in leaves of AMF inoculated EV plants, a report on AMF-inoculated *Medicago* leaves described an alteration in phenylpropanoid metabolism due to AMF inoculation (Adolfsson et al. 2017). However, other studies have reported only increases in particular secondary metabolites upon AMF inoculation, and not a general increase in phenolics associated with AMF colonization (Cosme et al. 2014; Schweiger et al. 2014).

In contrast to leaves, levels of most amino acids in roots showed a very clear pattern related to AMF inoculation, which mostly followed the additive model in both inoculated genotypes: levels were higher in EV than in irCCaMK plants, and hence the increase in irCCaMK plants is probably due to the percentage of EV roots mixed up with irCCaMK providing a good indicator that these compounds are AMF-induced. These results are in clear contrast to the findings for tomato roots colonized by two different AMF species, which showed a reduction in basic and aromatic amino acids compared to non-inoculated roots (Rivero et al. 2015). Increases in the levels of aspartic acid, asparagine and glutamic acid in inoculated roots is a more consistently observed response across different host species and inocula (Schliemann et al. 2008; Rivero et al. 2015) and it is thought that these are related to N-uptake (Govindarajulu et al. 2005). Levels of other amino acids appear to be more plant species-specific and this also applies to phenylpropanoids. Flavonoids and lignins increase in some species (Lopez-Raez et al. 2010; Rivero et al. 2015; Zubek et al. 2015), but the direction of change as well as the type of metabolites differ among the studies. For example, while we observed a significant increase in caffeic acid and chlorogenic acid in AMF inoculated roots, in clover a significant decline was observed in response to inoculation with two mycorrhizal species (Lopez-Raez et al. 2010), though in both studies an increase in ferulic acid was shown.

In this context it is important to note that though the overall pattern was similar between the two inocula, the absolute levels as well as the strength of induction differed, which is in agreement with previous studies indicating that different inoculum types can lead to different plant responses (Lopez-Raez et al. 2010; Rivero et al. 2015; Walder et al. 2015; Zubek et al. 2015; Walder et al. 2016).

In conclusion, the present study underscores the importance of the identity of the fungal partner in plant-AMF interactions to evaluate systemic changes in the plants due to AMF colonization. Plants impaired in their interactions with AMF clearly display strong signs of P-starvation and have a fitness disadvantage when competing for limited soil nutrients with a fully functional isogenic line. Furthermore, there is growing evidence that AMF-specific phosphate transporters are more versatile than previously thought. The data presented here demonstrate an expression pattern of the AMF-specific *PT5* in leaves which is independent of AMF colonization. An in-depth functional characterization is needed to clarify the role and the molecular mechanism of *NaPT5*.

MATERIALS AND METHODS

Fungal inoculum, plant germination and growth

Native soil was obtained from the New Plot site (N 37.1412, W 114.0275) at the Lytle Ranch Preserve, in SW Utah, USA, a native habitat of *Nicotiana attenuata* in Utah, USA. The soil was mixed with autoclaved sand (1:3) and *Medicago* and leek plants were grown in the same pot and used as trap plants to amplify the AMF in the soil. Six weeks after planting, shoots were removed, and the roots cut into small pieces and mixed with autoclaved sand (1:10). This field mycorrhizal mixture (FMM) was used as active inoculum and after autoclaving (twice at 121°C for 30 min) for non-inoculated controls. Additional experiments were performed with living and dead (autoclaved at 121°C for 30 min) commercial *Rhizophagus irregularis* inoculum (Biomyc Vital), which was also diluted 1:10 with autoclaved expanded clay (2–4 mm) (Figure 1). Empty vector (EV) plants carrying the empty construct (line A-04–266-3-1) and plants silenced in the expression of a calcium- and calmodulin-dependent protein kinase *irCCaMK* (*irCCaMK* 2 line A09-1212-1, (Groten et al. 2015a)), were germinated on Gamborg B5 medium according to Kruegel et al. (2002). EV and *irCCaMK* plants were grown as dual-plant communities in 2 L pots filled with either living or dead inoculum (FMM or *R. irregularis*). At the bottom of the pot we placed a layer of expanded clay (size 4–8 mm) for better drainage and on top a layer of sand (about 1 cm) to prevent any cross-contamination. Plants were irrigated with hydroponic fertilizer (Groten et al. 2015a) with 1/10 of the regular

inorganic P_i concentration during rosette stage, and starting with the elongation stage with 1/4 P_i concentration. Leaf and stalk length measurements were taken every 5 and 3 d, respectively. Rosette leaves (1st and 2nd source leaf) were harvested 2 weeks post-inoculation (wpi), and stem leaves (1st–3rd) and root material 6 wpi. The biomass of the leaves and shoots was measured and the plant material immediately frozen in liquid nitrogen. To compare the *irCCaMK* phenotype of plants grown with and without competitors in 1 and 2 L pots, we also grew plants in single pots under low P conditions with the commercial inoculum. In addition to 1 L pots with individual plants only, we also used 2 L pots separated by a barrier penetrable for hyphae but not for roots (mesh size 30 μ M), so that plants were connected by a common mycorrhizal network, but roots could not directly interact (Supporting Figure S1). We repeated the competition experiment in 2 L pots with an isogenic *N. attenuata* line ectopically expressing a green fluorescent protein (GFP)-sporamin fusion protein (line A06-349-6) instead of EV (Zhang et al. 2010). As GFP from jellyfish should only be present in GFP overexpressing plants, we used these plants as an additional marker (see below).

Root harvest, root staining, mycorrhizal feature visualization and evaluation

For harvests, roots of the two plants in each pot were carefully disentangled and washed with tap water to remove the remaining substrate. However, roots of glasshouse-grown *N. attenuata* plants are very delicate and partially mix up when two plants are grown together in a pot, which makes a clean harvest very difficult. We discarded all root parts for which we could not be not sure if they were from a single genotype. Additionally, in an independent experiment we used the GFP-SPOR lines grown in competition with *irCCaMK* plants to find out if the root systems were fully entwined. Roots were cut into 1 cm pieces and the pieces well-mixed. A subset was collected from each genotype with and without AMF inoculation and stored in a solution consisting of 99% ethanol and 60% acetic acid (3:1, v:v) at 4°C. The remaining root material was immediately frozen in liquid nitrogen. For fungal colonization analysis, root tissue was stained with trypan blue according to Riedel et al. (2008). For colonization analysis, up to 15 randomly picked root pieces were mounted on a slide and scored at $\times 20$

magnification with an Axiomager Z1 microscope (Zeiss, Jena, Germany) using a magnified gridline intersect method (McGonigle et al. 1990; Groten et al. 2015a). 100 intersections per sample (slide) were counted.

Characterization of the Field Mycorrhizal Mixture

For the characterization of the FFM in EV and irCCaMK roots, we followed the protocol described in detail in Groten et al. (2015a). In brief, the FastDNA SPIN Kit for Soil (MP Biomedicals) was used for DNA extraction according to the manufacturer's instructions. PCR reactions using the AML1 and AML2 primer pair (Lee et al. 2008) were done in a 50 µL volume using Phusion High-Fidelity DNA Polymerase (New England BioLabs Inc., Beverly, MA, USA) following the manufacturer's protocol. For the second PCR with the N31 and AM1 primer pair (Simon et al. 1992; Helgason et al. 1999), PCR products of the first PCR were diluted 1:50 with Milli-Q water. PCR products (550 bp) were run on a 1% agarose gel, excised and then purified using the QIAquick Gel Extraction Kit. Purified DNA fragments were ligated into the pGEM-T Easy vector according to the manufacturer's protocol. Twenty-four positive clones were selected and sequenced using ABI Genetic Analyzer 3100 (Applied Biosystems, Germany). Using the Geneious R6 (ver. 6.0.5, available from <http://www.geneious.com/>) software, overlapping sequences of T7 and Sp6 were extracted and shortened in accordance to the (~550 bp) alignment with N31 and AM1 primer flanking the AMF the small subunit (SSU). The chromatogram of this sequence was checked for mis-spaced peaks (i.e. missing nucleotides, confused nucleotides) and the sequence was edited accordingly. After completion of sequence annotation, the fungal taxa were identified by a BLAST search with MaarjAM (<http://maarjam.botany.ut.ee/>) and NCBI (<http://blast.ncbi.nlm.nih.gov/Blast.cgi>) database.

Determination of total P content

Leaf and root material (6 wpi) were thoroughly ground to fine powder with mortar and pestle in liquid nitrogen. 200 mg ground material for each sample was freeze-dried at -50°C for 48 h. The total P content of the freeze-dried material was analyzed at the Laboratory for Spectrometry at the Max Planck Institute for Biogeochemistry, Jena, Germany.

Total RNA isolation and quality check

For large-scale transcriptome profiling, three replicates per time-point (2 and 6 wpi) and per treatment

(inoculated/non-inoculated) were analyzed for each genotype. RNA was extracted using Qiagen RNeasy Mini Kit columns (Qiagen, www.qiagen.com) according to the manufacturer's protocols, in combination with on-column DNase-I treatment (Qiagen). Aliquots (1 µL) of purified RNA were pipetted for quantification and quality assessment of total RNA using the Agilent 2100 Bioanalyzer system in combination with RNA 6000 n kit (Agilent, Santa Clara, CA, USA). Only RNA that displayed intact 18S and 25S peaks was used for microarray analysis. For the additional set-ups with irCCaMK, EV and GFP-SPOR RNA was extracted from leaves and roots using the NucleoSpin RNA plant kit (Machery-Nagel, <http://www.mn-net.com/>) according to the manufacturer's instructions including on-column DNA digestion.

Microarray analysis

Extracted RNA was labeled and hybridized according to the protocol of the Quick Amp labeling kit (Agilent, <http://www.agilent.com/home>). Agilent single-color technology arrays (60 k) were used to form hybrids from each sample. Raw intensity data were normalized with the quantile method, and subsequently the low expression probes were after log₂ transformation. Differentially expressed probes were filtered after pair-wise comparison ($FDR \leq 0.05$, fold change ≥ 1.5).

Gene ontology enrichment analysis

Significantly overrepresented gene ontology (GO) categories and distribution of differentially expressed genes (DEG) were identified using ClueGO (2.1.7) + CluePedia (1.1.7) plugin for Cytoscape (3.2.1). The overrepresented GO terms were computed through enrichment/depletion (Two-sided hypergeometric test) and Bonferroni correction ($pV \leq 0.05$, Kappa Score threshold = 0.4, Percentage for a significant cluster $\geq 60\%$) based on aspects of "Biological Process" and "Molecular Function".

qPCR of selected genes

RNA concentrations were determined using Nanodrop, and equal amounts reverse transcribed with the RevertAid H Minus First Strand cDNA Synthesis Kit (Thermo Fisher, <https://www.thermofisher.com>). qPCRs were performed using a Stratagene Mx3005P qPCR system using the primers listed in Table S6.

Amino acid analysis

Metabolites (amino acids) were analyzed by solid-phase extraction based sample preparation and analyzed by UHPLC–HESI–MS/MS according to Schäfer et al. (2016).

Statistical analysis

R version 3.1.1 and Microsoft Excel version 2007 were used for statistical analysis.

Nucleotide accession numbers

All microarray data were deposited in NCBI GEO database (GSE85375).

ACKNOWLEDGEMENTS

We thank Nam Nguyen for help with plant harvest, Shuqing Xu for substantial support with microarray analysis and Klaus Gase for submission of microarray results. This study was funded by the Max Planck Society, by Advanced Grant 293926 from the European Research Council to I.T.B., by a JSMC grant to J.W. and by the Collaborative Research Centre “Chemical Mediators in Complex Biosystems - ChemBioSys” (SFB 531 1127).

AUTHOR CONTRIBUTIONS

M. Wang, J. Wilde and K. Groten setup the experiments, recorded plant growth and harvested the material. J. Wilde characterized the FMM and analyzed the growth and P data. M. Wang performed and analyzed the microarray, the qPCRs and metabolite measurements, and the phylogenetic analysis of *Pht1* family transporters. K. Groten performed the qPCRs and counted the root colonization structures for the validation of *irCCaMK*. M. Wang, J. Wilde and K. Groten drafted the manuscript. I.T. Baldwin and K. Groten revised the manuscript. M. Wang, J. Wilde, K. Groten and I.T. Baldwin conceived and designed the study.

REFERENCES

- Adolfsson L, Nziengui H, Abreu IN, Šimura J, Beebo A, Herdean A, Aboalazadeh J, Široká J, Moritz T, Novák O, Ljung K, Schoefs B, Spetea C (2017) Enhanced secondary- and hormone metabolism in leaves of arbuscular mycorrhizal *Medicago truncatula*. **Plant Physiol** 175: 392–411
- Baldwin IT, Morse L (1994) Up in smoke 2. germination of *Nicotiana attenuata* in response to smoke-derived cues and nutrients in burned and unburned soils. **J Chem Ecol** 20: 2373–2391
- Baldwin IT, Staszakozinski L, Davidson R (1994) Up in smoke 1. smoke-derived germination cues for postfire annual, *Nicotiana attenuata* Torr ex Watson. **J Chem Ecol** 20: 2345–2371
- Balzergrue C, Puech-Pages V, Becard G, Rochange SF (2011) The regulation of arbuscular mycorrhizal symbiosis by phosphate in pea involves early and systemic signalling events. **J Exp Bot** 62: 1049–1060
- Banba M, Gutjahr C, Miyao A, Hirochika H, Paszkowski U, Kouchi H, Imaizumi-Anraku H (2008) Divergence of evolutionary ways among common sym genes: CASTOR and CCaMK show functional conservation between two symbiosis systems and constitute the root of a common signaling pathway. **Plant Cell Physiol** 49: 1659–1671
- Bandoly M, Grichnik R, Hilker M, Steppuhn A (2016) Priming of anti-herbivore defence in *Nicotiana attenuata* by insect oviposition: Herbivore-specific effects. **Plant Cell Environ** 39: 848–859
- Bonfante P, Genre A (2010) Mechanisms underlying beneficial plant-fungus interactions in mycorrhizal symbiosis. **Nat Commun** 1: 48
- Bucher M (2007) Functional biology of plant phosphate uptake at root and mycorrhiza interfaces. **New Phytol** 173: 11–26
- Caretto S, Linsalata V, Colella G, Mita G, Lattanzio V (2015) Carbon fluxes between primary metabolism and phenolic pathway in plant tissues under stress. **Int J Mol Sci** 16: 26378–26394
- Cervantes-Gamez RG, Alonso Bueno-Ibarra M, Cruz-Mendivil A, Ligne Calderon-Vazquez C, Maria Ramirez-Douriet C, Eduardo Maldonado-Mendoza I, Angel Villalobos-Lopez M, Valdez-Ortiz A, Lopez-Meyer M (2016) Arbuscular mycorrhizal symbiosis-induced expression changes in *Solanum lycopersicum* leaves revealed by RNA-seq analysis. **Plant Mol Biol Rep** 34: 89–102
- Chen A, Chen X, Wang H, Liao D, Gu M, Qu H, Sun S, Xu G (2014) Genome-wide investigation and expression analysis suggest diverse roles and genetic redundancy of *Pht1* family genes in response to Pi deficiency in tomato. **BMC Plant Biol** 14: 61–61
- Chen A, Hu J, Sun S, Xu G (2007) Conservation and divergence of both phosphate- and mycorrhiza-regulated physiological responses and expression patterns of phosphate transporters in solanaceous species. **New Phytol** 173: 817–831
- Chiou TJ, Lin SI (2011) Signaling network in sensing phosphate availability in plants. **Ann Rev Plant Biol** 62: 185–206
- Cosme M, Franken P, Mewis I, Baldermann S, Wurst S (2014) Arbuscular mycorrhizal fungi affect glucosinolate and mineral element composition in leaves of *Moringa oleifera*. **Mycorrhiza** 24: 565–570

- Daram P, Brunner S, Persson BL, Amrhein N, Bucher M (1998) Functional analysis and cell-specific expression of a phosphate transporter from tomato. **Planta** 206: 225–233
- Douds D, Pfeffer P, Shachar-Hill Y (2000) *Arbuscular Mycorrhizas Physiology and Function*. Kluwer Academic Publisher, Dordrecht, The Netherlands. pp. 107–130
- Facelli E, Duan T, Smith SE, Christophersen HM, Facelli JM, Smith FA (2014) Opening the black box: Outcomes of interactions between arbuscular mycorrhizal (AM) and non-host genotypes of *Medicago* depend on fungal identity, interplay between P uptake pathways and external P supply. **Plant Cell Environ** 37: 1382–1392
- Facelli E, Smith SE, Facelli JM, Christophersen HM, Smith FA (2010) Underground friends or enemies: Model plants help to unravel direct and indirect effects of arbuscular mycorrhizal fungi on plant competition. **New Phytol** 185: 1050–1061
- Fester T, Fetzter I, Buchert S, Lucas R, Rillig MC, Haertig C (2011) Towards a systemic metabolic signature of the arbuscular mycorrhizal interaction. **Oecologia** 167: 913–924
- Fiorilli V, Catoni M, Miozzi L, Novero M, Accotto G, Lanfranco L (2009) Global and cell-type gene expression profiles in tomato plants colonized by an arbuscular mycorrhizal fungus. **New Phytol** 184: 975–987
- Ganie AH, Ahmad A, Pandey R, Aref IM, Yousuf PY, Ahmad S, Iqbal M (2015) Metabolite profiling of low-P tolerant and low-P sensitive maize genotypes under phosphorus starvation and restoration conditions. **PLoS ONE** 10: e0129520
- Gerlach N, Schmitz J, Polatajko A, Schlueter U, Fahrenstich H, Witt S, Fernie AR, Uroic K, Scholz UWE, Sonnewald UWE, Bucher M (2015) An integrated functional approach to dissect systemic responses in maize to arbuscular mycorrhizal symbiosis. **Plant Cell Environ** 38: 1591–1612
- Govindarajulu M, Pfeffer P, Jin H, Abubaker J, Douds D, Allen J, Bucking H, Lammers P, Shachar-Hill Y (2005) Nitrogen transfer in the arbuscular mycorrhizal symbiosis. **Nature** 435: 819–823
- Groten K, Nawaz A, Nguyen NHT, Santhanam R, Baldwin IT (2015a) Silencing a key gene of the common symbiosis pathway in *Nicotiana attenuata* specifically impairs arbuscular mycorrhizal infection without influencing the root-associated microbiome or plant growth. **Plant Cell Environ** 38: 2398–2416
- Groten K, Pahari NT, Xu S, van Doorn MM, Baldwin IT (2015b) Virus-induced gene silencing using tobacco rattle virus as a tool to study the interaction between *Nicotiana attenuata* and *Rhizophagus irregularis*. **PLoS ONE** 10: e0136234
- Gu M, Chen A, Sun S, Xu G (2016) Complex regulation of plant phosphate transporters and the gap between molecular mechanisms and practical application: What is missing? **Mol Plant** 9: 396–416
- Guether M, Balestrini R, Hannah M, He J, Udvardi M, Bonfante P (2009) Genome-wide reprogramming of regulatory networks, transport, cell wall and membrane biogenesis during arbuscular mycorrhizal symbiosis in *Lotus japonicus*. **New Phytol** 182: 200–212
- Guimil S, Chang HS, Zhu T, Sesma A, Osbourn A, Roux C, Ionnidis V, Oakeley EJ, Docquier M, Descombes P, Briggs SP, Paszkowski U (2005) Comparative transcriptomics of rice reveals an ancient pattern of response to microbial colonization. **Proc Natl Acad Sci USA** 102: 8066–8070
- Gutjahr C, Banba M, Croset V, An K, Miyao A, An G, Hirochika H, Imaizumi-Anraku H, Paszkowski U (2008) Arbuscular mycorrhiza-specific signaling in rice transcends the common symbiosis signaling pathway. **Plant Cell** 20: 2989–3005
- Gutjahr C, Parniske M (2013) Cell and developmental biology of arbuscular mycorrhiza symbiosis. **Ann Rev Cell Dev Biol** 29: 593–617
- Harrison MJ, Dewbre GR, Liu JY (2002) A phosphate transporter from *Medicago truncatula* involved in the acquisition of phosphate released by arbuscular mycorrhizal fungi. **Plant Cell** 14: 2413–2429
- Helgason T, Fitter AH, Young JPW (1999) Molecular diversity of arbuscular mycorrhizal fungi colonising *Hyacinthoides non-scripta* (bluebell) in a seminatural woodland. **Mol Ecol** 8: 659–666
- Hogekamp C, Kuester H (2013) A roadmap of cell-type specific gene expression during sequential stages of the arbuscular mycorrhiza symbiosis. **BMC Genomics** 14: 306
- Jakobsen I, Rosendahl L (1990) Carbon flow into soil and external hyphae from roots of mycorrhizal cucumber plants. **New Phytol** 115: 77–83
- Jeong K, Mattes N, Catausan S, Chin JH, Paszkowski U, Heuer S (2015) Genetic diversity for mycorrhizal symbiosis and phosphate transporters in rice. **J Integ Plant Biol** 57: 969–979
- Jung SC, Martinez-Medina A, Lopez-Raez JA, Pozo MJ (2012) Mycorrhiza-induced resistance and priming of plant defenses. **J Chem Ecol** 38: 651–664
- Juszczuk IM, Wiktorowska A, Malusá E, Rychter AM (2004) Changes in the concentration of phenolic compounds and exudation induced by phosphate deficiency in bean plants (*Phaseolus vulgaris* L.). **Plant Soil** 267: 41–49
- Kai M, Takazumi K, Adachi H, Wasaki J, Shinano T, Osaki M (2002) Cloning and characterization of four phosphate transporter cDNAs in tobacco. **Plant Sci** 163: 837–846
- Karandashov V, Bucher M (2005) Symbiotic phosphate transport in arbuscular mycorrhizas. **Trends Plant Sci** 10: 22–29
- Karandashov V, Nagy R, Wegmuller S, Amrhein N, Bucher M (2004) Evolutionary conservation of a phosphate transporter in the arbuscular mycorrhizal symbiosis. **Proc Natl Acad Sci USA** 101: 6285–6290
- Kistner C, Winzer T, Pitzschke A, Mulder L, Sato S, Kaneko T, Tabata S, Sandal N, Stougaard J, Webb KJ, Szczygłowski K, Parniske M (2005) Seven *Lotus japonicus* genes required for transcriptional reprogramming of the root during fungal and bacterial symbiosis. **Plant Cell** 17: 2217–2229

- Koeppel DE, Southwick LM, Bittell JE (1976) The relationship of tissue chlorogenic acid concentrations and leaching of phenolics from sunflowers grown under varying phosphate nutrient conditions. **Can J Bot** 54: 593–599
- Kogel KH, Voll LM, Schäfer P, Jansen C, Wu Y, Langen G, Imani J, Hofmann J, Schmiedl A, Sonnewald S, von Wettstein D, Cook RJ, Sonnewald U (2010) Transcriptome and metabolome profiling of field-grown transgenic barley lack induced differences but show cultivar-specific variances. **Proc Natl Acad Sci USA** 107: 6198–6203
- Kruegel T, Lim M, Gase K, Halitschke R, Baldwin IT (2002) Agrobacterium-mediated transformation of *Nicotiana attenuata*, a model ecological expression system. **Chemoecology** 12: 177–183
- Lee J, Lee S, Young JPW (2008) Improved PCR primers for the detection and identification of arbuscular mycorrhizal fungi. **FEMS Microbiol Ecol** 65: 339–349
- Lehmann A, Barto EK, Powell JR, Rillig MC (2012) Mycorrhizal responsiveness trends in annual crop plants and their wild relatives—a meta-analysis on studies from 1981 to 2010. **Plant Soil** 355: 231–250
- Levy J, Bres C, Geurts R, Chalhoub B, Kulikova O, Duc G, Journet E, Ane J, Lauber E, Bisseling T, Denarie J, Rosenberg C, Debelle F (2004) A putative Ca^{2+} and calmodulin-dependent protein kinase required for bacterial and fungal symbioses. **Science** 303: 1361–1364
- Liu H, Trieu AT, Blaylock LA, Harrison MJ (1998) Cloning and characterization of two phosphate transporters from *Medicago truncatula* roots: Regulation in response to phosphate and to colonization by arbuscular mycorrhizal (AM) fungi. **Mol Plant-Microbe Interact** 11: 14–22
- Liu J, Maldonado-Mendoza I, Lopez-Meyer M, Cheung F, Town CD, Harrison MJ (2007) Arbuscular mycorrhizal symbiosis is accompanied by local and systemic alterations in gene expression and an increase in disease resistance in the shoots. **Plant J** 50: 529–544
- Lopez-Raez JA, Flors V, Garcia JM, Pozo MJ (2010) AM symbiosis alters phenolic acid content in tomato roots. **Plant Signal Behav** 5: 1138–1140
- Lou YG, Baldwin IT (2004) Nitrogen supply influences herbivore-induced direct and indirect defenses and transcriptional responses to *Nicotiana attenuata*. **Plant Physiol** 135: 496–506
- Lynds GY, Baldwin IT (1998) Fire, nitrogen, and defensive plasticity in *Nicotiana attenuata*. **Oecologia** 115: 531–540
- Marschner H (1996) Mineral nutrient acquisition in non-mycorrhizal and mycorrhizal plants. **Phyton-Ann Rei Bot** 36: 61–68
- McGonigle TP, Miller MH, Evans DG, Fairchild GL, Swan JA (1990) A new method which gives an objective measure of colonization by vesicular arbuscular mycorrhizal fungi. **New Phytol** 115: 495–501
- Merrild MP, Ambus P, Rosendahl S, Jakobsen I (2013) Common arbuscular mycorrhizal networks amplify competition for phosphorus between seedlings and established plants. **New Phytol** 200: 229–240
- Nagy R, Drissner D, Amrhein N, Jakobsen I, Bucher M (2009) Mycorrhizal phosphate uptake pathway in tomato is phosphorus-repressible and transcriptionally regulated. **New Phytol** 181: 950–959
- Nagy R, Karandashov V, Chague W, Kalinkevich K, Tamasloukht M, Xu GH, Jakobsen I, Levy AA, Amrhein N, Bucher M (2005) The characterization of novel mycorrhiza-specific phosphate transporters from *Lycopersicon esculentum* and *Solanum tuberosum* uncovers functional redundancy in symbiotic phosphate transport in solanaceous species. **Plant J** 42: 236–250
- Nagy R, Vasconcelos MJ, Zhao S, McElver J, Bruce W, Amrhein N, Raghothama KG, Bucher M (2006) Differential regulation of five Pht1 phosphate transporters from maize (*Zea mays* L.). **Plant Biol (Stuttg)** 8: 186–197
- Nouri E, Breuillin-Sessoms F, Feller U, Reinhardt D (2014) Phosphorus and nitrogen regulate arbuscular mycorrhizal symbiosis in *Petunia hybrida*. **PLoS ONE** 9: e90841
- Parniske M (2008) Arbuscular mycorrhiza: The mother of plant root endosymbioses. **Nat Rev Microbiol** 6: 763–775
- Paszowski U, Kroken S, Roux C, Briggs SP (2002) Rice phosphate transporters include an evolutionarily divergent gene specifically activated in arbuscular mycorrhizal symbiosis. **Proc Natl Acad Sci USA** 99: 13324–13329
- Rausch C, Daram P, Brunner S, Jansa J, Laloi M, Leggewie G, Amrhein N, Bucher M (2001) A phosphate transporter expressed in arbuscule-containing cells in potato. **Nature** 414: 462–466
- Redecker D, Kodner R, Graham L (2000) Glomalean fungi from the Ordovician. **Science** 289: 1920–1921
- Riedel T, Groten K, Baldwin IT (2008) Symbiosis between *Nicotiana attenuata* and *Glomus intraradices*: Ethylene plays a role, jasmonic acid does not. **Plant Cell Environ** 31: 1203–1213
- Rillig MC, Ramsey PW, Gannon JE, Mummey DL, Gadkar V, Kapulnik Y (2008) Suitability of mycorrhiza-defective mutant/wildtype plant pairs (*Solanum lycopersicum* L. cv Micro-Tom) to address questions in mycorrhizal soil ecology. **Plant Soil** 308: 267–275
- Rivero J, Gamir J, Aroca R, Pozo MJ, Flors V (2015) Metabolic transition in mycorrhizal tomato roots. **Front Microbiol** 6: 598
- Schäfer M, Brütting C, Baldwin IT, Kallenbach M (2016) High-throughput quantification of more than 100 primary- and secondary-metabolites, and phytohormones by a single solid-phase extraction based sample preparation with analysis by UHPLC–HESI–MS/MS. **Plant Methods** 12: 30
- Schliemann W, Ammer C, Strack D (2008) Metabolite profiling of mycorrhizal roots of *Medicago truncatula*. **Phytochemistry** 69: 112–146
- Schlueter U, Colmsee C, Scholz U, Braeutigam A, Weber APM, Zellerhoff N, Bucher M, Fahnenstich H, Sonnewald U (2013) Adaptation of maize source leaf metabolism to stress related disturbances in carbon, nitrogen and phosphorus balance. **BMC Genomics** 14: 442
- Schweiger R, Baier MC, Persicke M, Mueller C (2014) High specificity in plant leaf metabolic responses to arbuscular mycorrhiza. **Nat Commun** 5: 3886

- Simon L, Lalonde M, Bruns TD (1992) Specific amplification of 18S fungal ribosomal genes from vesicular-arbuscular endomycorrhizal fungi colonizing roots. **Appl Environ Microbiol** 58: 291–295
- Smith SE, Jakobsen I, Gronlund M, Smith FA (2011) Roles of arbuscular mycorrhizas in plant phosphorus nutrition: Interactions between pathways of phosphorus uptake in arbuscular mycorrhizal roots have important implications for understanding and manipulating plant phosphorus acquisition. **Plant Physiol** 156: 1050–1057
- Smith SE, Read D (2008) *Mycorrhizal Symbiosis*. 3rd edn. Elsevier, Amsterdam, The Netherlands. pp. 787
- Smith SE, Smith FA, Jakobsen I (2004) Functional diversity in arbuscular mycorrhizal (AM) symbioses: The contribution of the mycorrhizal P uptake pathway is not correlated with mycorrhizal responses in growth or total P uptake. **New Phytol** 162: 511–524
- Sun H, Wang L, Zhang B, Ma J, Hettenhausen C, Cao G, Sun G, Wu J, Wu J (2014) Scopoletin is a phytoalexin against *Alternaria alternata* in wild tobacco dependent on jasmonate signalling. **J Exp Bot** 65: 4305–4315
- Tamura Y, Kobae Y, Mizuno T, Hata S (2012) Identification and expression analysis of arbuscular mycorrhiza-inducible phosphate transporter genes of soybean. **Biosci Biotechnol Biochem** 76: 309–313
- Tan Z, Hu Y, Lin Z (2012) Expression of NtPT5 is correlated with the degree of colonization in tobacco roots inoculated with *Glomus etunicatum*. **Plant Mol Biol Rep** 30: 885–893
- Tan Z, Hu Y, Lin Z (2013) Expression of SYMRK affects the development of arbuscular mycorrhiza in tobacco roots. **Acta Physiol Plant** 35: 85–94
- van der Heijden MGA, Horton TR (2009) Socialism in soil? The importance of mycorrhizal fungal networks for facilitation in natural ecosystems. **J Ecol** 97: 1139–1150
- Volpe V, Giovannetti M, Sun XG, Fiorilli V, Bonfante P (2016) The phosphate transporters LjPT4 and MtPT4 mediate early root responses to phosphate status in non mycorrhizal roots. **Plant Cell Environ** 39: 660–671
- Walder F, Boller T, Wiemken A, Courty PE (2016) Regulation of plants' phosphate uptake in common mycorrhizal networks: Role of intraradical fungal phosphate transporters. **Plant Signal Behav** 11: e1131372
- Walder F, Brulé D, Koegel S, Wiemken A, Boller T, Courty PE (2015) Plant phosphorus acquisition in a common mycorrhizal network: Regulation of phosphate transporter genes of the Pht1 family in sorghum and flax. **New Phytol** 205: 1632–1645
- Walder F, Niemann H, Natarajan M, Lehmann MF, Boller T, Wiemken A (2012) Mycorrhizal networks: Common goods of plants shared under unequal terms of trade. **Plant Physiol** 159: 789–797
- Wang X, Pan Q, Chen F, Yan X, Liao H (2011) Effects of co-inoculation with arbuscular mycorrhizal fungi and rhizobia on soybean growth as related to root architecture and availability of N and P. **Mycorrhiza** 21: 173–181
- Willmann M, Gerlach N, Buer B, Polatajko A, Nagy R, Koebe E, Jansa J, Flisch R, Bucher M (2013) Mycorrhizal phosphate uptake pathway in maize: Vital for growth and cob development on nutrient poor agricultural and greenhouse soils. **Front Plant Sci** 4: 533
- Wu QS, Srivastava AK, Li YF (2015) Effects of mycorrhizal symbiosis on growth behavior and carbohydrate metabolism of trifoliate orange under different substrate P levels. **J Plant Growth Regul** 34: 499–508
- Yan J, Zhao C, Zhou J, Yang Y, Wang P, Zhu X, Tang G, Bressan RA, Zhu JK (2016) The miR165/166 mediated regulatory module plays critical roles in ABA homeostasis and response in *Arabidopsis thaliana*. **PLoS Genet** 12: e1006416
- Yang H, Zhang Q, Dai Y, Liu Q, Tang J, Bian X, Chen X (2015) Effects of arbuscular mycorrhizal fungi on plant growth depend on root system: A meta-analysis. **Plant Soil** 389: 361–374
- Zhang L, Gase K, Baldwin IT, Galis I (2010) Enhanced fluorescence imaging in chlorophyll-suppressed tobacco tissues using virus-induced gene silencing of the phytoene desaturase gene. **Biotechniques** 48: 125–133
- Zubek S, Rola K, Szewczyk A, Majewska ML, Turnau K (2015) Enhanced concentrations of elements and secondary metabolites in *Viola tricolor* L. induced by arbuscular mycorrhizal fungi. **Plant Soil** 390: 129–142

SUPPORTING INFORMATION

Additional Supporting Information may be found online in the supporting information tab for this article: <http://onlinelibrary.wiley.com/doi/10.1111/jipb.12609/supinfo>

Figure S1. Comparisons of transcript abundances and inoculation rates of AMF-inoculated irCCaMK plants in single pots, in 2 L pots separated by a barrier not penetrable for roots and in 2 L pots with an isogenic line of *N. attenuata* ectopically expressing GFP confirm that irCCaMK roots are not internally colonized by AMF

Figure S2. Expression box plots after data normalization, sequential multi-dimensional scaling (MDS) and measurement of selected, significantly changed gene expressions by qPCR indicate that data adjustment and the validity of the data-set for downstream analyses are valid

Figure S3. Phylogenetic tree of PHT1 family and hierarchical cluster analysis of PHT1 family members in *N. attenuata*

Table S1. AMF root colonization rates 6 weeks post-inoculation

Table S2. Amino acid analysis of leaves and roots 6 wpi from plants grown on Rhizophagus inoculum (+) and non-inoculated plants (–). For the experimental set-up see **Figure 1**

Table S3. Amino acid analysis of leaves and roots 6 wpi from plants grown on FMM (+) and non-inoculated plants (–). For the experimental set-up see [Figure 1](#)

Table S4. Secondary metabolite levels of leaves and roots 6 wpi from plants grown on *R. irregularis* (+)

and non-inoculated plants (–). For the experimental set-up see [Figure 1](#)

Table S5. Secondary metabolite levels of leaves and roots 6 wpi from plants grown on FMM (+) and non-inoculated plants (–). For the experimental set-up see [Figure 1](#)

Table S6. qPCR primers used in this study



Scan using WeChat with your smartphone to view JIPB online



Scan with iPhone or iPad to view JIPB online

Supporting Information

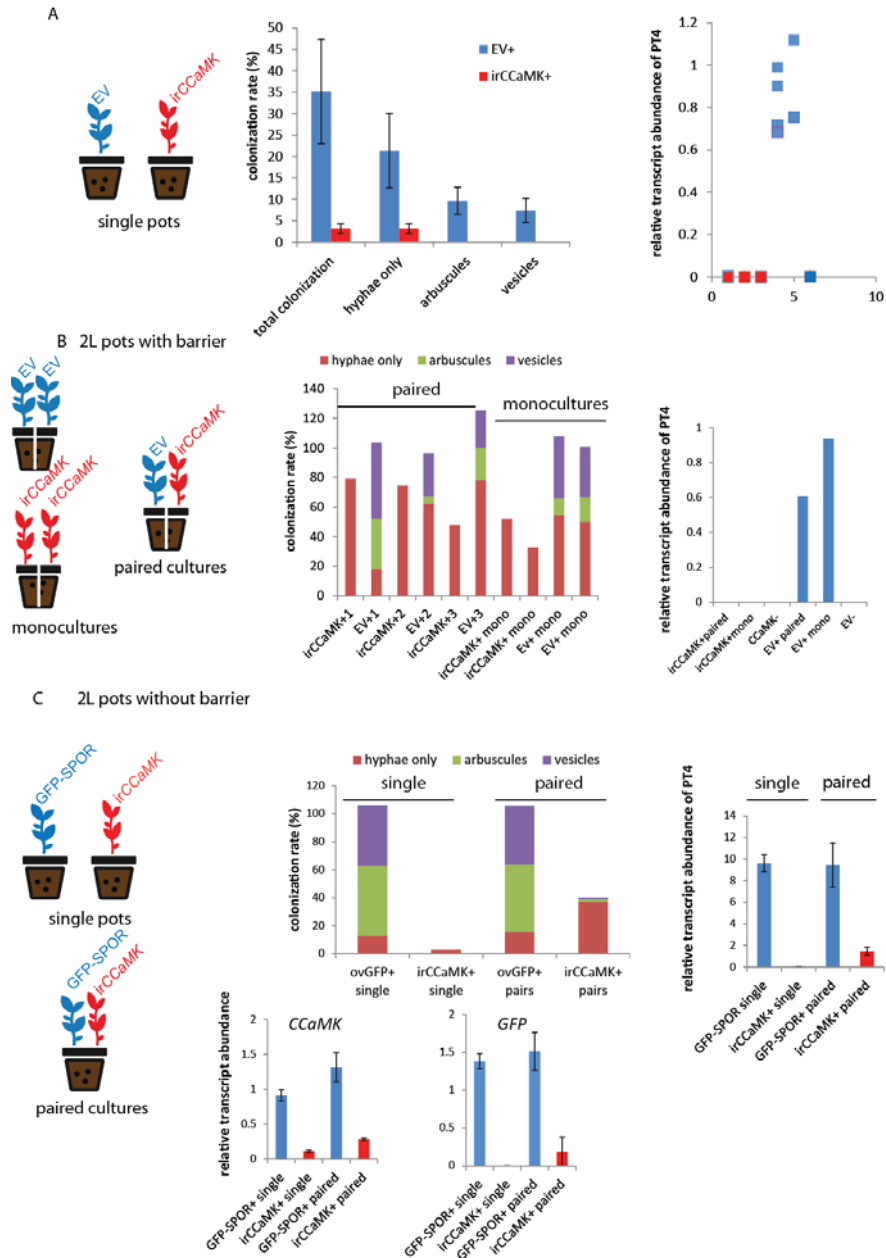


Fig. S1. Comparisons of transcript abundances and inoculation rates of AMF-inoculated *irCCaMK* plants in single pots, in 2L pots separated by a barrier not penetrable for roots and in 2L pots with a line of an isogenic line of *N. attenuata* ectopically expressing GFP confirm that *irCCaMK* roots are not internally colonized by AMF.

Plants were grown for at least six weeks with *Rhizophagus* inoculum. Roots were harvested and used to determine fungal colonization rates by Trypan Blue staining and to determine transcript abundance of *NaPT4*. A) Plants were grown in single pots. B) EV and *irCCaMK* plants were grown in 2 L pots with a barrier not penetrable for roots, but for fungal hyphae. Plants were grown either with the same genotype (mono) or in pairs with the other genotype (paired). C) Plants expressing a GFP-sporamin fusion protein (GFP-SPOR) and *irCCaMK* plants were grown either in single 1 L pots (single) or in mixed pairs (paired) in 2 L pots and in addition to *NaPT4* relative transcript abundances of *GFP* and of *CCaMK* were determined. Data shown are N=4, mean±se. Elongation factor $\alpha 1$ was used to compare transcript abundances among samples.

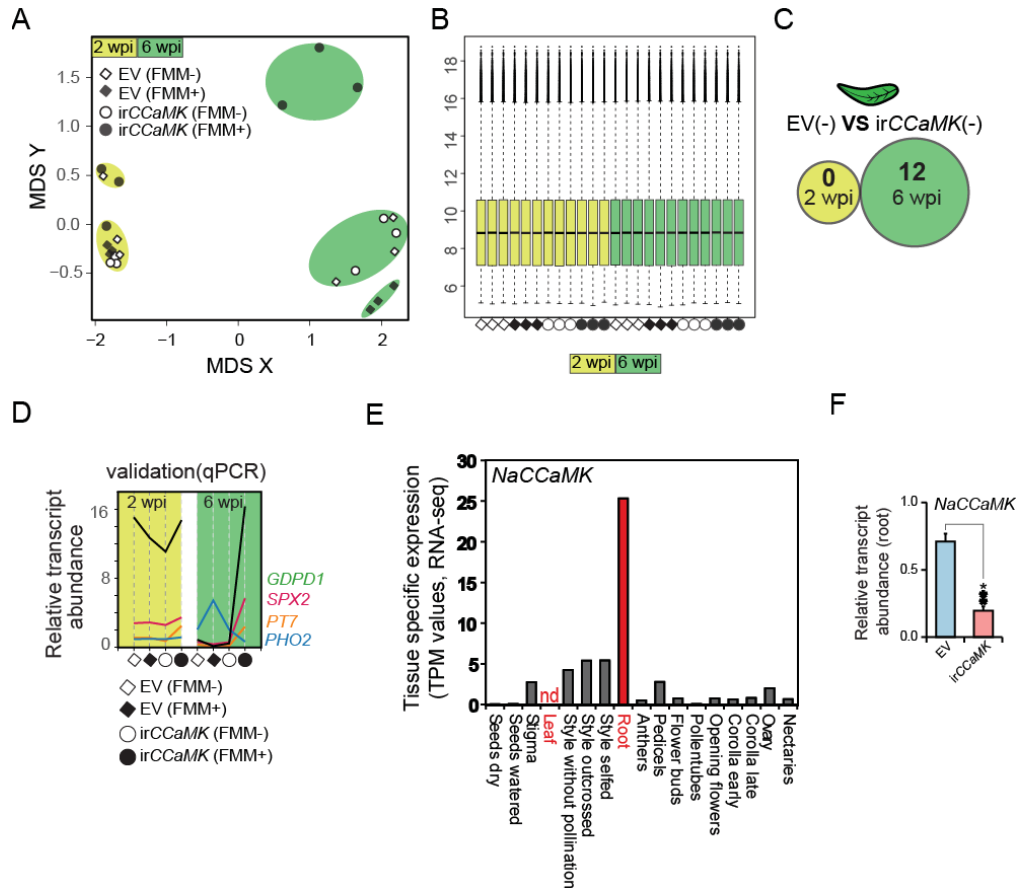


Fig. S2. Expression box plots after data normalization, sequential multi-dimensional scaling (MDS) and measurement of selected, significantly changed gene expressions by qPCR indicate that data adjustment and the validity of the data-set for downstream analyses are valid.

(A) **Multi-dimensional scaling (MDS) plot of all samples.** Manhattan distances (statistically calculated from 33,798 informative probe sets) were used to generate the MDS plot. The largest differences occurred among inoculated and non-inoculated plants, in particular with data from *irCCaMK* plants, while at the early harvest time-point most samples grouped closely together without showing a clear pattern among the different samples. (B) Box plots of expression values after quantile normalization. Rank-average expression values of non-inoculated (blank) and inoculated (filled) at 2wpi (yellow) and 6 wpi (green) samples were used to replace the specific microarray expression values of pre-quantile normalization. The post-normalized box plots distribute in the same intervals with the same density center, indicating successful adjustment of data for further analysis. (C) Venn-diagram showing the number of DEGs (fold

change ≥ 1.5 or ≤ -1.5 , $FDR \leq 0.05$) in leaves between EV and *irCCaMK* without AMF inoculation. Genotype based pair-wise comparisons were performed at 2 wpi (yellow) and 6 wpi (green) harvest. (D) **qRT-PCR validation of selected DEGs confirmed the reliability of microarray datasets. Data shown are mean \pm SE (N=3).** (E) Tissue-specific gene expression pattern of *NaCCaMK* analyzed by RNA-seq. Data are TPM (transcripts per million) values after transformation. Relative higher transcript levels of *NaCCaMK* are present in root and floral tissues, but not in leaves. (F) *CCaMK* transcript level is silenced (72.4%) in *irCCaMK* roots. Transcript abundance was tested by **qRT-PCR** (relative to EIF5A3; mean \pm SE; N=6; Student's *t* test, *** $p \leq 0.005$).

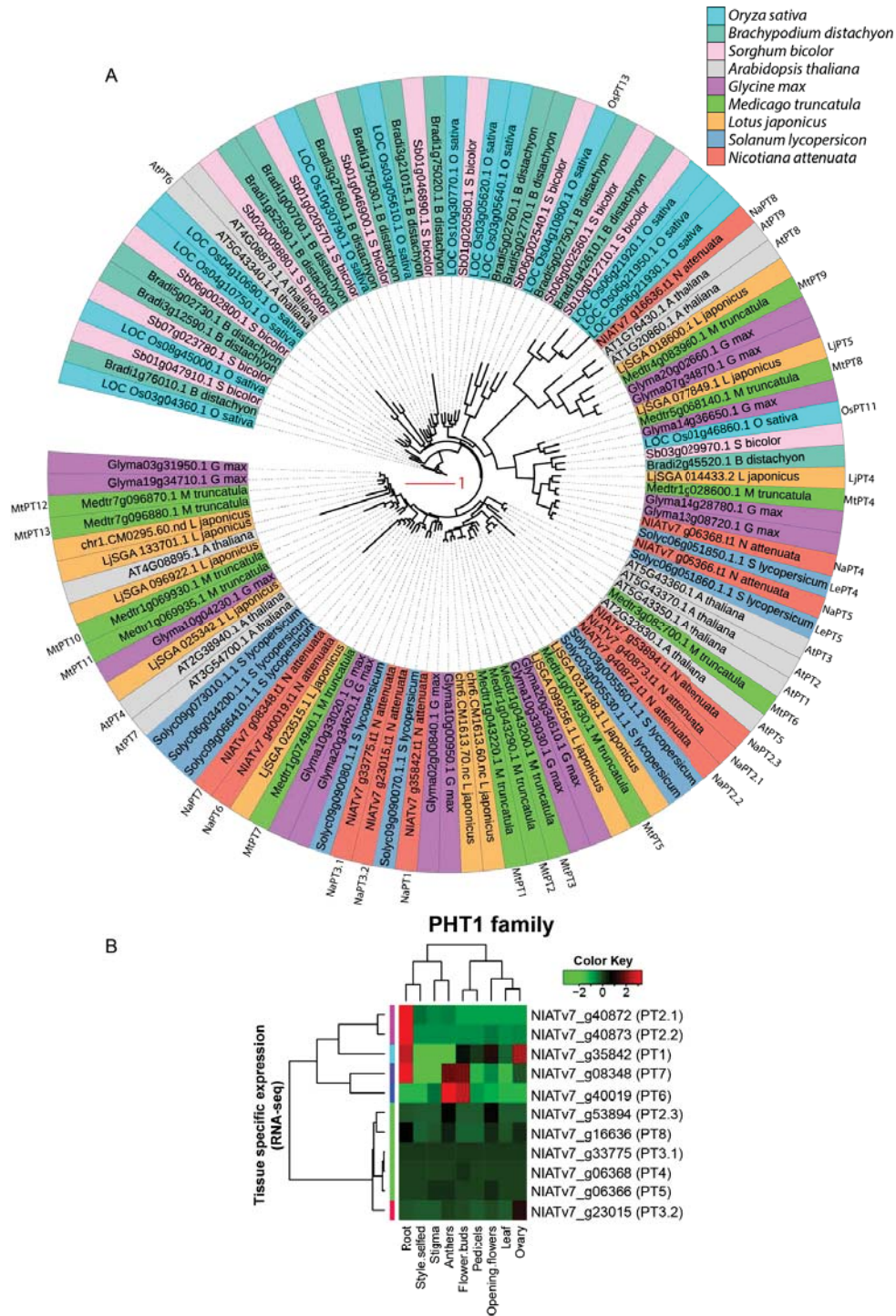


Fig. S3. Phylogenetic tree of PHT1 family and hierarchical cluster analysis of PHT1 family members in *N. attenuata*.

(A) Phylogenetic tree showing all phosphate transporters of the PHT1 family identified in *N. attenuata* and their homologues in rice, Sorghum, Arabidopsis, soybean, Medicago, Lotus and Brachypodium. The full-length amino acid sequences of PHT1 family were obtained by blasting the published sequences from Arabidopsis, rice, medicago and tomato against the *N. attenuata* database (Xu et al. 2017). These sequences were used to build a phylogenetic tree with Phylogeny.fr (<http://phylogeny.lirmm.fr/phylo.cgi/index.cgi>); the full mode of MUSCLE was used for alignment. The approximately maximum likelihood phylogenetic tree was generated using PhyML with the Jones-Taylor-Thornton (JTT) model. Each branch division shows local support values with the approximate likelihood-ratio test (aLRT). (B) Expression of *PTH1* family members in different tissues based on RNAseq data. Hierarchical cluster analysis was conducted by heatmap.2.

Table S1. AMF root colonization rates 6 weeks post inoculation.

Genotype	Relative root colonization (%)	Relative arbuscule colonization (%)	Relative vesicle colonization (%)
EV (FMM+)	87±4.93	54±4.33**	19±2.03*
irCCaMK (FMM+)	77±6.36	29±5.33	8±1.86
EV (R. irr.+)	93±2.03	80±24.73	23±1.20**
irCCaMK (R. irr.+)	73±11.06	28±7.31	6±2.67

Asterisks indicate significant differences (paired Students *t*-test, **p*≤0.05, ***p*≤0.01, N=3, mean±SE).

Table S2. Amino acid analysis of leaves and roots 6 wpi from plants grown on *R. irregularis* inoculum (+) and non-inoculated plants (-). For the experimental set-up see Fig. 1.

Amino acid	Leaf – 6 wpi				Root – 6wpi			
	EV-	EV+	irCCaMK-	irCCaMK+	EV-	EV+	irCCaMK-	irCCaMK+
Threonine	11.63±0.57	14.60±0.95	13.97±1.57	29.19±3.75*	5.51±0.32	11.24±0.59	5.79±0.36	13.93±0.70
L-Alanine	6.00±0.52	8.82±0.71	8.76±1.32	9.64±1.04	1.14±0.07	4.88±0.30*	1.19±0.07	2.86±0.22
L-Arginine	2.86±0.24	4.63±0.39	2.86±0.20	4.89±0.7	2.87±0.28	213.09±19.01*	3.26±0.16	62.46±5.96
L-Aspartic Acid	14.69±1.91	7.99±0.75	18.03±3.83*	18.91±1.24*	2.27±0.08 a	8.30±0.47 *	2.39±0.11	5.85±1.16
L-Asparagine	0.90±0.29	0.57±0.05	0.67±0.09	4.34±1.35*	1.24±0.1	19.66±1.48 *	1.30±0.10	9.43±0.85
L-Glutamic acid	71.39±6.33	59.37±4.32	76.49±9.92	108.74±6.24*	19.97±0.95	72.27±3.84*	20.05±1.14	35.48±2.30
L-Glutamine	26.17±7.83	8.19±0.86	23.30±8.28	117.51±34.23*	11.28±0.67	37.77±2.15*	11.24±0.98	27.95±2.53
L-Isoleucine	7.44±1.08	9.57±0.40	6.10±0.61	26.09±7.41*	2.34±0.14a	4.69±0.33	2.44±0.19	5.22±0.32
L-Leucine	2.63±0.21	4.01±0.18	2.53±0.16	8.70±2.07*	3.58±0.16	4.55±0.23	3.80±0.21	6.08±0.33*
L-Lysine	12.82±0.9	10.18±1.19	13.18±1.88	16.04±2.63	9.03±1.78a	13.81±1.50*	6.74±0.34a	8.66±0.86
L-Phenylalanine	6.95±0.34	7.37±0.40	7.92±0.60	10.97±0.96*	3.96±0.20a	4.05±0.18a	4.19±0.20a	5.10±0.2*
L-Proline	10.63±0.81	13.45±1.52	13.91±0.88	31.37±5.49*	1.63±0.07	3.12±0.29	1.77±0.06	3.51±0.72
L-Serine	7.77±0.94	10.26±0.93	9.23±1.22	13.91±0.83*	5.45±0.43	9.87±0.98 *	5.20±0.27	7.82±0.65
L-Valine	7.69±1.26	10.09±0.45	6.28±0.32	26.39±7.05	2.54±0.15	5.70±0.42*	2.52±0.22	4.86±0.41
L-Tyrosine	3.66±0.70	3.94±0.22	2.99±0.32	16.03±4.66 *	3.44±0.29	5.28±0.29	3.59±0.39	7.73±0.52
L-Tryptophane	18.86±5.34	13.29±1.02	12.48±1.58	105.50±34.87*	20.61±2.21	31.08±2.36	24.71±3.14	76.44±4.41*

Values are in ng/g FM. Asterisks indicate significant differences between AMF-inoculated and non-inoculated plants of the same genotype (unpaired Students t-test, N=8, mean±SE, $p \leq 0.05$). Values were $\log_2(x+1)$ –transformed before statistical analysis.

Table S3. Amino acid analysis of leaves and roots 6 wpi from plants grown on FMM (+) and non-inoculated plants (-). For the experimental set-up see Fig. 1.

Amino acid	Leaf – 6 wpi				Root – 6wpi			
	EV-	EV+	CCaMK-	irCCaMK+	EV-	EV+	CCaMK-	irCCaMK+
Threonine	8.08±0.76	9.58±0.39	10.65±0.64	12.99±1.04	4.69±0.21	11.66±0.90*	5.29±0.63	9.48±0.59*
L-Alanine	4.34±0.36	5.30±0.37	5.25±0.33	6.01±0.59	1.24±0.09	7.49±0.77*	1.63±0.25	5.14±0.98*
L-Arginine	1.56±0.29	2.25±0.19	1.89±0.20	11.48±8.88*	1.48±0.09	161.16±23.08*	1.61±0.15	93.43±22.05*
L-Aspartic Acid	4.59±0.35	4.68±0.28	4.90±0.29	9.78±1.18*	2.34±0.13	6.60±0.69*	2.55±0.18	4.61±0.49*
L-Asparagine	0.04±0.04	0.15±0.08	0.03±0.03	1.45±0.94*	1.49±0.1	13.51±1.62*	1.63±0.22	7.66±1.40*
L-Glutamic acid	29.78±2.97	26.67±1.32	35.63±2.89*	58.40±5.09*	19.53±1.04	52.78±5.19*	19.24±1.34	37.39±4.40*
L-Glutamine	2.66±0.34	2.43±0.28	3.30±0.41	11.07±2.34*	7.89±0.96	43.62±4.83*	8.75±0.93	27.45±4.51*
L-Isoleucine	4.33±0.77	5.66±0.41	5.17±0.64	6.75±0.78	1.70±0.09	4.44±0.36*	1.92±0.3	3.50±0.31*
L-Leucine	<0.01	0.33±0.33	0.27±0.27	0.49±0.48	0.20±0.2	0.74±0.51	0.98±0.39	1.34±0.69
L-Lysine	8.40±0.64	4.60±0.43*	6.30±0.33	5.50±0.69	1.14±0.12	0.75±0.27	1.06±0.18	1.04±0.23
L-Phenylalanine	4.31±0.37	5.04±0.46	5.45±0.33	5.02±0.44	2.48±0.12	3.53±0.19*	2.54±0.21	3.87±0.20*
L-Proline	6.50±0.59	7.57±0.45	8.53±0.52	12.20±0.85*	1.37±0.11	6.77±0.81*	1.40±0.20	6.93±2.30*
L-Serine	5.12±0.59	5.27±0.37	6.55±0.48*	8.10±0.48*	4.71±0.20	9.13±0.60*	6.94±2.00	7.99±0.53*
L-Valine	4.52±0.79	5.85±0.55	5.48±0.70	7.14±0.72	2.14±0.11	6.32±0.50*	2.63±0.43	4.68±0.49*
L-Tyrosine	2.17±0.40	2.58±0.23	2.83±0.39	4.29±0.32*	2.27±0.13	4.31±0.24*	2.61±0.29	4.60±0.27*
L-Tryptophane	5.03±1.04	6.29±0.77	6.55±1.08	13.46±1.97*	8.87±0.64	18.86±1.37*	9.10±0.84 a	22.03±1.58*

Values are in ng/g FM. Asterisks indicate significant differences between AMF-inoculated and non-inoculated plants of the same genotype (unpaired Students t-test, N=7, mean±SE, $p \leq 0.05$). Values were $\log_2(x+1)$ –transformed before statistical analysis.

Table S4. Secondary metabolite levels of leaves and roots 6 wpi from plants grown on *R. irregularis* inoculated (+) and non-inoculated plants (-). For the experimental set-up see Fig. 1.

Leaf – 6 wpi					Root – 6 wpi			
Metabolite	EV-	EV+	irCCaMK-	irCCaMK+	EV-	EV+	irCCaMK-	irCCaMK+
IAA	1.31± 0.36	1.99±0.16	1.73±0.49	3.68±2.09	2.83±0.26	2.96± 0.15	2.75±0.26	3.99± 0.17*
Caffeic acid	59.17± 6.17	53.69± 3.73	60.95±3.72	81.55±10.28	69.48±6.26	182.17± 15.95*	70.98±8.5	124.75± 10.81*
Cinnamic acid	0.69± 0.19	0.33±0.13	0.75±0.15	2.24±0.51*	0.05±0.04	0.45± 0.05*	0±0	0.35± 0.05*
Coniferyl aldehyde	9.47± 1.11	7.41±0.39	9.12±1.00	8.99±0.68	7.02±0.55	15.99± 0.79*	7.39±0.60	10.42± 0.51*
Ferulic acid	3.47±0.62	1.81±0.23*	3.19±0.49	4.31±0.64	2.24±0.18	8.49± 0.98*	2.49±0.21	5.18± 0.41*
Fraxetin	0.04±0.02	0.02±0.01	0.04±0.02	0.2±0.04*	0.17±0.03	0.41± 0.07	0.15±0.03	0.84± 0.18*
Scopoletin	1.35± 0.65	0.13±0.03	0.4±0.12	9.93±5.53*	1.33±0.26	17.48± 3.08*	1.27±0.21	24.36± 5.93*
Scopolin	65.57± 24.20	18.22±2.23	39.91±9.00	194.63±77.72	36.72±9.98	292.84± 55.97*	46.67±9.56	226.59± 51.66*
Sinapic acid	53.47± 4.60	45.1±2.79	50.01±3.19	65.82±6.33*	2.37±0.20	28.65± 3.50*	2.56±0.46	10.23± 0.80*
Sinapyl aldehyde	0.58± 0.21	0.7±0.06	0.99±0.22	0.7±0.15	0.50±0.04	0.74± 0.08	0.51±0.06	0.51±0.02
Malic acid	3422.28± 257.65	2179.66± 216.15*	3230.43± 316.00	1879.57± 274.08*	911.87± 71.10	447.58± 37.31*	1053.6±54.02	500.09± 30.21*
Rutin	338.89± 34.01	252.04± 17.28	430.18± 25.42	611.37± 46.69*	0.19±0.05	0.01± 0.01*	0.18±0.07	0.01± 0.01*
Tyramine	18.11± 4.86	20±3.94	15.7±1.63	47.92±8.11*	74.46±8.99	193.39± 23.26*	88.21± 13.44	228.51± 40.62*
Caffeoylputrescine	167.82± 69.50	69.06±6.97*	219.14±86.79	711.58± 123.72*	4.99±1.13	14.05± 5.76	6.74±2.06	30.42± 12.17*
Chlorogenic acid	477.26± 60.85	363.51± 25.34	505.22± 50.51	598.52± 60.09	231.51± 13.29	474.86± 55.89*	294.82± 49.39	470.3± 103.20

Values are in ng/g FM. Asterisks indicate significant differences between inoculated and non-inoculated plants of the same genotype (unpaired Students t-test, N=8, mean±SE, $p \leq 0.05$). Values were $\log_2(x+1)$ –transformed before statistical analysis.

Table S5. Secondary metabolite levels of leaves and roots 6 wpi from plants grown on FMM (+) and non-inoculated plants (-). For the experimental set-up see Fig. 1.

metabolite	Leaf – 6 wpi				Root – 6 wpi			
	EV-	EV+	irCCaMK-	irCCaMK+	EV-	EV+	irCCaMK-	irCCaMK+
IAA	4.30± 0.71	4.08± 0.47	4.10± 0.50	7.19± 1.59	6.93± 0.40	9.26± 0.62*	6.85± 0.39	10.29± 0.72*
Caffeic acid	33.24± 2.98	37.46± 3.89	30.94± 3.56	41.90± 3.69	82.94± 3.80	157.30± 11.16*	74.89± 3.49	99.28± 13.03
Cinnamic acid	0.19± 0.12	0.00± 0.00	0.10± 0.10	0.54± 0.15*	0.10± 0.05	3.84± 0.59*	0.26± 0.09	2.27± 0.51*
Coniferyl aldehyd	0.00± 0.00	0.00± 0.00	0.00± 0.00	0.00± 0.00	13.09± 1.02	17.46± 1.40*	13.29± 1.23	13.81± 2.18
Ferulic acid	1.97± 0.28	2.78± 0.44	1.74± 0.49	1.74± 0.30	1.67± 0.08	7.08± 0.97*	1.63± 0.11	3.91± 0.97*
Fraxetin	0.00± 0.00	0.01± 0.01	0.03± 0.01	0.08± 0.01	0.12± 0.03	0.71± 0.08*	0.14± 0.03	0.44± 0.12*
Scopoletin	0.37± 0.25	0.31± 0.08	0.13± 0.07	0.46± 0.35	2.03± 0.40	135.41± 17.08*	2.78± 0.40	67.45± 24.94*
Scopolin	20.52± 2.09	41.36± 10.21	19.14± 3.85	29.40± 10.83	46.23± 6.96	1201.91± 150.05*	63.21± 7.69	675.77± 172.28*
Sinapic acid	38.45± 2.62	35.51± 1.53	34.99± 4.08	41.64± 1.55	1.57± 0.28	19.06± 3.37*	1.59± 0.15	8.52± 4.65*
Sinapyl aldehyd	0.35± 0.05	0.55± 0.09	0.74± 0.11	0.80± 0.12	1.46± 0.16	0.93± 0.23*	1.30± 0.24	1.03± 0.33
Malic acid	2387.12± 902.25	1851.13± 699.66*	2025.71± 765.65	1740.21± 657.74	897.17± 299.06	394.72± 131.57*	795.47± 265.16	544.24± 192.42
Rutin	201.15± 12.12	186.99± 15.69	252.73± 16.42	315.25± 57.11*	0.38± 0.07	0.17± 0.07	0.11± 0.04	0.06± 0.02
Tyramine	11.38± 4.30	69.74± 6.36*	13.04± 4.93	62.50± 3.62*	83.08± 7.69	939.40± 13.13*	112.56± 37.52	583.38± 206.26*
Caffeoylputrescine	18.72± 2.30	27.65± 4.26	25.23± 4.58	129.00± 18.37*	1.53± 0.26	248.93± 28.35*	1.86± 0.32	168.50± 44.51*
Chlorogenic acid	379.80± 12.32	360.47± 33.46	442.30± 25.72	523.21± 38.82	534.12± 41.60	1795.11± 181.84*	628.20± 56.06	1334.19± 205.39*
Citric acid	6.26± 1.13	2.12± 0.38*	5.06± 0.94	10.41± 3.91	2.32± 0.27	3.45± 0.52	2.05± 0.35	3.58± 0.92
Fumaric acid	0.73± 0.28	0.95± 0.57	0.73± 0.28	0.30± 0.30	0.63± 0.32	1.00± 0.24	0.49± 0.21	0.96± 0.32

Values are in ng/g FM. Asterisks indicate significant differences between inoculated and non-inoculated plants of the same genotype (unpaired Students t-test, N=8, mean±SE, $p \leq 0.05$). Values were $\log_2(x+1)$ –transformed before statistical analysis.

Table S6. qPCR primers used in this study

Gene	Forward Primer	Reverse Primer
NaCCaMK	TTGGAGCTTTGTTCTGGTGGT	ATACTTGCCCCGTGTAGCG
NaPT1	GGGGCATTGAAACCTGGAT	CCACCCGAAAAACAGTTGACC
NaPT3.1	GTTGCTCTTATTATTGCTGGTGC	TCCAAACATAATCAGCTTCAGGT
NaPT4	GGGGCTCGTTTCAATGATTA	AACACGATCCGCCAAACAT
NaPT4-1*	GGGGCTCGTTTCAATGATTA	AGCAGTGTAACGCCCTGTTT
NaPT5	TTGGCGAATAGTATTGATGCT	TCAAGAACCTTTCCCATGTCAA
NaPT7	GTTACAGTGTTCTCATTGACAG	GCGAATAGAGAACACGAATCC
NaIF5a	GTCGGACGAAGAACCATT	CACATCACAGTTGTGGGAGG
NaWRKY70	TCGACGAGGACGCTACAAAA	TGCATGGCCATCATCCACTAAA
NaR1B-12	CTGGTGCTTGAATTTTGCAGGA	TGCACATTGGAGGGGAAAATTG
NaPMPI-1	TGGTGGTGAAGGTTTCTGTCT	CAGTGTGTCGTCACCGTTTTG
NaRIN4	AACGTCGCGTGAGTAAAGAAC	ATCCACGACCAGCTCCATTAC
GFP	GGACACGATGTCCAAATGCG	CCGGAAAAGTCTGGTAGGTCG
NaEF- α 1	ACACTTCCACATTGCTGTCA	AAACGACCAATGGAGGGTAC

*NaPT4-1 was used in Supporting Fig. S1

Manuscript III:
**Blumenols as effective shoot markers for root symbiosis with arbuscular
mycorrhizal fungi**

Ming Wang, Martin Schäfer, Dapeng Li, Rayko Halitschke, Chuanfu Dong, Erica McGale, Christian Paetz, Yuanyuan Song, Suhua Li, Junfu Dong, Sven Heiling, Karin Groten, Philipp Franken, Michael Bitterlich, Maria Harrison, Uta Paszkowski and Ian T. Baldwin
Submitted to *eLife* (2018)

Blumenols as effective shoot markers for root symbiosis with arbuscular mycorrhizal fungi

Ming Wang^{1#}, Martin Schäfer^{1#}, Dapeng Li¹, Rayko Halitschke¹, Chuanfu Dong^{2Y}, Erica McGale¹, Christian Paetz³, Yuanyuan Song^{1†}, Suhua Li¹, Junfu Dong^{1,4}, Sven Heiling^{1‡}, Karin Groten¹, Philipp Franken^{5,6}, Michael Bitterlich⁷, Maria Harrison⁸, Uta Paszkowski⁹ and Ian T. Baldwin^{1*}

¹ Max Planck Institute for Chemical Ecology, Department of Molecular Ecology, Hans Knöll Str. 8, 07745 Jena, Germany.

² Max Planck Institute for Chemical Ecology, Department of Bioorganic Chemistry, Hans Knöll Str. 8, 07745 Jena, Germany.

³ Max Planck Institute for Chemical Ecology, Research Group Biosynthesis / NMR, Hans Knöll Str. 8, 07745 Jena, Germany.

⁴ College of Life Sciences, University of Chinese Academy of Sciences, 101408 Beijing, China

⁵ Leibniz-Institute of Vegetable and Ornamental Crops Großbeeren/Erfurt e.V, Kühnhäuser Str. 101, 99090 Erfurt, Germany

⁶ Humboldt Universität zu Berlin, Institute of Biology, Philippstr. 13, 10115 Berlin, Germany.

⁷ Leibniz-Institute of Vegetable and Ornamental Crops Großbeeren/Erfurt e.V, Theodor-Echtermeyer-Weg 1, 14979 Großbeeren, Germany.

⁸ Boyce Thompson Institute for Plant Research, Tower Road, Ithaca, New York 14853, USA.

⁹ University of Cambridge, Department of Plant Sciences, Street Downing, Cambridge CB2 3EA, United Kingdom.

^Y Current address: Max Planck Institute for Developmental Biology, Department of Integrative Evolutionary Biology, Max-Planck-Ring 1, 72076 Tübingen, Germany

[†] Current address: College of crop science, Fujian Agriculture and Forestry University, China

[‡] Current address: Institute of Clinical Chemistry and Laboratory Diagnostics and integrated Biobank Jena, Jena University Hospital, Am Klinikum 1, 07747 Jena, Germany

[#] Equal contribution

E-mail addresses: MW: mwang@ice.mpg.de, MS: mschaefer@ice.mpg.de, DL: dli@ice.mpg.de, RH: rhalitschke@ice.mpg.de, CD: chuanfu.dong@tuebingen.mpg.de, EM: emcgale@ice.mpg.de, CP: cpaetz@ice.mpg.de, YS: yyuansong@163.com, SL: sli@ice.mpg.de, JD: jdong@ice.mpg.de, SH: sheiling@ice.mpg.de, KG: kgroten@ice.mpg.de, PF: Franken@erfurt.igzev.de, MB: Bitterlich@igzev.de, MH: mjh78@cornell.edu, UP: up220@cam.ac.uk, ITB: baldwin@ice.mpg.de.

Running title: Leaf markers indicative of mycorrhization.

* Correspondence: Ian T. Baldwin, Department of Molecular Ecology, Max Planck Institute for Chemical Ecology. Hans-Knöll-Straße 8, 07745 Jena, Germany. E-mail: baldwin@ice.mpg.de

Abstract

The green revolution created high-yielding, but fertilizer-demanding crops; with P supplies dwindling, crop varieties harboring P-delivering mutualisms with arbuscular mycorrhizal fungi (AMF) are needed. High-through-put (HTP) screening for functional AMF-associations is challenging because roots must be excavated and colonization evaluated by transcript analysis or microscopy. Here we show that specific leaf-metabolites provide broadly applicable accurate proxies of these associations, suitable for HTP-screens. With a combination of untargeted and targeted metabolomics, we show that shoot accumulations of hydroxy- and carboxyblumenol C-glucosides mirror root AMF-colonization in *Nicotiana attenuata* plants. Genetic/ pharmacologic manipulations indicate that these AMF-indicative foliar blumenols are synthesized and transported from roots to shoots. Such foliar markers, found in many di- and monocotyledonous crop and model plants (*Solanum lycopersicum*, *Solanum tuberosum*, *Hordeum vulgare*, *Triticum aestivum*, *Medicago truncatula* and *Brachypodium distachyon*), are not restricted to particular mycorrhizal species, and are shown to be applicable for field-based QTL mapping of AMF-related genes.

eLife Digest

More than 70% of all higher plants, including crop plants, form symbiotic associations with arbuscular mycorrhizal fungi (AMF). While the fungus facilitates the uptake of mineral nutrients, in particular phosphorous (P) and nitrogen, the plant supplies the fungus with carbon. Currently, phosphate fertilizer is derived from phosphate rock, a non-renewable resource, which is predicted to be depleted within the next decade. Unfortunately, the characterization of AMF-associations is laborious and time-consuming, typically requiring destructive root harvesting and microscopic examination or transcript analyses. Here we describe a discovery that will enable crop breeding programs to select varieties that have negotiated AMF symbioses that deliver high yields with minimal P inputs, a discovery that could help steer the “green revolution” agricultural crops that currently feed the world’s growing populations away from intense fertilizer inputs and the collateral environmental damage they cause.

AMF-interactions influence whole-plant performance, hence systemic metabolic responses have been anticipated, searched for, but no widespread and specific AMF-induced responses have been found. We performed different metabolomics analyses combining methods that are suitable for the identification of new target metabolites, sophisticated biostatistics approaches, as well as methods most suitable for the quantification of minute amounts of compounds even in highly complex mixtures. We found blumenols, a group of compounds derived from carotenoids, to accumulate in the roots of coyote tobacco plants with AMF-interaction. Interestingly, these metabolites also accumulated in shoot tissues and were highly correlated with mycorrhizal colonization rates as determined by classical methods.

To clarify the origins (local biosynthesis vs. transport) of these leaf blumenols, we genetically manipulated the carotenoid biosynthesis in particular leaves of coyote tobacco plants. Treated leaves showed clear signs of bleaching, indicating impaired carotenoid biosynthesis but the levels of the AMF-indicative foliar blumenols were not affected. Additional, pharmacological experiments showed that seedlings have the capacity to transport blumenols from the root to the shoot. Therefore, we propose that AMF-indicative blumenols are produced in the root and are transported to shoot tissues.

We demonstrate the utility of these foliar metabolite markers for plant breeding by screening a full population of recombinant inbred lines (728 plants) of a forward genetics experiment grown across a 7200 m² field plot in Utah. The marker analysis took less than two weeks, something that would not have been possible with currently available techniques. Importantly, these foliar metabolites accurately reflected AMF associations in various major crop and model plants tested (tomato, potato, weed, barley, barrel clover, and purple false brome) and in associations with a variety of different mycorrhizal inoculum sources. The compounds are stable and can be

analyzed in dried leaves. We propose that the analysis of blumenols in the shoot provides a convenient, easy-to-conduct and minimally destructive tool to interrogate plant-AMF interactions to empower plant breeding programs to produce mycorrhizal-responsive and P-efficient high-yielding lines of crops.

Introduction

More than 70% of all higher plants, including crop plants, form symbiotic associations with arbuscular mycorrhizal fungi (AMF) (Brundrett and Tedersoo 2018). While the fungus facilitates the uptake of mineral nutrients, in particular phosphorous (P) and nitrogen, the plant supplies the fungus with carbon (Helber *et al.* 2011, Bravo *et al.* 2017, Jiang *et al.* 2017, Keymer *et al.* 2017, Luginbuehl and Menard 2017). The interaction affects plant growth (Rooney *et al.* 2009, Adolfsson *et al.* 2015) and resistance to various abiotic and biotic stresses (Pineda *et al.* 2010, Vannette *et al.* 2013, Chitarra *et al.* 2016, Sharma *et al.* 2017). Although AMF interactions are physically restricted to the roots, they influence whole-plant performance, hence systemic metabolic responses have been anticipated, and searched for, but no general AMF-specific responses have been found (Bi *et al.* 2007, Toussaint 2007, Schweiger and Müller 2015). While, changes in foliar levels of carbohydrates, proteins, and amino acids, as well as secondary metabolites and phytohormones in response AMF inoculation have been shown (Schweiger *et al.* 2014, Aliferis *et al.* 2015, Adolfsson *et al.* 2017), these changes are not specific to AMF interactions and tend to be general responses to various abiotic and biotic stresses. Moreover, these metabolic responses also tend to be taxa-specific, and many are likely indirect consequences of AMF-mediated effects on plant growth and development.

In contrast, large amounts of blumenol-type metabolites accumulate in roots after AMF inoculation. These compounds are apocarotenoids, in particular C₁₃ cyclohexenone derivatives, produced by the cleavage of carotenoids. After AMF colonization, a C₄₀ carotenoid is cleaved by carotenoid cleavage dioxygenase 7 (CCD7) to produce a C₁₃ cyclohexenone and a C₂₇ apocarotenoid which is further cleaved by CCD1 to yield a second C₁₃ cyclohexenone (Floss *et al.* 2008, Vogel *et al.* 2010, Hou *et al.* 2016). The compounds have been found to accumulate in the roots of AMF-colonized plants in a manner highly correlated with the fungal colonization rate (Fester *et al.* 1999). Other stimuli such as pathogen infection and abiotic stresses, do not induce their accumulations (Maier *et al.* 1997). The AMF-induced accumulation of these compounds is widespread and has been observed in roots of plant species from different families, including mono- and dicotyledons, (*Hordeum vulgare*, Peipp *et al.* 1997, *Solanum lycopersicum* and *Nicotiana tobaccum*, Maier *et al.* 2000, e.g., *Zea mays*, Fester *et al.* 2002, *Lotus japonicus* and *Medicago truncatula*, Fester *et al.* 2005, *Ornithogalum umbellatum*, Schliemann *et al.* 2006, *Allium porrum*, Schliemann *et al.* 2008).

Blumenols are classified into 3 major types; blumenol A, blumenol B and blumenol C (Figure 1A). However, previous studies reported that only blumenol glycosides that contain a blumenol C-based aglycone are positively correlated with mycorrhizal colonization. The aglycone can be additionally hydroxylated at the C11 or carboxylated at the C11 or C12 position (Maier *et al.*

1997, Maier *et al.* 2000). Additionally, 7,8-didehydro versions of blumenol C have been reported (Peipp *et al.* 1997). The glycosylation usually occurs as an *O*-glycoside at the C9 position (Strack and Fester 2006), but glycosylations at the hydroxylated C11 position have also been observed (Schliemann *et al.* 2008). The glycosyl moiety can be a single sugar or combinations of glucose (Glc), rhamnose, apiose, arabinose and/or glucuronic acid, which, in turn can be additionally malonylated or contain a 3-hydroxy-3-methylglutarate decoration (Strack and Fester 2006, Schliemann *et al.* 2008). The connections among sugar components can also vary (e.g., glucose-(1''→4')-glucose or glucose-(1''→6')-glucose; Maier *et al.* 2000, Fester *et al.* 2002). The particular type of decorations appears to be highly species-specific and it is likely that additional structural variants remain to be discovered. Exemplary structures are shown in Figure 1B.

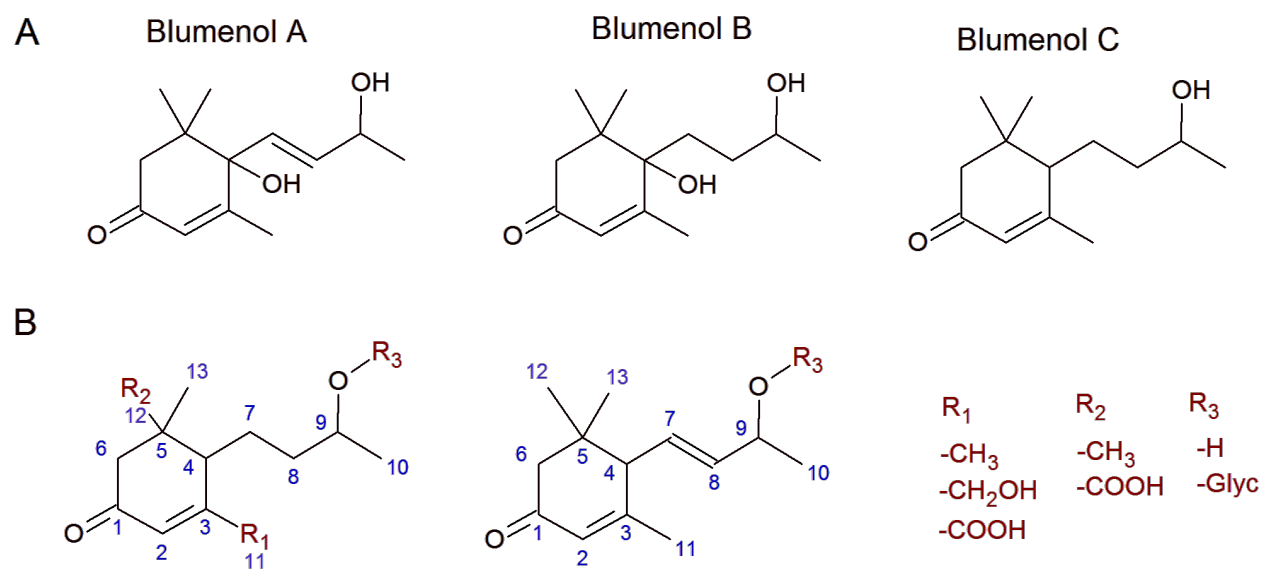


Figure 1 Blumenol core structures and exemplary modifications

A Structure of blumenol A, blumenol B and blumenol C. **B** Exemplary blumenol C derivatives. Glyc, glycoside.

Interestingly, blumenols such as blumenol A, blumenol A-9-*O*-Glc, blumenol B, blumenol C and blumenol C-9-*O*-Glc, were also reported to occur in the aerial parts of various plant species (Galbraith and Horn 1972, Bhakuni *et al.* 1974, Takeda *et al.* 1997). However, most of these studies focused on the identification of natural products using large scale extractions (up to several kg of plant material) and were not performed in the context of AMF colonization. Furthermore, some blumenol compounds were also found in plant families that are known to have lost their ability to establish AMF interactions (Brassicaceae: Cutillo *et al.* 2005, Urticaceae: Aishan *et al.* 2010). These reports indicate AMF-independent constitutive levels of particular blumenols in aerial plant parts. Adolfsson *et al.* (2017) analyzed blumenol accumulations together with other metabolites in leaves of plants with and without AMF colonization. None of these studies reported AMF-specific accumulations of blumenols or transcripts specific for their biosynthesis. The concentrations of some blumenol derivatives were even reported to be down-regulated in response to AMF colonization (Adolfsson *et al.* 2017).

The identification of a reliable metabolite marker in aerial plant tissues might be highly useful for AMF research since the characterization of AMF-associations is still laborious and time-consuming, typically requiring destructive root harvesting and microscopic examination or transcript analyses (Vierheilig *et al.* 2005, Paradi *et al.* 2010). To identify readily accessible AMF-indicative shoot metabolites, we hypothesized that a subset of the AMF-induced root metabolites would accumulate in shoots as a result of transport or systemic signaling.

Results

Blumenols are AMF-indicative metabolic fingerprints in roots

We performed an untargeted metabolomics analysis of root tissues in a transgenic line of *Nicotiana attenuata*, silenced in the calcium- and calmodulin-dependent protein kinase (*irCCaMK*) and empty vector (EV) plants co-cultured with or without *Rhizophagus irregularis* (Figure 2A). By using *irCCaMK* plants, unable to establish a functional AMF-association (Groten *et al.* 2015), we were able to dissect the AMF association-specific metabolic responses from those changes that result from more general plant-fungus interactions. Untargeted metabolome profiling of roots using liquid chromatography (LC) coupled to time-of-flight mass spectrometry (qTOF-MS) resulted in a concatenated data matrix consisting of 943 mass features (*m/z* signals detected at particular retention times). A co-expression network analysis was conducted in which nodes represent *m/z* features and edges connect metabolite mass features originating from similar in-source fragmentations and sharing biochemical relationships (Li *et al.* 2015, Li *et al.* 2016). For example, features representing well-known compounds, like nicotine and phenylalanine, were tightly connected (Figure 2B). A STEM clustering pipeline was performed to recognize patterns of metabolite accumulations in the genotype \times treatment data matrix [(EV/*irCCaMK*) \times (-/+ AMF inoculation)]. As a result, 5 of 8 computed distinct expression patterns were mapped onto the covariance network in Figure 2B (shown in different colors). A tightly grouped cluster of unknown metabolites, highlighted in red (Figure 2B) occupied a distinct metabolic space. Metabolites grouped in this cluster were highly elicited upon mycorrhizal colonization in EV, but not in *irCCaMK* plants and not found in plants without AMF associations (Figure 2C). The structures of the compounds of this cluster were annotated based on tandem-MS and NMR data. Five metabolites were annotated as blumenols: 11-hydroxyblumenol C-9-*O*-Glc (Figure 2C; Compound 1), 11-carboxyblumenol C-9-*O*-Glc (Figure 2C; Compound 2), 11-hydroxyblumenol C-9-*O*-Glc-Glc (Compound 3), blumenol C-9-*O*-Glc-Glc (Compound 4) and blumenol C-9-*O*-Glc (Compound 5).

To quantify these compounds throughout the plant, we used a more sensitive and specifically targeted metabolomics approach based on LC-triple-quadrupole-MS. The abundance of the five blumenol C-glycosides continually increased with mycorrhizal development (Figure 2—figure supplement 1A) and was highly correlated with the mycorrhizal colonization rate as determined by the transcript abundances of classical arbuscular mycorrhizal symbiosis-marker genes (fungal house-keeping gene, *Ri-tub*; plant marker genes, *Vapyrin*, *RAM1*, *STR1* and *PT4*; Park *et al.* (2015); Figure 2—figure supplement 1B, Data Set 1).

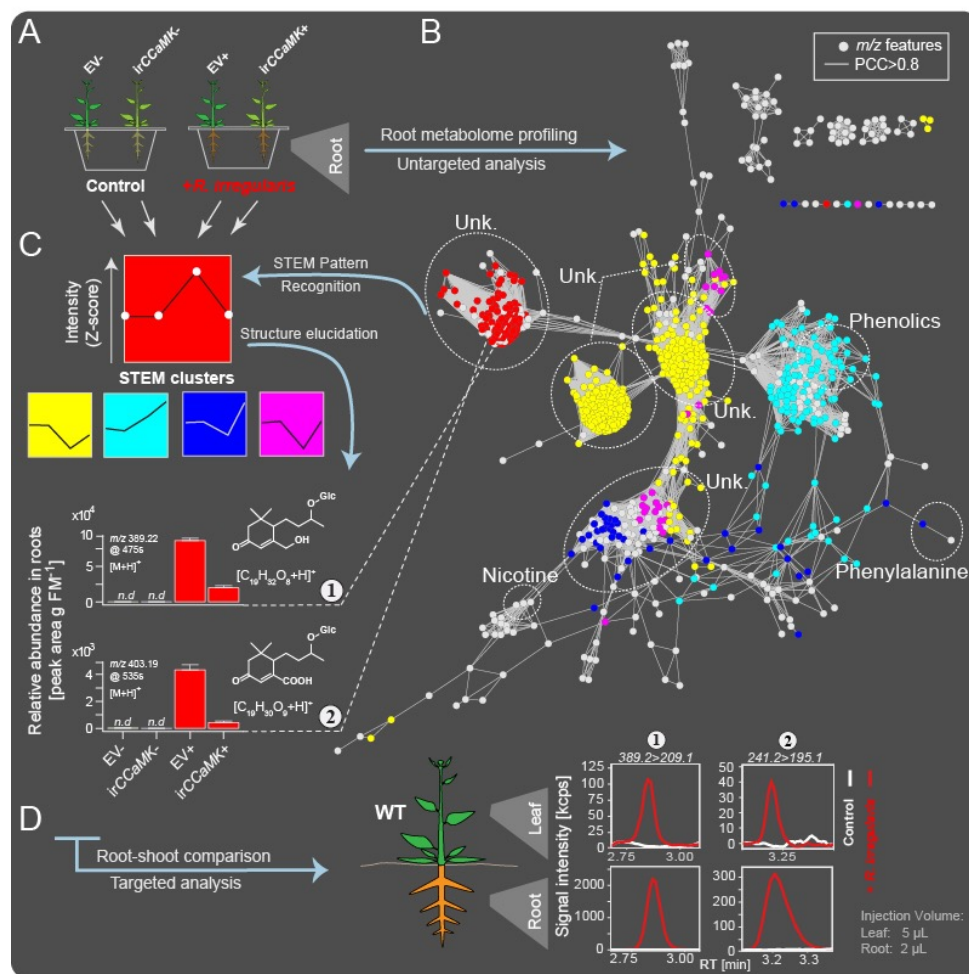


Figure 2 Combined targeted and untargeted metabolomics identified blumenol derivatives as AMF-indicative *in-planta* metabolic fingerprints in the roots and leaves of *Nicotiana attenuata* plants.

A Experimental set-up. EV and irCCaMK plants were co-cultured and inoculated with or without *R. irregularis*. Six weeks after inoculation (wpi), root samples were harvested for metabolite profiling. **B** Covariance network visualizing m/z features from UHPLC-qTOF-MS untargeted analysis ($n=8$). Known compounds, including nicotine, phenylalanine and various phenolics, and unknown metabolites (Unk.) are annotated by dashed ellipses. **C** Normalized Z-scored of m/z features were clustered using STEM Clustering; 5 of 8 significant clusters are shown in different colors and mapped onto the covariance network. The intensity variation (mean + SE) of 2 selected features (Compounds 1 and 2) are shown in bar plots (n.d., not detected). **D** Representative chromatograms of Compounds 1 and 2 in roots and leaves of plants with and without AMF inoculation, as analyzed by targeted UHPLC-triple quadrupole-MS metabolomics.

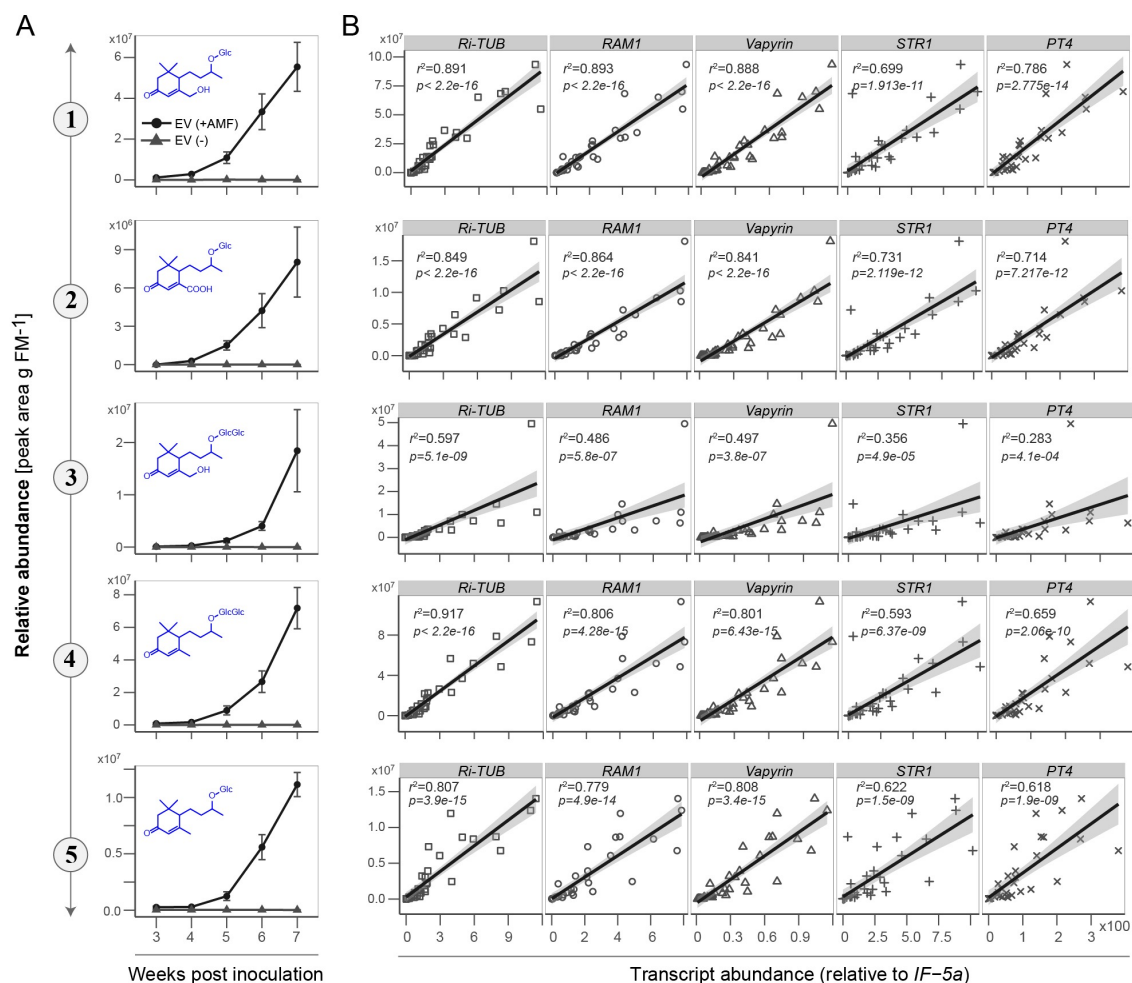


Figure 2—figure supplement 1 Abundance of root blumenol derivatives correlates positively with root AMF colonization.

A Time lapse accumulations (3-7 weeks post inoculation, $n \geq 3$ for each time point) of Compounds 1, 2, 3, 4 and 5 in roots of plants with (EV+, black lines with circles) and without (EV-, grey lines with triangle) AMF inoculation. The experiment was conducted with empty vector (EV) transformed plants. Data are means \pm SE. **B** Abundance of Compounds 1, 2, 3, 4 and 5 relative to the transcript abundance of the *R. irregularis* specific housekeeping gene, *Ri-tub* (GenBank: EXX64097.1), as well as to the plant derived marker genes *RAM1*, *Vapyrin*, *STR1* and *PT4* (Gene ID and transcripts abundance are listed in Data Set 1). The transcript abundance was quantified by q-PCR, relative to *NaIF-5a* (NCBI Reference Sequence: XP_019246749.1). The correlations among blumenol derivatives and the transcript abundances of marker genes were analyzed by linear regression (lm) models.

Hydroxy- and carboxyblumenol C-glucoside levels in leaves positively correlate with root colonizations

Compounds 1 and 2 showed a similar AMF-specific accumulation in the leaves, as observed in the roots (Figure 2D). The other analyzed blumenols were not detected in leaves (Compounds 3 and 4; Figure 3—figure supplement 1A) or showed a less consistent AMF-specific accumulation (Compound 5; due to its constitutive background level; Figure 3—figure supplement 1A). The identity of Compounds 1 and 2 in the leaves was verified by high resolution qTOF-MS (Figure 3—figure supplement 1B-E).

Next, we determined the correlations between the contents of AMF-indicative foliar Compounds 1 and 2 and root colonization rates. In a kinetic experiment, the amount of both compounds steadily increased in the leaves of plants inoculated with *R. irregularis* (Figure 3A). In contrast, the classical AMF-marker-genes, which are usually analyzed in the roots, did not respond in the leaves (Figure 4). In an inoculum-gradient experiment using increasing inoculum concentrations, proportionally higher Compound 1 and 2 levels were observed (Figure 3B), accurately reflecting the differential colonization of roots across treatments (Figure 3E). In addition to inoculation with a single AMF species (*R. irregularis*), we also tested mycorrhizal inoculum originally collected from the plant's native habitat, the Great Basin Desert in Utah, USA, which mainly consists of *Funneliformis mosseae* and *R. irregularis*. EV plants inoculated with this 'natural inoculum' also accumulated Compounds 1 and 2 in leaves, while *irCCaMK* plants did not (Figure 3C). When planted into the plant's natural environment in Utah, both EV and *irCCaMK* plants could be clearly distinguished by their leaf Compound 1 and 2 contents. The signature of Compound 2 provided a better quality marker in these field-grown plants (Figure 3D, Figure 3—figure supplement 2). The foliar contents of these two compounds were highly correlated with the percentage of arbuscules in roots, the core structure of AMF interactions (Figure 3F). In contrast, other biotic or abiotic stresses, including herbivory, pathogen infection and drought stress, did not elicit the foliar accumulations of Compounds 1 and 2 (Figure 5). Such stimuli also do not induce blumenol accumulation in roots (Maier *et al.* 1997). An analysis of various plant tissues, including different leaf positions, stem pieces, flowers and capsules revealed that these AMF-specific signatures accumulated throughout the shoot (Figure 3G). Taken together, we conclude that the contents of particular blumenols in aerial plant parts robustly reflect the degree of mycorrhizal colonization in *N. attenuata* plants.

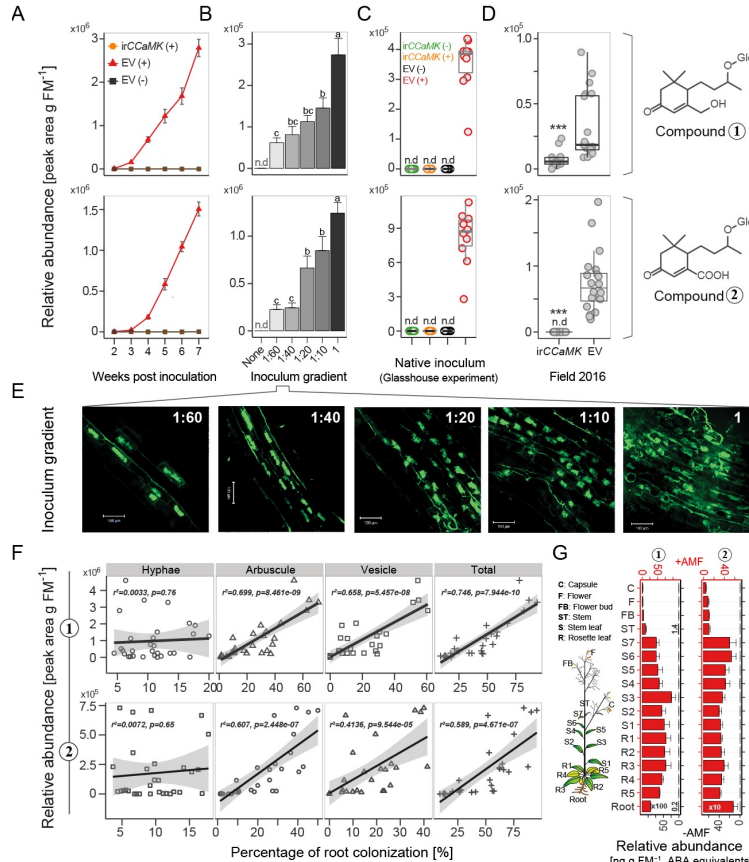


Figure 3 Compounds 1 and 2 are leaf markers of root AMF colonization in *N. attenuata*.

A Time lapse accumulations of Compounds 1 and 2 in leaves of EV plants with (EV+, red) or without (EV-, black) AMF-inoculation and of irCCaMK plants with AMF-inoculation (irCCaMK+, orange, covered by black) (means \pm SE, $n \geq 5$). **B** Leaf abundances of Compounds 1 and 2 (5 wpi) of plants inoculated with different inoculum concentrations (means \pm SE, $n \geq 4$); different letters indicate significant differences ($p < 0.05$, one-way ANOVA followed by Fisher's LSD). **C** Compounds 1 and 2 in leaf samples of EV and irCCaMK plants inoculated with (+) or without (-) AMF inoculum isolated from the plant's native habitat (6 wpi); different letters indicate significant differences ($p < 0.05$, one-way ANOVA followed by Tukey's HSD, $n = 10$). **D** Field experiment (Great Basin Desert, Utah, USA): Compounds 1 and 2 in leaf samples of EV ($n = 20$) and irCCaMK ($n = 19$) plants sampled 8 weeks after planting. (Student's t -test: ***, $p < 0.001$). **E** Representative images of WGA-488 stained roots of plants shown in **B** (bar = 100 μ m). **F** Leaf Compounds 1 and 2 relative to the percentage of root colonization by hyphae, arbuscules, vesicles and total root length colonization of the same plants (linear regression model). **G** Compounds 1 and 2 in 17 different tissues of plants with (+AMF, $n = 3$, red bars) or without (-AMF, $n = 1$, black bars) AMF-inoculation harvested at 6 wpi.

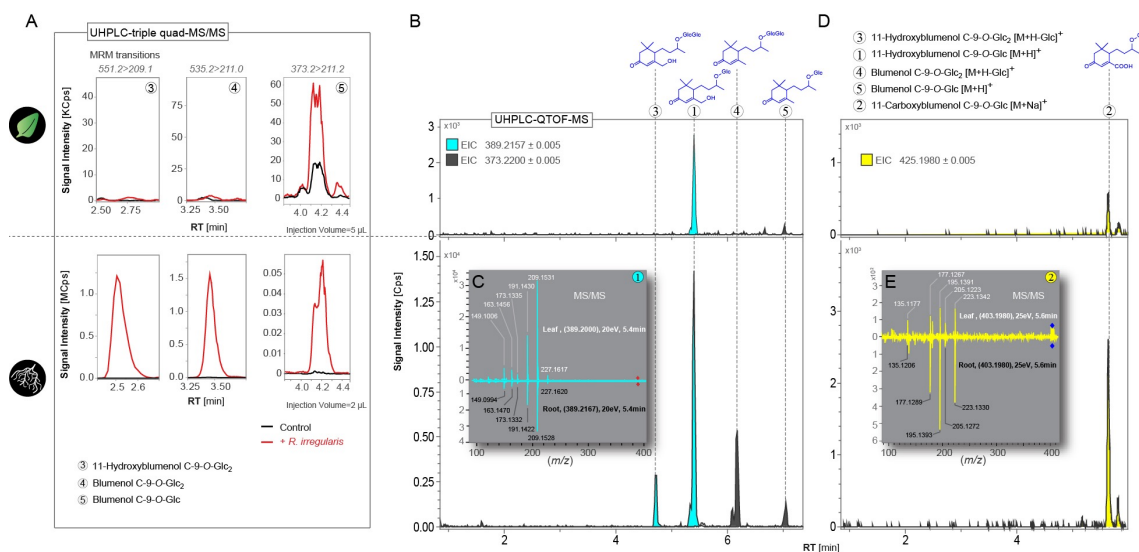


Figure 3—figure supplement 1 AMF-induced accumulation of blumenol derivatives in roots and leaves of *N. attenuata*.

A Representative chromatograms of targeted tandem MS-based analyses of Compounds 3, 4 and 5 in roots (bottom panel) and leaves (top panel) of *N. attenuata* plants after inoculation with *R. irregularis* (+*R. irregularis*, red line, 6wpi) and in untreated control plants (Control, black line). Experiments were conducted with wild type (WT) plants. The respective precursor-to-product ion transitions are indicated at the top. **B, D** Representative chromatograms of a high resolution MS-based analysis of Compounds 1, 3, 4 and 5 (**B**), as well as Compound 2 (**D**) in roots (bottom panel) and leaves (top panel) of *N. attenuata* plants after inoculation with *R. irregularis*. Extracted ion chromatograms (EIC) are labeled by colors and settings listed at the top. **C, E** Comparison of fragmentation patterns of Compounds 1 (**C**) and 2 (**E**) in both tissues by high resolution tandem MS.

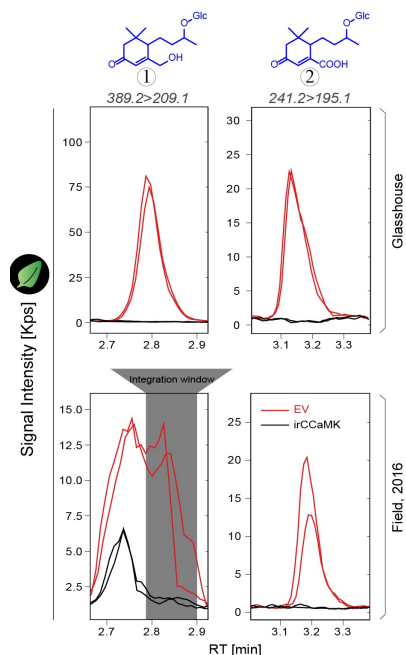


Figure 3—figure supplement 2 Signals from Compound 1 are partially disturbed in field samples, but not for Compound 2.

Leaf samples were harvested from glasshouse-(top panel) and field-grown, Utah, 2016 (bottom panel) plants for analysis. Representative chromatograms of two samples of each genotype, EV (red) and *irCCaMK* (black), were shown. Grey area indicates the peak integration window used for the quantification of Compound 1.

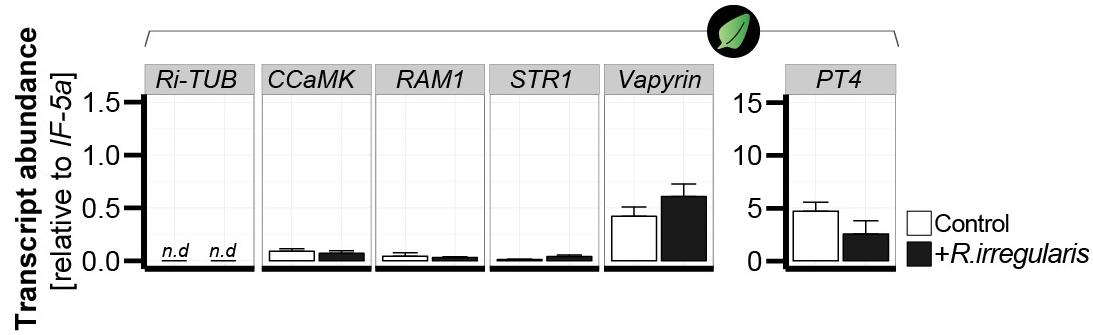
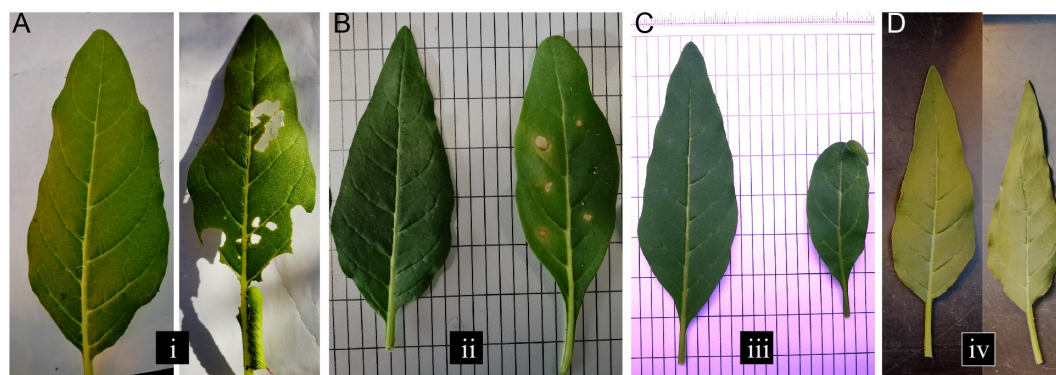


Figure 4 Transcript abundance of classical arbuscular mycorrhizal symbiosis-marker genes do not respond in leaves of mycorrhizal and control *N. attenuata* plants

The transcript abundance (relative to *NaIF-5a*) of classical root marker genes was analyzed in leaves of *N. attenuata* plants in the presence (+*R. irregularis*, black bars) and absence (control, white bars) of root colonization with *R. irregularis*. The marker genes include the *R. irregularis* specific housekeeping gene, *Ri-tub*, as well as the plant-derived marker genes *CCaMK*, *Vapyrin*, *PT4*, *STR1* and *RAM1*. Leaf samples were harvested 6 weeks after inoculation and analyzed by qPCR. Data represent means + SE ($n \geq 3$), n.d., not detected.



E

Treatment	Compound 1	Compound 2
i. Herbivory (<i>M. sexta</i>)	n.d.	n.d.
ii. Pathogen infection (<i>B. cinerea</i>)	n.d.	n.d.
iii. Bacteria & virus infection	n.d.	n.d.
iv. Drought (3 days)	n.d.	n.d.

n.d., not detected

iii. Infection with *A. tumefaciens* carrying the Tobacco Rattle Virus

Figure 5 Different biotic and abiotic stresses do not elicit accumulations of Compounds 1 and 2 in leaves.

A-D Representative leaves of *N. attenuata* plants subjected to different stresses (right leaf), as well as the untreated controls (left leaf): **A** *Manduca sexta* feeding for 10 days; **B** *Botrytis cinerea* infection for 5 days. **C** Infection for 2 weeks with *Agrobacterium tumefaciens* carrying the Tobacco Rattle Virus; **D** Dehydration for 3 days. For each treatment, four biological replicates were used. **E** Accumulation of Compounds 1 and 2 in treated samples from **A-D**. n.d., not detected.

AMF-indicative blumenols in shoots most likely originate from the roots

Blumenols are apocarotenoids originating from a side branch of the carotenoid pathway (Hou *et al.* 2016). Most of the candidate genes for blumenol biosynthesis were upregulated in roots, but not in leaves of *N. attenuata* plants in response to mycorrhizal colonization (Figure 6A, Figure 6—figure supplement 1A). We inferred that these AMF-indicative leaf apocarotenoids are transported from their site of synthesis in colonized roots to other plant parts. This is consistent with the occurrence of blumenols in stem sap (Figure 6—figure supplement 1B) which was collected by centrifuging small stem pieces. To clarify the origins (local biosynthesis vs. transport) of these leaf blumenols, we genetically manipulated the carotenoid biosynthesis of *N. attenuata* plants. To minimize the effects of a disturbed carotenoid biosynthesis on the AMF-plant interaction, we used the dexamethasone (DEX)-inducible pOp6/LhGR system to silence phytoene desaturase (PDS) expression in a single DEX-treated leaf position (Schäfer *et al.* 2013). Treated leaves showed clear signs of bleaching, indicating PDS silencing (Figure 6B, Figure 6—figure supplement 1C), but levels of the AMF-indicative Compounds 1 and 2 were not affected, consistent with their transport from other tissues, likely the highly accumulating roots. As a control, we analyzed the non-AMF-inducible Compound 6, showing constitutive levels in aerial tissues (Figure 6—figure supplement 2). In DEX-treated leaves, Compound 6 concentrations were reduced by nearly 40%, consistent with local production (Figure 6B, Figure 6—figure supplement 1D). To confirm the within-plant transport potential of blumenols, we dipped roots of seedlings into aqueous solutions of Compounds 1 or 2. After overnight incubation, the blumenol derivatives were clearly detected not only in roots, but also in shoots (Figure 6C, Figure 6—figure supplement 1E).

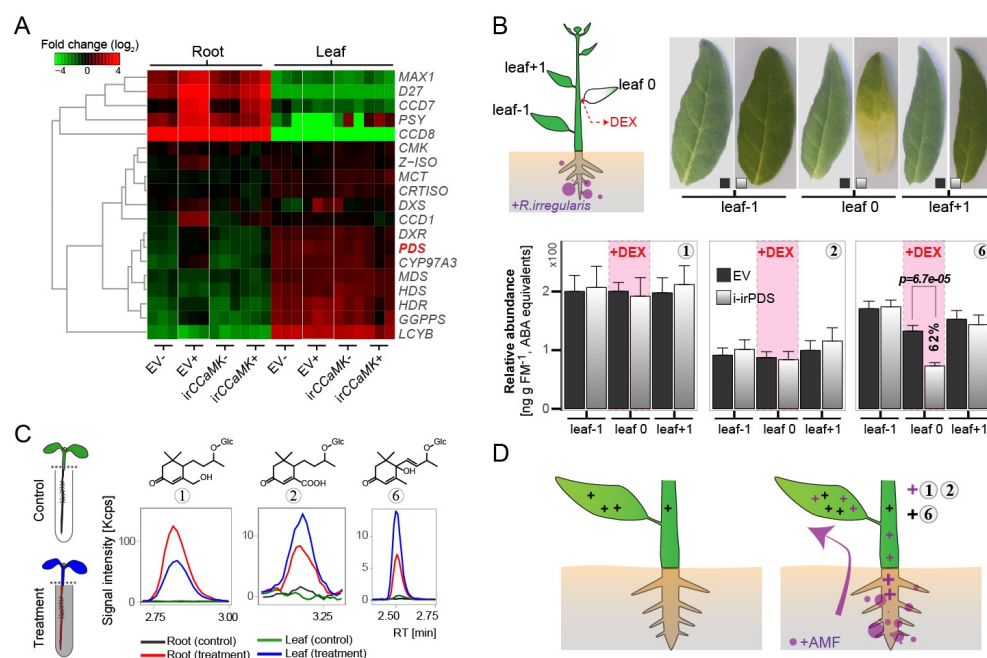


Figure 6 AMF-indicative Compounds 1 and 2 in shoots of mycorrhizal plants originate from the roots.

A Hierarchical clustering analysis of transcript abundance from RNA-seq of methylerythritol 4-phosphate (MEP) and (apo)carotenoid biosynthetic genes (for details see Figure S6A). **B** Compounds 1, 2 (AMF-specific) and 6 (not AMF-specific) in AMF-inoculated i-irPDS and EV plants. On each plant, a single stem leaf (leaf 0) was elicited with 100 μ M DEX-containing paste for 3 weeks; treated and adjacent, untreated control leaves (leaf -1 and leaf+1) were harvested. Representative leaves are shown (bleaching indicates PDS silencing); (means \pm SE, $n \geq 6$). The same leaf positions in i-irPDS and EV plants were compared by Student's *t*-tests. **C** Contents of Compounds 1, 2 and 6 in the roots and shoots of seedlings whose roots were dipped for 1 d into an aqueous solution with (treatment) or without (control) AMF-indicative blumenols. **D** Model of blumenol distribution in plants with (right panel) and without (left panel) AMF colonization. The model illustrates constitutive blumenols (e.g., Compound 6 in *N. attenuata*) and AMF-indicative ones (e.g., Compounds 1 and 2 in *N. attenuata*) and their inferred transport.

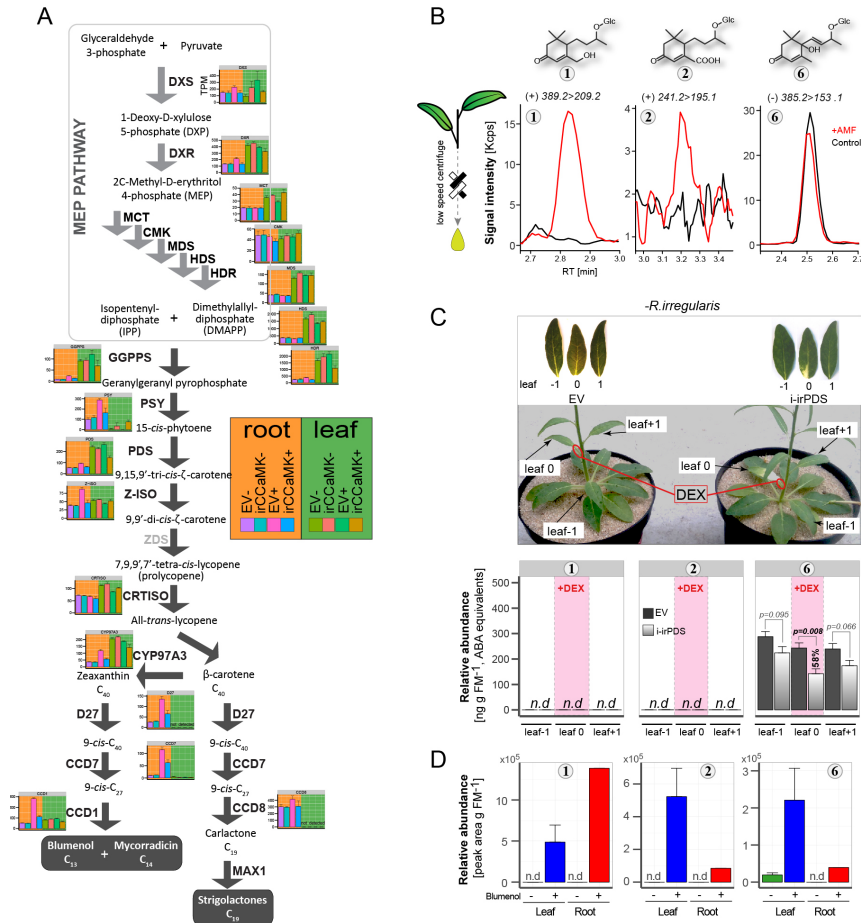


Figure 6—figure supplement 1 Foliar levels of Compounds 1 and 2 are derived from roots

A Transcript abundance of MEP and apocarotenoid pathway biosynthetic genes (based on homologies to tomato, Arabidopsis and tobacco). Plant materials from same experimental set-up as in Figure 1A were used for sequencing. Data are means + SE (n=3) generated by RNA-seq and the abundance of each transcript is expressed in TPM (Transcripts per kilobase of exon model per million mapped reads). Transcripts were analyzed in roots (left panel, orange background) and leaf tissues (right panel, green background) of EV and *irCCaMK* plants with (EV+ and *irCCaMK*+ respectively) and without (EV- and *irCCaMK*- respectively) inoculations with *R. irregularis*. Gene abbreviations; CRTISO: carotenoid isomerase; GGPPs: geranylgeranyl diphosphate synthase; PSY: phytoene synthase; PDS: phytoene desaturase; ZDS: ζ-carotene desaturase; Z-ISO: ζ-carotene isomerase; CCD: carotenoid cleavage dioxygenase; MAX1: cytochrome P450-type monooxygenase CYP711A1; DXS: 1-deoxy-D-xylulose 5-phosphate synthase; DXR: 1-deoxy-D-xylulose 5-phosphate reductoisomerase; MCT: 2-C-methyl-D-erythritol 4-phosphate cytidyltransferase; CMK: 4-(cytidine 5'-diphospho)-2-C-methyl-D-erythritol kinase; MDS: 2-C-methyl-D-erythritol 2,4-cyclodiphosphate synthase; HDS: 4-

hydroxy-3-methylbut-2-enyl-diphosphate synthase; HDR: 4-hydroxy-3-methylbut-2-enyl diphosphate reductase; D27: carotenoid isomerase. **B** Representative chromatograms from a targeted tandem MS-based analysis of Compounds 1, 2 and 6 in stem sap fluid of *N. attenuata* plants after *R. irregularis* inoculation (+AMF, red line, 6wpi) and of untreated control plants (Control, black line). The respective precursor-to-product ion transitions are indicated at top. **C** Accumulations of Compounds 1, 2 and 6 in non AMF-inoculated plants after local silencing of the carotenoid biosynthesis in the DEX-treated leaf. The experiment was performed with plants harboring a transformation construct of the chemically-inducible silencing of the phytoene desaturase (i-irPDS), as well as with empty vector (EV) plants. On each plant, a single stem leaf (leaf 0) was treated with a 100 μ M dexamethasone (DEX) containing lanolin paste for 3 weeks. The adjacent, untreated leaves (leaf -1 and leaf+1) were harvested as controls. Representative leaves are shown (bleaching indicates functional PDS silencing). Data are means + SE ($n \geq 6$). For statistical analysis, the samples from the same leaf positions in i-irPDS and EV plants were compared by Student's *t* test. **D** Contents of Compounds 1, 2 and 6 in the roots (red bars) and shoots (blue bars) of seedlings whose roots were dipped into an aqueous solution with or without addition of the respective blumenols. Seedlings were incubated for 1d before analysis. Data are means + SE (shoot, $n=3$; root, $n=1$). The data originate from the same experiment presented in Figure 6C.

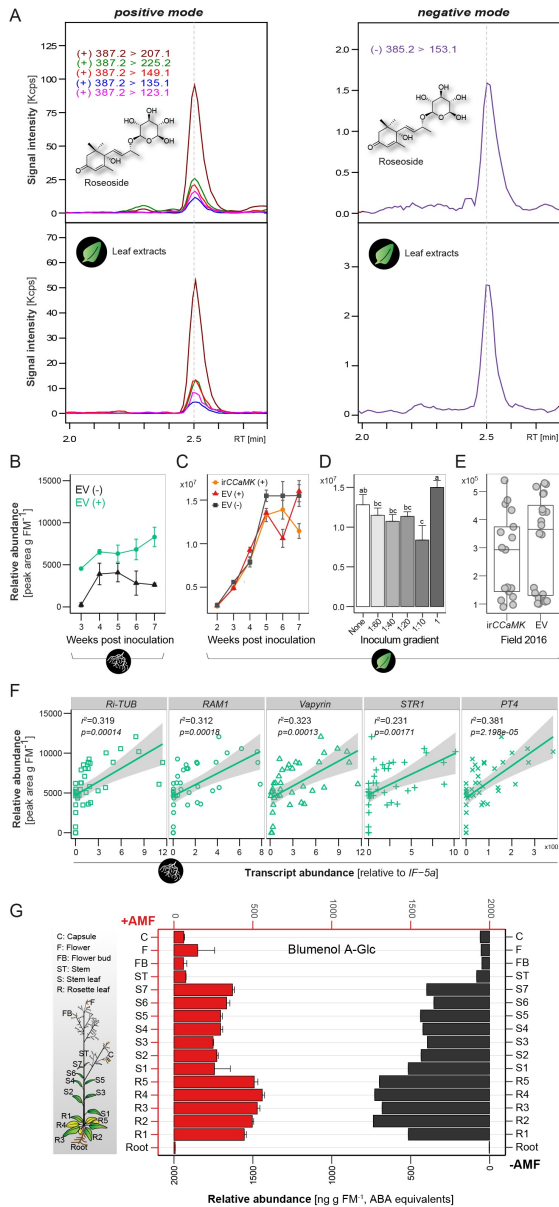


Figure 6—figure supplement 2 Compound 6 is constitutively produced in shoots of *N. attenuata* and not indicative of AMF associations.

A Representative chromatograms from a targeted tandem MS-based analysis of Compound 6 in leaves of *N. attenuata* (bottom panel) and as comparison, a blumenol A-9-O-glucoside (roseoside) standard (top panel). The precursor-to-product ion transitions are indicated. **B** Time lapse accumulations of Compound 6 in roots of EV plants with (EV+, green line) or without (EV-, black line) AMF-inoculation. Data represent means \pm SE ($n \geq 3$). **C** Time lapse accumulations of Compound 6 in leaves of EV plants with (EV+, red line) or without (EV-, black line) AMF-inoculation and of irCCaMK plants with AMF-inoculation (irCCaMK+, orange line).

Data represent means \pm SE ($n \geq 5$). **D** Comparison of the abundances of Compound 6 in leaves of plants inoculated with different inoculum concentrations, samples were harvested at 5 weeks-post-inoculation (wpi). Data are means \pm SE ($n \geq 4$). Different letters indicate significant differences ($p < 0.05$, one-way ANOVA followed by Fisher's LSD). **E** Field experiment (Great Basin Desert, Utah, USA): leaf samples of EV ($n=20$) and *irCCaMK* ($n=19$) plants were sampled 8 weeks after planting and amounts of Compound 6 were analyzed. For statistical analysis, Student's *t* test was applied. **F** Abundance of Compound 6 relative to the transcript abundance of the *R. irregularis* specific housekeeping gene, *Ri-tub* (GenBank: EXX64097.1), as well as to the plant derived marker genes *RAM1*, *Vapyrin*, *STR1* and *PT4*. The transcript abundance was quantified by q-PCR, relative to *NaIF-5a* (NCBI Reference Sequence: XP_019246749.1). The correlation between compound 6 and transcript abundance of marker genes was analyzed by linear regression (lm) models. **G** Distribution of Compound 6 in different plant tissues, as indicated, of plants with (+AMF, $n=3$, red bars) or without (-AMF, $n=1$, black bars) AMF-inoculation. Samples were harvested at 6 wpi.

The analysis of AMF-indicative blumenols as HTP screening tool for forward genetics approaches

To test the potential of the foliar AMF-indicative metabolites as a screening tool, we quantified the concentration of Compounds 1 and 2 in leaves of plants of a population of recombinant inbred lines (RILs) of a forward genetics experiment, an experiment which would be challenging with the classical screening tools of root staining or nucleic acid analysis. We focused our analysis on Compound 2 due to the superior quality of its signature in the leaves of field-grown plants (Figure 3—figure supplement 2). The experiment consisted of a population of RILs from a cross of two *N. attenuata* accessions (Utah, UT and Arizona, AZ)(Zhou *et al.* 2017) which differ in their mycorrhizal colonization (Figure 7A-B, Figure 7—figure supplement 1) and accumulation of foliar Compound 2 in the glasshouse (Figure 7C). A QTL analysis of 728 plants grown across a 7200 m² field plot (Figure 7D) revealed that the abundance of Compound 2 mapped to a single locus on linkage group 3 (Figure 7E), which harbored a homologue of *NOPE1(NIATv7_g02911)*, previously shown to be required for the initiation of AMF symbioses in maize and rice (Nadal *et al.* 2017). While clearly requiring additional follow-up work, these results highlight the value of these signature metabolites for HTP screens, which form the basis of most crop improvement programs.

AMF-indicative blumenols in shoots are a widespread response of various plant species to different kinds of AMF

The AMF-specific accumulation of blumenol C-derivatives in roots is a widespread phenomenon within higher plants (Strack and Fester 2006); however, how general are the observed blumenol changes in aerial parts across different combinations of plants and AMF species? We analyzed *Solanum lycopersicum*, *Triticum aestivum* and *Hordeum vulgare* plants with and without AMF inoculation and again we found an overlap in the AMF-specific blumenol responses in roots and leaves, consistent with the transport hypothesis. Further analyses led to the identification of additional AMF-indicative blumenols in the leaves of *Medicago truncatula*, *Solanum tuberosum* and *Brachypodium distachyon*. We identified various types of blumenols that showed an AMF-specific accumulation in the shoot, including blumenol B (Compound 7), which has not previously been reported in an AMF-dependent context (Figure 7F; Figure 7—figure supplement 2). As reported for roots, the particular blumenol types were species-dependent, but the general pattern was widespread across monocots and dicots in experiments conducted at different research facilities. In tests with diverse fungal species (*R. irregularis*, *F. mosseae* and *Glomus versiforme*), the observed effects were not found to be restricted to specific AMF taxa (Figure 7F; Figure 7—figure supplement 2). In short, the method is robust.

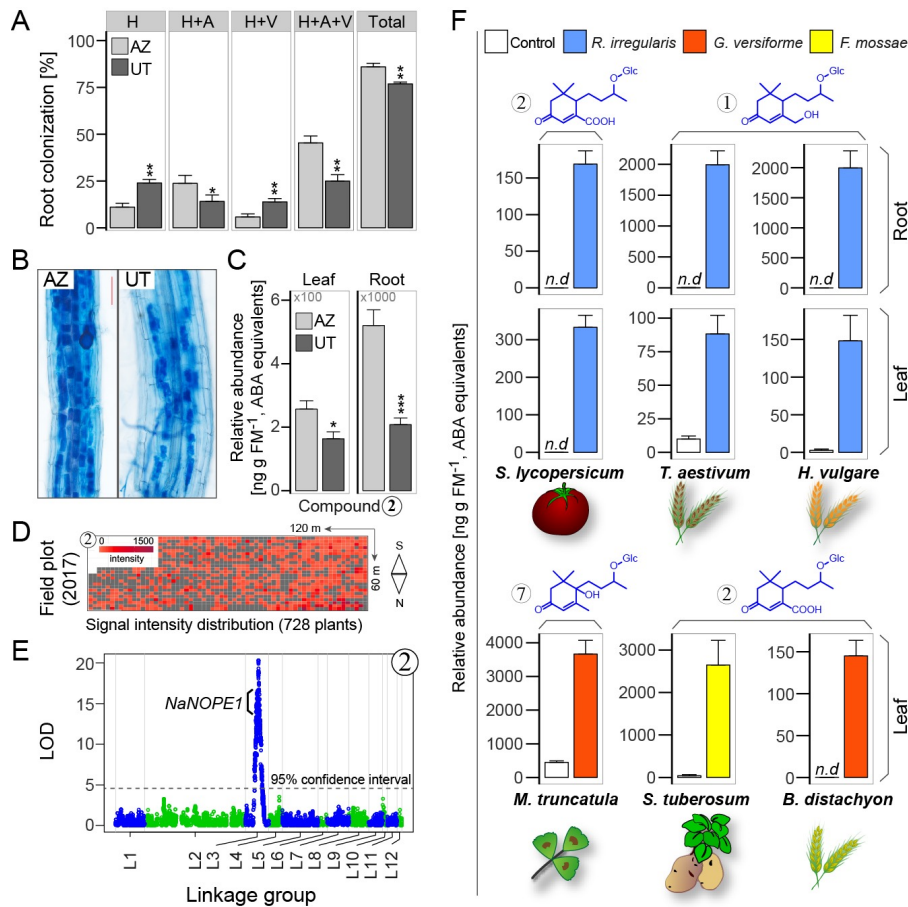


Figure 7 AMF-indicative changes in blumenols in aerial plant parts are valuable research tools providing accurate assessments of functional AMF associations in high-throughput screenings of multiple plant and AMF species.

A Root colonization analysis in two *N. attenuata* accessions (UT/ AZ). H: hyphae; A: arbuscules; V: vesicles; T: total colonization (n=4; Student's *t*-test, *, $p < 0.05$, **, $p < 0.01$, ***, $p < 0.001$). **B** Representative images of trypan blue stained roots (6 wpi; bar=100 μ m). **C** Compound 2 in roots and leaves of UT and AZ plants with and without AMF-inoculation (means + SE, n=8). **D** Heatmap of the normalized abundance of foliar Compound 2 in plants of a UT-AZ RIL population (728 plants) planted across a 7,200 m² field plot. **E** QTL mapping analysis of the data from **D**. QTL locus on linkage group 3 contains *NaNOPE1*, an AMF-associated gene, in addition to others. LOD, logarithm of the odds ratio. **F** Blumenol contents of different crop and model plants with and without AMF inoculation (*S. lycopersicum* (n=6), *T. aestivum* (n=10), *H. vulgare* (n=5): 8 wpi; *M. truncatula* (n=3): 7 wpi; *S. tuberosum* (n=5): 6 wpi; *B. distachyon* (n=4): 5 wpi). Different plant and AMF species were used as indicated (means + SE; n.d., not detected).

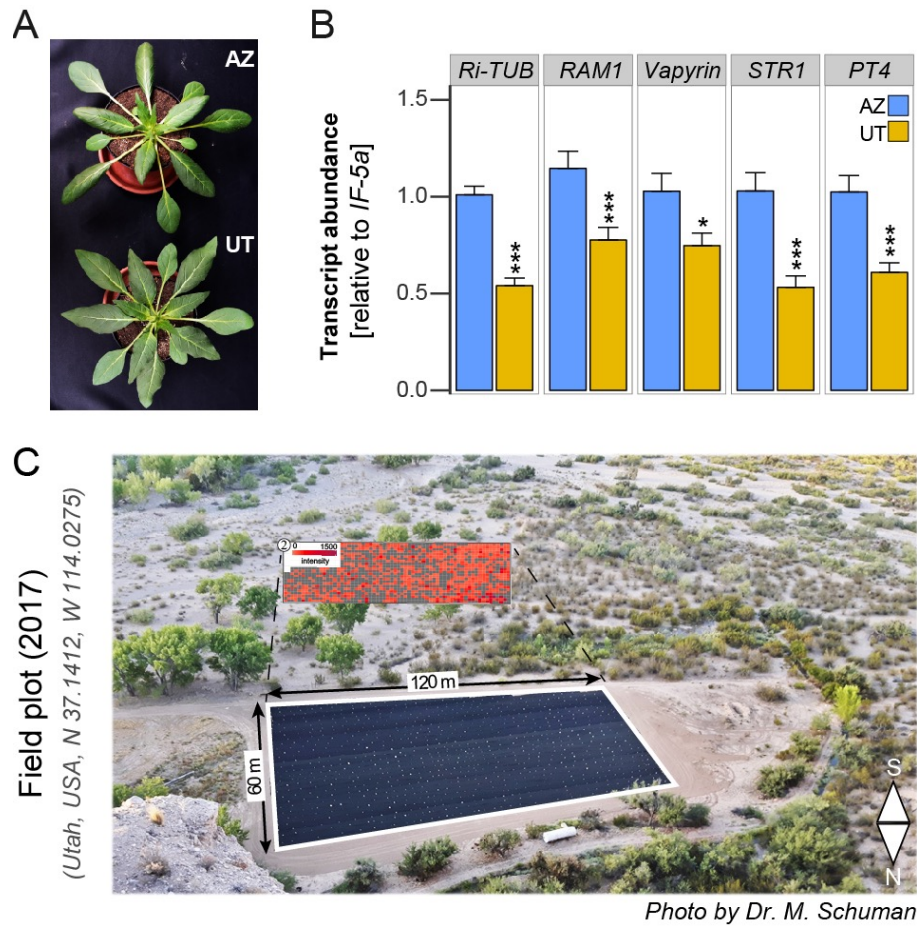


Figure 7—figure supplement 1 Phenotypes of UT and AZ accessions and field plot planting design.

A Representative *N. attenuata* plants of the UT and AZ accessions in the rosette stages of growth (12 days after potting). **B** Transcripts of marker genes in roots responding to AMF colonization in UT and AZ after 6 wpi inoculated with *R. irregularis* were quantified by qPCR in the same samples as in Fig 4A-C (n=8); Student's *t* test *, $p < 0.05$, **, $p < 0.01$, ***, $p < 0.001$. **C** Field plot of 728 sampled individual plants in Utah, USA, 2017.

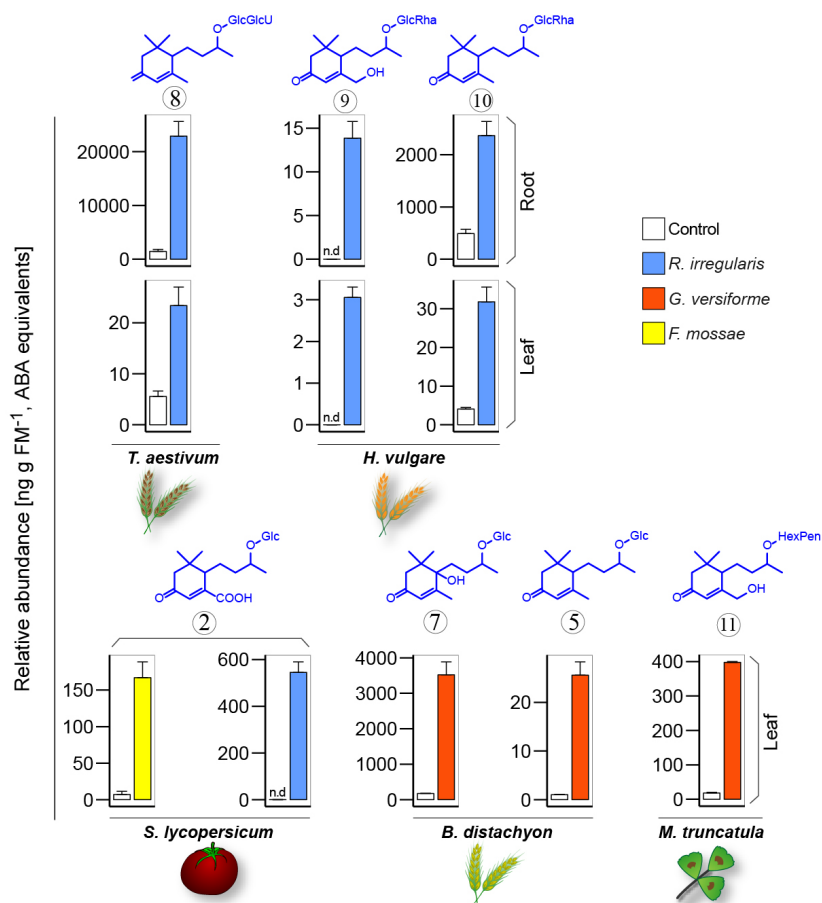


Figure 7—figure supplement 2 AMF-indicative changes in blumenols in aerial plant part are valuable research tools providing accurate assessments of functional AMF associations of multiple plant and AMF species (continued from Figure 7F).

Blumenol contents of different crop plants with and without AMF inoculation (*T. aestivum*: 8 wpi, n=5; *H. vulgare*: 8 wpi, n=10; *S. lycopersicum* with *F. mossae*: 6wpi, n=5; *S. lycopersicum* with *R. irregularis*: 11wpi, n=6; *B. distachyon*: 5 wpi, n=4; *M. truncatula*: 7 wpi, n=3). Different plant and AMF species were used, as indicated; means + SE, n.d., not detected.

Discussion

AMF-interactions are proposed to have played an important role for the colonization of land by plants and still play an important role for a majority of plants by improving the function of their roots and increasing whole-plant performance. Consequently, the investigation of AMF-mediated effects on a host plant's physiology has been an important research field for many decades and characteristic transcriptional and metabolic changes have been observed in the roots of AMF-colonized plants. However, the cumbersome analysis of AMF-interactions, involving destructive harvesting of root tissues and microscopic or transcript analysis, restrains large-scale investigations and commercial applications. AMF interactions were also shown to affect the primary and secondary metabolism in the systemic, aerial tissues of plants; however none of these responses proved to be widespread and sufficiently specific to function as reliable markers (Schweiger and Müller 2015). Here we describe the discovery of particular blumenols as AMF-indicative markers in leaves and other systemic aerial tissues and illustrate their potential application as tools for research and plant breeding.

Systemic AMF-mediated metabolite changes

Improvements in analytical instrumentation has enabled the study of minute amounts of compounds with unprecedented accuracy and sensitivity and different types of instrumentation have allowed for different workflows each with specific advantages and drawbacks. While untargeted metabolomics allow for a less biased view of metabolic responses, they are more affected by co-occurring compounds and the post-run analysis is usually cumbersome. Targeted methods, in contrast, are often more sensitive and specific, but limited to the targeted metabolites. We capitalized on the strengths of these two approaches by applying a combination of targeted and untargeted LC-MS based metabolomics approaches coupled with a sophisticated biostatistical analysis (Figure 2). Metabolites and metabolite responses are often specific to particular parts and tissues of a plant (Li *et al.* 2016, Lee *et al.* 2017), but it is also known that local responses can spread to other plant parts. Additionally, metabolites do not only accumulate at their place of biosynthesis but can be readily transported throughout the plant (Baldwin 1989). Therefore, we hypothesized that local changes in the roots might be also be reflected in the systemic aerial tissues, either by signaling or transport. This more focused view allowed us to identify specific AMF-indicative blumenols in the shoot (Figure 3) despite the occurrence of other highly abundant and constitutively produced compounds and not AMF-indicative blumenols. Interestingly, the confirmation of compound identities in leaf samples with high resolution MS techniques proved to be challenging and required additional sample purification steps. Likely, such matrix effects thwarted the detection of these AMF-indicative, systemic

blumenol responses in previous investigations. The discovery of these AMF-indicative blumenol compounds in diverse plant species interacting with different AMF species (Figure 7, Figure 7—figure supplement 2) further indicates that these responses are widespread.

Root-to-shoot transport of AMF-indicative blumenols

Despite the AMF-induced accumulation of blumenols in the shoot, putative candidate genes of the apocarotenoid biosynthesis pathway were only induced in the roots of AMF-inoculated plants (Figure 6A, Figure 6—figure supplement 1A). To exclude other mechanisms (e.g., post-transcriptional regulation) mediating the local production of the blumenol compounds in the leaves, we genetically manipulated the carotenoid pathway in a tissue-specific manner. It is challenging to manipulate blumenols without affecting the AMF-colonization of the plant, since other carotenoid-derived compounds, such as strigolactones, are known to play an important role in this process (Lanfranco *et al.* 2017). To circumvent these problems, we used the LhGR/pOp6 system for chemically-inducible RNAi-mediated gene silencing of PDS (Schäfer *et al.* 2013) to impair carotenoid biosynthesis only in a particular leaf of AMF-inoculated plants. Interestingly, only the constitutively produced Compound 6 was reduced in the treated leaves, while the AMF-indicative Compounds 1 and 2 were not affected by our treatment (Figure 6B). This indicated that instead of being locally produced, Compound 1 and 2 are translocated from the roots, an inference consistent with the occurrence of AMF-indicative blumenols in stem sap and the capacity of seedlings to transport blumenols from the root to the shoot from hydroponic solution (Figure 6C, Figure 6—figure supplement 1B, D). It seems likely that the AMF-indicative blumenols are transported in the xylem with the transpiration stream (Figure 6D). The blumenol glucosides (Compounds 1, 2 and 6) are hydrophilic low-molecular weight (402, 388 and 386 Da), compounds that are unlikely to pass membranes without further support, e.g., by transporters and it will remain an interesting research question to identify the involved mechanisms.

Functional implication of blumenol accumulation and transport

Blumenols were shown to accumulate in large amounts in the roots of various plants after AMF-inoculation (Strack and Fester 2006) and our data indicate that they are subsequently distributed throughout the plant (Figure 3G). While the conservation of this response in various plants after inoculation with different AMF species (Figure 7F, Figure 7—figure supplement 2) indicates an important functional role in the AMF-plant interaction, this function remains to be explored. Genetic manipulation of DXS and CCD1 indicate a role in arbuscule maintenance (Floß *et al.* 2008, Floss *et al.* 2008). However, DXS is located upstream in the carotenoid biosynthesis

pathway and its manipulation might have caused pleiotrophic effects, while CCD1 silencing only results in a partial reduction in blumenol levels. Other studies showed that direct application of blumenols suppresses root colonization and arbuscule formation at early stages of mycorrhiza development (Fester *et al.* 1999) and inhibit the growth of soil born plant-pathogens (Park *et al.* 2004). Unfortunately, these soil-born activities do not shed light on the systemic function of AMF-induced blumenols in shoot tissues observed here. Activity studies on vomifoliol, the aglycone of the not AMF-indicative Compound 6, showed that this compound induces stomatal closure similar to the structurally related abscisic acid (Stuart and Coke 1975). Additionally, blumenols are known to suppress seed germination and plant growth (Kato-Noguchi *et al.* 2012, Kato-Noguchi *et al.* 2015). Therefore, AMF-induced blumenols could serve as systemic signals that mediate the large-scale adjustments in general physiology that are thought to accompany AMF-interactions. For example, AMF-induced blumenols could be involved in the regulation of differential susceptibility of AMF-inoculated plants to stresses, such as drought or pathogen infection.

AMF-indicative blumenols as tool for research and plant breeding

Classical tools for the quantification of AMF-plant interactions are labor intensive and highly destructive which limits their application in studies that require high sample throughput, as well as in experiments that require repeated analysis of plants. We propose that the analysis of AMF-indicative blumenols in the shoot provides a convenient, easy-to-conduct, and minimally destructive tool to interrogate plant-AMF interactions in a HTP manner that allows for forward genetic studies even under field conditions (Figure 7E) and empowers plant breeding programs to produce mycorrhiza-responsive and P-efficient high-yielding lines (van de Wiel *et al.* 2016). Currently, phosphate fertilizer is derived from phosphate rock, a non-renewable resource, which is predicted to be soon depleted (Vaccari and Strigul 2011). By enabling breeding programs to select crop varieties that have negotiated AMF symbioses that deliver high yields with minimal P inputs, this discovery could help steer the “green revolution” away from intense agricultural inputs and the collateral environmental damage they cause.

Materials and Methods

Plant material and AMF inoculation

For our experiments with *Nicotiana attenuata* (Torr. ex S. Wats.), we used plants from the 31st inbred generation of the inbred ‘UT’ line, irCCaMK (A-09-1212-1; Groten *et al.* 2015) plants that are stably silenced in CCaMK via RNAi, i-irPDS plants (A-11-92-4 × A-11-325-4; Schäfer *et al.* 2013) harboring the LhGR/pOp6 system for chemically-inducible RNAi-mediated gene silencing of phytoene desaturase (PDS) and the respective empty vector (EV) transformed plants (A-04-266-3; Bubner *et al.* 2006) as controls. Details about the transformation and screening of the irCCaMK plants are described by Groten *et al.* (2015) and for the i-irPDS plants by Schäfer *et al.* (2013). Seeds were germinated on Gamborg B5 as described by Krügel *et al.* (2002). The advance intercross recombinant inbred line (RIL) population was developed by crossing two *N. attenuata* inbred lines originating from accessions collected in Arizona (AZ) and Utah (UT), USA (Glawe *et al.* 2003, Zhou *et al.* 2017). Additionally, we used *Solanum lycopersicum* ‘MoneyMaker’, *Hordeum vulgare* ‘Elbany’ and *Triticum aestivum* ‘Chinese Spring’ plants.

For glasshouse experiments, plants were treated according to Groten *et al.* (2015). In brief, they were transferred into dead (autoclaved twice at 121 °C for 30 min; non-inoculated controls) or living inoculum (*R. irregularis*, Biomyc Vital, inoculated plants) diluted 1:10 with expanded clay (size: 2–4 mm). Pots were covered with a thin layer of sand. Plants were watered with distilled water for 7 d and subsequently fertilized every second day either with a full strength hydroponic solution (for 1 L: 0.1292 g CaSO₄ × 2H₂O, 0.1232 g MgSO₄ × 7H₂O, 0.0479 g K₂HPO₄, 0.0306 g KH₂PO₄, 2mL KNO₃ (1 M), 0.5 mL micronutrients, 0.5 mL Fe diethylene triamine pentaacetic acid) or with a low P hydroponics solution containing only 1/10 of the regular P-concentration (0.05 mM). Plants were grown separately in 1L pots, if not stated otherwise. In the paired design (Figure 2), irCCaMK plants were grown together with EV plants in 2L pots and the watering regime was changed to ¼ of the regular P-concentration after plants started to elongate. Glasshouse experiments with natural inoculum (Figure 3C) were conducted in a mesocosm system (4 boxes, each 2 pairs of EV and irCCaMK plants). Plants were maintained under standard glasshouse conditions (16 h light, 24-28 °C, and 8 h dark, 20- 24 °C and 45 -55% humidity) with supplemental light supplied by high-pressure sodium lamps (Son-T-Agro).

The field experiments were conducted as described by Schuman *et al.* (2012). Seedlings were transferred to Jiffy pots and planted into a field plot at the Lytle Ranch Preserve in the Great Basin Desert (Utah, USA: N 37.1412, W 114.0275). Field season 2016 (Figure 3D): field experiments were conducted under the US Department of Agriculture Animal and Plant Health Inspection Service (APHIS) import permission numbers 10-004-105m (irCCaMK) and 07-341-101n (EV) and the APHIS release permission number 16-013-102r. EV and irCCaMK plants were planted in communities of six plants, either of the same genotype or with both genotypes in equal number.

Sample collection

During harvests, roots were washed and briefly dried with a paper towel. Subsequently, they were cut into 1 cm pieces and mixed. Plant tissues were shock-frozen in liquid nitrogen immediately after collection, ground to a fine powder and stored at -20°C (short-term storage)/-80°C (long-term storage) until extraction. From the root samples, an aliquot was stored in root storage solution (25% ethanol and 15% acetic acid in water) at 4 °C for microscopic analysis.

For stem sap collection, branches of *N. attenuata* plants were cut into 1.5cm long pieces and placed into small 0.5 mL reaction tubes with a small hole in the tip, which were placed in a larger 1.5 mL reaction tube. The tubes were centrifuged for 15 min at 10 000 × g. The stem sap from the larger reaction tubes was collected and stored at -20°C.

Samples prepared at other laboratory facilities

Medicago truncatula (Figure 7 and Figure 7—figure supplement 2) and *Brachypodium distachyon* (Figure 7 and Figure 7—figure supplement 2) samples were prepared at the laboratory of Prof. Maria Harrison from the Boyce Thompson Institute for Plant Research (Ithaca, NY, USA). *M. truncatula* plants were grown in a growth chamber with a 16 h light (25°C)/8 h dark (22°C) cycle. *B. distachyon* plants were grown in growth chamber with a 12 h light (24 °C) / 12 h dark (22 °C) cycle. All experiments were carried out in surface sterilized containers, autoclaved growth substrates and with surface sterilized spores and seeds as described previously (Liu *et al.* 2004, Hong *et al.* 2012, Floss *et al.* 2013). The growth substrates were mixtures of play sand (average particle 200-300 µm), black sand (heterogeneous particle size 50 – 300 µm) and gravel (heterogeneous particle size 300 µm -10 mm) as outlined below. For *M. truncatula*, 2 d-old seedlings were planted into 20.5 cm cones (Cone-tainers) containing a 1:1 mixture of sterile black sand and gravel with 200 surface-sterilized *G. versiforme* spores placed on a layer of play sand positioned 4 cm below the top of the cones. Five seedlings were planted into each cone. Plants were fertilized twice weekly with 20 mL of with modified 1/2-strength Hoagland's solution (Millner and Kitt 1992) containing with 100 µM potassium phosphate. Plants were harvested 49 d post planting and tissue frozen in liquid nitrogen and stored at -80 C. One cone containing 5 seedlings represents one biological replicate. The harvest date was 3/3/2015. *B. distachyon* seedlings were planted into cones (Cone-tainers) containing a 2:1:1 mixture of black sand:play sand:gravel with 300 surface-sterilized *G. versiforme* spores placed on a layer of play sand positioned 4 cm below the top of the cones. Plants were fertilized twice weekly with 20 mL of modified 1/4-strength Hoagland's solution (Millner and Kitt 1992) containing with 20 µM potassium phosphate. Plants were harvested 35 d post planting and tissue frozen in liquid nitrogen and stored at -80 C. Each cone contained 3 plants and each biological replicate consisted of a pool of 4 cones. The harvest date was 6/20/2016.

S. lycopersicum 'Moneymaker' (Figure 7—figure supplement 2) and *Solanum tuberosum* 'Wega' (Figure 7) samples were prepared at the laboratory of Prof. Philipp Franken by Dr. Michael Bitterlich from the Leibniz-Institute of Vegetable and Ornamental Crops (Großbeeren/Erfurt Germany). *S. lycopersicum* were transplanted into 10 L open pots containing a sand/vermiculite

mixture (sand: grain size 0.2–1 mm; Euroquarz, Ottendorf-Okrilla, Germany, vermiculite:agra vermiculite, Pullrhenen, Rhenen, The Netherlands; 1:1 v:v) and grown in the glass house from March to May (20:28:17°C day:night, PAR: 300-2000 $\mu\text{mol m}^{-2} \text{s}^{-1}$). Mycorrhizal plants were inoculated with a commercial inoculum either containing *R. irregularis* DAOM 197198 (INOQ, Schnega, Germany) or *F. mosseae* BEG12 (MycAgro Laboratory, Breteniere, France) with 10 % of the substrate volume and were harvested after 11 or 6 weeks, respectively. *S. tuberosum* tubers of similar size were planted into 3 L pots filled with the same substrate and grown in a growth cabinet (20:16°C day:night, 16 h light, 8 h dark; PAR: 250-400 $\mu\text{mol m}^{-2} \text{s}^{-1}$, 50 % rH). Mycorrhizal plants were inoculated with a commercial inoculum either containing *F. mosseae* BEG12 (MycAgro Laboratory, Breteniere, France) with 10 % of the substrate volume and were harvested after 6 weeks. Non-mycorrhizal counterparts were inoculated with the same amount of autoclaved (2 h, 121°C) inoculum and a filtrate. The filtrate was produced for every pot by filtration of 200 mL deionized water through Whatman filter (particle retention 4–7 μm ; GE Healthcare Europe GmbH, Freiburg, Germany) containing approx. 200 mL of inoculum. The same amount of deionized water (200 mL) was added to mycorrhizal pots. Plants were irrigated every other day with 400- 600 mL nutrient solution (De Kreij *et al.* 1997); 40% of full strength) with 10% of the standard phosphate to guarantee good colonization (N:10.32 mM; P: 0.07 mM, K: 5.5 mM, Mg: 1.2 mM, S: 1.65 mM, Ca: 2.75 mM, Fe: 0.02 mM, pH: 6.2, EC: 1.6 mS). For the experiment in the glasshouse, additional irrigation was carried out with deionized water until pot water capacity every other day. The pooled bulk leaf sample was dried at 60°C for 48 h, ground to a fine powder and stored under dry conditions at room temperature until further analyses.

Stress treatments

Herbivory treatments were conducted by placing *Manduca sexta* neonates, originating from an in-house colony, on the plants. After feeding for 2 weeks, rosette leaves were harvested. As controls, we harvested leaves from untreated plants.

For bacteria and virus infection, plants were inoculated with *Agrobacterium tumefaciens* carrying the Tobacco Rattle Virus. The inoculation was conducted by infiltrating leaves with a bacteria solution using a syringe. The treatment was conducted as described for virus-induced gene silencing described by Ratcliff *et al.* (2001) and by Saedler and Baldwin (2004). After incubation for 3 weeks, stem leaves of the treated plants and untreated control plants were harvested.

The fungal infection was done with *Botrytis cinerea*. On each plant, three leaves were treated by applying 6 droplets each containing 10 μL of *B. cinerea* spore suspension (10^6 spores mL^{-1} in Potato Extract Glucose Broth, Carl Roth GmbH) to the leaf surface. As control, plants were treated with broth without spores in the same way. Samples were collected after 4 days incubation.

Drought stress was induced by stopping the watering for 4 d. Subsequently, stem leaves of the drought-stressed plants and the continuously watered control plants were harvested. In contrast

to the other samples of the stress experiment, leaves were dried before analysis to compensate for weight differences caused by changes in the water content.

Sample preparation - extraction and purification

For extraction, samples were aliquoted into reaction tubes, containing two steel balls. Weights were recorded for later normalization. Per 100 mg plant tissues (10 mg in case of dry material), approximately 1 mL 80% MeOH was added to the samples before being shaken in a GenoGrinder 2000 (SPEX SamplePrep) for 60 s at 1150 strokes min⁻¹. After centrifugation, the supernatant was collected and analyzed. For triple-quadrupole MS quantification, the extraction buffer was spiked with stable isotope-labeled abscisic acid (D₆-ABA, HPC Standards GmbH) as an internal standard.

Stem sap was diluted 1:1 with MeOH spiked with D₆-ABA as an internal standard. After centrifugation, the supernatant was collected and analyzed.

The purification of *N. attenuata* leaf extracts for high resolution MS was conducted by solid-phase-extraction (SPE) using the Chromabond HR-XC 45 µm benzenesulfonic acid cation exchange columns (Machery-Nagel) to removed abundant constituents, such as nicotine and phenolamides. After purification the samples were evaporated to dryness and reconstituted in 80% methanol.

Compound identification was conducted by NMR with purified fractions of root and leaf extracts. Compounds 1, 3 and 4 were extracted from root tissues of *N. attenuata* and purified by HPLC (Agilent-HPLC 1100 series; Grom-Sil 120 ODS-4 HE, C18, 250 × 8 mm, 5 µm; equipped with a Gilson 206 Abimed fraction collector). Compounds 2 and 7 were extracted from a mixture of leaf tissues from different plant species (*M. truncatula*, *Z. mays*, *S. lycopersicum* and *N. attenuata*). The first purification step was conducted by SPE using the Chromabond HR-XC 45 µm benzenesulfonic acid cation exchange columns (Machery-Nagel) to remove hydrophilic and cationic constituents. Additional purification steps were conducted via HPLC (Agilent-HPLC 1100 series; Phenomenex Luna C18(2), 250 × 10 mm, 5 µm; equipped with a Foxy Jr. sample collector) and UHPLC (Dionex UltiMate 3000; Thermo Acclaim RSLC 120 C18, 150 × 2.1 mm, 2.2 µm; using the auto-sampler for fraction collection).

Untargeted MS based analyses

For high resolution mass spectrometry (MS), indiscriminant tandem mass spectrometry (idMS/MS), tandem MS (MS²) and pseudo-MS³ were used. Ultra-high performance liquid chromatography (UHPLC) was performed using a Dionex UltiMate 3000 rapid separation LC system (Thermo Fisher), combined with a Thermo Fisher Acclaim RSLC 120 C18, 150 × 2.1 mm, 2.2 µm column. The solvent composition changed from a high % A (water with 0.1% acetonitrile and 0.05% formic acid) in a linear gradient to a high % B (acetonitrile with 0.05 %

formic acid) followed by column equilibration steps and a return to starting conditions. The flow rate was 0.3 mL/min. MS detection was performed using a micrOTOF-Q II MS system (Bruker Daltonics), equipped with an electrospray ionization (ESI) source operating in positive ion mode. ESI conditions for the micrOTOF-Q II system were end plate offset 500 V, capillary voltage 4500 V, capillary exit 130 V, dry temperature 180°C and a dry gas flow of 10 L min⁻¹. Mass calibration was performed using sodium formate (250 mL isopropanol, 1 mL formic acid, 5 mL 1 M NaOH in 500 mL water). Data files were calibrated using the Bruker high-precision calibration algorithm. Instrument control, data acquisition and reprocessing were performed using HyStar 3.1 (Bruker Daltonics).

idMS/MS was conducted in order to gain structural information on the overall detectable metabolic profile. For this, samples were first analyzed by UHPLC-ESI/qTOF-MS using the single MS mode (producing low levels of fragmentation that resulted from in-source fragmentation) by scanning from *m/z* 50 to 1400 at a rate of 5000 scans/s. MS/MS analyses were conducted using nitrogen as collision gas and involved independent measurements at the following 4 different collision-induced dissociation (CID) voltages: 20, 30, 40 and 50 eV. The quadrupole was operated throughout the measurement with the largest mass isolation window, from *m/z* 50 to 1400. Mass fragments were scanned between *m/z* 50 to 1400 at a rate of 5000 scans/s. For the idMS/MS assembly, we used a previously designed precursor-to-product assignment pipeline (Li *et al.* 2015, Li *et al.* 2016) using the output results for processing with the R packages XCMS and CAMERA (Data Set 2).

Additional MS/MS experiments were performed on the molecular ion at various CID voltages. For the fragmentation of the proposed aglycones via pseudo-MS³, we applied a 60 eV in-source-CID transfer energy which produced spectra reflecting the loss of all sugar moieties.

Structure elucidation by NMR

Purified fractions were completely dried with N₂ gas and reconstituted with MeOH-d₃ prior to analysis by nuclear magnetic resonance spectroscopy (NMR). Structure elucidation was accomplished on an Avance III AV700 HD NMR spectrometer (Bruker-Biospin, Karlsruhe, Germany) at 298 K using a 1.7 mm TCI CryoProbeTM with standard pulse programs as implemented in Bruker TopSpin (Version 3.2). Chemical shift values (δ) are given relative to the residual solvent peaks at δ_H 3.31 and δ_C 49.05, respectively. Carbon shifts were determined indirectly from ¹H-¹³C HSQC and ¹H-¹³C HMBC spectra. The data are shown in Table 1.

Table 1 ^1H and ^{13}C NMR data for compounds 1-4 and 7

No.	Compound 1			Compound 2			Compound 3			Compound 4			Compound 7		
Pos.	δ_{H}	mult., J [Hz]	δ_{C}	δ_{H}	mult., J [Hz]	δ_{C}	δ_{H}	mult., J [Hz]	δ_{C}	δ_{H}	mult., J [Hz]	δ_{C}	δ_{H}	mult., J [Hz]	δ_{C}
1	-	-	202.3	-	-	203.1	-	-	202.2	-	-	202.3	-	-	200.9
2	6.0	dd,	121.3	6.4	s	128.5	6.0	s br	121.3	5.8	s br	125.2	5.8	s	126.4
3	-	-	172.4	-	-	172.6	-	-	172.2	-	-	169.8	-	-	171.5
4	1.9	dd,	47.8	2.6	m	46.3	1.9	dd,	48.0	1.9	dd,	52.4	-	-	79.2
5	2	5.2/5.2	37.2	4	-	36.9	2	5.2/5.2	37.2	7	5.0/5.0	37.2	-	-	42.9
6	2.5	d, 17.5	48.5	2.0	d, 17.4	48.0	2.5	d, 17.6	47.7	2.4	d, 17.3	48.0	2.1	d, 18.0	50.8
7	2.0	d, 17.5	26.8	2.6	d, 17.4	27.6	2.0	d, 17.6	27.1	1.9	d, 17.3	26.5	2.1	d, 18.0	34.6
8	1.6	m	37.1	1.6	m	36.0	1.6	m	37.2	1.6	m	37.4	1.4	m	32.7
9	3.8	dd,	77.2	3.8	m	77.7	3.8	dd,	77.7	3.8	dd,	77.7	3.8	ddd,	78.2
10	1.2	d, 6.2	21.6	1.2	d, 6.1	21.9	1.2	d, 6.3	21.9	1.2	d, 6.3	21.9	1.2	d, 6.3	21.9
11	4.3	dd,	64.9	-	-	160.1	4.3	m/m	64.9	2.0	d, 1.2	24.9	2.0	d, 1.0	21.7
12	1.0	s	28.4	1.0	s	28.4	1.0	s	28.6	1.0	s	28.7	1.0	s	24.3
13	1.1	s	27.5	1.1	s	27.5	1.1	s	27.5	1.1	s	27.4	1.0	s	23.7
1'	4.3	d, 7.9	103.8	4.3	d, 7.9	104.1	4.3	d, 7.9	103.8	4.3	d, 7.8	104.0	4.3	d, 7.9	104.0
2'	3.1	dd,	75.0	3.1	dd,	75.1	3.1	dd,	75.1	3.1	dd,	75.2	3.1	dd, 7.9/8.9	75.1
3'	3.3	dd,	77.9	3.3	dd,	78.0	3.3	m	77.8	3.3	dd,	78.0	3.3	dd, 8.9/8.9	77.8
4'	3.2	dd,	71.4	3.2	dd,	71.5	3.3	m	71.4	3.3	dd,	71.5	3.2	dd, 8.9/8.9	71.4
5'	3.2	m	77.6	3.2	m	77.6	3.4	m	77.0	3.4	m	76.9	3.2	m	77.7
6'	3.8	dd,	62.5	3.8	dd,	62.6	4.1	dd,	69.6	4.1	dd,	69.7	3.8	d, 11.7	62.3
1"	3.6	dd,	11.8/5.5	3.6	dd,	11.8/5.5	3.7	dd,	11.7/5.7	3.7	dd,	11.6/5.9	3.6	dd, 4.5/11.7	62.3
2"	-	-	-	-	-	-	4.4	d, 7.9	104.6	4.4	d, 7.8	104.8	-	-	-
3"	-	-	-	-	-	-	3.2	dd,	74.9	3.2	dd,	75.0	-	-	-
4"	-	-	-	-	-	-	3.3	dd,	77.9	3.3	dd,	77.9	-	-	-
5"	-	-	-	-	-	-	3.2	dd,	71.4	3.2	dd,	71.5	-	-	-
6"	-	-	-	-	-	-	3.2	m	77.9	3.2	dd,	78.0	-	-	-
	-	-	-	-	-	-	3.8	dd,	62.5	3.8	dd,	62.7	-	-	-
	-	-	-	-	-	-	3.6	0	62.5	3.6	dd,	62.7	-	-	-

s, singlet; s br, broad singlet; d, doublet; dd, doublet of doublet; m, multiplet

Targeted metabolite analysis

For chromatographic separations, a UHPLC (Dionex UltiMate 3000) was used to provide a maximum of separation with short run times. This reduced the interference from other extract components (matrix effects), increased the specificity of the method, and met the requirements of a HTP analysis. The auto-sampler was cooled to 10°C. As a stationary phase, we used a reversed phase column (Agilent ZORBAX Eclipse XDB C18, 50 × 3.0 mm, 1.8 µm) suitable for the separation of moderately polar compounds. Column temperature was set to 42°C. As mobile phases, we used: A, 0.05% HCOOH, 0.1% ACN in H₂O and B, MeOH, the composition of which was optimized for an efficient separation of blumenol-type compounds within a short run time. We included in the method a cleaning segment at 100% B and an equilibration segment allowing for reproducible results across large samples sets. The gradient program was as follows: 0–1 min, 10% B; 1–1.2 min, 10–35% B; 1.2–5 min, 35–50% B; 5–5.5 min, 50–100% B; 5.5–6.5 min, 100% B; 6.5–6.6 min, 100–10% B and 6.6–7.6 min, 10% B. The flow rate was set to 500 µL min⁻¹. Analysis was performed on a Bruker Elite EvoQ triple quadrupole MS equipped with a HESI (heated electrospray ionization) ion source. Source parameters were as follows: spray voltage (+), 4500V; spray voltage (-), 4500V; cone temperature, 350°C; cone gas flow, 35; heated probe temperature, 300°C; probe gas flow, 55 and nebulizer gas flow, 60. Samples were analyzed in multi-reaction-monitoring (MRM) mode; the settings are described in Table 2.

Table 2 MRM-settings used for targeted blumenol analysis

Nr.	Compound Name	RT		Q1 [m/z] ^a ^b	Q3 [m/z] ^{c, d} (CE [V])
1	11-hydroxyblumenol C-Glc ^{f, g}	2.82	+	389.22	227.16 (-2.5), 209.15 (-7.5) , 191.14 (-12.5), 163.10 (-15), 149.10 (-17.5)
2	11-carboxyblumenol C-Glc ^{f, g}	3.22	+	403.22	241.16 (-2.5), 223.15 (-7.5), 177.10 (-15), 195.14 (-12.5)
			+	241.16 ^e	223.15 (-5), 177.10 (-15), 195.14 (-10)
3	11-hydroxyblumenol C-Glc-Glc ^{f, g}	2.5	+	551.27	389.22 (-2.5), 227.16 (-7.5), 209.15 (-10) , 191.14 (-15), 149.10 (-20)
4	Blumenol C – Glc-Glc ^{f, g}	3.47	+	535.27	373.22 (-2.5), 211.00 (-10) , 193.10 (-17.5), 135.00 (-22.5), 109.00 (-22.5)
5	Blumenol C - Glc ^{f, h}	4.18	+	373.22	211.20 (-6) , 193.16 (-9), 175.10 (-15), 135.12 (-16), 109.10 (-20)
6	Blumenol A - Glc ^{f, h}	2.51	-	385.20	153.10 (14)
			+	387.20	225.15 (-5), 207.14 (-8), 149.10 (-18), 135.12 (-16), 123.08 (-23)
7	Blumenol B - Glc ^{f, g}	2.5	+	389.22	227.16 (-5), 209.15 (-7.5) , 191.14 (-12.5), 153.10 (-17.5), 149.10 (-17.5)
8	Blumenol C – Glc-GlcU ^{f, i}	3.25 & 3.38	+	549.27	373.22 (-2.5), 211.00 (-10) , 193.10 (-17.5), 135.00 (-22.5), 109.00 (-22.5)
9	11-hydroxylumenol C – Glc-Rha ⁱ	2.8	+	535.27	389.22 (-2.5), 227.16 (-7.5) , 209.15 (-10), 191.14 (-15), 149.10 (-20)
10	Blumenol C – Glc-Rha ^{f, i}	4.1	+	519.27	373.22 (-2.5), 211.00 (-10) , 193.10 (-17.5), 135.00 (-22.5), 109.00 (-22.5)
11	Hydroxyblumenol C-Hex-Pen ⁱ	2.5	+	521.27	389.22 (-2.5), 227.16 (-7.5), 209.15 (-10) , 191.14 (-15), 149.10 (-20)
	D ₆ -ABA ^h	4.5	-	269.17	159.00 (10)

RT: retention time

CE: collision energy

Glc: glucose

GlcU: glucuronic acid

Rha: rhamnose

Hex: hexose

Pen: pentose

^a Resolution: 0.7^b [M+H]⁺ or [M-H]⁻ if not stated differently^c Resolution: 2^d Quantifiers are depicted in bold^e [M+H-Glc]⁺^f Verified by high resolution MS^g Verified by NMR^h Optimized with commercial available standardsⁱ Transitions predicted based on structural similar compounds and literature information

Adjusted method for targeted blumenol analysis in *N. attenuata*

The compound list was limited to the AMF-indicative markers in *N. attenuata*, Compound 1 and 2, the not AMF-indicative Compound 6 and the internal standard (D₆-ABA). Accordingly, the gradient program was adjusted as follows: 0–1 min, 10% B; 1–1.2 min, 10–35% B; 1.2–3 min, 35–42% B; 3–3.4 min, 42–100% B; 3.4–4.4 min, 100% B; 4.4–4.5 min, 100–10% B and 4.5–5.5 min, 10% B. The MRM settings are given in Table 3.

Table 3 MRM-settings for the analysis of selected blumenols in *N. attenuata*

Nr.	Compound Name	RT	Q1 [m/z] ^{a, b}	Q3 [m/z] ^{c, d} (CE [V])
1	11-hydroxyblumenol C-Glc ^{f, g}	2.82	+ 389.22	227.16 (-2.5), 209.15 (-7.5) , 191.14 (-12.5), 163.10 (-15), 149.10 (-17.5)
2	11-carboxyblumenol C-Glc ^{f, g}	3.22	+ 403.22	241.16 (-2.5), 223.15 (-7.5), 177.10 (-15), 195.14 (-12.5)
			+ 241.16 ^e	223.15 (-5), 177.10 (-15), 195.14 (-10)
6	Blumenol A - Glc ^{f, h}	2.51	- 385.20	153.10 (14)
			+ 387.20	225.15 (-5), 207.14 (-8), 149.10 (-18), 135.12 (-16), 123.08 (-23)
	D ₆ -ABA ^h	4.0	- 269.17	159.00 (10)

RT: retention time

CE: collision energy

Glc: glucose

Hex: hexose

Pen: pentose

^a Resolution: 0.7

^b [M+H]⁺ or [M-H]⁻ if not stated differently

^c Resolution: 2

^d Quantifiers are depicted in bold

^e [M+H-Glc]⁺

^f Verified by high resolution MS

^g Verified by NMR

^h Optimized with commercial available standards

Determination of the AMF colonization rate

To determine the fungal colonization rates and mycorrhizal structures, root samples were stained and analyzed by microscopy. For WGA-Alexa Fluor 488 staining, roots were first washed with distilled water and then soaked in 50% (v/v) ethanol overnight. Roots were then boiled in a 10% (w/v) KOH solution for 10 minutes. After rinsing with water, the roots were boiled in 0.1 M HCl solution for 5 minutes. After rinsing with water and subsequently with 1x phosphate-buffered saline solution, roots were stained in 1x phosphate-buffered saline buffer containing 0.2 mg mL⁻¹ WGA-Alexa Fluor 488 overnight in the dark. Zeiss confocal microscopy (LSM 510 META) was used to detect the WGA-Alexa Fluor 488 (excitation/emission maxima at approximately 495/519 nm) signal. Trypan blue staining was performed as described by Brundrett *et al.* (1984) to visualize mycorrhizal structures. For the counting of mycorrhizal colonization, 15 root fragments, each about 1 cm long, were stained with either trypan blue or WGA-488 followed by slide mounting. More than 150 view fields per slide were surveyed with 20x object magnification and classified into 5 groups: no colonization, only hyphae (H), hyphae with arbuscules (H+A), hyphae with vesicles (V+H), and hyphae with arbuscules and vesicles (A+V+H). The proportions of each group were calculated by numbers of each group divided by total views.

For the molecular biological analysis of colonization rates, RNA was extracted from the roots using the RNeasy Plant Mini Kit (Qiagen) or NucleoSpin® RNA Plant (Macherey-Nagel) according to the manufacturer's instructions and cDNA was synthesized by reverse transcription using the PrimeScript RT-qPCR Kit (TaKaRa). Quantitative (q)PCR was performed on a Stratagene Mx3005P qPCR machine using a SYBR Green containing reaction mix (Eurogentec, qPCR Core kit for SYBR Green I No ROX). We analyzed the *R. irregularis* specific housekeeping gene, *Ri-tub* (GenBank: EXX64097.1), as well as the transcripts of the AMF-induced plant marker genes *RAM1*, *Vapyrin*, *STR1* and *PT4*. The signal abundance was normalized to *NaIF-5a* (NCBI Reference Sequence: XP_019246749.1). The primer sequences are summarized in Table 4.

Table 4 Sequences of primers used for qPCR-based analysis of AMF-colonization rates

Gene	Forward primer	Reversed primer
<i>NaIF-5a</i>	GTCGGACGAAGAACCATT	CACATCACAGTTGTGGGAGG
<i>NaRAM1</i>	ACGGGGTCTATCGCTCCTT	GTGCACCAGTTGTAAGCCAC
<i>NaVapryrin</i>	GGTCCCAAGTGATTGGTTCAC	GACCTTCAAAGTCAACTGAGTCAA
<i>NaSTR1</i>	TCAGGCTTCCACCTTCAATATCT	GACTCTCCGACGTTCTCCC
<i>NaPT4</i>	GGGGCTCGTTTCAATGATTA	AACACGATCCGCCAAACAT
<i>NaCCaMK</i>	TTGGAGCTTTGTTCTGGTGGT	ATACTTGCCCCGTGTAGCG
<i>Ri-TUB</i>	TGTCCAACCGTTTAAAGT	AAAGCACGTTTGGCGTACAT

Transcript analysis of the apocarotenoid pathway

The transcript analysis of the (apo)carotenoid pathway was conducted based on RNA-seq (Data Set 3) by using *N. attenuata* roots with or without *R. irregularis* inoculations. The data analysis methods are based on the previously published pipeline of Ling *et al.* (2015). Representative values for transcripts abundances are TPM (Transcripts per kilobase of exon model per million mapped reads).

Blumenol transport experiment

To analyze the root-to-shoot transfer potential of blumenols, we placed three *N. attenuata* seedlings, previously germinated on petri dishes with GB5 Agar for approximately 10 days, into 0.5 mL reaction tubes. The roots were placed into the tube, while the shoot projected out of the tube. The tubes were carefully covered with parafilm, which held the seedlings in place and isolated roots from shoots (see Figure 6C). The tubes were filled with tap water supplemented with 0.5% v/v plant extracts enriched in Compounds 1 or 2 (unknown concentration; purified fractions), or a commercial available standard of Compound 6 (25 ng μL^{-1} end concentration; Roseoside; Wuhan ChemFaces Biochemical Co., Ltd.). Compound 1 or 2 were prepared from a mix of leaf tissues from different plant species (*M. truncatula*, *Z. mays*, *S. lycopersicum* and *N. attenuata*) by methanol extraction followed by purification by SPE (Chromabond HR-XC column) and HPLC (Agilent-HPLC 1100 series; Phenomenex Luna C18(2), 250 \times 10 mm, 5 μm ; equipped with a Foxy Jr. fraction collector). As a control, we used tap water supplemented with the respective amounts of MeOH. The seedlings were incubated for 1d in a Percival climate chamber (16 h of light at 28 °C, and 8 h of dark at 26 °C). During sample collection, roots and shoots were separated and the roots were rinsed in water (to reduce the surface contamination with the incubation medium). While the shoots were analyzed separately, the roots of all seedlings from the same treatment were pooled. Sample extraction was conducted as described above.

Inducible PDS silencing

For the temporal and spatial restriction of PDS gene silencing, we treated the petiole of the second oldest stem leaf of AMF-inoculated and non AMF-inoculated i-ir*PDS* and EV plants with a 100 μ M dexamethasone-containing lanolin paste (1% v/v DMSO). The lanolin paste was prepared and applied as described by Schäfer *et al.* (2013). The treatment started 3 weeks after potting and was conducted for 3 weeks. The lanolin paste was refreshed twice per week. On each plant the treated leaf and the adjacent, untreated leaves were harvested for analysis.

QTL analysis

The field experiments for QTL analysis were conducted in 2017. Collected leaf samples were extracted as described with 80% MeOH spiked with D₆-ABA as internal standard and analyzed with the method described under '*Adjusted method for targeted blumenol analysis in N. attenuata*'. The peak areas for Compound 2 were normalized by amount of extracted tissue, internal standard and log-transformed. Samples with missing genotype or phenotype information were removed. In total, 728 samples were used for QTL mapping analysis. For quantitative trait loci (QTL) mapping, we used the AZ-UT RIL population described by Zhou *et al.* (2017).

Statistics

Statistical analysis of the data was performed with R version 3.0.3 (<http://www.R-project.org/>). The statistical methods used and the number of replicates are indicated in the figure legends.

References

- Adolfsson, L., Nziengui, H., Abreu, I.N., Šimura, J., Beebo, A., Herdean, A., Aboalizadeh, J., Široká, J., Moritz, T., Novák, O., Ljung, K., Schoefs, B. and Spetea, C.** (2017) Enhanced secondary- and hormone metabolism in leaves of arbuscular mycorrhizal *Medicago truncatula*. *Plant Physiology*, 10.1104/pp.16.01509
- Adolfsson, L., Solymosi, K., Andersson, M.X., Keresztes, A., Uddling, J., Schoefs, B. and Spetea, C.** (2015) Mycorrhiza symbiosis increases the surface for sunlight capture in *Medicago truncatula* for better photosynthetic production. *PLoS ONE*, **10**, e0115314. 10.1371/journal.pone.0115314
- Aishan, H., Baba, M., Iwasaki, N., Kuang, H. and Okuyama, T.** (2010) The constituents of *Urtica cannabina* used in Uighur medicine. *Pharmaceutical Biology*, **48**, 577-583. 10.3109/13880200903214215
- Aliferis, K.A., Chamoun, R. and Jabaji, S.** (2015) Metabolic responses of willow (*Salix purpurea* L.) leaves to mycorrhization as revealed by mass spectrometry and H-1 NMR spectroscopy metabolite profiling. *Frontiers in Plant Science*, **6**, 15. 10.3389/fpls.2015.00344
- Baldwin, I.T.** (1989) Mechanism of damage-induced alkaloid production in wild tobacco. *Journal of Chemical Ecology*, **15**, 1661-1680. 10.1007/bf01012392
- Bhakuni, D.S., Joshi, P.P., Uprety, H. and Kapil, R.S.** (1974) Roseoside-A C₁₃ glycoside from *Vinca rosea*. *Phytochemistry*, **13**, 2541-2543. 10.1016/S0031-9422(00)86933-2
- Bi, H.H., Song, Y.Y. and Zeng, R.S.** (2007) Biochemical and molecular responses of host plants to mycorrhizal infection and their roles in plant defence. *Allelopathy Journal*, **20**, 15-27.
- Bravo, A., Brands, M., Wewer, V., Dormann, P. and Harrison, M.J.** (2017) Arbuscular mycorrhiza-specific enzymes FatM and RAM2 fine-tune lipid biosynthesis to promote development of arbuscular mycorrhiza. *New Phytologist*, **214**, 1631-1645. 10.1111/nph.14533
- Brundrett, M.C., Piché, Y. and Peterson, R.L.** (1984) A new method for observing the morphology of vesicular–arbuscular mycorrhizae. *Canadian Journal of Botany*, **62**, 2128-2134. 10.1139/b84-290
- Brundrett, M.C. and Tedersoo, L.** (2018) Evolutionary history of mycorrhizal symbioses and global host plant diversity. *New Phytologist*. 10.1111/nph.14976
- Bubner, B., Gase, K., Berger, B., Link, D. and Baldwin, I.T.** (2006) Occurrence of tetraploidy in *Nicotiana attenuata* plants after *Agrobacterium*-mediated transformation is genotype specific but independent of polysomaty of explant tissue. *Plant Cell Reports*, **25**, 668-675. 10.1007/s00299-005-0111-4
- Chitarra, W., Pagliarani, C., Maserti, B., Lumini, E., Siciliano, I., Cascone, P., Schubert, A., Gambino, G., Balestrini, R. and Guerrieri, E.** (2016) Insights on the impact of arbuscular mycorrhizal symbiosis on tomato tolerance to water stress. *Plant Physiology*, **171**, 1009-1023. 10.1104/pp.16.00307
- Cuttillo, F., Dellagrecia, M., Previtera, L. and Zarrelli, A.** (2005) C₁₃ norisoprenoids from *Brassica fruticulosa*. *Natural Product Research*, **19**, 99-103. 10.1080/14786410410001686409

- De Kreijl, C., Voogt, W., van den Bos, A.L. and Baas, R.** (1997) *Voedingsoplossingen voor de teelt van tomaat in gesloten teeltsystemen*: Naaldwijk: Brochure VG Tomaat.
- Fester, T., Hause, B., Schmidt, D., Halfmann, K., Schmidt, J., Wray, V., Hause, G. and Strack, D.** (2002) Occurrence and localization of apocarotenoids in arbuscular mycorrhizal plant roots. *Plant and Cell Physiology*, **43**, 256-265. [10.1093/pcp/pcf029](#)
- Fester, T., Maier, W. and Strack, D.** (1999) Accumulation of secondary compounds in barley and wheat roots in response to inoculation with an arbuscular mycorrhizal fungus and co-inoculation with rhizosphere bacteria. *Mycorrhiza*, **8**, 241-246. [10.1007/s005720050240](#)
- Fester, T., Wray, V., Nimtz, M. and Strack, D.** (2005) Is stimulation of carotenoid biosynthesis in arbuscular mycorrhizal roots a general phenomenon? *Phytochemistry*, **66**, 1781-1786. [10.1016/j.phytochem.2005.05.009](#)
- Floß, D.S., Hause, B., Lange, P.R., Küster, H., Strack, D. and Walter, M.H.** (2008) Knock-down of the MEP pathway isogene 1-deoxy-d-xylulose 5-phosphate synthase 2 inhibits formation of arbuscular mycorrhiza-induced apocarotenoids, and abolishes normal expression of mycorrhiza-specific plant marker genes. *The Plant Journal*, **56**, 86-100. [10.1111/j.1365-313X.2008.03575.x](#)
- Floss, D.S., Levy, J.G., Levesque-Tremblay, V., Pumplin, N. and Harrison, M.J.** (2013) DELLA proteins regulate arbuscule formation in arbuscular mycorrhizal symbiosis. *Proceedings of the National Academy of Sciences of the United States of America*, **110**, E5025-5034. [10.1073/pnas.1308973110](#)
- Floss, D.S., Schliemann, W., Schmidt, J., Strack, D. and Walter, M.H.** (2008) RNA interference-mediated repression of MtCCD1 in mycorrhizal roots of *Medicago truncatula* causes accumulation of C₂₇ apocarotenoids, shedding light on the functional role of CCD1. *Plant Physiology*, **148**, 1267-1282. [10.1104/pp.108.125062](#)
- Galbraith, M.N. and Horn, D.H.S.** (1972) Structures of the natural products blumenols A, B, and C. *Journal of the Chemical Society, Chemical Communications*, 113-114. [10.1039/C39720000113](#)
- Glawe, G.A., Zavala, J.A., Kessler, A., Van Dam, N.M. and Baldwin, I.T.** (2003) Ecological costs and benefits correlated with trypsin protease inhibitor production in *Nicotiana attenuata*. *Ecology*, **84**, 79-90. [10.1890/0012-9658\(2003\)084\[0079:ECABCW\]2.0.CO;2](#)
- Groten, K., Nawaz, A., Nguyen, N.H.T., Santhanam, R. and Baldwin, I.T.** (2015) Silencing a key gene of the common symbiosis pathway in *Nicotiana attenuata* specifically impairs arbuscular mycorrhizal infection without influencing the root-associated microbiome or plant growth. *Plant, Cell & Environment*, **38**, 2398-2416. [10.1111/pce.12561](#)
- Helber, N., Wippel, K., Sauer, N., Schaarschmidt, S., Hause, B. and Requena, N.** (2011) A versatile monosaccharide transporter that operates in the arbuscular mycorrhizal fungus *Glomus* sp is crucial for the symbiotic relationship with plants. *The Plant Cell*, **23**, 3812-3823. [10.1105/tpc.111.089813](#)
- Hong, J.J., Park, Y.S., Bravo, A., Bhattarai, K.K., Daniels, D.A. and Harrison, M.J.** (2012) Diversity of morphology and function in arbuscular mycorrhizal symbioses in *Brachypodium distachyon*. *Planta*, **236**, 851-865. [10.1007/s00425-012-1677-z](#)

- Hou, X., Rivers, J., León, P., McQuinn, R.P. and Pogson, B.J.** (2016) Synthesis and function of apocarotenoid signals in plants. *Trends in Plant Science*, **21**, 792-803. [10.1016/j.tplants.2016.06.001](https://doi.org/10.1016/j.tplants.2016.06.001)
- Jiang, Y., Wang, W., Xie, Q., Liu, N. and Liu, L.** (2017) Plants transfer lipids to sustain colonization by mutualistic mycorrhizal and parasitic fungi. *Science*, **356**, 1172-1175. [10.1126/science.aam9970](https://doi.org/10.1126/science.aam9970)
- Kato-Noguchi, H., Hamada, N. and Clements, D.R.** (2015) Phytotoxicities of the invasive species *Plantago major* and non-invasive species *Plantago asiatica*. *Acta Physiologiae Plantarum*, **37**, 60. [10.1007/s11738-015-1794-y](https://doi.org/10.1007/s11738-015-1794-y)
- Kato-Noguchi, H., Tamura, K., Sasaki, H. and Suenaga, K.** (2012) Identification of two phytotoxins, blumenol A and grasshopper ketone, in the allelopathic Japanese rice variety Awaakamai. *Journal of Plant Physiology*, **169**, 682-685. [10.1016/j.jplph.2012.01.009](https://doi.org/10.1016/j.jplph.2012.01.009)
- Keymer, A., Pimprikar, P., Wewer, V., Huber, C. and Brands, M.** (2017) Lipid transfer from plants to arbuscular mycorrhiza fungi. *Elife*, **6**, e29107. [10.7554/eLife.29107](https://doi.org/10.7554/eLife.29107)
- Krügel, T., Lim, M., Gase, K., Halitschke, R. and Baldwin, I.T.** (2002) *Agrobacterium*-mediated transformation of *Nicotiana attenuata*, a model ecological expression system. *Chemoecology*, **12**, 177-183. [10.1007/PL00012666](https://doi.org/10.1007/PL00012666)
- Lanfranco, L., Fiorilli, V., Venice, F. and Bonfante, P.** (2017) Strigolactones cross the kingdoms: plants, fungi, and bacteria in the arbuscular mycorrhizal symbiosis. *Journal of Experimental Botany*, **erx432-erx432**. [10.1093/jxb/erx432](https://doi.org/10.1093/jxb/erx432)
- Lee, G., Joo, Y., Kim, S.G. and Baldwin, I.T.** (2017) What happens in the pith stays in the pith: tissue-localized defense responses facilitate chemical niche differentiation between two spatially separated herbivores. *The Plant Journal*, **92**, 414-425. [10.1111/tpj.13663](https://doi.org/10.1111/tpj.13663)
- Li, D., Baldwin, I.T. and Gaquerel, E.** (2015) Navigating natural variation in herbivory-induced secondary metabolism in coyote tobacco populations using MS/MS structural analysis. *Proceedings of the National Academy of Sciences of the United States of America*, **112**, E4147-E4155. [10.1073/pnas.1503106112](https://doi.org/10.1073/pnas.1503106112)
- Li, D., Heiling, S., Baldwin, I.T. and Gaquerel, E.** (2016) Illuminating a plant's tissue-specific metabolic diversity using computational metabolomics and information theory. *Proceedings of the National Academy of Sciences of the United States of America*, **113**, E7610-E7618. [10.1073/pnas.1610218113](https://doi.org/10.1073/pnas.1610218113)
- Ling, Z., Zhou, W., Baldwin, I.T. and Xu, S.** (2015) Insect herbivory elicits genome-wide alternative splicing responses in *Nicotiana attenuata*. *The Plant Journal*, **84**, 228-243. [10.1111/tpj.12997](https://doi.org/10.1111/tpj.12997)
- Liu, J., Blaylock, L.A. and Harrison, M.J.** (2004) cDNA arrays as a tool to identify mycorrhiza-regulated genes: identification of mycorrhiza-induced genes that encode or generate signaling molecules implicated in the control of root growth. *Canadian Journal of Botany*, **82**, 1177-1185. [10.1139/b04-048](https://doi.org/10.1139/b04-048)
- Luginbuehl, L.H. and Menard, G.N.** (2017) Fatty acids in arbuscular mycorrhizal fungi are synthesized by the host plant. *Science*, **356**, 1175-1178. [10.1126/science.aan0081](https://doi.org/10.1126/science.aan0081)
- Maier, W., Hammer, K., Dammann, U., Schulz, B. and Strack, D.** (1997) Accumulation of sesquiterpenoid cyclohexenone derivatives induced by an arbuscular mycorrhizal fungus in members of the *Poaceae*. *Planta*, **202**, 36-42. [10.1007/s004250050100](https://doi.org/10.1007/s004250050100)

- Maier, W., Schmidt, J., Nimtz, M., Wray, V. and Strack, D.** (2000) Secondary products in mycorrhizal roots of tobacco and tomato. *Phytochemistry*, **54**, 473-479. [10.1016/S0031-9422\(00\)00047-9](#)
- Millner, P.D. and Kitt, D.G.** (1992) The Beltsville method for soilless production of vesicular-arbuscular mycorrhizal fungi. *Mycorrhiza*, **2**, 9-15. [10.1007/bf00206278](#)
- Nadal, M., Sawers, R., Naseem, S., Bassin, B., Kulicke, C., Sharman, A., An, G., An, K., Ahern, K.R., Romag, A., Brutnell, T.P., Gutjahr, C., Geldner, N., Roux, C., Martinoia, E., Konopka, J.B. and Paszkowski, U.** (2017) An *N*-acetylglucosamine transporter required for arbuscular mycorrhizal symbioses in rice and maize. *Nature plants*, **3**, 17073-17073. [10.1038/nplants.2017.73](#)
- Paradi, I., van Tuinen, D., Morandi, D., Ochatt, S., Robert, F., Jacas, L. and Dumas-Gaudot, E.** (2010) Transcription of two blue copper-binding protein isogenes is highly correlated with arbuscular mycorrhizal development in *Medicago truncatula*. *Molecular Plant-Microbe Interactions*, **23**, 1175-1183. [10.1094/mpmi-23-9-1175](#)
- Park, H.-J., Floss, D.S., Levesque-Tremblay, V., Bravo, A. and Harrison, M.J.** (2015) Hyphal branching during arbuscule development requires *Reduced Arbuscular Mycorrhiza1*. *Plant Physiology*, **169**, 2774-2788. [10.1104/pp.15.01155](#)
- Park, S., Takano, Y., Matsuura, H. and Yoshihara, T.** (2004) Antifungal compounds from the root and root exudate of *Zea mays*. *Bioscience, Biotechnology, and Biochemistry*, **68**, 1366-1368. [10.1271/bbb.68.1366](#)
- Peipp, H., Maier, W., Schmidt, J., Wray, V. and Strack, D.** (1997) Arbuscular mycorrhizal fungus-induced changes in the accumulation of secondary compounds in barley roots. *Phytochemistry*, **44**, 581-587. [10.1016/S0031-9422\(96\)00561-4](#)
- Pineda, A., Zheng, S.J., van Loon, J.J., Pieterse, C.M. and Dicke, M.** (2010) Helping plants to deal with insects: the role of beneficial soil-borne microbes. *Trends in Plant Science*, **15**, 507-514. [10.1016/j.tplants.2010.05.007](#)
- Ratcliff, F., Martin-Hernandez, A.M. and Baulcombe, D.C.** (2001) Technical Advance. Tobacco rattle virus as a vector for analysis of gene function by silencing. *The Plant Journal*, **25**, 237-245. [10.1046/j.0960-7412.2000.00942.x](#)
- Rooney, D.C., Killham, K., Bending, G.D., Baggs, E., Weih, M. and Hodge, A.** (2009) Mycorrhizas and biomass crops: opportunities for future sustainable development. *Trends in Plant Science*, **14**, 542-549. [10.1016/j.tplants.2009.08.004](#)
- Saedler, R. and Baldwin, I.T.** (2004) Virus-induced gene silencing of jasmonate-induced direct defences, nicotine and trypsin proteinase-inhibitors in *Nicotiana attenuata*. *Journal of Experimental Botany*, **55**, 151-157. [10.1093/jxb/erh004](#)
- Schäfer, M., Brütting, C., Gase, K., Reichelt, M., Baldwin, I. and Meldau, S.** (2013) “Real time” genetic manipulation: A new tool for ecological field studies. *The Plant Journal*, **76**, 506-518. [10.1111/tpj.12301](#)
- Schliemann, W., Kolbe, B., Schmidt, J., Nimtz, M. and Wray, V.** (2008) Accumulation of apocarotenoids in mycorrhizal roots of leek (*Allium porrum*). *Phytochemistry*, **69**, 1680-1688. [10.1016/j.phytochem.2008.02.015](#)

- Schliemann, W., Schmidt, J., Nimtz, M., Wray, V., Fester, T. and Strack, D.** (2006) Accumulation of apocarotenoids in mycorrhizal roots of *Ornithogalum umbellatum*. *Phytochemistry*, **67**, 1196-1205. [10.1016/j.phytochem.2006.05.005](#)
- Schuman, M.C., Barthel, K. and Baldwin, I.T.** (2012) Herbivory-induced volatiles function as defenses increasing fitness of the native plant *Nicotiana attenuata* in nature. *Elife*, **1**, e00007. [10.7554/eLife.00007](#)
- Schweiger, R., Baier, M.C., Persicke, M. and Müller, C.** (2014) High specificity in plant leaf metabolic responses to arbuscular mycorrhiza. *Nature Communications*, **5**, 11. [10.1038/ncomms4886](#)
- Schweiger, R. and Müller, C.** (2015) Leaf metabolome in arbuscular mycorrhizal symbiosis. *Current Opinion in Plant Biology*, **26**, 120-126. [10.1016/j.pbi.2015.06.009](#)
- Sharma, E., Anand, G. and Kapoor, R.** (2017) Terpenoids in plant and arbuscular mycorrhiza-reinforced defence against herbivorous insects. *Annals of Botany*, **119**, 791-801. [10.1093/aob/mcw263](#)
- Strack, D. and Fester, T.** (2006) Isoprenoid metabolism and plastid reorganization in arbuscular mycorrhizal roots. *New Phytologist*, **172**, 22-34. [10.1111/j.1469-8137.2006.01837.x](#)
- Stuart, K.L. and Coke, L.B.** (1975) The effect of vomifoliol on stomatal aperture. *Planta*, **122**, 307-310. [10.1007/bf00385281](#)
- Takeda, Y., Zhang, H., Masuda, T., Honda, G., Otsuka, H., Sezik, E., Yesilada, E. and Handong, S.** (1997) Megastigmane glucosides from *Stachys byzantina*. *Phytochemistry*, **44**, 1335-1337. [10.1016/S0031-9422\(96\)00751-0](#)
- Toussaint, J.P.** (2007) Investigating physiological changes in the aerial parts of AM plants: what do we know and where should we be heading? *Mycorrhiza*, **17**, 349-353. [10.1007/s00572-007-0133-6](#)
- Vaccari, D.A. and Strigul, N.** (2011) Extrapolating phosphorus production to estimate resource reserves. *Chemosphere*, **84**, 792-797. [10.1016/j.chemosphere.2011.01.052](#)
- van de Wiel, C.C.M., van der Linden, C.G. and Scholten, O.E.** (2016) Improving phosphorus use efficiency in agriculture: opportunities for breeding. *Euphytica*, **207**, 1-22. [10.1007/s10681-015-1572-3](#)
- Vannette, R.L., Hunter, M.D. and Rasmann, S.** (2013) Arbuscular mycorrhizal fungi alter above- and below-ground chemical defense expression differentially among *Asclepias* species. *Frontiers in Plant Science*, **4**, 361. [10.3389/fpls.2013.00361](#)
- Vierheilig, H., Schweiger, P. and Brundrett, M.** (2005) An overview of methods for the detection and observation of arbuscular mycorrhizal fungi in roots. *Physiologia Plantarum*, **125**, 393-404. [10.1111/j.1399-3054.2005.00564.x](#)
- Vogel, J.T., Walter, M.H., Giavalisco, P., Lytovchenko, A., Kohlen, W., Charnikhova, T., Simkin, A.J., Goulet, C., Strack, D., Bouwmeester, H.J., Fernie, A.R. and Klee, H.J.** (2010) SlCCD7 controls strigolactone biosynthesis, shoot branching and mycorrhiza-induced apocarotenoid formation in tomato. *The Plant Journal*, **61**, 300-311. [10.1111/j.1365-3113.2009.04056.x](#)
- Zhou, W., Kugler, A., McGale, E., Haverkamp, A., Knaden, M., Guo, H., Beran, F., Yon, F., Li, R., Lackus, N., Kollner, T.G., Bing, J., Schuman, M.C., Hansson, B.S., Kessler, D., Baldwin, I.T. and Xu, S.** (2017) Tissue-specific emission of (E)-alpha-bergamotene

helps resolve the dilemma when pollinators are also herbivores. *Current Biology*, **27**, 1336-1341. [10.1016/j.cub.2017.03.017](https://doi.org/10.1016/j.cub.2017.03.017)

4. Discussion

Nicotiana attenuata was developed as a model system to study plant developmental growth, resistance and productive traits. In its native habitat, abiotic stresses such as high UV radiation, drought, heterogeneity of nutrient distribution and smoke residues from fires in the Great Basin Desert represent crucial environmental factors to which *N. attenuata* has adapted. Over millions of years, and with a myriad of interactions with microbiomes in the soil, this plant has evolved sophisticated systemic responses. Integrated ecological factors have interplayed in multiple layers to sculpt *N. attenuata*'s diversified adaption mechanisms for its survival in nature (Baldwin & Morse, 1994; Baldwin *et al.*, 1994; Kessler & Baldwin, 2002; Wu & Baldwin, 2010; Schuman & Baldwin, 2016).

4.1. From the abiotic perspective: a new compound, catechol, which exists in natural environments, is involved in root growth

We investigated the impact of smoke on root growth and development, rather than only on seed germination stimulation, **in manuscript I**. The active compounds from smoke which enhance seed germination have been well characterized and include karrikin and cyanohydrin (Flematti *et al.*, 2004; Flematti *et al.*, 2013). Previous data indicates that smoke cues are easily transported out of the burn area, but the activity which results from their initial presence can remain for many years. From the emergence of roots from the seed, it is inevitable that they will contact these cues for their whole life span. Smoke cues can be found in artificial food condiments such as barbeque sauce and a dilution of these sauces are referred to as “liquid smoke”, with no significant differences detected between brands (Baldwin & Morse, 1994; Baldwin *et al.*, 1994; Preston & Baldwin, 1999; Krock *et al.*, 2002; Preston *et al.*, 2004; Wang *et al.*, 2017). By externally supplementing liquid smoke to GB5 growth medium, root morphology was changed with primary roots showing a longer phenotype with no elongated root hairs. Here, bioactivity-guided fractionation helped isolate catechol as the main active compound resulting in the defects of root growth and development. Catechol has been identified in liquid smoke as highly abundant and moreover, targeted analysis of soils from different burn sites in the Great Basin

Desert demonstrated a fair amount of presence in burn soils, which supports the ecological relevance of this smoke cue in nature.

4.2. Auxin is not the main regulator that mediates catechol-induced root morphological changes

Plant roots mainly forage in the soil for nutrients and water. Based on the observations of root phenotypes in an in-vitro assay, the ecological importance was surmised to be that the promotion of primary root elongation and numbers of adventitious roots may facilitate a more efficient root growth rates to reach nutrients-rich patches or areas with higher water content. Additional research is certainly needed to better understand the local distribution and persistence of catechol in burn soil and its correlation with the presence of nutrients in order to fully understand its ecological role as an environmental signal. Large discrepancies of root morphology after comparison of addition of liquid smoke and karrikin1 (KAR1) ruled out that the effect is due to the well-characterized germination stimulant karrikin. This further indicates that *N. attenuata* perceives different substances in smoke for germination and for seedling establishment. To further understand underlying mechanisms for how smoke alters root morphology, an RNA-seq transcriptome profiling performed on kinetic samples was done to identify the potential regulatory pathway. Indeed, Gene Ontology (GO) enrichment of differential expressed genes (DEG) resulted in a few main physical responses networks such as those related to auxin biosynthesis, cell redox homeostasis and glucosyltransferases activity, which guided us to focus on two well-studied pathways: the auxin- and reactive oxygen species-related pathways (ROS).

Root phenotypes induced by smoke resembled some which resulted from root exposure to the auxin-biosynthesis inhibitors Kyn and yucasin (Nishimura *et al.*, 2014), which included longer but hairless roots. We initially hypothesized that the decrease of auxin production ascribed to the inhibitory effect of smoke substances on biosynthesis may be an important factor in the root morphological response to smoke. However, evidence was obtained via the following auxin-related tests to corroborate that auxin production doesn't play a primary role in the modifications of root phenotype upon smoke or catechol treatments.

- 1) External auxin application failed to rescue the deficient root phenotype induced by smoke.

- 2) The content of auxin showed the opposite accumulation as expected: an increase of IAA in roots was observed after smoke or catechol exposure.
- 3) NaSHY2, a molecular reporter bi-directionally regulated by auxin and cytokinins (Tian & Reed, 1999), did not significantly change after smoke incubation.
- 4) In line with previous publications (Peng *et al.*, 2013; Perrot-Rechenmann, 2013), synthetic NAA supplementation increased proliferation of meristematic cells leading to an increase of cell numbers in the root tip, while the application of smoke did not.
- 5) By means of the reporter line in *Arabidopsis* DII-VENUS (Brunoud *et al.*, 2012), in which rapid fluorescence quenching accompanied with AUX/IAA degradation is elicited by an auxin signal, we found a sharp decline of fluorescence intensity with NAA induction, and smoke treatment slightly decreased fluorescence intensity, indicating an increase of auxin.
- 6) Inhibition of an auxin transport by application of NPA could not mimic the smoke-induced root phenotype. As reported, the signaling and polar distribution of auxin were also essential to for its full effects on root growth (Ljung *et al.*, 2001), and in particular, cell-to-cell transport of auxin forms gradients along the roots which determine the life cycle of each cell file (Sauer *et al.*, 2013).

Based on these six pieces of evidence, we corroborated that auxin is not the primary effector from smoke application. Nevertheless, the lack of diverse approaches for *N. attenuata* plants to study this question, such as auxin reporter transgenic lines to temporally/spatially study cell-to-cell changes in auxin gradient, limited the tests we could conduct and led us to conclude that we cannot completely rule out this possibility. However, the slight but significant elevation of auxin did not correspond to an increase of meristematic cell number from cell division. Likely the increase of IAA results from the primary physiological responses upon smoke treatment, rather than an initial input for root structure formation.

4.3. Spatial ROS homeostasis interruption caused by catechol treatment accounts for root defects

Another possibility is that the effect of the increase of auxin might be counteracted by decreased superoxide (O_2^-) levels. Another study investigated transcriptional changes of maize kernels in response to smoke treatment over one day. Interestingly, differential GO enrichment in redox processes were found (Soós *et al.*, 2009), overlapping with ours. Genetic evidence on the role of ROS homeostasis in root development and growth comes from research done in *Arabidopsis* on UPBEAT (UPB1) and MED25/PFT1 (Tsukagoshi *et al.*, 2010; Sundaravelpandian *et al.*, 2013), with both mutant lines showing alteration of ROS balance as the main regulator of corresponding phenotypic defects. To date, it is well known that ROS is an independent signaling pathway involved in root development. Hydrogen peroxide (H_2O_2) and superoxide (O_2^-) are two important reactive oxygen species in roots. H_2O_2 is enriched in the EZ/DZ, and is confined to the apoplast and the extending root hairs; in contrast, O_2^- is differentially localized in MZ to coordinate cell proliferation. In accordance with such patterns in other plant species, ROS has the same distribution pattern in *N. attenuata* roots. It has been reported that in *pfl1* and *upb1* in *Arabidopsis*, perturbed ROS distribution resulted in reduced accumulation of H_2O_2 in the EZ/TZ, but had a reverse pattern of O_2^- in MZ, ultimately leading to an increase of meristem size which could be positively associated with meristem cell length.

The increase in root length resulting from the application of catechol or smoke is mainly due to longitudinal increases of cell size, rather than increases in meristem cell numbers. Consistent with previous data, no changes in cell proliferation in the MZ were associated with simple alteration of O_2^- content; however, the increase in cell length did not correspond to a decrease in H_2O_2 content in the EZ/DZ, but in fact a small increase, contrary to expectations (Tsukagoshi *et al.*, 2010). This is not in agreement with the conical theory about how ROS affect root development. Interestingly, with the help of BES- H_2O_2 -AC fluorescence dye to track the polar location of H_2O_2 spatially (Maeda *et al.*, 2004), we observed that in seedlings free of catechol incubation, H_2O_2 was mainly distributed around the cell files of the epidermis and cortex, while catechol treated seedlings had misplaced H_2O_2 to the tissue surrounding the stele, and only sporadic signals of H_2O_2 could be visualized in the outer layers. It became obvious that the content of H_2O_2 around the cell walls in the epidermis and cortex layers was much lower, even though in total amounts, catechol treated seedling roots seemed to have a higher overall

quantity. It is widely accepted that H_2O_2 is an important factor to loosen cell walls and to directly regulate the cell wall matrix to eventually determine cell size. We speculated that the reduction in H_2O_2 around cell walls might be ascribed to catechol's ability to produce hydroxyl radicals ($\cdot OH$) via the Fenton reaction with H_2O_2 (Pignatello *et al.*, 2006). In this case, external catechol spatially meeting with apoplast H_2O_2 would be a precondition to generate hydroxyl radicals ($\cdot OH$). In another words, catechol itself would need to cross the plasma membrane to react and thereby would produce a redox signal, which would then be transmitted into cells to be perceived through a signaling cascade that would ultimately activate adaptive responses. Importantly, the catechol transport and Fenton reaction hypotheses presented in this story are still hypothetical, and further experimental evidence is needed. However, if differential transcription of ROS response genes is indicative, then there is evidence which may suggest the validity of these hypotheses: a number of ROS related genes were found to have altered transcript accumulation, including RBOHD, CAT, GPX, SOD, and some peroxidases.

Besides ROS-response genes, some genes which are mediated by ROS also had altered transcripts, including extensin (EXT). Extensin has been intensively investigated as one of the members of the hydroxy-Pro-rich glycoprotein superfamily, generically referred to as HRGPs (Velasquez *et al.*, 2011; Mangano *et al.*, 2017; Mangano *et al.*, 2018; Marzol *et al.*, 2018). It is mainly involved in hydroxylation of Pro residues into Hyp, and then O-glycosylation of Hyp and Ser, which will ultimately form intra- and inter-EXT linkages through putative type-III peroxidases (PERs). These may functionally overlap with other cell wall constituents to create the final cell wall matrix. From genetic research in *Arabidopsis thaliana*, loss of function mutants for each of the leucine-rich repeat extensins, extensins 1 and extensins 2 (lrx1 and lrx2 respectively), along with extensin 6, 7 and 10 (ext6, ext7 and ext10) demonstrated aberrant root hair formation due to genetic disruption which had resulted in the disturbance of O-glycosylation (Velasquez *et al.*, 2011). Interestingly, in our transcriptome data, 21 extensins were strongly down-regulated, similarly to these loss of function mutants. Integrating our results of interrupted homeostasis of ROS, strongly decreased transcript abundance of a bulk of EXTs and increased cell length, led us to propose that catechol/liquid smoke addition weakens cross-linking composition in cell walls, which facilitates cell expansion, and can be ascribed to attenuated

linking strength mediated by EXTs and ROS. However, this inference needs additional work to be corroborated.

Returning to biochemical properties: dihydroxybenzene isomers consist of catechol, resorcinol, and hydroquinone. After comparison of the antioxidant capacity of each of these, we report that catechol had the highest activity, and facilitates the Fenton reaction most readily. We detected that young seedlings were much more sensitive to catechol under the concentration of 0.01 mM and that catechol incubated seedlings displayed fewer root hairs and longer roots, when compared to seedlings treated with the other two isomers. Applying these isomers, or derivatives, of catechol caused observable differences in antioxidant capacity and the corresponding root phenotypes supported the concept that disruption of ROS homeostasis is mainly responsible for root defects. Importantly, in a biochemical complementation assay, external H₂O₂ addition largely rescued defects in root length and root hairs and this assay thus supported the significance of catechol-disrupted H₂O₂ spatial distribution. Interestingly, previous data indicated that liquid smoke contains various phenolic compounds such as hydroquinone and guaiacol, and these also exist along with catechol in burned soil, so an influence of smoke on *N. attenuata*'s growth, development and production as a result of root morphology changes, and not only the stimulation of germination, could largely be expected in nature.

In conclusion, we have provided evidence to reveal another impact of smoke on plant development and growth, besides the impact of karrikin on seed germination. Smoke promotes *N. attenuata* root growth and suppresses root hair elongation in a dose-dependent manner. Bioassay-driven fractionation and elucidation revealed that catechol is the main active compound that corresponds to these observed smoke-induced root defects. Transcriptional profiling under smoke induction highlighted the potential involved mechanistic pathways: auxin and ROS. Genetic and biochemical trials provided evidence of the independence of the auxin pathway from these effects, even though it was initially expected to play a major role. The potential involvement of ROS homeostasis disruption by catechol was determined based on transcriptional responses and its hyperactive antioxidation property has been shown.

Further quantitative and qualitative analyses on ROS demonstrated that total amounts of H₂O₂ were slightly but significantly elevated, while histochemical staining specifically visualized the misplaced H₂O₂ from outer layers to inner ones. The interruption of the distribution of H₂O₂ resulted in the decrease in amounts located directly adjacent to cell walls, which may have caused the longer root phenotype.

4.4. From the biotic perspective: growth responses of plant communities in mesocosms colonized with arbuscular mycorrhizal fungi (AMF)

Arbuscular mycorrhizal structures have been clearly observed in field roots of *N. attenuata*, in addition to the ability of *N. attenuata* to associate with AMF being confirmed by sequencing, and the ecological importance of this interaction is a subject of ongoing research (Riedel *et al.*, 2008; Groten *et al.*, 2015a; Groten *et al.*, 2015b; Wang *et al.*, 2018). Regarding the complexity of an ecosystem at community level, and in particular, in an extreme abiotic environment, it is interesting to explore the plant's benefit and global response from this symbiotic relationship.

To mimic the natural growth competitive condition of *N. attenuata* in monoculture communities, two *N. attenuata* host plants were planted in the same pot in the glasshouse with either a commercial AMF inoculum or native inoculum isolates, referred to as FMM (field mycorrhizae mixture). These were compared to non-inoculated plant pair controls. In each pot, one plant was an empty vector control (EV), and the other was from an RNAi line deficient in the formation of AMF symbioses, irCCaMK (calcium-calmodulin-dependent kinase), which was made by knocking down the core CCaMK gene in the signaling cascade involved in central stages of AMF symbiosis with plant roots. As reported in rice (*Oryza sativa*), high phosphate fertilization leads to a rapid decrease of arbuscule density and inhibition of hyphal branching. Such suppression can be exaggerated in mutants, such as the rice *pt11-1* mutant that is impaired in P uptake in its arbuscule branches, and which leads to suppression, indicating that an output of P is a critical regulator to stabilize arbuscules (Yang *et al.*, 2012). To facilitate a prominent competitive difference in the above genotypes by ensuring AMF inoculation and optimal association, low P fertilizer was used on these plants for watering, and the P amount was

progressively increased with development, reaching a maximum of 25% of the normal fertilizing formula for glasshouse *N. attenuata*.

However, a serious problem emerged in that irCCaMK plants, which had previously been observed not to be colonized by AMF in monoculture, were now colonized (Groten *et al.*, 2015a). The sampling process was carefully checked to rule out potential contamination of irCCaMK root samples from EV samples during the harvesting process. The silencing efficiency of CCaMK gene was also assessed and reflected a 73% silencing in all irCCaMK plants, regardless of treatment, which had been sufficient silencing to dampen colonization in a previous monoculture experiment. This suggested that other factors involved in this abnormal upregulation of root colonization may exist. Though root colonization of irCCaMK co-cultured with EV was significantly increased, the transcript abundance of AMF-indicative markers NaPT5/NaPT4 that normally increase with association, was still far lower in irCCaMK upon mycorrhization than in EV. In previous studies using rice (*O. sativa*), the genetic mutant *hebiba* (*hb*) was used because it has a 169kb deletion containing 26 genes, of which one is *kai2* (*karrikin insensitive*). Genetic complementation phenotypically deciphered the essential roles of KAI2 in symbiotic partnership establishment with AMF. When *hb* mutants were co-cultured with WT plants, numbers of hyphopodia, intraradical hyphae and arbuscules in the roots were significantly increased compared to the roots of *hb* in monoculture. Authors proposed that the lack of fungus development was partially recovered by the increase of inoculum strength gained from active fungus interaction occurring in neighboring WT plants (Gutjahr *et al.*, 2015). Likewise, increased root colonization of irCCaMK could largely be due to the same reason, though it could also be that RNAi remains “leaky” to a certain extent with still ca. 27% of CCaMK being produced and inducing the CCaMK-dependent pathway, a common drawback of the knock-down technique.

4.5. AMF-mediated preferential Pi uptake in EV plants leads to better growth

Regularly monitoring growth traits such as seedling diameter and stalk height clearly showed a suppression effect on plant growth from AMF inoculation, which agrees with previous data (Riedel *et al.*, 2008; Groten *et al.*, 2015a). Interestingly, such suppression was exacerbated in

irCCaMK plants. Initially, only small differences in irCCaMK plant growth were expected, though significant differences in growth may be due to the abortion of AMF colonization compromising plant growth, as previously reported for *N. attenuata* plants. In fact, severely dampened growth in co-cultured irCCaMK plants were recorded, which indicated the existence of a third factor behind these growth changes, aside the treatment and genotype effects, respectively. Because Pi-limited fertilizer enhanced the growth differences in irCCaMK plants which were both in competition and inoculated with AMF, versus in competition and not inoculated, a preferential Pi allocation to the EV in the pair, mediated by the AMF network, was hypothesized. Indeed, after Pi measurement it was found that more Pi content accumulated in EV plants, indicating the importance of partner identity in the outcome of plants' competitive interactions. Similarly, AMF preferentially allocating nutrients has been previously tested in non-host (*A. thaliana*) and host (*Trifolium pratense* or *Lolium multiflorum*) plants, with or without AMF inoculum (Veiga *et al.*, 2013). These plants were grown in dual compartments separated by mesh that was only hyphae-penetrable. The results were a clear growth inhibition effect (up to 50%) observed in *A. thaliana*, the non-host plant, versus itself in non-inoculated pairs, suggesting that host plants took full advantage of their symbiotic partners at the expense of competitive non-host plants. In extremely complex ecosystems, it is likely that unequal nutrient allocation, mediated as well by symbionts, could be one of the selective strengths that evolutionarily sculpt the landscape of terrestrial plants.

On the one hand, growth differences helped us to better understand the reason behind the impeded growth of irCCaMK as a result of uneven nutrient uptake by its neighbor through AMF involvement. On the other hand, such an unexpected third effect introduced into experiments from inconsistent growth may result in unpredicted complexity of results. To further dissect the effects as being from AMF inoculation or from simple growth differences, a leaf transcriptome analysis was performed, using samples with FMM inoculation and their controls. Differentially expressed genes (DEGs) were summarized in two modules comprising additive and interactive DEGs, which inspired us to undertake subsequent studies.

4.6. Interactive model aspect summarized from foliar DEGs: the third regulator behind differential plants growth

***NaPT5* is a dual response gene triggered both by root AMF colonization and leaf Pi-starvation**

Manuscripts II and III contain transcriptome and metabolome data that were analyzed based on additive and interactive models after comparison the effect between genotype (EV vs. irCCaMK) and treatment (AMF vs. not-AMF inoculated) , and led to the discovery of foliar AMF-indicative chemical markers.

To better understand effects of phosphate availability and AMF-plant interaction on plant competitive growth, DEGs were screened from microarray datasets in manuscript II and were analyzed at length. Interestingly, Gene Ontology analysis of these DEGs revealed their physiological functions to be highly associated with the phosphate starvation process, phosphate transport and galactolipid metabolism, which is an indirect consequence of Pi shortage. The transcript accumulation patterns of these genes exhibited **an interactive model** in EV and irCCaMK plants: showing a decrease in EV plants (AMF vs. not-AMF inoculated) and an increase in irCCaMK plants (AMF vs. not-AMF inoculated), but this trend could only be detected six weeks post inoculation (6 wpi), and not in an earlier root sample harvest at two weeks post inoculation (2 wpi).

In the earlier stage, it is possible that the symbiosis establishment was not yet complete, including particularly the formation of arbuscules, which are widely accepted as the phosphate exchange site between fungus and host and usually occur normally in a late stage of the symbiosis. However, sporadic arbuscules were observed with their main arbuscule trunk and branches by microscopy. We thus inferred that it is more likely in the earlier stage that the symbiotic structures are already formed, but that the limited occurrence of such functional structures is not sufficient for competitive acquisition. In later stages, with the progressively growing arbuscules in the roots, more phosphate can be put into the “trade market”, can preferentially go to EV plants, and this then can eventually lead to a severe Pi shortage in irCCaMK plants.

Considering the importance of phosphate transporters (PT) in Pi uptake, PTs were particularly focused. **In manuscript II**, we demonstrated the potential function of NaPT3/4/5 in transporting Pi into plants during AMF association. *NaPT1/7* were clustered closely together as non-AMF-specific members of the PT family, with obvious phosphate deficit responses in leaves even at an early time point (2 wpi). *NaPT3/4* were grouped together showing low expression in leaves and in non-AMF inoculated root samples, and highly induced transcript levels in AMF-inoculated root samples, indicating that *NaPT3/4* are AMF-specific, in line with the results from *Nicotiana tabacum* (Tan et al., 2012). Similarly, PT4 isoologues were broadly investigated as AMF-specific markers in different species such as tomato, potato, rice and *Medicago* [reviewed in (Harrison et al., 2010)] as they mediate Pi uptake at the arbuscules.

Interestingly, we found that transcript levels of *NaPT5* exhibited a dual inducibility in roots and leaves. On the one hand, *NaPT5* transcripts in irCCaMK plants were induced in leaf samples from both two and six wpi presenting similar expression profile with *NaPT1/7*. On the other hand, in roots, *NaPT5* transcripts behaved in the same way as *NaPT3/4*, being highly induced by AMF colonization as validated mycorrhization indicative genes, resulting in clustering classified *NaPT5*, the homologue of *NtPT5* (Tan et al., 2012) into a distinctive clade compared to the clade of *NaPT1/7* and *NaPT3/4*. Based on this observation, we hypothesized that *NaPT5* might played dual roles in Pi-starvation and AMF colonization responses. Independent repeat by using field mycorrhizal mixture (FMM) inoculum corroborated the consistence of these 5 PTs transcripts profile relative to that only inoculated with commercial *R. irregularis*.

To determine the role of Pi status in *NaPT5* transcript accumulation, a Pi-starvation experiment was conducted, the same set of genes were analysed, and we found that transcript abundance of *NaPHO2* was inhibited by Pi-starvation as expected as negative repressor, *NaPT4* did not change, and *NaPT5* was induced not in roots, but in the leaves of Pi-deficient samples, which suggested a tissue-specific effect. Given that foliar *NaPT5* responds to Pi-starvation, but belowground it is highly induced with AMF colonization, the dual responses of *NaPT5* were then inferred, A detailed study was performed to research the role of PT4 in *Lotus japonicas* and

Medicago truncatula during Pi-starvation responses, and the authors verified the increase of GUS stain coupled with PT4 in the root tips when Pi availability was depleted (Kobae *et al.*, 2016). In contrast, *NaPT4* expression in roots had no detectable changes under Pi-starvation conditions, which might be due to species specificity, but is most likely due to whole root harvesting resulting in an over dilution of an increase which is most likely confined to the root tip. Taking these two observations together, under the instruction of an interactive model, the reason for the huge growth differences between EV and irCCaMK when AMF inoculated is presented as being mainly due to Pi preferentially being allocated to EV plants by AMF, and the up-regulation of *NaPT3/4/5* in plants potentially facilitates this more efficient Pi acquisition mediated by AMF. An additional function of *NaPT5* was proposed to be as a Pi-starvation response in systemic tissues, in addition to its function as a conical AMF-indicative marker in roots.

4.7. Additive model aspect 1: predication of AMF-indicative markers genes in leaves

As we found that the expression of AMF-induced makers *NaPT4/PT5* was much higher in EV roots than in irCCaMK roots showing **an additive effect**, a bulk of other markers were tested as well which exhibited the same additive pattern. DEGs with such a pattern of expression were searched for as potential “reporters” of AMF colonization in the leaves, parallel with that in roots.

Hierarchal clustering was performed to specifically target DEGs with an additive effect, and indeed such clusters helped us to obtain some candidates as potential foliar markers. However, further investigation by comparing the common responses with two different inocula (*R. irregularis* vs. FMM native inoculum) failed to find a general expression pattern as originally expected. This unexpected result reminded us to think of the differences between the two set-ups. Apart from the culture substrate (clay vs. sand) and inoculum (FMM vs. single *R. irregularis*), other growth conditions were strictly controlled to maintain the same conditions for every plant within the same batch, including light intensity and photoperiod, irrigation plan and nutrient supply. The parameters we monitored also indicated comparability between the two set-ups, including growth record and the transcripts of AMF marker genes. One hand, we speculated that

the genes with additive effects that were picked up were not surrogates of general AMF colonization effects and possibly resulted from some unknown environmental factors. On the other hand, more likely, the different partner identities from the AMF inoculum accounted for the discrepancies of the systemic responses in two set-ups.

Consistently with our results, research comparing Pi uptake efficiency within various AMF species has demonstrated that the same host plant colonized with a few AMF species separately can differ in many growth traits per the identity of the AMF symbiotic partner. Not only the growth of these plants differed, but also the distinctive response in coping with abiotic stress varied with the fungus partner. Drought tolerance was surveyed in tomato (*Solanum lycopersicum*) in response to two AMF species (*Funneliformis mosseae* and *Rhizophagus intraradices*) (Chitarra *et al.*, 2016). Under sufficient water conditions, obvious growth variation in terms of plant height and shoot biomass were observed between two inoculum colonized groups, and notably, such differences were erased under water stress. Overall, plants associated with AMF performed much better than control plants under water stress, but within AMF-inoculated plants, performance largely depended on the symbiotic partner. For example, *R. irregularis*-associated plants significantly increased water use efficiency in comparison to *F. mosseae*-inoculated plants. The complicated mechanism was multifaceted and included modification in stomatal density, ABA content and ABA responses. Similarly, plants of the same species grown in pairs revealed that in the presence of some fungal species, genotypes with a lower capacity to interact with a fungus produced less biomass and received less Pi in comparison to their better- interacting competitor (Facelli *et al.*, 2010; Willmann *et al.*, 2013; Facelli *et al.*, 2014). In nature, plants also broadly interact with different fungal and bacterial microbes, who in turn interact with many different plants, to create a belowground network linking plants together (Lehmann *et al.*, 2012; Merrild *et al.*, 2013). Partner identity in partnerships of plants and fungus has been shown to change competitive interactions among plants, altering growth and fitness outcomes (Van Der Heijden & Horton, 2009; Walder *et al.*, 2012; Wu *et al.*, 2015; Yang *et al.*, 2015). All of these studies together demonstrate that factors specific to individual fungal and host plant species determine the outcome of a symbiosis in terms of growth and resistance.

4.8. Additive model aspect 2: searching AMF-indicative chemicals in leaves

We next hypothesized that metabolic changes in the leaves resembling the inducibility of root AMF-indicative marker genes could also biochemically represent the extent of AMF colonization in the roots, and show an additive effect between EV and irCCaMK plants. The aforementioned root samples (EV vs. irCCaMK) associated with *R. irregularis* were analyzed for untargeted metabolite profiling to search for candidates. In this process, sample extraction methods and profiling approaches technically determined the output of feature acquisition. Computationally generated coexpression networks and STEM pipeline application successfully narrowed the range from thousands of features to hundreds. As we expected, a number of metabolic candidates were screened meeting the requirements of the additive effect: exhibiting higher inducibility in EV with AMF colonization than in irCCaMK plants. Still, the numbers of candidate were beyond manageable and testable, and most of them were only putatively annotated with structures. Extend of metabolic inducibility and actual amount of candidates in roots was then considered to further facilitated compound selection, fractionation and structure elucidation. Taken all together, five metabolites were identified based on tandem-MS and NMR data as blumenols: 11-hydroxyblumenol C-9-*O*-Glc (Figure 2C; Compound 1), 11-carboxyblumenol C-9-*O*-Glc (Figure 2C; Compound 2), 11-hydroxyblumenol C-9-*O*-Glc-Glc (Compound 3), blumenol C-9-*O*-Glc-Glc (Compound 4) and blumenol C-9-*O*-Glc (Compound 5), which all belonged to a class of compounds already reported in other plant species to be associated with AMF, but only in root tissue, rather than in aerial tissues. We then asked whether these chemical markers could be AMF-indicative markers in leaves, which was the same question we had for our transcriptome analysis. Before we switched to focus on the shoot, the validation of these 5 chemicals as AMF-indicative markers in roots was necessary, and indeed, the amount of these chemicals positively correlated with the transcript abundance of marker genes in the roots, as well as with the degree of root colonization, particularly reflecting the percentage of arbuscules per root length. Hereafter, we started to test the hypothesis that a subset of the AMF-induced root metabolites could accumulate in shoots as a result of transport or systemic signaling. Fortunately, 2 of 5 verified compounds in roots (11-hydroxyblumenol C-9-*O*-Glc, 11-carboxyblumenol C-9-*O*-Glc) can be traced in leaf tissue with high inducibility triggered by AMF colonization (*R. irregularis*)

although the absolute amount was not comparable with that in local root tissue. This same pattern was also detected in leaves of FMM-inoculated plants as well, which increased the reliability of these 2 compounds as foliar AMF-indicative markers. So far, we purified only 5 features in the present study based on their amount and inducibility, and they were proved to be robust as AMF-indicative markers, but details on their physiological functions and ecological consequences are still largely unknown.

Though the discovery of Myc-LCO and CO as elicitors derived from AMF is a breakthrough in this research topic, very few studies focus on how metabolites from host plants affect symbiosis establishment. Strigolactones are one of the main plant exudates that have been revealed to stimulate AMF spore germination and hyphal branching, though the confounding results of root colonization phenotyping from studies in different species suggest that more investigations need to be done on this topic (Akiyama *et al.*, 2005; Akiyama & Hayashi, 2006). Recently, four independent groups reported that plant lipids play critical roles in symbiosis. Misallocation of 2-monoacylglycerols from plants to fungus in *Mtstr1/str2* mutants resulted in defective symbiosis establishment success (Bravo, A. *et al.*, 2017; Jiang *et al.*, 2017; Keymer *et al.*, 2017; Luginbuehl *et al.*, 2017). By silencing the *DXS* gene in *Medicago* to block blumenol biosynthesis, it was found that colonization significantly decreased, which indicated that blumenols have a function in AMF symbiosis. However, the side-effect of silencing *DXS* to study the function of blumenols was that it concomitantly impaired other critical metabolite biosynthesis including that of strigolactones and of ABA derived from the *DXS*-mediated carotenoid biosynthesis pathway, both of which play important roles for the AMF symbiotic process (Floss *et al.*, 2008a). Therefore, more focused research on the role of blumenols in AMF symbiosis is needed. As mentioned before, only 5 metabolites from our additive analysis were structurally elucidated, and studying the rest of the candidates belonging to this additive model may enhance the understanding of how plant-derived metabolites mediate this mutualistic partnership establishment.

Improvements in analytical instrumentation have enabled the study of minimal amounts of compounds with higher accuracy and sensitivity, and different types of instrumentation have

allowed for different workflows, each with specific advantages and disadvantages. While untargeted metabolomics allow for a less biased view of metabolic responses, they are more affected by co-occurring compounds and the post-run analysis is usually cumbersome. Targeted methods, in contrast, are often more sensitive and specific, but limit the number of metabolites analyzed. We imposed on the power of these two approaches by applying a comprehensive combination of targeted and untargeted LC-MS methodology coupled with genetically transformed plants: including irCCaMK in set-ups. Through a sophisticated biostatistical analysis, an expected additive pattern was screened. Metabolites and metabolic responses are often specific to particular tissues of a plant (Li *et al.*, 2016; Lee *et al.*, 2017) , but it is also known that local responses can spread to systemic tissues, just as foliar herbivore-induced responses can cause a large increase of defensive metabolites in roots (Gulati *et al.*, 2013; Gulati *et al.*, 2014). Additionally, specific metabolite accumulation has been shown to not be confined to their locations of biosynthesis and to be readily transported to other places, such as phytohormones (Baldwin, 1989). Therefore, we hypothesized that in the metabolic layer of AMF responses, some local responses in the roots might be statistically associated with similar responses in the systemic aerial tissues, due either to signaling or transport. This concept allowed us to identify specific AMF-indicative blumenols in the shoot despite the occurrence of other highly abundant and constitutively produced compounds and non-AMF-indicative blumenols. The confirmation of compound identities in leaf samples with high-resolution MS techniques proved to be challenging and required additional sample purification steps. Likely, such matrix effects compromised the detection of these AMF-indicative, systemic blumenol responses in previous investigations. The discovery of these AMF-indicative blumenol compounds in diverse plant species with different AMF species colonization further indicates that these responses are widespread.

Despite the AMF-induced accumulation of blumenols in the shoot, putative candidate genes of the apocarotenoid biosynthesis pathway were merely induced in the roots after AMF inoculation via transcriptome profiling. To determine the likelihood that the root mediates the production of these blumenol compounds, we genetically manipulated the carotenoid pathway in a tissue-specific manner. It is challenging to manipulate blumenol production without affecting

the AMF colonization of the plant, since other carotenoid-derived compounds, such as strigolactones, are known to play an important role in this process (Akiyama *et al.*, 2005) and are affected by this manipulation. To circumvent these problems, we used the LhGR/pOp6 system for chemically-inducible RNAi-mediated gene silencing of PDS (Schäfer *et al.*, 2013) to impair carotenoid biosynthesis only in a dexamethasone-induced leaf. Interestingly, only the constitutively produced Compound 6 was reduced in the treated leaves, while the AMF-indicative Compounds 1 and 2 were not affected by our treatment. This indicated that instead of being locally produced, Compound 1 and 2 are translocated from the roots, an inference consistent with the occurrence of AMF-indicative blumenols in stem sap and the capacity of seedlings to transport blumenols from the root to the shoot from hydroponic solution. It seems likely that the AMF-indicative blumenols are transported in the xylem with the transpiration stream. The blumenol glucosides (Compounds 1, 2 and 6) are hydrophilic and have a low-molecular weight (402, 388 and 386 Da), but are still compounds that are unlikely to freely diffuse through membranes. Instead, active transport is likely required, for example by ABC-type transporters, and it will remain an interesting research question to identify the involved mechanisms.

4.9. Functional implication of blumenol accumulation and transport

Blumenols were shown to accumulate in large amounts in the roots after AMF inoculation (Strack & Fester, 2006) and our data indicate that they are subsequently distributed throughout the plant. While the conservation of this response in various plants after inoculation with different AMF species implicates an important functional role in the AMF-plant interaction, this function remains to be further explored. Previous studies mainly focus on the function of AMF-induced blumenols in roots as plant-derived signals mediating the AMF colonization process. Genetic manipulation of DXS and CCD1 indicate a role in arbuscule maintenance (Floss *et al.*, 2008a; Floss *et al.*, 2008b). However, DXS is located upstream in the carotenoid biosynthesis pathway and its manipulation might have caused pleiotrophic effects, while CCD1 silencing only results in a partial reduction in blumenol levels. Other studies showed that direct application of blumenols suppresses root colonization and arbuscule formation at early stages of mycorrhiza

development (Fester *et al.*, 1999) and inhibits the growth of soil born plant-pathogens (Park *et al.*, 2004). Unfortunately, these soil-born activities do not shed light on the systemic function of AMF-induced blumenols in shoot tissues observed here. But indirect evidence from functional studies in the shoot inspires hypotheses regarding the ecological relevance of shoot AMF-induced blumenols. Activity studies on vomifoliol, the aglycone of the non-AMF-indicative Compound 6, showed that this compound induces stomatal closure similar to the structurally related abscisic acid (Stuart & Coke, 1975). Additionally, blumenols are known to suppress seed germination and plant growth (Park *et al.*, 2004; Kato-Noguchi *et al.*, 2012). Therefore, AMF-induced blumenols could serve as systemic signals that mediate the large-scale adjustments in general physiology that are thought to accompany AMF interactions. For example, AMF-induced blumenols could be involved in the regulation of differential susceptibility of AMF-inoculated plants to stresses, such as drought or pathogen infection.

4.10. Using AMF-indicative blumenols as a powerful tool for research and plant breeding

As previously mentioned, there are many drawbacks to conventional phenotyping approaches of AMF colonization, including destructive sampling and time-consuming analyses. Therefore, we propose that the analysis of AMF-indicative blumenols in the shoot provides a convenient, easy-to-conduct, and minimally destructive tool to harbingering plant-AMF interactions in a HTP manner that allows for large-scale studies (e.g. forward genetics studies) even under field conditions and empowers plant breeding programs to produce mycorrhiza-responsive and P-efficient high-yielding lines (van de Wiel *et al.*, 2016). Currently, phosphate fertilizer is derived from phosphate rock, a non-renewable resource, which is predicted to be soon depleted (Vaccari & Strigul, 2011). By enabling breeding programs to select crop varieties that have negotiated AMF symbioses that deliver high yields with minimal P inputs, this discovery could help steer the “green revolution” away from intense agricultural inputs and the collateral environmental damage they cause.

5. Summary

As one of well-established plant model systems, *Nicotiana attenuata* has been intensively researched in plant resistance/tolerance, plant physiology and interactions with other environmental components in the last two decades. Although root systems, hidden belowground, are much harder to study than other organs, considering their importance in dynamic regulation of plant physiology, morphology, biochemistry, flowering and synthesis of metabolites, and their rich environmental interactions, the exploration of root responses to abiotic and biotic factors in *N. attenuata* will help to better understand mechanisms of how plants cope with multifaceted environmental factors.

Smoke cues are long-live chemical signals in native habitats which play important roles in many aspects for *N.attenuata* plants, for example by promoting seed germination. Roots are likely exposed to smoke cues in the soil, but how roots respond to such chemical cues was poorly understand. We observed clear root developmental defects in primary root and root hair elongation with liquid smoke incubation. Bioassay-guided fractionation allowed us to obtain the active compound (catechol) responsible for these root defects. Amongst many root growth regulators, comparative transcriptomics narrowed them down to auxin and reactive oxygen species (ROS) signaling pathways. Auxin was excluded as the main regulator to mediate smoke-induced root morphological alteration. Extenal catechol application caused a spatial disruption of H₂O₂ accumulation, although no bulk quantitative differences. Such misslocation of H₂O₂ is likely responsible for root defects caused by catechol, which can be partially recovered by H₂O₂ supplementation that suggested catechol is the main regulator in smoke leads to the smoke-mediated root defects. Further investigation demonstared the existense of catechol in burned areas in the native habitat of Utah, indicating possible ecological functions of smoke cues tuning root growth in nature.

As one the 80% of higher plants associated with arbuscular mycorrhizal (AMF) for a mutualistic relationship, *N.attenuata* has been observed to harbor the characteristic symbiotic fungus structure in roots along with sequence identity confirmation; *R. irregularis* and *F.mosesa* are domestic fungus species colonizing *N.attenuata* roots in a native habitat. We were aiming to

seek representative systemic responses in leaves by transcripts or metabolites after AMF colonization. Comparative transcriptomics and metabolomics were performed to compare changes in EV and irCCaMK plants after AMF colonization, and a class of blumenols were targeted for their specificity and high inducibility. By optimizing quantification methods for an improvement of sensitivity, 11-hydroxyblumenol C-9-*O*-Glc and 11-carboxyblumenol C-9-*O*-Gl were traced in aerial tissues as foliar markers to mirror root colonization ratio belowground. By application of “real-time” genetic modification using a chemically inducible promoter, we locally blocked biosynthesis of these two compounds in leaves, but their levels in modified leaves were not reduced. Thus, we inferred a root-to-shoot translocation mechanism. Using these more easily applied foliar markers of AMF association, a large screening was performed for a QTL analysis, and we successfully targeted some reported genes regulating symbioses such as *NOPE1*. We further confirmed that such foliar markers, found in many di- and monocotyledonous crop and model plants (*Solanum lycopersicum*, *Solanum tuberosum*, *Hordeum vulgare*, *Triticum aestivum*, *Medicago truncatula* and *Brachypodium distachyon*), are not restricted to particular mycorrhizal species.

6. Zusammenfassung

Nicotiana attenuata ist ein gut etabliertes Pflanzenmodellsystem und wurde innerhalb der letzten zwanzig Jahre intensiv mit Blick auf Pflanzenresistenz/Toleranz, Pflanzenphysiologie und Interaktionen mit weiteren Umweltfaktoren untersucht. Obwohl das Wurzelsystem aufgrund seiner unterirdischen Lage schwerer zu untersuchen ist als andere Pflanzenorgane, bietet es die Möglichkeit abiotische und biotische Wachstumsfaktoren von *N. attenuata* zu erforschen und kann somit zu einem besseren Verständnis führen, wie Pflanzen ihr Überleben in einer facettenreichen Umwelt meistern.

Da Rauch ein chemisches Signal im natürlichen Habitat der Pflanze ist, dass lange überdauert, ist es für viele Aspekte der Pflanze wie zum Beispiel die Samenkeimung von entscheidender Bedeutung. Die Wurzeln der Pflanze sind wahrscheinlich vom ersten Moment an Rauchsignalen ausgesetzt, jedoch ist bisher wenig darüber bekannt, wie Wurzeln solche chemischen Signale adaptieren. In unseren Experimenten beobachteten wir Defekte bei der Entwicklung von primären Wurzeln und Wurzelhaarstreckung nach Inkubation mit flüssiger Rauchlösung. Die Bioassay-getriebene Isolierung führte zu dem Ergebnis, dass die aktive Komponente (Catechol) für die beobachteten Defekte verantwortlich war. Mit Hilfe vergleichender Transkriptomik konnten die möglichen Wurzelwachstumsfaktoren auf Auxin und reaktive Sauerstoffspezies (ROS) eingegrenzt werden. Durch den Vergleich von physiologischen und biochemischen Reaktionen der Wurzel auf Auxin, konnte Auxin als Hauptregulator bei rauch-induzierten Änderungen der Wurzelmorphologie ausgeschlossen werden. Die externe Applikation von Catechol bekräftigte eine räumliche aber keine quantitative Veränderung von H_2O_2 . Diese Lageveränderungen von H_2O_2 bewirkten Wurzeldefekte durch Catechol und können teilweise durch Supplementierung von H_2O_2 behoben werden, was darauf hinweist, dass Catechol als der Hauptregulator in Rauch diese rauch-induzierten Wurzeldefekte bewirkt. Weitere Untersuchungen zeigten die Existenz von Catechol in Brandflächen im natürlichen Habitat in Utah, was eine bestimmte ökologische Funktion bietet, inwiefern Rauchsignale das Wurzelwachstum von Pflanzen in der Natur regulieren.

N. attenuata gehört zu den 80% der höheren Pflanzen, die eine mutualistische Beziehung mit arbuskulären Mykorrhizapilzen (AMF) eingehen. Mittels Sequenzierung konnte die

charakteristische symbiotische Pilzstruktur in den Wurzeln aufgedeckt werden: *R. irregularis* und *F. mosesa* sind heimische Pilzarten und kolonisieren die Wurzeln von *N. attenuata* als abiotische Interaktionspartner. Unser Ziel war es nach charakteristischen systemischen Antworten im Blatt auf der metabolischen Ebene zu suchen, die nach AMF Kolonisierung auftreten und somit nicht nur erleichtern würden, bestimmen zu können, welche Individuen von AMF kolonisiert sind, sondern auch unser Verständnis von funktionellen Konsequenzen in systemischen Geweben verbessern könnten. Der Ansatz der vergleichende Metabolomik wurde genutzt, um metabolische Veränderungen in EV und irCCaMK Pflanzen nach AMF Kolonisierung zu messen, wodurch eine Klasse von Blumenolen gefunden wurde, die Spezifität und hohe Induzierbarkeit zeigte. Durch Optimierung der Quantifizierungsmethode, wodurch eine erhöhte Sensitivität erreicht werden konnte, war es möglich 11-hydroxyblumenol C-9-*O*-Glc und 11-carboxyblumenol C-9-*O*-Gl zu identifizieren, die die Kolonisierungsrate in Wurzeln widerspiegeln und somit als Blattmarker genutzt werden können. Durch Nutzung genetischer “real-time“ Toolbox, wurden irPDS Pflanzen hergestellt, die in der Biosynthese dieser zwei Stoffe in Blättern blockiert sind, was jedoch zu keiner Reduktion der Menge führte, wodurch sich ein Mechanismus der Translokation von der Wurzel in den Spross vermuten lässt. Für eine breitere Anwendung dieser „Vorbotten“ in Blättern für AMF Kolonisierung wurde ein großes Screening für eine QTL Analyse durchgeführt. Dabei wurden einige Gene ins Auge genommen wie zum Beispiel *NOPE1*, von denen bereits berichtet wurde, dass sie in die Regulierung von Symbiosen involviert sind und somit weitere Anhaltspunkte für die Forward Genetics Forschung bieten. Weiterhin konnten wir bestätigen, dass solche Blattmarker, wie sie in vielen ein- und zweikeimblättrigen Kultur- und Modellpflanzen (*Solanum lycopersicum*, *Solanum tuberosum*, *Hordeum vulgare*, *Triticum aestivum*, *Medicago truncatula* and *Brachypodium distachyon*) zu finden sind, nicht auf eine bestimmte Mykorrhiza-Art beschränkt sind.

7. References

- Adolfsson L, Solymosi K, Andersson MX, Keresztes A, Uddling J, Schoefs B, Spetea C. 2015.** Mycorrhiza Symbiosis Increases the Surface for Sunlight Capture in *Medicago truncatula* for Better Photosynthetic Production. *Plos One* **10**(1).
- Akiyama K, Hayashi H. 2006.** Strigolactones: Chemical signals for fungal symbionts and parasitic weeds in plant roots. *Annals of Botany* **97**(6): 925-931.
- Akiyama K, Matsuzaki K, Hayashi H. 2005.** Plant sesquiterpenes induce hyphal branching in arbuscular mycorrhizal fungi. *Nature* **435**(7043): 824-827.
- Aliferis KA, Chamoun R, Jabaji S. 2015.** Metabolic responses of willow (*Salix purpurea* L.) leaves to mycorrhization as revealed by mass spectrometry and H-1 NMR spectroscopy metabolite profiling. *Frontiers in Plant Science* **6**.
- Amasino R. 2005.** 1955: Kinetin arrives. The 50th anniversary of a new plant hormone. *Plant Physiology* **138**(3): 1177-1184.
- Apel K, Hirt H. 2004.** Reactive oxygen species: Metabolism, oxidative stress, and signal transduction. *Annual Review of Plant Biology* **55**: 373-399.
- Bahulikar RA, Stanculescu D, Preston CA, Baldwin IT. 2004.** ISSR and AFLP analysis of the temporal and spatial population structure of the post-fire annual, *Nicotiana attenuata*, in SW Utah. *BMC ecology* **4**(1): 12.
- Bais HP, Weir TL, Perry LG, Gilroy S, Vivanco JM. 2006.** The role of root exudates in rhizosphere interactions with plants and other organisms. *Annu. Rev. Plant Biol.* **57**: 233-266.
- Baldwin IT. 1989.** Mechanism of Damage-Induced Alkaloid Production in Wild Tobacco. *Journal of Chemical Ecology* **15**(5): 1661-1680.
- Baldwin IT, Morse L. 1994.** Up in Smoke .2. Germination of *Nicotiana-Attenuata* in Response to Smoke-Derived Cues and Nutrients in Burned and Unburned Soils. *Journal of Chemical Ecology* **20**(9): 2373-2391.
- Baldwin IT, Staszakozinski L, Davidson R. 1994.** Up in Smoke .1. Smoke-Derived Germination Cues for Postfire Annual, *Nicotiana-Attenuata* Torr Ex Watson. *Journal of Chemical Ecology* **20**(9): 2345-2371.
- Bravo A, Brands M, Wewer V, Dormann P, Harrison MJ. 2017.** Arbuscular mycorrhiza-specific enzymes FatM and RAM2 fine-tune lipid biosynthesis to promote development of arbuscular mycorrhiza. *New Phytologist* **214**(4): 1631-1645.
- Bravo A, Brands M, Wewer V, Dörmann P, Harrison MJ. 2017.** Arbuscular mycorrhiza-specific enzymes FatM and RAM2 fine-tune lipid biosynthesis to promote development of arbuscular mycorrhiza. *New Phytologist* **214**(4): 1631-1645.

- Brundrett MC, Tedersoo L. 2018.** Evolutionary history of mycorrhizal symbioses and global host plant diversity. *New Phytologist*.
- Brunoud G, Wells DM, Oliva M, Larrieu A, Mirabet V, Burrow AH, Beeckman T, Kepinski S, Traas J, Bennett MJ, Vernoux T. 2012.** A novel sensor to map auxin response and distribution at high spatio-temporal resolution. *Nature* **482**(7383): 103-U132.
- Bürkle L, Cedzich A, Döpke C, Stransky H, Okumoto S, Gillissen B, Kühn C, Frommer WB. 2003.** Transport of cytokinins mediated by purine transporters of the PUP family expressed in phloem, hydathodes, and pollen of Arabidopsis. *Plant Journal* **34**(1): 13-26.
- Chitarra W, Pagliarani C, Maserti B, Lumini E, Siciliano I, Cascone P, Schubert A, Gambino G, Balestrini R, Guerrieri E. 2016.** Insights on the Impact of Arbuscular Mycorrhizal Symbiosis on Tomato Tolerance to Water Stress. *Plant Physiology* **171**(2): 1009-1023.
- De Smet I, Vassileva V, De Rybel B, Levesque MP, Grunewald W, Van Damme D, Van Noorden G, Naudts M, Van Isterdael G, De Clercq R, Wang JY, Meuli N, Vanneste S, Friml J, Hilson P, Jurgens G, Ingram GC, Inze D, Benfey PN, Beeckman T. 2008.** Receptor-like kinase ACR4 restricts formative cell divisions in the Arabidopsis root. *Science* **322**(5901): 594-597.
- Dello Ioio R, Linhares FS, Scacchi E, Casamitjana-Martinez E, Heidstra R, Costantino P, Sabatini S. 2007.** Cytokinins Determine Arabidopsis Root-Meristem Size by Controlling Cell Differentiation. *Current Biology* **17**(8): 678-682.
- Desalegn G, Turetschek R, Kaul HP, Wienkoop S. 2016.** Microbial symbionts affect *Pisum sativum* proteome and metabolome under *Didymella pinodes* infection. *Journal of Proteomics* **143**: 173-187.
- Facelli E, Duan T, Smith SE, Christophersen HM, Facelli JM, Smith FA. 2014.** Opening the black box: Outcomes of interactions between arbuscular mycorrhizal (AM) and non-host genotypes of *Medicago* depend on fungal identity, interplay between P uptake pathways and external P supply. *Plant, Cell and Environment* **37**(6): 1382-1392.
- Facelli E, Smith SE, Facelli JM, Christophersen HM, Andrew Smith F. 2010.** Underground friends or enemies: Model plants help to unravel direct and indirect effects of arbuscular mycorrhizal fungi on plant competition. *New Phytologist* **185**(4): 1050-1061.
- Ferrieri AP, Machado RAR, Arce CCM, Kessler D, Baldwin IT, Erb M. 2017.** Localized micronutrient patches induce lateral root foraging and chemotropism in *Nicotiana attenuata*. *Journal of Integrative Plant Biology* **59**(10): 759-771.
- Fester T, Maier W, Strack D. 1999.** Accumulation of secondary compounds in barley and wheat roots in response to inoculation with an arbuscular mycorrhizal fungus and co-inoculation with rhizosphere bacteria. *Mycorrhiza* **8**(5): 241-246.
- Flematti GR, Ghisalberti EL, Dixon KW, Trengove RD. 2004.** A compound from smoke that promotes seed germination. *Science* **305**(5686): 977.

- Flematti GR, Waters MT, Scaffidi A, Merritt DJ, Ghisalberti EL, Dixon KW, Smith SM. 2013.** Karrikin and Cyanohydrin Smoke Signals Provide Clues to New Endogenous Plant Signaling Compounds. *Molecular Plant* **6**(1): 29-37.
- Floss DS, Hause B, Lange PR, Kuster H, Strack D, Walter MH. 2008a.** Knock-down of the MEP pathway isogene 1-deoxy-D-xylulose 5-phosphate synthase 2 inhibits formation of arbuscular mycorrhiza-induced apocarotenoids, and abolishes normal expression of mycorrhiza-specific plant marker genes. *Plant Journal* **56**(1): 86-100.
- Floss DS, Schliemann W, Schmidt J, Strack D, Walter MH. 2008b.** RNA Interference-Mediated Repression of MtCCD1 in Mycorrhizal Roots of *Medicago truncatula* Causes Accumulation of C-27 Apocarotenoids, Shedding Light on the Functional Role of CCD1. *Plant Physiology* **148**(3): 1267-1282.
- Friml J. 2003.** Auxin transport—shaping the plant. *Current opinion in plant biology* **6**(1): 7-12.
- Gapper C, Dolan L. 2006.** Control of plant development by reactive oxygen species. *Plant Physiology* **141**(2): 341-345.
- Genre A, Chabaud M, Balergue C, Puech–Pagès V, Novero M, Rey T, Fournier J, Rochange S, Bécard G, Bonfante P. 2013.** Short-chain chitin oligomers from arbuscular mycorrhizal fungi trigger nuclear Ca²⁺ spiking in *Medicago truncatula* roots and their production is enhanced by strigolactone. *New Phytologist* **198**(1): 190-202.
- Gerlach N, Schmitz J, Polatajko A, Schluter U, Fahnenstich H, Witt S, Fernie AR, Uroic K, Scholz U, Sonnewald U, Bucher M. 2015.** An integrated functional approach to dissect systemic responses in maize to arbuscular mycorrhizal symbiosis. *Plant Cell and Environment* **38**(8): 1591-1612.
- Gillissen B, Bürkle L, André B, Kühn C, Rentsch D, Brandl B, Frommer WB. 2000.** A new family of high-affinity transporters for adenine, cytosine, and purine derivatives in *Arabidopsis*. *Plant Cell* **12**(2): 291-300.
- Grieneisen VA, Xu J, Maree AFM, Hogeweg P, Scheres B. 2007.** Auxin transport is sufficient to generate a maximum and gradient guiding root growth. *Nature* **449**(7165): 1008-1013.
- Groten K, Nawaz A, Nguyen NHT, Santhanam R, Baldwin IT. 2015a.** Silencing a key gene of the common symbiosis pathway in *Nicotiana attenuata* specifically impairs arbuscular mycorrhizal infection without influencing the root-associated microbiome or plant growth. *Plant Cell and Environment* **38**(11): 2398-2416.
- Groten K, Pahari NT, Xu SQ, van Doorn MM, Baldwin IT. 2015b.** Virus-Induced Gene Silencing Using Tobacco Rattle Virus as a Tool to Study the Interaction between *Nicotiana attenuata* and *Rhizophagus irregularis*. *Plos One* **10**(8).

- Gulati J, Baldwin IT, Gaquerel E. 2014.** The roots of plant defenses: integrative multivariate analyses uncover dynamic behaviors of gene and metabolic networks of roots elicited by leaf herbivory. *Plant Journal* **77**(6): 880-892.
- Gulati J, Kim SG, Baldwin IT, Gaquerel E. 2013.** Deciphering Herbivory-Induced Gene-to-Metabolite Dynamics in *Nicotiana attenuata* Tissues Using a Multifactorial Approach. *Plant Physiology* **162**(2): 1042-1059.
- Gutjahr C, Gobbato E, Choi J, Riemann M, Johnston MG, Summers W, Carbonnel S, Mansfield C, Yang SY, Nadal M, Acosta I, Takano M, Jiao WB, Schneeberger K, Kelly KA, Paszkowski U. 2015.** Rice perception of symbiotic arbuscular mycorrhizal fungi requires the karrikin receptor complex. *Science* **350**(6267): 1521-1524.
- Harrison MJ. 2005.** Signaling in the arbuscular mycorrhizal symbiosis. *Annual Review of Microbiology* **59**: 19-42.
- Harrison MJ, Pumplin N, Breuillin FJ, Noar RD, Park HJ. 2010.** Phosphate Transporters in Arbuscular Mycorrhizal Symbiosis. *Arbuscular Mycorrhizas: Physiology and Function*: 117-135.
- Helber N, Wipfel K, Sauer N, Schaarschmidt S, Hause B, Requena N. 2011.** A Versatile Monosaccharide Transporter That Operates in the Arbuscular Mycorrhizal Fungus *Glomus* sp Is Crucial for the Symbiotic Relationship with Plants. *Plant Cell* **23**(10): 3812-3823.
- Hirose N, Makita N, Yamaya T, Sakakibara H. 2005.** Functional characterization and expression analysis of a gene, OsENT2, encoding an equilibrative nucleoside transporter in rice suggest a function in cytokinin transport. *Plant Physiology* **138**(1): 196-206.
- Hwang I, Sheen J, Muller B. 2012.** Cytokinin Signaling Networks. *Annual Review of Plant Biology*, Vol **63** **63**: 353-380.
- Jiang YN, Wang WX, Xie QJ, Liu N, Liu LX, Wang DP, Zhang XW, Yang C, Chen XY, Tang DZ, Wang ET. 2017.** Plants transfer lipids to sustain colonization by mutualistic mycorrhizal and parasitic fungi. *Science* **356**(6343): 1172-1175.
- Kato-Noguchi H, Tamura K, Sasaki H, Suenaga K. 2012.** Identification of two phytotoxins, blumenol A and grasshopper ketone, in the allelopathic Japanese rice variety Awaakamai. *Journal of Plant Physiology* **169**(7): 682-685.
- Kerr ID, Bennett MJ. 2007.** New insight into the biochemical mechanisms regulating auxin transport in plants. *Biochemical Journal* **401**: 613-622.
- Kessler A, Baldwin IT. 2002.** Plant responses to insect herbivory: The emerging molecular analysis. *Annual Review of Plant Biology* **53**: 299-328.
- Keymer A, Pimprakar P, Wewer V, Huber C, Brands M, Bucerius SL, Delaux PM, Klingl V, von Ropenack-Lahaye E, Wang TL, Eisenreich W, Dormann P, Parniske M, Gutjahr C. 2017.** Lipid transfer from plants to arbuscular mycorrhiza fungi. *Elife* **6**.

- Kobae Y, Ohmori Y, Saito C, Yano K, Ohtomo R, Fujiwara T. 2016.** Phosphate treatment strongly inhibits new arbuscule development but not the maintenance of arbuscule in mycorrhizal rice roots. *Plant Physiology*: pp. 00127.02016.
- Kratsch H, Heflebower R. 2013.** Gardening guide for high-desert urban landscapes of Great Basin regions in Nevada and Utah. *SP-13-09. Reno, NV: University of Nevada, Cooperative Extension.* Online: <http://www.unce.unr.edu/publications/files/ho/2013/sp1309.pdf>.
- Krock B, Schmidt S, Hertweck C, Baldwin IT. 2002.** Vegetation-derived abscisic acid and four terpenes enforce dormancy in seeds of the post-fire annual, *Nicotiana attenuata*. *Seed Science Research* 12(4): 239-252.
- Kyozuka J. 2007.** Control of shoot and root meristem function by cytokinin. *Current opinion in plant biology* 10(5): 442-446.
- Leach JE, Triplett LR, Argueso CT, Trivedi P. 2017.** Communication in the Phytobiome. *Cell* 169(4): 587-596.
- Lee G, Joo Y, Kim SG, Baldwin IT. 2017.** What happens in the pith stays in the pith: tissue-localized defense responses facilitate chemical niche differentiation between two spatially separated herbivores. *Plant Journal* 92(3): 414-425.
- Lehmann A, Barto EK, Powell JR, Rillig MC. 2012.** Mycorrhizal responsiveness trends in annual crop plants and their wild relatives-a meta-analysis on studies from 1981 to 2010. *Plant and Soil* 355(1-2): 231-250.
- Leyser O. 2017.** Auxin Signaling. *Plant Physiology*.
- Li DP, Heiling S, Baldwin IT, Gaquerel E. 2016.** Illuminating a plant's tissue-specific metabolic diversity using computational metabolomics and information theory. *Proceedings of the National Academy of Sciences of the United States of America* 113(47): E7610-E7618.
- Ljung K, Bhalerao RP, Sandberg G. 2001.** Sites and homeostatic control of auxin biosynthesis in *Arabidopsis* during vegetative growth. *Plant Journal* 28(4): 465-474.
- Long HH, Sonntag DG, Schmidt DD, Baldwin IT. 2010.** The structure of the culturable root bacterial endophyte community of *Nicotiana attenuata* is organized by soil composition and host plant ethylene production and perception. *New Phytologist* 185(2): 554-567.
- Luginbuehl LH, Menard GN, Kurup S, Van Erp H, Radhakrishnan GV, Breakspear A, Oldroyd GED, Eastmond PJ. 2017.** Fatty acids in arbuscular mycorrhizal fungi are synthesized by the host plant. *Science* 356(6343): 1175-1178.
- Lynds GY, Baldwin IT. 1998.** Fire, nitrogen, and defensive plasticity in *Nicotiana attenuata*. *Oecologia* 115(4): 531-540.
- Maeda H, Futkuyasu Y, Yoshida S, Fukuda M, Saeki K, Matsuno H, Yamauchi Y, Yoshida K, Hirata K, Miyamoto K. 2004.** Fluorescent probes for hydrogen peroxide based on a non-oxidative mechanism. *Angewandte Chemie-International Edition* 43(18): 2389-2391.

- Maillet F, Poinot V, Andre O, Puech-Pages V, Haouy A, Gueunier M, Cromer L, Giraudet D, Formey D, Niebel A, Martinez EA, Driguez H, Becard G, Denarie J. 2011.** Fungal lipochitooligosaccharide symbiotic signals in arbuscular mycorrhiza. *Nature* **469**(7328): 58-U1501.
- Mangano S, Denita-Juarez SP, Choi HS, Marzol E, Hwang Y, Ranocha P, Velasquez SM, Borassi C, Barberini ML, Aptekmann AA, Muschietti JP, Nadra AD, Dunand C, Cho HT, Estevez JM. 2017.** Molecular link between auxin and ROS-mediated polar growth. *Proceedings of the National Academy of Sciences of the United States of America* **114**(20): 5289-5294.
- Mangano S, Pacheco JM, Marino-Buslje C, Estevez JM. 2018.** How Does pH Fit in with Oscillating Polar Growth? *Trends in Plant Science*.
- Marchant A, Bhalerao R, Casimiro I, Eklöf J, Casero PJ, Bennett M, Sandberg G. 2002.** AUX1 promotes lateral root formation by facilitating indole-3-acetic acid distribution between sink and source tissues in the Arabidopsis seedling. *The Plant Cell* **14**(3): 589-597.
- Martin FM, Uroz S, Barker DG. 2017.** Ancestral alliances: Plant mutualistic symbioses with fungi and bacteria. *Science* **356**(6340).
- Marzol E, Borassi C, Bringas M, Sede A, Garcia DRR, Capece L, Estevez JM. 2018.** Filling the Gaps to Solve the Extensin Puzzle. *Molecular Plant*.
- Mashiguchi K, Tanaka K, Sakai T, Sugawara S, Kawaide H, Natsume M, Hanada A, Yaeno T, Shirasu K, Yao H, McSteen P, Zhao YD, Hayashi K, Kamiya Y, Kasahara H. 2011.** The main auxin biosynthesis pathway in Arabidopsis. *Proceedings of the National Academy of Sciences of the United States of America* **108**(45): 18512-18517.
- Matsuzaki Y, Ogawa-Ohnishi M, Mori A, Matsubayashi Y. 2010.** Secreted Peptide Signals Required for Maintenance of Root Stem Cell Niche in Arabidopsis. *Science* **329**(5995): 1065-1067.
- Meldau DG, Long HH, Baldwin IT. 2012.** A native plant growth promoting bacterium, *Bacillus* sp B55, rescues growth performance of an ethylene-insensitive plant genotype in nature. *Frontiers in Plant Science* **3**.
- Meldau DG, Meldau S, Hoang LH, Underberg S, Wunsche H, Baldwin IT. 2013.** Dimethyl Disulfide Produced by the Naturally Associated Bacterium *Bacillus* sp B55 Promotes *Nicotiana attenuata* Growth by Enhancing Sulfur Nutrition. *Plant Cell* **25**(7): 2731-2747.
- Merrild MP, Ambus P, Rosendahl S, Jakobsen I. 2013.** Common arbuscular mycorrhizal networks amplify competition for phosphorus between seedlings and established plants. *New Phytologist* **200**(1): 229-240.
- Miyawaki K, Matsumoto-Kitano M, Kakimoto T. 2004.** Expression of cytokinin biosynthetic isopentenyltransferase genes in Arabidopsis: tissue specificity and regulation by auxin, cytokinin, and nitrate. *Plant Journal* **37**(1): 128-138.

- Newman E. 1978.** Root microorganisms: their significance in the ecosystem. *Biological Reviews* **53**(4): 511-554.
- Nishimura T, Hayashi KI, Suzuki H, Gyohda A, Takaoka C, Sakaguchi Y, Matsumoto S, Kasahara H, Sakai T, Kato JI, Kamiya Y, Koshiba T. 2014.** Yucasin is a potent inhibitor of YUCCA, a key enzyme in auxin biosynthesis. *Plant Journal* **77**(3): 352-366.
- Oldroyd GE. 2013.** Speak, friend, and enter: signalling systems that promote beneficial symbiotic associations in plants. *Nature Reviews Microbiology* **11**(4): 252.
- Overvoorde P, Fukaki H, Beeckman T. 2010.** Auxin Control of Root Development. *Cold Spring Harbor Perspectives in Biology* **2**(6).
- Park S, Takano Y, Matsuura H, Yoshihara T. 2004.** Antifungal compounds from the root and root exudate of *Zea mays*. *Bioscience Biotechnology and Biochemistry* **68**(6): 1366-1368.
- Parniske M. 2008.** Arbuscular mycorrhiza: the mother of plant root endosymbioses. *Nature Reviews Microbiology* **6**(10): 763-775.
- Pearce G, Moura DS, Stratmann J, Ryan CA. 2001.** RALF, a 5-kDa ubiquitous polypeptide in plants, arrests root growth and development. *Proceedings of the National Academy of Sciences of the United States of America* **98**(22): 12843-12847.
- Peng Q, Wang H, Tong J, Kabir MH, Huang Z, Xiao L. 2013.** Effects of indole-3-acetic acid and auxin transport inhibitor on auxin distribution and development of peanut at pegging stage. *Scientia Horticulturae* **162**: 76-81.
- Perrot-Rechenmann C. 2013.** Auxin-Binding Protein 1 is a negative regulator of the SCFTIR1/AFB pathway. *Auxin signaling in primary roots*.
- Phillips JM, Hayman DS. 1970.** Improved Procedures for Clearing Roots and Staining Parasitic and Vesicular-Arbuscular Mycorrhizal Fungi for Rapid Assessment of Infection. *Transactions of the British Mycological Society* **55**: 158-+.
- Pignatello JJ, Oliveros E, MacKay A. 2006.** Advanced oxidation processes for organic contaminant destruction based on the Fenton reaction and related chemistry. *Critical Reviews in Environmental Science and Technology* **36**(1): 1-84.
- Pineda A, Zheng SJ, van Loon JJA, Pieterse CMJ, Dicke M. 2010.** Helping plants to deal with insects: the role of beneficial soil-borne microbes. *Trends in Plant Science* **15**(9): 507-514.
- Preston CA, Baldwin IT. 1999.** Positive and negative signals regulate germination in the post-fire annual, *Nicotiana attenuata*. *Ecology* **80**(2): 481-494.
- Preston CA, Becker R, Baldwin IT. 2004.** Is 'NO' news good news? Nitrogen oxides are not components of smoke that elicits germination in two smoke-stimulated species, *Nicotiana attenuata* and *Emmenanthe penduliflora*. *Seed Science Research* **14**(1): 73-79.

- Raya-González J, Ortiz-Castro R, Ruíz-Herrera LF, Kazan K, López-Bucio J. 2014.** Phytochrome and flowering time/mediator25: Regulates lateral root formation via auxin signaling in arabidopsis. *Plant Physiology* **165**(2): 880-894.
- Reinhardt D, Pesce ER, Stieger P, Mandel T, Baltensperger K, Bennett M, Traas J, Friml J, Kuhlemeier C. 2003.** Regulation of phyllotaxis by polar auxin transport. *Nature* **426**(6964): 255-260.
- Rich MK, Nouri E, Courty PE, Reinhardt D. 2017.** Diet of Arbuscular Mycorrhizal Fungi: Bread and Butter? *Trends in Plant Science* **22**(8): 652-660.
- Riedel T, Groten K, Baldwin IT. 2008.** Symbiosis between *Nicotiana attenuata* and *Glomus intraradices*: ethylene plays a role, jasmonic acid does not. *Plant Cell and Environment* **31**(9): 1203-1213.
- Roberts JKM, Callis J, Jardetzky O, Walbot V, Freeling M. 1984a.** Cytoplasmic Acidosis as a Determinant of Flooding Intolerance in Plants. *Proceedings of the National Academy of Sciences of the United States of America-Biological Sciences* **81**(19): 6029-6033.
- Roberts JKM, Jardetzky O, Callis J, Walbot V, Freeling M. 1984b.** Cytoplasmic Acidosis as a Determinant of Flooding Intolerance in Plants. *Plant Physiology* **75**: 66-66.
- Rooney DC, Killham K, Bending GD, Baggs E, Weih M, Hodge A. 2009.** Mycorrhizas and biomass crops: opportunities for future sustainable development. *Trends in Plant Science* **14**(10): 542-549.
- Sakakibara H. 2006.** Cytokinins: Activity, biosynthesis, and translocation. *Annual Review of Plant Biology* **57**: 431-449.
- Santhanam R, Luu VT, Weinhold A, Goldberg J, Oh Y, Baldwin IT. 2015.** Native root-associated bacteria rescue a plant from a sudden-wilt disease that emerged during continuous cropping. *Proceedings of the National Academy of Sciences of the United States of America* **112**(36): E5013-E5020.
- Sauer M, Robert S, Kleine-Vehn J. 2013.** Auxin: Simply complicated. *Journal of Experimental Botany* **64**(9): 2565-2577.
- Schäfer M, Brütting C, Gase K, Reichelt M, Baldwin I, Meldau S. 2013.** ‘Real time’ genetic manipulation: a new tool for ecological field studies. *The Plant Journal* **76**(3): 506-518.
- Schuman MC, Baldwin IT. 2016.** The Layers of Plant Responses to Insect Herbivores. *Annual Review of Entomology, Vol 61* **61**: 373-394.
- Schweiger R, Baier MC, Muller C. 2014a.** Arbuscular Mycorrhiza-Induced Shifts in Foliar Metabolism and Photosynthesis Mirror the Developmental Stage of the Symbiosis and Are Only Partly Driven by Improved Phosphate Uptake. *Molecular Plant-Microbe Interactions* **27**(12): 1403-1412.
- Schweiger R, Baier MC, Persicke M, Muller C. 2014b.** High specificity in plant leaf metabolic responses to arbuscular mycorrhiza. *Nature Communications* **5**.
- Schweiger R, Muller C. 2015.** Leaf metabolome in arbuscular mycorrhizal symbiosis. *Current opinion in plant biology* **26**: 120-126.

- Sharma E, Anand G, Kapoor R. 2017.** Terpenoids in plant and arbuscular mycorrhiza-reinforced defence against herbivorous insects. *Annals of Botany* **119**(5): 791-801.
- Silverstone AL, Chang CW, Krol E, Sun TP. 1997.** Developmental regulation of the gibberellin biosynthetic gene GA 1 in *Arabidopsis thaliana*. *Plant Journal* **12**(1): 9-19.
- Soós V, Sebestyén E, Juhász A, Pintér J, Light ME, Staden J, Balázs E. 2009.** Stress-related genes define essential steps in the response of maize seedlings to smoke-water. *Functional and Integrative Genomics* **9**(2): 231-242.
- Strack D, Fester T. 2006.** Isoprenoid metabolism and plastid reorganization in arbuscular mycorrhizal roots. *New Phytologist* **172**(1): 22-34.
- Stuart K, Coke L. 1975.** The effect of vomifoliol on stomatal aperture. *Planta* **122**(3): 307-310.
- Sun TP, Gubler F. 2004.** Molecular mechanism of gibberellin signaling in plants. *Annual Review of Plant Biology* **55**: 197-223.
- Sundaravelpandian K, Chandrika NNP, Schmidt W. 2013.** PFT1, a transcriptional Mediator complex subunit, controls root hair differentiation through reactive oxygen species (ROS) distribution in *Arabidopsis*. *New Phytologist* **197**(1): 151-161.
- Swarup R, Friml J, Marchant A, Ljung K, Sandberg G, Palme K, Bennett M. 2001.** Localization of the auxin permease AUX1 suggests two functionally distinct hormone transport pathways operate in the *Arabidopsis* root apex. *Genes & development* **15**(20): 2648-2653.
- Takei K, Yamaya T, Sakakibara H. 2004.** *Arabidopsis* CYP735A1 and CYP735A2 encode cytokinin hydroxylases that catalyze the biosynthesis of trans-Zeatin. *Journal of Biological Chemistry* **279**(40): 41866-41872.
- Tan ZJ, Hu YL, Lin ZP. 2012.** Expression of NtPT5 Is Correlated with the Degree of Colonization in Tobacco Roots Inoculated with *Glomus etunicatum*. *Plant Molecular Biology Reporter* **30**(4): 885-893.
- Tian Q, Reed JW. 1999.** Control of auxin-regulated root development by the *Arabidopsis thaliana* SHY2/IAA3 gene. *Development* **126**(4): 711-721.
- Tormo J, Moreira B, Pausas J. 2014.** Field evidence of smoke-stimulated seedling emergence and establishment in Mediterranean Basin flora. *Journal of vegetation science* **25**(3): 771-777.
- Tsukagoshi H, Busch W, Benfey PN. 2010.** Transcriptional regulation of ROS controls transition from proliferation to differentiation in the root. *Cell* **143**(4): 606-616.
- Ubeda-Tomás S, Federici F, Casimiro I, Beemster GTS, Bhalerao R, Swarup R, Doerner P, Haseloff J, Bennett MJ. 2009.** Gibberellin Signaling in the Endodermis Controls *Arabidopsis* Root Meristem Size. *Current Biology* **19**(14): 1194-1199.
- Vaccari DA, Strigul N. 2011.** Extrapolating phosphorus production to estimate resource reserves. *Chemosphere* **84**(6): 792-797.

- van de Wiel CCM, van der Linden CG, Scholten OE. 2016.** Improving phosphorus use efficiency in agriculture: opportunities for breeding. *Euphytica* **207**(1): 1-22.
- Van Der Heijden MGA, Horton TR. 2009.** Socialism in soil? the importance of mycorrhizal fungal networks for facilitation in natural ecosystems. *Journal of Ecology* **97**(6): 1139-1150.
- Vannette RL, Hunter MD, Rasmann S. 2013.** Arbuscular mycorrhizal fungi alter above- and below-ground chemical defense expression differentially among *Asclepias* species. *Frontiers in Plant Science* **4**.
- Veiga RS, Faccio A, Genre A, Pieterse CM, Bonfante P, HEIJDEN MG. 2013.** Arbuscular mycorrhizal fungi reduce growth and infect roots of the non-host plant *Arabidopsis thaliana*. *Plant, cell & environment* **36**(11): 1926-1937.
- Velasquez SM, Ricardi MM, Dorosz JG, Fernandez PV, Nadra AD, Pol-Fachin L, Egelund J, Gille S, Harholt J, Ciancia M, Verli H, Pauly M, Bacic A, Olsen CE, Ulvskov P, Petersen BL, Somerville C, Iusem ND, Estevez JM. 2011.** O-glycosylated cell wall proteins are essential in root hair growth. *Science* **332**(6036): 1401-1403.
- Walder F, Niemann H, Natarajan M, Lehmann MF, Boller T, Wiemken A. 2012.** Mycorrhizal networks: Common goods of plants shared under unequal terms of trade. *Plant Physiology* **159**(2): 789-797.
- Wang M, Schoettner M, Xu SQ, Paetz C, Wilde J, Baldwin IT, Groten K. 2017.** Catechol, a major component of smoke, influences primary root growth and root hair elongation through reactive oxygen species-mediated redox signaling. *New Phytologist* **213**(4): 1755-1770.
- Wang M, Wilde J, Baldwin IT, Groten K. 2018.** *Nicotiana attenuata*'s capacity to interact with arbuscular mycorrhiza alters its competitive ability and elicits major changes in the leaf transcriptome. *Journal of Integrative Plant Biology* **60**(3): 242-261.
- Weller DM, Raaijmakers JM, Gardener BBM, Thomashow LS. 2002.** Microbial populations responsible for specific soil suppressiveness to plant pathogens. *Annual Review of Phytopathology* **40**: 309-+.
- Werner T, Motyka V, Laucou V, Smets R, Van Onckelen H, Schmülling T. 2003.** Cytokinin-Deficient Transgenic *Arabidopsis* Plants Show Multiple Developmental Alterations Indicating Opposite Functions of Cytokinins in the Regulation of Shoot and Root Meristem Activity. *Plant Cell* **15**(11): 2532-2550.
- Werner T, Motyka V, Strnad M, Schmülling T. 2001.** Regulation of plant growth by cytokinin. *Proceedings of the National Academy of Sciences of the United States of America* **98**(18): 10487-10492.
- Willemsen V, Scheres B. 2004.** Mechanisms of pattern formation in plant embryogenesis. *Annual Review of Genetics* **38**: 587-614.

- Willmann M, Gerlach N, Buer B, Polatajko A, Nagy R, Koebeke E, Jansa J, Flisch R, Bucher M. 2013.** Mycorrhizal phosphate uptake pathway in maize: Vital for growth and cob development on nutrient poor agricultural and greenhouse soils. *Frontiers in Plant Science* **4**(DEC).
- Won C, Shen XL, Mashiguchi K, Zheng ZY, Dai XH, Cheng YF, Kasahara H, Kamiya Y, Chory J, Zhao YD. 2011.** Conversion of tryptophan to indole-3-acetic acid by TRYPTOPHAN AMINOTRANSFERASES OF ARABIDOPSIS and YUCCAs in Arabidopsis. *Proceedings of the National Academy of Sciences of the United States of America* **108**(45): 18518-18523.
- Wu JQ, Baldwin IT. 2010.** New Insights into Plant Responses to the Attack from Insect Herbivores. *Annual Review of Genetics, Vol 44* **44**: 1-24.
- Wu JS, Kurten EL, Monshausen G, Hummel GM, Gilroy S, Baldwin IT. 2007.** NaRALF, a peptide signal essential for the regulation of root hair tip apoplastic pH in *Nicotiana attenuata*, is required for root hair development and plant growth in native soils. *Plant Journal* **52**(5): 877-890.
- Wu QS, Srivastava AK, Li Y. 2015.** Effects of Mycorrhizal Symbiosis on Growth Behavior and Carbohydrate Metabolism of Trifoliolate Orange Under Different Substrate P Levels. *Journal of Plant Growth Regulation* **34**(3): 499-508.
- Yang H, Zhang Q, Dai Y, Liu Q, Tang J, Bian X, Chen X. 2015.** Effects of arbuscular mycorrhizal fungi on plant growth depend on root system: a meta-analysis. *Plant and Soil* **389**(1-2): 361-374.
- Yang SY, Gronlund M, Jakobsen I, Grotemeyer MS, Rentsch D, Miyao A, Hirochika H, Kumar CS, Sundaresan V, Salamin N, Catausan S, Mattes N, Heuer S, Paszkowski U. 2012.** Nonredundant Regulation of Rice Arbuscular Mycorrhizal Symbiosis by Two Members of the PHOSPHATE TRANSPORTER1 Gene Family. *Plant Cell* **24**(10): 4236-4251.

8. Acknowledgment

Thanks to everyone who helped me and encourage me to get all the things done!

Thanks to **Ian** for his supervision, suggestions, discussion and support. Particularly I would like to thanks your professional spirit, your office lights peaking time is always before 7 pm in the morning, no matter summer or winter. Your diligence has been promoted me to keep moving on!

Thanks to **Merry** for my thesis revision!

Thanks to **Karin** for recruiting me as an IMPRS member and your always kindly help!

Thanks to **Evelyn** for her organization to help me get accommodated in Jena, and your reminding email to woke me up every Friday morning before 8:30.

Thanks to manage team, **Rayko**, **Merry** and **Klaus**, if our group is a flying airplane, you are pilots!

Thanks to the best engineer / technician / transformation team, **Eva**, **Thomas**, **Matthias**, **PuKe Wibke**, **Gundega** and **Klaus**, your contribution is just like the fuel for this plane.

Thanks to Greenhouse team, **Danny**, **Elke**, **Andreas.S**, **Andreas.W**, **Birgit.A**, **Birgit.Z** and **Jana** for all your herbal-skills, and all other gardeners for keeping the plants growing.

Thanks to office mates, **Henrique**, **Yang**, for ignoring my noises I made basically I called my family every day, and also for your kindly sharing snacks, coffee and jokes.

Thanks to my lab mates, **Suhua**, **Jiancai**, **Erica**, **Merry** for sharing everything in the lab and joint lab cleaning.

Thanks to **Shuqing** and **Ran** for technical teaching, and very important is that I learnt a lot from both you particularly the way of thinking of a scientific question and how to figure it out, along with your working style, work hard but very efficient!

Thanks to my collaborators **Dapeng**, **Martin**, **Suhua**, you are wonderful! No more words to express my appreciation, I was really enjoying to work with you! You guys are so brilliant!

Thanks to **Erica** for your help with thesis revision and many other experimental help!

Thanks to Friday night dinner crew, **Chuanfu**, **Yuanyuan**, **Huili**, **Zhiling**, **Lingling**, **Suhua** and **Junfu**, for sharing your stories and your always support! Thanks to all Chinese friends in this institute, **Han**, **Jun**, **Yong**!

Thanks to every member in this department!

And last many thanks to **my family**, without your support, I can't make it! I love you all!

9. Curriculum Vitae

Ming Wang

Born: 05.19.1986

Nationality: China

Email: wangmingxl09@gmail.com

Gender: Male

Education

2013-2018: Ph. D. (Molecular Ecology)

Max-Planck-Institute for Chemical Ecology, Jena, Germany

Dissertation: “A hidden mystery: root adaptive responses to environmental factors in *Nicotiana attenuata*”

2009-2012: M. Sc (Cell Biology), Lanzhou University, Lanzhou, China

2005-2009: B. Sc (Bio-technology), Tsinghai University, Xi'ning, China

Publication:

1. Wang, M., Schäfer, M., Li, D., Halitschke, R., Dong, C., McGale, E., Paetz, C., Song, Y., Li, S., Baldwin, I. T. (2018). Blumenols as effective shoot markers for root symbiosis with arbuscular mycorrhizal fungi. *eLife* (under review)
2. Song, Y., Wang, M., Groten, K., Wilde, J., Zeng, R., Baldwin, I.T. (2018). Priming of anti-herbivore defense in neighbouring plants of *Nicotiana attenuata* via common mycorrhizal network. *New Phytologist* (in preparation)
3. Wang, M., Wilde, J., Baldwin, I. T., Groten, K. (2018). *Nicotiana attenuata*'s capacity to interact with arbuscular mycorrhiza alters its competitive ability and elicits major changes in the leaf transcriptome. *Journal of Integrative Plant Biology*, 60(3), 242-261. doi:10.1111/jipb.12609
4. Wang, M., Schoettner, M., Xu, S., Paetz, C., Wilde, J., Baldwin, I. T., Groten, K. (2017). Catechol, a major component of smoke, influences primary root growth and root hair elongation through reactive oxygen species-mediated redox signaling. *New Phytologist*, 213(4), 1755-1770. doi:10.1111/nph.14317.

5. Li, R., Wang, M., Wang, Y., Schuman, M. C., Weinhold, A., Schäfer, M., Jimenez-Aleman, G. H., Barthel, A., Baldwin, I. T. (2017). Flower-specific jasmonate signaling regulates constitutive floral defenses in wild tobacco. *Proceedings of the National Academy of Sciences of the United States of America*, 114(34), E7205-E7214. doi:10.1073/pnas.1703463114
6. Zhou, Z.Y., Zhang, C.G., Wu, L., Chai, J., Wang, M., Jha, A., Jia, P.F., Cui, S.J., Yang, M., Chen, R. and Guo, G.Q. (2011) Functional characterization of the *CKRC1/TAA1* gene and dissection of hormonal actions in the Arabidopsis root. *Plant Journal*, 66, 516-527

Patents

1. Leaf markers for root colonization by arbuscular mycorrhizal fungi in plants. (patent reference: EP 18 15 8922.7, 2018)

Selected Oral Presentations

1. Ming W (2017). Jasmonate signaling mediates mycorrhization in *Nicotiana attenuata* by interfering with strigolactone biosynthesis in a COI1-dependent manner. IMPRS symposium
2. Ming W (2015). Smoke – more than a germination cue? Institute symposium

Selected Poster Presentations

1. Ming W, Julia W, Shuqing X, Ian.T.B and Karin G (2016). AMF-induced local and systemic changes in gene expression and metabolite levels under low Pi condition. 2nd international Molecular Mycorrhiza Meeting (iMMM)
2. Ming W, Karin G, and Ian.T.B (2014). The ecological effect of smoke on plant growth and development in *Nicotiana attenuata*. IMPRS symposium

10. Eigenständigkeitserklärung

Ich erkläre hiermit, dass die geltende Promotionsordnung der Biologisch-Pharmazeutischen Fakultät der Friedrich-Schiller-Universität Jena mir bekannt ist. Diese vorliegende Dissertation habe ich selbst angefertigt und keine anderen als die angegebenen Hilfsmittel, Mitteilungen oder Quellen benutzt. Bei der Auswahl und Auswertung des Materials haben mich die in der Danksagung meiner Dissertation genannten Personen unterstützt. Personen, die bei der Anfertigung wissenschaftlicher Daten beteiligt waren, sind auch in der Arbeit angegeben. Ich erkläre, dass ich keine Hilfe eines Promotionsberaters in Anspruch genommen habe und dass Dritte weder unmittelbar, noch mittelbar geldwerte Leistungen von mir für Arbeiten genommen haben, die im Zusammenhang mit dem Inhalt der vorliegenden Dissertation stehen. Weiterhin erkläre ich, dass ich die Dissertation nicht als Prüfungsarbeit für eine staatliche oder andere wissenschaftliche Prüfung eingereicht habe. Ferner habe ich nicht versucht, diese Doktorarbeit oder eine andere Abhandlung dieser Arbeit bei einer anderen Hochschule als Dissertation einzureichen.

Jena, May 22, 2018

Ming Wang

Universität Jena

2018